



## City Research Online

### City, University of London Institutional Repository

---

**Citation:** Morrison, P.D.J. (1994). Performance of foundations in a rising groundwater environment. (Unpublished Doctoral thesis, City University London)

This is the accepted version of the paper.

This version of the publication may differ from the final published version.

---

**Permanent repository link:** <https://openaccess.city.ac.uk/id/eprint/7421/>

**Link to published version:**

**Copyright:** City Research Online aims to make research outputs of City, University of London available to a wider audience. Copyright and Moral Rights remain with the author(s) and/or copyright holders. URLs from City Research Online may be freely distributed and linked to.

**Reuse:** Copies of full items can be used for personal research or study, educational, or not-for-profit purposes without prior permission or charge. Provided that the authors, title and full bibliographic details are credited, a hyperlink and/or URL is given for the original metadata page and the content is not changed in any way.

**Performance of foundations in a rising  
groundwater environment.**

**by**

**Paul Robert James Morrison**

**A dissertation submitted for the  
Degree of Doctor of Philosophy**

**at**

**The City University, London  
Department of Civil Engineering**

**May 1994**

**BEST COPY**

**AVAILABLE**

Variable print quality

CONTENTS	2	
LIST OF TABLES	7	
LIST OF FIGURES	8	
ACKNOWLEDGEMENTS	15	
DECLARATIONS	16	
ABSTRACT	17	
LIST OF SYMBOLS	18	
CHAPTER 1	INTRODUCTION	21
1.1	Background	21
1.1.1	Historical background in London	21
1.1.2	Ground conditions and foundations	22
1.2	Modelling of foundation behaviour in soil with rising pore pressures	24
1.2.1	Physical modelling	24
1.2.2	Numerical modelling	25
1.3	Objectives of the research	26
1.4	Outline of thesis	26
1.5	Summary	28
CHAPTER 2	LITERATURE REVIEW	29
2.1	Deep and shallow foundation design and behaviour	29
2.1.1	Ultimate load capacity of piles	30
2.1.1.1	Pile shaft capacity	30
2.1.1.2	Pile base capacity	33
2.1.2	Pile settlements	34
2.1.2.1	Shaft load displacement response	34
2.1.2.2	Base load displacement response	35
2.1.2.3	Composite pile settlement	36
2.1.3	Shallow footing load capacity	38
2.1.4	Shallow footing settlement	38
2.2	In-situ soil stresses	38
2.2.1	Initial one dimensional loading	39
2.2.2	One dimensional unloading	39
2.2.3	One dimensional reloading	40
2.2.4	Earth pressure and changing pore water pressure	41

2.3	Case histories of foundation behaviour with changing pore water pressure	42
2.3.1	Wilkinson (1984): An introduction to the problem	42
2.3.2	Armishaw and Cox (1979): Rising groundwater levels and driven piles in granular soils	42
2.3.3	Troughton and Platis (1989): A large scale pile test with modelling of changing effective stresses in sand	43
2.3.4	Simpson et al. (1987 and 1989): CIRIA SP69	44
2.3.5	Kulhawy and Beech (1987): The effect of recovering water levels on foundation side resistance	45
2.3.6	Andersen (1990): An initial series of centrifuge tests modelling rising groundwater in clay	46
2.3.7	Challa and Poulos (1992): Model tests of piles in swelling clay	46
2.4	A simple "by hand" settlement calculation	47
2.4.1	Friction piles	48
2.4.2	End bearing piles	48
2.5	Summary	49
CHAPTER 3	CRITICAL STATE SOIL MODELS AND TRIAXIAL TESTING	50
3.1	Introduction	50
3.2	Introduction to critical state soil mechanics	50
3.3	Schofield model	51
3.4	Three surface kinematic hardening model (Stallebrass model)	52
3.4.1	State boundary surface	53
3.4.2	Overconsolidated behaviour	53
3.5	Triaxial testing	55
3.5.1	Triaxial apparatus	55
3.5.2	Controlling software	55
3.5.3	Controlling hardware	56
3.5.4	Instrumentation	57
3.6	Testing and test results	58
3.6.1	Sample and cell preparation	58
3.6.2	$K_0$ effective stress paths	59
3.6.3	Volumetric conditions during $K_0$ stress paths	60
3.6.4	Shearing	61
CHAPTER 4	CENTRIFUGE MODELLING AND MODEL TEST PROCEDURE	62
4.1	Introduction	62

4.2	Centrifuge scaling laws	62
	4.2.1 Stress and dimensions	63
	4.2.2 Time	63
	4.2.3 Mass	64
	4.2.4 Summary	64
4.3	Centrifuge model and preparation	64
	4.3.1 Soil stress errors during preparation	66
4.4	Centrifuge modelling errors	68
	4.4.1 Vertical acceleration field	68
	4.4.2 Radial acceleration field	69
	4.4.3 Model foundation orientation in gravity field	69
	4.4.4 Coriolis acceleration errors	70
4.5	Test equipment	70
	4.5.1 Acutronic 661 centrifuge	70
	4.5.2 Data recovery	71
	4.5.3 Model containers	72
	4.5.4 Foundation types and installation	72
	4.5.5 Loading rigs	73
	4.5.6 Standpipe	74
	4.5.7 Instrumentation	74
	4.5.8 Piezocone and actuator	75
4.6	Pore pressures and downward hydraulic gradient consolidation	76
4.7	Test procedure	77
CHAPTER 5	CENTRIFUGE TESTS AND RESULTS	80
5.1	Introduction	80
	5.1.1 Data obtained from tests	82
5.2	Generalised pore water pressure changes in the model	83
	5.2.1 Spin up and subsequent dissipation	83
	5.2.2 Rising groundwater event	84
	5.2.3 Spin down	85
5.3	Moisture contents at end of test	85
5.4	Piezocone tests	86
	5.4.1 Piezocone test results	87
	5.4.1.1 Tests at 0.2mm/sec	87
	5.4.1.2 Tests at 2.0mm/sec	88

5.4.2	Discussion of piezocone results	89
5.4.2.1	Rate of penetration	89
5.4.2.2	Correlation with undrained strength ( $S_u$ )	89
5.4.2.3	Correlation with drained strength	91
5.4.2.4	Comparison of drained and undrained strength	91
5.5	Piled foundation load behaviour prior to rising groundwater	92
5.5.1	Piled foundations during initial pore water pressure equilibrium stage	94
5.5.2	Initial foundation loading	95
5.6	Foundation behaviour during a rising groundwater event	96
5.6.1	Tests RW3 and RW6: Comparison of pre-loaded and non pre-loaded piles	97
5.6.2	Test RW10: Influence of initial factor of safety on settlement	99
5.6.3	Test RW13: The behaviour of different foundation types and different initial pore pressure distributions	100
5.6.4	Test RW15: Comparison of two different pile geometries	102
5.7	Comparison of piled foundation load capacity before and after the rising groundwater event	104
5.7.1	Shaft capacity	104
5.7.2	Base capacity	105
5.8	Factors effecting foundation movements during a rising groundwater event	105
5.8.1	The influence of factor of safety on pile settlement	106
5.8.2	The influence of slenderness ratio on pile settlement	107
5.8.3	The influence of different pore water pressure on foundation movements	107
5.8.4	The influence of pile length on pile settlement	108
5.9	Summary	108
CHAPTER 6	NUMERICAL ANALYSIS OF PILED FOUNDATIONS	110
6.1	Introduction: Finite element modelling	110
6.2	Introduction to finite element program - CRISP	111
6.2.1	Types of analysis	111
6.2.2	Element types and boundary conditions	111

6.3	Modelling of pile installation	112
6.3.1	Mesh and material properties	113
6.3.2	Initial in-situ stress conditions	113
6.3.3	Soil stress state before pile installation	114
6.3.4	Pile installation results: 1PIEXC	115
6.3.5	Pile installation results: 1P2MOD	116
6.3.6	Comments on prototype and model pile installations	117
6.4	Piles in a rising groundwater event after pile installation	118
6.4.1	Pile shaft in a rising groundwater event	120
6.4.1.1	After analysis 1PIEXC	120
6.4.1.2	After analysis 1P2MOD	121
6.4.1.3	Comparison of smooth shaft analyses	121
6.5	Piles in a rising groundwater event using Schofield model	122
6.6	Conclusions from finite element analyses	124
6.7	Simple "by hand" analysis of pile settlement during a rising groundwater event	125
6.7.1	Prediction of centrifuge model behaviour	126
6.8	Summary	127
CHAPTER 7	CONCLUDING REMARKS AND SUGGESTIONS FOR FURTHER WORK	129
7.1	Methodology	129
7.2	Soil in a rising groundwater environment	130
7.3	Foundations in a rising groundwater environment	130
7.4	Implications for foundation behaviour and design	132
7.5	Limitations of the work	133
7.6	Further work	134
REFERENCES		136
TABLES		
FIGURES		
APPENDIX A	Centrifuge test raw data	A.1
APPENDIX B	Calculation of pile settlement	B.1

## LIST OF TABLES

- Table 4.1    Scaling for typical centrifuge test
- Table 5.1    Summary of centrifuge tests:  
a:    Tests RW1 to RW5  
b:    Tests RW6 to RW11  
c:    Tests RW12 to RW16
- Table 5.2    Summary of piezocone penetration tests
- Table 5.3    Summary of foundation load tests:  
a:    Tests RW1 to RW5  
b:    Tests RW6 to RW11  
c:    Tests RW12 to RW16
- Table 5.4    Summary of foundation behaviour during rising groundwater event:  
a:    Tests RW1 to RW5  
b:    Tests RW6 to RW11  
c:    Tests RW12 to RW16
- Table 5.5    Ultimate shaft capacity before and after rising groundwater event for instrumented under-reamed piles
- Table 5.6    Ultimate base capacity before and after rising ground event for instrumented piles
- Table 6.1    Pile installation analyses summary
- Table 6.2    Summary of material properties for finite element modelling
- Table 6.3    Summary of rising groundwater events using Schofield model

## LIST OF FIGURES

- Figure 1.1 Schematic of groundwater levels beneath London
- Figure 1.2 Geology of the London basin
- Figure 1.3 Pore water pressure profiles through London Clay (After Simpson et al., 1989)
- Figure 2.1 Stresses around a bored pile shaft (After Lopes, 1979)
- Figure 2.2 Hyperbolic function applied to pile settlement (After Chin 1972)
- Figure 2.3 Undrained bearing capacity factor (After Skempton, 1951, see Poulos and Davis, 1980)
- Figure 2.4 Schematic of one-dimensional stress history
- Figure 2.5 Driven pile (in terrace gravel deposit) end bearing capacity against vertical effective stress (After Armishaw and Cox, 1979)
- Figure 2.6a Bored pile (in Thanet sand deposit) end bearing resistance against vertical effective stress (after Troughton and Platis, 1989)
- Figure 2.6b Bored pile (in Thanet sand deposit) end bearing resistance against mean normal effective stress (after Troughton and Platis, 1989)
- Figure 2.7 Anticipated modes of behaviour of shallow and deep foundations in clay during a rising groundwater event (After Simpson et al. 1989)
- Figure 2.8 Centrifuge model set up (After Andersen 1990)
- Figure 2.9 Loss of model pile load capacity after swelling clay event (After Challa and Poulos, 1993)
- Figure 2.10 Tension in model piles after swelling clay event (After Challa and Poulos, 1993)
- Figure 2.11 Model pile and soil displacements after swelling clay event (After Challa and Poulos, 1993)
- Figure 2.12 Schematic of the effects of rising groundwater levels on friction piles
- Figure 2.13 Schematic of the effects of rising groundwater levels on end bearing piles
- Figure 3.1 Schofield Model:  
a)  $p' - q$  space  
b)  $v - \ln(p')$  space

- Figure 3.2 Three surface kinematic yield hardening model in  $p' - q$  space: Stallebrass model
- Figure 3.3 Stiffness with shear stress for different stress path rotations (After Stallebrass, 1990)
- Figure 3.4 Stress path rotation for Figure 3.3 (After Stallebrass, 1990)
- Figure 3.5 Layout of triaxial stress path cell
- Figure 3.6 Stress path for  $K_0$  normally consolidated Speswhite Kaolin, horizontal effective stress against vertical effective stress
- Figure 3.7 Stress path for  $K_0$  unloading of Speswhite Kaolin, horizontal effective stress against vertical effective stress:  
a) Tests 7 $\phi$  and 10 $\phi$   
b) Tests T8 and T9  
c) Test L1
- Figure 3.8 Variation of  $K_{ou}/K_{onc}$  with overconsolidation ratio
- Figure 3.9 Cycles of pore water pressure under  $K_0$  conditions, horizontal effective stress against vertical effective stress, stress path from A to B to C:  
a) Test T8                      b) Test T10  
c) Test L1                      d) Test L3
- Figure 3.10 Change in horizontal effective stress with change in vertical effective stress during pore water pressure cycles, stress path from A to B to C
- Figure 3.11  $K_0$  compression data,  $\ln(v)$  against  $\ln(p')$  for tests in Figure 3.6
- Figure 3.12  $K_0$  compression and swelling data for samples compressed to  $\sigma'_{vmax} = 600\text{kPa}$  during pore water pressure cycles in  $\ln(v) - \ln(p')$  space
- Figure 3.13 Variation of  $\kappa^*$  with overconsolidation ratio during primary unloading (After Al-Tabbaa, 1987)
- Figure 3.14 Variation of  $\kappa^*$  with overconsolidation ratio during reloading (After Al-Tabbaa, 1987)
- Figure 3.15 Ultimate stress states for constant  $p'$  shearing in compression
- Figure 3.16 Comparison of volumetric and shear strain during constant  $p'$  shearing in compression
- Figure 4.1a Layout of computer controlled hydraulic consolidometer

- Figure 4.1b Stress states in sample using downward hydraulic gradient technique
- Figure 4.2 Placement of aluminium pile in excavated hole
- Figure 4.3a View of typical centrifuge model prior to loading onto centrifuge swing
- Figure 4.3b Set up of a typical centrifuge model with two similar piles
- Figure 4.4 Schematic of pore water pressure profile with downward seepage and variation due to different profiles of maximum preconsolidation pressure
- Figure 4.5 Swing and centrifuge arm geometry for calculation of acceleration errors
- Figure 4.6 Comparison of model and prototype total stress profiles along centre line of model
- Figure 4.7 Comparison of model and prototype total stress profiles along line offset by 0.18m (model scale) from centre line of model
- Figure 4.8 Schematic of Acutronic 661 centrifuge and centrifuge testing facility
- Figure 4.9 Foundation sizes and base load instrumentation
- Figure 4.10 Foundation loading mechanism
- Figure 4.11 Basal aquifer pore water pressure control mechanism
- Figure 4.12 Calibration data for transducers used in test RW15:  
a) Displacement transducers, gain = 2  
b) Pore pressure transducers, gain = 100  
c) Load cells, gain = 200
- Figure 4.13a Schematic of pore water pressure profile with downward seepage and a perched water table before groundwater rising event
- Figure 4.13b Schematic of pore water profile pressure with sealed top surface before groundwater rising event
- Figure 5.1 Pore water pressure response during spin-up from test RW10
- Figure 5.2a Dissipation of pore water pressure after spin-up from test RW10 with perched water table
- Figure 5.2b Dissipation of pore water pressure after spin-up from test RW13 with sealed surface
- Figure 5.3 Vertical effective stress profiles before (line 'a') and after (line 'b') rising groundwater event for nine tests with a perched water table

- Figure 5.4 Vertical effective stress profiles before (line 'a') and after (line 'b') rising groundwater event for two tests with a sealed surface
- Figure 5.5 Increase in pore water pressure with time during a model rising groundwater event from test RW10 with a perched water table
- Figure 5.6 Increase in pore water pressure with time during a rising groundwater event with a sealed surface, test RW13
- Figure 5.7 Pore water pressure response during spin-down from test RW16
- Figure 5.8 Final moisture contents for tests with downward seepage
- Figure 5.9 Final moisture contents for tests with a sealed surface
- Figure 5.10 Piezocone tests at 0.2mm/sec:  
a) Uncorrected cone resistance -  $q_c$   
b) Excess pore water pressure -  $u_e$
- Figure 5.11 Pore water pressure ratio for tests at 0.2mm/sec
- Figure 5.12 Corrected cone resistance ( $q_n$ ) against vertical effective stress at 0.2mm/sec
- Figure 5.13 Corrected cone resistance ( $q_n$ ) against mean normal effective stress at 0.2mm/sec
- Figure 5.14 Piezocone tests at 2.0mm/sec:  
a) Uncorrected cone resistance -  $q_c$   
b) Excess pore water pressure -  $u_e$
- Figure 5.15 Pore water pressure ratio for tests at 2.0mm/sec
- Figure 5.16 Corrected cone resistance ( $q_n$ ) against vertical effective stress at 2.0mm/sec
- Figure 5.17 Corrected cone resistance ( $q_n$ ) against mean normal effective stress at 2.0mm/sec
- Figure 5.18 Comparison of corrected cone resistance for test at 2.0mm/sec against with calculated cone resistance ( $N_c = 8.0$ )
- Figure 5.19 Load displacement results for pile loading prior to rising groundwater event:  
a) Piles with top and base load measurement  
b) Piles with only top load measurement
- Figure 5.20 Pile load distribution during loading to failure and subsequent unloading:  
a) Pile in test RW4, under-reamed  
b) Pile in test RW3, straight 16mm diameter

- Figure 5.21 Changing pile load distribution during a rising groundwater event against vertical effective stress at 150mm clay depth, test RW3
- Figure 5.22 Ultimate shaft stress against average vertical effective stress at pile shaft face, test RW3
- Figure 5.23 Foundation and surface movements during rising groundwater event against vertical effective stress at 150mm clay depth, test RW6  
Inset: Pore pressure profiles at four marked stages during rising groundwater event
- Figure 5.24 Foundation loads during rising groundwater event, test RW6
- Figure 5.25 Loading of Pile 1 prior to rising groundwater event, test RW10
- Figure 5.26 Load distribution during rising groundwater event for Pile 1, test RW10
- Figure 5.27 Foundation and surface movements during rising groundwater event against vertical effective stress at 150mm clay depth, test RW10  
Inset: Pore pressure profiles at four marked stages during rising groundwater event
- Figure 5.28 Foundation, buried plate and surface movements during rising groundwater event against vertical effective stress at 150mm clay depth, test RW13  
Inset: Pore pressure profiles at four marked stages during rising groundwater event
- Figure 5.29 Load distribution during rising groundwater event for pile and pad, test RW13
- Figure 5.30 Foundation, buried plate and surface movements during rising groundwater event against vertical effective stress at 150mm clay depth, test RW15  
Inset: Pore pressure profiles at four marked stages during rising groundwater event
- Figure 5.31a Pile end bearing capacity against calculated mean normal effective stress at pile base level
- Figure 5.31b Pile end bearing capacity against vertical effective stress at pile base level
- Figure 5.32 Correlation of pile initial factor of safety with settlement relative to soil surface during rising groundwater event for three pile geometries
- Figure 5.33 Correlation of pile initial factor of safety with settlement relative to soil at pile base level during rising groundwater event for three pile geometries

- Figure 5.34 Correlation of pile slenderness ratio (pile length -  $L_p/D_p$  -pile base diameter) with settlement relative to the ground surface, with general trends for different initial factors of safety
- Figure 5.35 Correlation of pile slenderness ratio (pile length -  $L_p/D_p$  -pile base diameter) with settlement relative to soil at pile base level, with general trends for different initial factors of safety
- Figure 5.36 Comparison of settlement of straight piles for different initial pore pressure profiles
- Figure 6.1 Mesh used for pile installation and rising groundwater analyses with Stallebrass model
- Figure 6.2 Variation of  $p'_c$  with  $\sigma'_v$  during one dimensional unloading from  $\sigma'_v = 1250\text{kPa}$
- Figure 6.3 Vertical effective stress profiles before, during and after modelling effects of recent stress history, analysis 1PIEXC
- Figure 6.4 Vertical and horizontal effective stress profiles after modelling effects of recent stress history, analysis 1PIEXC
- Figure 6.5 Comparison of  $K_0$  profile from Figure 6.4 and calculated profile from Eqn 3.8 and 2.20
- Figure 6.6 Vertical and horizontal effective stress profiles after modelling effects of recent stress history, analysis 1P2MOD
- Figure 6.7 Stress distributions with open excavation, analysis 1PIEXC:  
a) Vertical effective stress  
b) Radial effective stress  
c) Hoop effective stress
- Figure 6.8 Stress path during pile installation, analysis 1PIEXC:  
a) Element 336, 10m depth 0.8m from shaft  
b) Element 497, 10m depth 0.15m from shaft
- Figure 6.9 Vertical, radial and hoop effective stress distributions at 10m depth, analysis 1PIEXC:  
a) Open shaft  
b) After installation
- Figure 6.10 Stress distributions after pile installation, analysis 1PIEXC:  
a) Vertical effective stress  
b) Radial effective stress  
c) Hoop effective stress
- Figure 6.11 Horizontal displacements during pile installation at 1.0m and 5.5m from pile axis, analysis 1PIEXC

- Figure 6.12 Stress distributions after pile installation, analysis 1P2MOD:  
a) Vertical effective stress  
b) Radial effective stress  
c) Hoop effective stress
- Figure 6.13 Vertical, radial and hoop effective stress distributions at 0.10 depth, analysis 1P2MOD:  
a) Open shaft  
b) After installation
- Figure 6.14 Horizontal displacements during pile installation at 0.01 and 0.055m from pile axis, analysis 1P2MOD
- Figure 6.15 Shear stress at 0.9m and 5.5m from pile axis after rising groundwater event, analysis 1PIEXC
- Figure 6.16 Vertical effective stress at 0.1 and 5.5m from shaft after rising groundwater event, analysis 1PIEXC
- Figure 6.17 Stress ratio  $\eta$  at 0.1 and 5.5m from shaft after rising groundwater event, analysis 1PIEXC
- Figure 6.18 Displacement due to rising groundwater event, analysis 1PIEXC
- Figure 6.19 Detail of mesh with stress and strain controlled elements
- Figure 6.20 Variation of radial and hoop effective stresses with vertical effective stress during rising groundwater event with smooth pile shaft, analysis 1PIEXC
- Figure 6.21 Variation of radial and hoop effective stresses with vertical effective stress during rising groundwater event with smooth pile shaft, analysis 1P2MOD
- Figure 6.22 Vertical and horizontal effective stress distributions before and after rising groundwater event using Schofield model
- Figure 6.23 Rising groundwater event, analysis SCH5  
a) Surface and pile displacement  
b) Pile base load
- Figure 6.24 Rising groundwater event, analysis SCH2M  
a) Surface and pile displacement  
b) Pile base load
- Figure 6.25 Comparison of predicted (simple "by hand" method) pile settlements with centrifuge test results

## ACKNOWLEDGEMENTS

My stay at the Geotechnical Engineering Research Centre at City University has been both enjoyable and rewarding. The members of staff have all been supportive and helpful in finding answers to problems as they have arisen. I would especially like to thank my supervisor Dr Neil Taylor. His help, guidance and general good humour during my stay at City have been valued greatly. Secondly I would like to thank Dr Sarah Stallebrass for her friendship and insight on all things to do with finite elements.

The experimental part of the work would not have happened without able technical support of several people:

Harvey Skinner for driving the centrifuge and solving many problems which tend to arise at inopportune moments during testing.

Keith Osborne for always, when needed, finishing things yesterday.

Reg Allen for machining the most improbable shapes to exacting details.

Lloyd Martyka for help with electronics and computers.

I would also like to thank Dr Heleni Pantelidou for her encouragement and friendship during the writing of this thesis, and my parents for spending an immense amount of time in finding me a home.

The research was funded for two years (10/91 to 6/93 and 10/93 to 12/93) by the Science and Engineering Research Council under Grant Reference No. GR/G55723 and by the Geotechnical Engineering Research Centre during my final four months at City.

## DECLARATIONS

I certify that, except where specific reference is made in the text to the work of others, the contents of this dissertation are original and have not been submitted to any other university. This thesis is the result of my own work and contains nothing which is the outcome of work done in collaboration.

I grant powers of discretion to the University Librarian to allow this dissertation to be copied in whole or in part without further reference to me. This permission covers only single copies made for study purposes, subject to normal conditions of acknowledgement.

*P. R. J. Moman*

## ABSTRACT

In recent years an increase in the groundwater level in the basal aquifer beneath London has been observed. The result of this water level rise, if it were to reach equilibrium levels of two centuries ago, would be to cause a reduction in effective stress levels in the founding strata beneath London. The effect that such an increase in pore pressure would have on foundations in overconsolidated clay was investigated.

The performance of foundations in stiff clay during a rising ground water event was investigated by means of centrifuge model tests. The model tests included comparisons of the behaviour of bored piles with different factors of safety on load, piles with different length to base diameter ratios, comparison of shallow and deep foundation behaviour and the effect of different initial pore pressure distributions. In two tests piezocone tests were carried out in low and high pore water pressure regimes. Triaxial testing and numerical analyses were used to provide information for use in analysis of the centrifuge test results.

The main findings of the project were:

The geometry of a pile foundation (slender or under-reamed) and the manner by which load is transferred from pile to soil were seen to effect pile settlement relative to the ground surface during a rising groundwater event. Piles which require mobilisation of end bearing resistance at working loads will typically settle more than predominantly friction piles of the same length.

For similar geometry piles the initial factor of safety will effect settlement during a rising groundwater event. Piles with lower initial factors of safety settle more than those with higher initial factors of safety during a rising groundwater event.

Differential settlements between shallow and deep foundations were almost entirely due to the deep foundation settlement relative to the heaving ground surface where there was a surface perched water table. Where there was no perched surface water both shallow and deep foundations settled relative to the surface. Soil heave, in this latter case, was largely due to the high percentage loss in vertical effective stress near the surface compared to the case where a perched water table existed.

Piled foundation load capacity was seen to reduce as a result of a rising groundwater event. Base capacity, measured under largely drained conditions, was seen to be linearly related to the mean normal effective stress in the ground as was cone end resistance of piezocone tests carried out at slow penetration rates. The piezocone tests also showed that the percentage loss in drained end bearing resistance was larger than the loss in undrained resistance.

Finite element analyses investigated pile installation effects for model and prototype piles and the effect that they have on pile behaviour during a rising groundwater event. The results have shown that, on a smooth pile surface, the prototype piles will suffer a larger percentage reduction in shaft capacity than the model piles. The analyses were valuable for assessing the applicability of the centrifuge model data to prototype situations.

## LIST OF SYMBOLS

Units

a	Centrifuge acceleration	$m/s^2$
a	Piezocone area ratio	-
c'	True cohesion	$kN/m^2$
$d_b$	Pile base diameter	mm or m
g	Earth's gravitational acceleration	$m/s^2$
k	Coefficient of permeability	m/s
l	Length	mm or m
n	Centrifuge model scale factor	-
p'	Mean normal effective stress	$kN/m^2$
$p_b$	Pile base load	N
$p'_0$	Intercept of state boundary surface with p' axis in q - p' space	$kN/m^2$
$p_s$	Pile shaft - soil interface load	N
$p_w$	Foundation working load	N
q	Deviator stress	$kN/m^2$
$q_b$	Pile base stress	$kN/m^2$
$q_c$	Measured cone resistance	$kN/m^2$
$q_n$	Corrected cone resistance ( $q_t - \sigma_{vt}$ )	$kN/m^2$
$q_s$	Pile shaft - soil interface stress	$kN/m^2$
$q_t$	Cone resistance corrected for ppt cavity	$kN/m^2$
r	Centrifuge model radius	m
$r_m$	Radius from pile shaft at which settlements become negligible	mm or m
$r_o$	Pile shaft radius	mm or m
u	Pore water pressure	$kN/m^2$
v	Specific volume	-
A	Area	$mm^2$ or $m^2$
$B_q$	Pore pressure coefficient	-
E	Young's modulus	$kN/m^2$
FOS	Factor of safety on ultimate load	-
G	Shear modulus	$kN/m^2$
$G_o$	Shear modulus at very small strain	$kN/m^2$
H	Depth	m
$I_p$	Influence factor in pile settlement calculation	-

K	Factor in pile settlement calculation	-
K'	Drained bulk modulus	kN/m <sup>2</sup>
K <sub>o</sub>	Earth pressure coefficient at rest	-
K <sub>onc</sub>	Earth pressure coefficient at rest in normally consolidated state	-
K <sub>or</sub>	Earth pressure coefficient at rest during reloading	-
K <sub>ou</sub>	Earth pressure coefficient at rest during unloading	-
K <sub>p</sub>	Earth pressure coefficient at passive failure	-
K <sub>s</sub>	Earth pressure coefficient at pile shaft ( $\sigma'_1/\sigma'_v$ )	-
M	Stress ratio at critical state ( $q/p'$ )	-
M <sub>s</sub>	Flexibility factor in pile shaft settlement calculation	-
N <sub>c</sub>	Bearing capacity factor on cohesion	-
N <sub>k</sub>	Cone factor on undrained strength	-
N <sub>o</sub>	Specific volume intercept of one dimensional compression line at $p' = 1 \text{ kN/m}^2$	-
N <sub>q</sub>	Bearing capacity factor on $\sigma'_v$	-
N <sub>q</sub> *	Bearing capacity factor on $p'$	-
P <sub>b</sub>	Ultimate pile base load	N
P <sub>s</sub>	Ultimate pile shaft - soil interface load	N
PI	Plasticity index	-
Q <sub>b</sub>	Ultimate pile base stress	kN/m <sup>2</sup>
Q <sub>s</sub>	Ultimate pile shaft - soil interface stress	kN/m <sup>2</sup>
R	Overconsolidation ratio in vertical effective terms	-
R <sub>max</sub>	Maximum previous overconsolidation ratio (R)	-
S <sub>u</sub>	Undrained shear strength	kN/m <sup>2</sup>
S <sub>ub</sub>	Undrained shear strength at pile base	kN/m <sup>2</sup>
$\alpha$	Undrained pile shaft adhesion factor	-
$\beta$	Drained pile shaft friction factor	-
$\Gamma$	Intercept of Critical State Line with $p' = 1 \text{ kN/m}^2$ in $v - \ln p'$ space	-
$\gamma$	Unit weight	kN/m <sup>3</sup>
$\delta$	Pile shaft-soil interface friction angle	deg
$\epsilon$	Strain	-
$\eta$	Stress ratio ( $q/p'$ )	-
$\kappa$	Slope of swelling line in $v - \ln p'$ space	-
$\kappa^*$	Slope of swelling line in $\ln v - \ln p'$ space	-

$\lambda^*$	Slope of CSL in $L_{nv} - L_{np}'$ space	-
$\nu$	Poisson's ratio	-
$\rho$	Settlement	mm
$\tau_s$	Shear stress at pile shaft	kN/m <sup>2</sup>
$\phi$	Friction angle	deg
$\phi'_r$	Residual friction angle	deg
$\sigma$	Stress	kN/m <sup>2</sup>
$\sigma_{vt}$	Vertical total stress at reference level	kN/m <sup>2</sup>
$\omega$	Angular velocity of centrifuge	radians/s

#### SUPERSCRIPTS

p	Plastic
'	Effective

#### SUBSCRIPTS

ave	Average
b	Pile base
cv	Critical state or Constant volume
h	Horizontal
m	Model
o	Background reading
p	Prototype
v	Volumetric
v	Vertical
r	Radial
s	Pile shaft
t	Total
ult	Ultimate
$\theta$	Hoop

## CHAPTER 1 INTRODUCTION

### 1.1 Background

During the past two centuries man's impact on the environment has been enormous. Industrialisation has led to ever increasing requirements of raw materials for both public and private needs. Materials such as fossil fuels, ores and water are recovered directly from the Earth. In this project the effects of water extraction are of major interest.

During, and following the period of the industrial revolution in the United Kingdom, man's requirement for water has increased due to increasing population (almost double in the past one hundred years) and due to the increased amount of water used per capita (Shaw, 1983). In the London area the requirements for water have contributed to a major reduction in the deep groundwater level through pumping from wells in the basal aquifer approximately 30m below ground level. In recent years the altered local extraction rates have led to a rise in water level back towards the pre 1800's level. The effect that this type of rising groundwater event has on foundation behaviour is being examined in this project.

The main motivation for carrying out the research project clearly lies in the current situation in London. However, the findings are appropriate to other industrial cities and to the general problems of foundation behaviour with changing water pressures.

#### 1.1.1 Historical background in London

In London, a significant contribution to the water supply has been through extraction of groundwater from the deep aquifers beneath the city during the past two hundred years. Water was obtained by sinking wells through the impermeable London Clay and Woolwich and Reading Clay layers into the underlying Basal Sands and Chalk layers. The first record of wells tapping the groundwater from the deep aquifer is in the late eighteenth century (Simpson et al., 1989). Initially the wells in central London close to the River Thames were artesian. During the

following 140 years, until about the time of the Second World War, water extraction from the deep aquifer increased causing a considerable lowering of the piezometric level of the groundwater. In the area around Trafalgar Square the piezometric level was reduced by over 95m from its pre 1800's level. A schematic of the groundwater levels is shown in Figure 1.1.

From the 1940's onwards the multiple effects of well damage due to bombing in the war, improved road and electronic communications removing the need for industry to be located in cities (Martin and Rowthorn, 1986) and licensing controls introduced with the 1945 Water Act (Simpson et al., 1989) have resulted in a reduction of water extraction from the deep aquifer beneath London. This has led to a gradual increase in the piezometric level in the aquifer from its low level of the 1950's. The piezometric level beneath central London (Trafalgar Square) was at -61mOD in 1987 and rising at a rate of approximately 0.8m/year; near Liverpool Street the level was rising at 1.5m/year. More recent results (Nuttall, 1994) show that, in certain areas, the rate of water level recovery is 2.0m/year. Though a political decision has not yet been made, there is a likelihood that lost or unused wells will be re-opened to halt the rise in water table level beneath London (Nuttall, 1994)

#### 1.1.2 Ground conditions and foundations

The area occupied by London is located in a synclinal fold running in an almost east-west direction, with the River Thames in a central position. In the central London area the geological succession shows a Tertiary clay cap (London Clay and Woolwich and Reading Clay) overlying sand layers (Woolwich and Reading sand and Thanet sand) which in turn overlie a great depth of Chalk as shown in Figure 1.2. To the north and south the chalk layer rises upwards and outcrops some distance from central London.

The reduction in groundwater level in the Basal sands and Chalk aquifer mentioned in section 1.1.1 above, between approximately 1800 and 1950 (Simpson et al., 1989), has led to under drainage of the overlying clay layers causing a significant drop in pore water pressure in these

deposits with a corresponding increase in effective stress. The perched water table in made ground and terrace gravel layers at the top of the London Clay is supplied by surface recharge (precipitation and leaking water mains and sewers etc) and has maintained a continual downward seepage creating a non hydrostatic pore pressure distribution between the upper and lower aquifer as shown in Figure 1.3.

More recently the groundwater level in the deep aquifer has begun to recover to pre 1800 levels. A continued increase in groundwater level, first noted in around 1970 will lead to a significant reduction in effective stress resulting in swelling and a loss in strength in the clay and underlying layers. If the groundwater level in the deep aquifer reaches the pre 1800 level where it intersected the ground surface there may also be flooding of fill and shallow quaternary deposits. The potential reductions in effective stress were not considered for foundations designed prior to the early 1980's. It is believed that the effect of the increase in pore water pressure on foundations will depend on the type and depth of the foundation.

In very simple terms foundations can be classified by their depth of penetration into the ground and by their method of load transfer from foundation to soil. In London, shallow foundations may be located in deposits above the London Clay where the water level is dominated by the surface water table. In such circumstances, the foundations are unlikely to experience distress due to the increase in pore water pressure in the underlying clay layers. There may be some problems if the deep water table becomes artesian as was the case in some areas two centuries ago. In contrast deep foundations, which extend to near the base of the London Clay or the Woolwich and Reading Clay, may experience the detrimental effects due to a rising pore water pressure of settlement relative to the ground surface and loss of load bearing capacity in the next 25 to 35 years as water levels return almost to their original levels (Simpson et al. 1989). The mix of foundations (eg. combining deep under-reamed piles with shallow surface pads) used for a structure will dictate the overall behaviour of the building (Simpson et al. 1989).

## 1.2 Modelling of foundation behaviour in soil with rising pore pressures

### 1.2.1 Physical modelling

Modelling of foundations at realistic stress levels has been widely carried out using downward hydraulic gradient techniques (Zelikson, 1969), miniature element studies in pressurised cells (Chandler and Martins, 1982; Anderson et al., 1985) and on geotechnical centrifuges (Craig, 1985). The uses of downward hydraulic gradient and centrifuge techniques allow variation of effective stress with depth in the model ground thus allowing scaled model tests of the whole foundation to be performed. Use of pressurised cells at constant stress with depth allows investigation of specific aspects of a soil-interaction problem. In this project the behaviour of both shallow and deep bored (replacement) foundations has been modelled using centrifuge testing techniques. The behaviour of soil with changing pore pressures has been investigated using single element testing in a triaxial stress path cell.

#### Centrifuge modelling:

A series of centrifuge tests has been undertaken to examine bored foundation behaviour in stiff clay with increasing pore pressures. During a test the model is allowed to come into pore water pressure equilibrium after spin-up of the centrifuge to the required test speed. Foundations are then loaded, this may or may not include loading to failure followed by unloading to working loads, prior to the increase of groundwater level at the base of the model. When swelling has finished further foundation load tests are carried out. The tests have used a variety of foundation geometries modelling shallow foundations, under-reamed piles and straight shafted piles with two different diameters to assess the behaviour of different foundation types. Factors of safety on load have been also been varied to assess the effect that this has on foundation settlement. Finally two different initial pore pressure distributions were used prior to groundwater level rise; one where there was negative pore pressure at the clay surface in hydrostatic equilibrium with the deep water table; the other had a surface perched water table

with downward seepage through the clay to the deep water table. During the tests preconsolidation pressure, model soil type, clay depth and pile depth have been kept constant during most of the model tests. The tests are a continuation and elaboration of those carried out by Andersen (1990).

#### **Triaxial testing:**

A limited number of triaxial tests were carried out in a Bishop and Wesley cell to obtain soil parameters and to assess soil behaviour during one dimensional consolidation, swelling and pore pressure change. The data demonstrate far field stress changes that occur during a rising groundwater event and have provided parameters for use in numerical modelling.

#### **1.2.2 Numerical modelling**

Finite element modelling and more simple hand analyses have been carried out to assess the centrifuge test results and to investigate other factors that have not been examined in the centrifuge tests.

#### **Finite element method analyses:**

Initial finite element calculations were carried out to compare the model pile installation process with that of a prototype pile to assess differences in behaviour that might occur during a rising groundwater event. After pile installation a rising groundwater level event was initiated. A second set of analyses was carried out which isolated the behaviour of a pile shaft after pile installation during a rising groundwater event. Finally a series of analyses was carried out of a wished-in-place pile behaviour during a rising groundwater event.

#### **Hand calculations:**

A set of calculations using existing soil and soil-foundation interaction models has been carried out and compared with the centrifuge test

results. The model that was used provided a relatively easy method to assess foundation behaviour during rising groundwater events.

### 1.3 Objectives of the research

From the previous sections in this chapter it is clear that qualitatively the effects of a rising groundwater level on foundations are understood:

- o Foundations will settle relative to the ground surface as the effective stresses reduce;
- o Foundations will suffer a loss in load carrying capacity as the effective stresses reduce.

However, quantitatively the effects are not fully known and it is this aspect that has been examined in this project. Consequently, the research objectives were identified as:

- o Develop centrifuge testing procedures and models to provide data on the effects of a rising groundwater level on foundations;
- o Assess the effects of geometry and factor of safety on foundation settlement and the loss of load carrying capacity during a rising groundwater event;
- o Carry out numerical analyses of the tests to assess the suitability of numerical procedures for analysis of this problem;

### 1.4 Outline of the thesis

The thesis has a further six chapters as follows:

#### Chapter 2:

Chapter 2 has three main sections covering a literature review of: foundation design and behaviour; in-situ soil stresses; and the effect of pore water pressures on foundation behaviour. In each section the current theories and empirical relationships, relevant to this project, are evaluated. Attention is given to the topics which have proved most problematic in the analyses presented in the subsequent chapters. The chapter finishes with a proposed method for assessment of foundation

settlement during a rising groundwater event using the topics reviewed in the previous three sections.

#### **Chapter 3:**

Chapter 3 has two main parts. Firstly the soil models used in the finite element modelling of the foundations in a rising groundwater environment are presented. Secondly results from the triaxial tests on Speswhite Kaolin under one dimensional conditions are presented. The results from the tests have also provided parameters for use in the numerical modelling presented in Chapter 6.

#### **Chapter 4:**

In Chapter 4 the geotechnical centrifuge testing technique and its relevance to modelling foundations in a rising groundwater environment are summarised. The equipment used in the tests is described and any shortcomings in the testing procedure are discussed.

#### **Chapter 5:**

The centrifuge test results are presented in Chapter 5. Firstly, typical model behaviour is presented from starting to stopping the centrifuge so that the general behaviour of the model foundations can be understood. A centrifuge test using in-flight site investigation techniques is then presented. Foundation load behaviour is reviewed prior to presenting typical foundation behaviour during a rising groundwater event. The chapter finishes with an assessment of loss of foundation load capacity due to a rising groundwater event and a summary of the main findings.

#### **Chapter 6:**

Comparisons were made between prototype and centrifuge model situations during pile installation. The behaviour of the installed piles was then investigated during simulated rising groundwater events. The finite element section of the chapter concludes with an assessment of wished-in-place pile behaviour during a rising groundwater event. The chapter finishes with an assessment of pile behaviour during a rising groundwater event using a non-computer based method.

## **Chapter 7:**

Chapter 7 summarises the main findings of this research project and proposes additional areas where further research could be carried out.

## **Appendix A:**

A brief description of each centrifuge model test undertaken including the main test results during the rising groundwater event is given in Appendix A.

## **Appendix B:**

A sample "by hand" calculation of centrifuge model settlement during a rising groundwater event is included in Appendix B. The method adopted allowed a relative simple procedure to be used for prediction of pile settlement.

## **1.5 Summary**

In this introductory chapter the events leading up to the reduction in groundwater level in the deep aquifer and the underdrainage of the overlying clay layers resulting in depressed pore water pressures have been described. A brief description of the qualitative effects of loss in load bearing capacity, settlement relative to the ground level and differential settlement between varying types of foundation resulting from an increase in groundwater level in the deep aquifer was presented. The investigative methods of centrifuge testing, triaxial testing and numerical analysis, used in the project were discussed. An outline of the thesis with brief comments on the following six chapters and two appendices was given.

The main phenomena which govern the behaviour of non-displacement foundations situated in clay when subjected to rising pore water pressures are considered. To understand the problem the behaviour of the soil and its interaction with foundations must be examined. Thus the following topics are reviewed in this chapter:

In section 2.1 the behaviour of deep (and shallow) foundations are reviewed in terms of load carrying capacity and load displacement response.

In section 2.2 the changes in stress that occur in a soil body, free from foundation loads, during deposition, erosion of overlying layers and variations in ground water level have been reviewed. Reductions in vertical effective stress and the consequential lowering of horizontal effective stress have a direct influence on both foundation load capacity and subsequent foundation settlement during a rising groundwater event.

In section 2.3 case histories involving foundation behaviour in a soil with changing pore water pressures are reviewed.

Section 2.4 uses the information presented in the previous sections and suggests how foundation settlement during a rising groundwater event might be calculated using existing inexpensive techniques.

### 2.1 Deep and shallow foundation design and behaviour

In this project foundations are differentiated by their formation depth below ground level and their method of load transfer to the soil. Shallow foundations are assumed to mobilise no side resistance to vertical loading. Piles are subdivided into predominantly friction piles and those mobilising significant end bearing as well as full shaft friction at working load.

The manner in which the shaft and the base of a pile transfer load to the soil is very different and will be considered independently for

calculation of ultimate load carrying capacity but will, by necessity, be drawn together when considering the overall load-displacement response of a pile.

The notation adopted for pile shaft - soil interface and base stresses and loads (with subscripts 's' for shaft and 'b' for base) is:

q	-	Mobilised stress (kN/m <sup>2</sup> )
Q	-	Ultimate stress (kN/m <sup>2</sup> )
p	-	Mobilised load (N)
P	-	Ultimate load (N)

### 2.1.1 Ultimate load capacity of piles

The ultimate load of a pile can be defined as either the load at which settlement continues to increase without further additional loading or the load which causes a settlement of 10% of the foundation base diameter (Fleming et al., 1992). Burland et al. (1966) point out that the latter category is likely to be the controlling factor for end bearing resistance (not for pile shaft resistance) for most soil conditions. The definition is likely to give a lower limit to ultimate load capacity as it is likely that only localised yielding will have occurred. In this project the failure load has been deemed to be the load, during a constant rate of loading (CRL) test, which gives a settlement of 10% pile base diameter. The rate of loading used in the centrifuge tests, while not slow enough to provide fully drained conditions, was sufficiently slow to create largely drained loading conditions.

#### 2.1.1.1 Pile shaft capacity

Until recently the shaft capacity of piles in clay was calculated in terms of undrained strength ( $S_u$ ) measured from quick undrained triaxial tests on undisturbed samples and an empirical adhesion factor ( $\alpha$ ) back calculated from pile tests:

$$Q_s = \alpha S_u \quad (2.1)$$

The value of empirical adhesion factor ' $\alpha$ ' depends on the strength, stiffness and plasticity of the clay. For a normally consolidated

deposit a value of  $\alpha = 1$  is typical but for overconsolidated or stiff clay a value of  $\alpha < 0.5$  would be common.

More recently researchers have shown that shaft friction can be calculated using effective stress terms Burland (1973). The shaft capacity is related to a parameter ' $\beta$ ' and the vertical effective stress ( $\sigma_v'$ ). The parameter ' $\beta$ ' is a function of the horizontal to vertical effective stress ratio at the pile shaft ( $K_s$ ) and the angle of friction between the shaft and the clay ( $\delta$ ). Any true cohesion ( $c'$ ) within the soil is assumed to have been reduced to zero along the shaft due to remoulding of the shaft surface during bore excavation. The shaft capacity at any point can be calculated using:

$$Q_s = K_s \cdot \sigma_v' \cdot \tan \delta - \beta \cdot \sigma_v' \quad (2.2)$$

or

$$Q_s = \sigma_{h \text{ at pile}}' \cdot \tan \delta \quad (2.3)$$

The choice of values of  $K_s$  ( $=\sigma_h'/\sigma_v'$ ) and  $\delta$  has been well documented, for example Chandler and Martins (1982), Anderson et al. (1985), Burland and Twine (1988) and Poulos (1989) and using numerical analyses by Potts and Martins (1982).

For bored piles  $K_s$  is assumed to have a maximum value equal to the coefficient of earth pressure at rest in the ground before the pile was installed. However, due to stress relief during pile construction and possible concrete shrinkage it is unlikely that the initial  $K_0$  will apply at the pile shaft. Lopes (1979) showed schematically the change in horizontal (radial) stress and pore water pressure around a bored pile prior to loading. Figure 2.1 shows a reduction in pore water pressure and total horizontal stress during shaft excavation (lines 2). During concrete placement and setting and subsequent consolidation the pore water pressure gradually returns to previous equilibrium values, while the total horizontal stress at the pile shaft does not similarly recover back to previous levels (lines 3 and 4). Chandler and Martins (1982) proposed that for piles in highly overconsolidated clay (which dilates during shearing) the loss in radial stress during pile installation is somewhat compensated for by the increase in radial stress during loading,

resulting in reestablishment of initial, pre-installation, horizontal effective stresses along the pile shaft.

Possible values of  $K_s$  for bored piles in stiff clay have been summarised by Poulos (1989) as being the lower of  $K_0$  or  $0.5(1 + K_0)$  or in the range of  $2/3K_0$  to  $K_0$  showing a large degree of uncertainty for design purposes.

The value of  $\delta$  is not known and will depend on the clay and on the condition on the soil-foundation interface. The value of  $\delta$  is likely to lie between the angle of friction of the remoulded soil ( $\phi'_{cv}$ ) and the residual angle of friction ( $\phi'_r$ ). If there is continuous smearing of the pile shaft during excavation or large displacements between the pile shaft and soil the value of  $\delta$  will tend towards  $\phi'_r$ .

Anderson et al. (1985) demonstrated, using a single element model of a bored pile shaft in overconsolidated clay, that the reduction in  $K_s$  resulting from shaft excavation and pile placement is largely recovered over a period of time. Tests in a carefully controlled environment demonstrated that  $K_s$  recovered to about 90% of  $K_0$  over a period of seven days (model scale, no scale factors were given) for soils with an overconsolidation ratio of five or higher. The final measured value of  $K_s$  did not appear to be affected by a delay between shaft excavation and concrete placement although such delays could result in  $K_s$  recovering more slowly. The friction angle at the shaft interface measured in model pile load tests was close to the residual angle of friction as measured in a ring shear apparatus (For Speswhite Kaolin in an overconsolidated state  $\phi'_r$  was measured as  $11^\circ$ ).  $K_0$  values measured in the clay body were close to those predicted by Wroth (1975). The model piles incorporated a total radial pressure transducer and a pore pressure transducer on the pile shaft from which the horizontal effective stress acting on the shaft was deduced. The clay body was instrumented with total earth pressure and pore water pressure transducers.

Twine (1987) and Burland and Twine (1988) used back analyses of prototype scale bored pile tests in stiff clays to demonstrate that a lower bound value of shaft capacity, measured in maintained load tests, can be calculated using the residual angle of friction ( $\phi'_r$ ) and the coefficient

of earth pressure at rest ( $K_0$ ). A literature review carried out by Patel (1991) confirmed these findings concluding that a pile shaft to soil interface angle of friction of  $\phi'_r$  or slightly higher linked with the initial  $K_0$  gives a realistic lower limit to bored pile shaft capacity.

$$Q_{s \text{ conservative}} = K_0 \cdot \sigma'_v \cdot \tan \phi'_r \quad (2.4)$$

#### 2.1.1.2 Pile base capacity

In contrast to shaft capacity, the base capacity for non displacement foundations in stiff clay is often calculated in terms of undrained shear strength.

For circular footings the bearing capacity is:

$$Q_b = s_c \cdot d_c \cdot N_c \cdot S_{ub} + \gamma \cdot H \quad (2.5)$$

Where

$N_c$	-	bearing capacity for surface strip foundation applied to $S_{ub}$
$s_c$	-	shape factor applied to $N_c$
$d_c$	-	depth factor applied to $N_c$
$S_{ub}$	-	undrained strength at the foundation base
$\gamma \cdot H$	-	is often compensated for by the pile self weight and therefore ignored.

The product of  $s_c \cdot d_c \cdot N_c$  is approximately 9.0 for circular footings where the depth exceeds four base diameters (Skempton, 1959). In principle the reduction in pile base bearing capacity during a rising groundwater event could be assessed by calculating the reduction in available  $S_{ub}$  at any particular stage.

In general, base capacity for piles has not been considered in terms of effective stress because (Fleming et al., 1992):

- o deformation required to mobilize full drained capacity would, in most circumstances, exceed allowable structural movements;
- o there must be sufficient short and intermediate term pile base capacity to prevent early failure.

However, during a rising groundwater event pile base behaviour should be considered in effective stress terms. It is therefore necessary to calculate ultimate end bearing capacity using drained bearing capacity parameters. If, as recommended by Poulos and Davis (1980), the soil is assumed to have zero true cohesion ( $c' = 0$ ) and the influence of the weight of the soil beneath the pile base is ignored then:

$$Q_b = N_q \cdot \sigma'_{vb} \quad (2.6)$$

where  $\sigma'_{vb}$  - vertical effective stress at pile base level  
(see comments in section 2.3.2)  
 $N_q$  - bearing capacity factor on vertical effective stress.

More recent research by Troughton and Platis (1989) suggested that, for piles in sand, drained bearing capacity should be related to the mean normal effective stress ( $p'$ ) and not  $\sigma'_v$ . A full review of the work by Troughton and Platis is included in section 2.3.3.

There is a degree of uncertainty for the value of  $N_q$  for soils with low friction angles. However, for comparison of the percentage change in drained pile base capacity before and after a rising groundwater event the actual value is not essential.

## 2.1.2 File settlements

Skempton (1959) drew the following conclusions concerning settlement from a series of pile load tests in London Clay:

- o settlement at ultimate load is approximately 8.5% (1 inch in a foot) of pile base diameter;
- o the shaft adhesion is fully mobilised at smaller settlements than the base resistance.

### 2.1.2.1 Shaft load displacement response

Analysis of pile tests carried out by Whitaker and Cooke (1966) show that pile shaft frictional resistance develops rapidly with settlement and is

generally fully mobilised when settlement has reached 0.5% of the pile shaft diameter (Burland and Cooke, 1974).

The shaft transfers load to the surrounding soil by means of shear stresses, which decrease in magnitude inversely with distance from the pile (Fleming et al., 1992). Changes in mean stress even close to the pile are relatively small resulting in small deflections (Poulos, 1989).

Fleming et al. (1992) presented an expression for pile shaft settlement due to shaft friction assuming the soil to be linearly elastic. All settlement was assumed to be as a direct result of shear strains:

$$\rho_s = \frac{p_s \cdot \ln \left( \frac{r_m}{r_o} \right)}{2 \pi l G_{ave}} \quad (2.7)$$

where

$\rho_s$	-	Shaft settlement
$p_s$	-	Load carried by pile shaft -soil interface
$l$	-	Shaft length
$G_{ave}$	-	Mean shear modulus of soil along pile shaft
$r_m$	-	Radius from pile at which strains become negligible $\approx 2.5l(1-\nu)$ (Randolph and Wroth, 1978).
$r_o$	-	Pile radius.

#### 2.1.2.2 Base load displacement response

In contrast to the shaft load displacement response the base load displacement response requires relatively large displacements (10% of pile base diameter or larger) to mobilise ultimate capacity fully. The base load-displacement response was non-linear especially when loads exceeded 1/3 ultimate base capacity (Burland and Cooke, 1974).

The calculation of settlement approaching ultimate capacity has not received much attention. For most structures these movements would be unacceptable.

Some work has been carried out in calculating pile base settlements under

typical working stresses. Many of the published formulae (Burland et al., 1966; Burland and Cooke, 1974; Fleming, 1992) although presented in differing formats are traceable to the Boussinesq solution for stresses, strains and displacements within an isotropic elastic half-space resulting from a point vertical surface load;

$$\rho_b = \frac{q_b \cdot d_b (1-\nu^2)}{E_b} \cdot I_p \quad (2.8)$$

where

$\rho_b$	-	Pile base settlement;
$d_b$	-	Pile base diameter;
$q_b$	-	Pile base stress;
$E_b$	-	Young's modulus of soil at pile base;
$I_p$	-	Influence factor = 0.5 for a uniform circular load at great depth.

In the method presented by Burland et al. (1966) the results from pile tests were back analyzed to allow pile settlements to be calculated on a site specific basis. The analysis is valid for base loads less than 30 percent of the ultimate base load where the load displacement response could be assumed linear:

$$\frac{\rho_b}{d_b} = K \cdot \frac{q_b}{Q_b} \quad (2.9)$$

K is a factor related to plate settlement on an elastic material back-calculated from plate load tests (a conservative value for London Clay is  $K = 0.02$ ). Thus to mobilise 30 percent of the ultimate base resistance a settlement of approximately 0.6% base diameter would be required, at which point it is likely that full shaft capacity will have been mobilised (especially for end bearing piles in clay where the pile base diameter is often enlarged).

### 2.1.2.3 Composite pile settlement

Fleming (1992) derived a pile settlement analysis using a composite approach incorporating both pile shaft and base components with elastic soil parameters and ultimate loads to describe the total pile response to maintained loading. The method uses a hyperbolic function as described by Chin (1972) to assess the ultimate pile shaft or base

capacity from the pile response to loading as defined in Figure 2.2; the offset K was used by Chin in defining the ultimate pile load from a hyperbolic load-displacement curve. The hyperbolic function is compared to an elastic solution for shaft or base settlement (similar to Eqns. 2.7 and 2.8 respectively) resulting in an expression for pile behaviour from negligible load to near failure. Eqns. 2.10 and 2.11 are typical expressions for base and shaft settlement calculations.

File base response:

$$\rho_b = \left( \frac{0.6 P_b P_b}{E_{25} d_b \cdot (P_b - P_b)} \right) \quad (2.10)$$

where

$\rho_b$	-	File base settlement
$P_b$	-	Ultimate pile base load as defined by Chin (1972) at which load displacement is infinite
$P_b$	-	Pile base load
$E_{25}$	-	Young's modulus at 25% of base failure stress
$d_b$	-	Pile base diameter.

File shaft response:

$$\rho_s = \frac{M_s d_s p_s}{P_s - p_s} \quad (2.11)$$

where

$\rho_s$	-	File shaft settlement.
$p_s$	-	File shaft load
$d_s$	-	File shaft diameter
$P_s$	-	Ultimate pile shaft load as in by Chin (1972)
$M_s$	-	Flexibility factor representing pile settlement caused by shaft friction

$$M_s = \zeta \cdot \frac{r_s}{2 G_{ave}}$$

$\zeta$	-	$\ln(r_m/r_o)$ (see Eqn. 2.7)
$G_{ave}$	-	Average soil shear modulus over length of pile
$r_s$	-	Average shear stress at shaft to soil interface.

This approach, whilst using only one elastic parameter to describe either the base ( $E_{25}$ ) or the shaft ( $G_{ave}$ ) settlement response to loading gives a

non-linear response representative of prototype pile behaviour. As either  $(P_b - p_b)$  or  $(P_s - p_s)$  become smaller so displacements become larger in a hyperbolic manner. By assuming that  $\rho_b = \rho_s$ , an expression for settlement of the whole pile can be derived. The pile settlement response to loading can be expanded to incorporate elastic pile shortening.

### 2.1.3 Shallow footing load capacity

The calculation of shallow footing load capacity in stiff clay, as with pile base capacity, is usually carried using the undrained strength. The product of the bearing capacity factor  $N_c$  and the shape and depth factors  $s_c$  and  $d_c$  in Eqn. 2.5 is 6.2 for a shallow circular footing and 5.1 for a strip footing at the ground surface (Skempton, 1951) and as shown in Figure 2.3.

### 2.1.4 Shallow footing settlement

The settlement of shallow footings follows closely that of base settlement of a pile described in section 2.1.2.2. The only difference that occurs between the settlement of the pile base and a shallow footing is due to the influence of the formation level.

The recent advent of cheap computing facilities has allowed more complex soil models to be used in settlement calculations (Padfield and Sharrock, 1983). The more accurate models include anisotropic elastic solutions and constitutive soil models. Examples of the latter are described in Chapter 3 and used in finite element analyses in Chapter 6 for analysis of pile behaviour during a rising groundwater event.

## 2.2 In-situ soil stresses

In section 2.1.1 it was shown that pile shaft load capacity is directly related to the horizontal effective stress magnitude, whilst in section 2.1.2 a settlement calculation using a failure load was presented. It is therefore necessary to understand the stress changes that occur within the soil body during a rising groundwater event to allow predictions of

foundation behaviour (load-displacement response) to be made.

The formation of an over-consolidated clay deposit commences with the deposition of a normally consolidated clay layer. This is followed by the removal of overlying deposits. All changes in vertical overburden stress are assumed to occur with zero horizontal strain.

During the processes of overburden increase and decrease the vertical and horizontal stresses ( $\sigma'_v, \sigma'_h$ ) are continuously changing. The horizontal effective stress is stress history dependant and is calculated from the coefficient of earth pressure at rest ( $K_0$ ) and the vertical effective stress:

$$\sigma'_h = K_0 \cdot \sigma'_v \quad (2.12)$$

### 2.2.1 Initial one dimensional loading

On initial one dimensional loading the horizontal effective stress increases linearly with the vertical effective stress. Jaky derived an equation for  $K_{onc}$  (the coefficient of earth pressure at rest for a normally consolidated deposit) which is commonly used in approximate form as (See Mayne and Kulhawy, 1982):

$$K_{onc} = 1 - \sin\phi' \quad (2.13)$$

### 2.2.2 One dimensional unloading

Brooker and Ireland (1965) found that when a normally consolidated deposit is unloaded the ratio of  $\sigma'_h/\sigma'_v$  changes. They also found that  $K_{ou}$  (coefficient of earth pressure during unloading from a normally consolidated state) was dependent on stress history as well as  $\phi'$ .

Mayne and Kulhawy (1982), who compiled data from over 170 different soils suggested that:

$$K_{ou} = (1 - \sin\phi') \cdot R^{\sin\phi'} \quad (2.14)$$

where  $R$  = overconsolidation ratio in terms of vertical effective stress

$K_{ou}$  is often assumed to have an upper limit equal to the coefficient of passive earth pressure ( $K_p$ ). When passive failure is reached the coefficient of passive earth pressure is often limited to:

$$K_p = \frac{(1 + \sin \phi'_{cv})}{(1 - \sin \phi'_{cv})} \quad (2.15)$$

where  $\phi'_{cv}$  = effective angle of friction at constant volume shearing.

However due to dilatant effects values of  $K_o$  in excess of  $K_p$  as defined in Eqn. 2.14 may be encountered at high overconsolidation ratios.

Al-Tabbaa (1987) investigated the behaviour of Speswhite Kaolin using a instrumented oedometer and found that:

$$K_o = 0.69R^{0.46} \quad (2.16)$$

Wroth (1975) recognised that the initial slope of the unloading curve in stress space was approximately constant. Using Poisson's ratio ( $\nu'$ ) and Hooke's Law the following equation was derived for lightly overconsolidated soil:

$$K_{ou} = K_{onc} \cdot R - \frac{\nu'}{1-\nu'} \cdot (R-1) \quad (2.17)$$

Al-Tabbaa (1987) measured Poisson's ratio ( $\nu'$ ) for Speswhite Kaolin to be  $0.3 \pm 0.05$ .

### 2.2.3 One dimensional reloading

On reloading Mayne and Kulhawy (1982) noticed that the change in  $\sigma_h'$  was less than  $\sigma_v'$ . With the limited data they had available the following empirical relationship between  $\sigma_h'$  and  $\sigma_v'$  on reloading was found (assuming that the passive failure line had not been reached at any time in the soil's stress history):

$$K_{or} = (1 - \sin \phi') \cdot \left[ \frac{R}{R_{max}^{(1 - \sin \phi')}} + 0.75 \left( \frac{R}{R_{max}} - 1 \right) \right] \quad (2.18)$$

where  $R_{max}$  = the maximum overconsolidation ratio the soil has been submitted to i.e.

$$R_{max} = \frac{\sigma'_{v \max}}{\sigma'_{v \min}} \quad (2.19)$$

Eqn. 2.17 simplifies to Eqn. 2.13 for initial unloading and Eqn. 2.12 for a normally consolidated deposit.

Burland and Hancock (1977) assumed that on loading the soil is initially behaving in an elastic manner. Wroth (1975) suggested that on reloading the slope of change in horizontal effective stress to the change in vertical effective stress is similar to that of the initial unloading slope where the soil is behaving elastically. The elastic relationship between change in horizontal stress with change in vertical stress is given by:

$$\Delta \sigma'_h = \Delta \sigma'_v \cdot \frac{\nu'}{1 - \nu'} \quad (2.20)$$

#### 2.2.4 Earth pressure and changing pore water pressure

The effect of reducing pore pressures in a deposit is similar, in effective stress path terms, to reloading the deposit. A rise in pore water pressure is analogous to unloading the deposit. Initial estimates of the loss in horizontal effective stress as a result of a rising groundwater table by Simpson et al. (1989) and Troughton and Platis (1989) assume that Eqn. 2.20 is valid where the soil stress ratio had not reached passive failure. For this assumption to be approximately correct the increase in pore pressures must have been preceded by a similar loading stage (usually a fall in pore pressure). For calculation of actual stress levels in the ground rather than changes of stress the initial value of  $K_0$  must be known using either on-site measurements or, in the case of centrifuge testing where the previous stress history is known, by use of the equations presented above.

## **2.3 Case histories of foundation behaviour with changing pore water pressure**

Possible loss of foundation bearing capacity and movements due to a rising groundwater event have been forecast by Wilkinson (1984), Simpson et al. (1987) and (1989) and Kulhawy and Beech (1987). Foundation behaviour in soil with a moving groundwater table has been studied by means of full scale tests (Armishaw and Cox, 1979; Troughton and Platis, 1989) and model scale tests (Andersen, 1990; Challa and Poulos, 1992). A numerical investigation of piled raft behaviour was carried out by Poulos (1993).

### **2.3.1 Wilkinson (1984): An introduction to the problem**

Wilkinson (1984), whilst introducing a discussion on the geotechnical consequences of rising groundwater levels, pointed out that in the London basin the rise in pore pressures could result in a loss of up to 50% of pile capacity due to the reduction in effective stresses. He suggested that this loss could be allowed for in design by increased area of pile bases to account for subsequent reductions in bearing capacity.

### **2.3.2 Armishaw and Cox (1979): Rising groundwater levels and driven piles in granular soils**

Armishaw and Cox (1979) carried out a series of driven piled tests in a sand and gravel stratum overlain by a peat and clay layer. Groundwater levels were controlled by wells which provided up to a 5m increase in groundwater level in the sand and gravel layer. Shaft capacity was measured by pull out tests at different groundwater levels. Overall pile capacity was measured by static load tests.

They found that the percentage loss in base capacity for a rise in pore pressure was less than the loss in vertical effective stress as shown in Figure 2.5. If the data from the individual pile tests are extrapolated to  $\sigma'_v = 0$ , the results suggest that the bearing capacity would not reduce to zero. This was explained by incorporating a term for effective pressure caused by driving ( $q_7$ ) in the following equation:

$$\frac{\Delta Q_b}{Q_b} = \frac{-\Delta u \cdot N_q}{q_\gamma + \sigma'_v \cdot N_q} \quad (2.21)$$

where  $q_\gamma$  = base resistance when  $\sigma'_v$  is extrapolated to zero.

The resulting loss in base capacity was 1/3 to 1/2 of that predicted when the apparent locked in stress caused by driving effects was ignored. This locked in stress suggests that the horizontal effective stress plays a part in end bearing capacity.

### 2.3.3 Troughton and Platis (1989): A large scale pile test with modelling of changing effective stresses in sand

Troughton and Platis (1989) reported on a large scale instrumented pile test carried out during the redevelopment of the London Docklands. The test was carried out on a base grouted bored pile with its tip embedded in the Thanet Sand stratum beneath the Woolwich and Reading Beds (see Figures 1.2 and 1.3). The test was carried out to assess the effect that the excavation of a basement above the pile and the effect that a change in groundwater level would have on the ultimate end resistance of the pile. The pile was surrounded by injection wells capable of reducing the vertical effective stress to levels representing the situation when the basement had been excavated and the long term case when the groundwater level had increased back to equilibrium levels as indicated by the pore pressure profiles from the Isle of Dogs in Figure 1.3. The pile was sheathed above the level where the pore water pressure was not influenced by the injection wells.

While the pile test was not carried out in a clay stratum it does demonstrate some of the potential detrimental effects that rising groundwater has on foundations. The results showed that:

- o when the pore pressure was increased (effective stress reduced) there was a reduction in ultimate pile base load;
- o when the pile base load was kept constant and the pore pressure increased there was a small pile base settlement.

Analysis of the results showed that there was a linear relationship between ultimate pile base load ( $P_b$ ) and vertical effective stress. The relationship did not pass through the origin of the axes as would be predicted from the classical bearing capacity and as shown in Figure 2.6(a).  $P_b$  was also compared with the mean normal effective stress ( $p'$ ):

$$p' = \frac{1}{3}(\sigma'_v + 2.\sigma'_h) = \frac{\sigma'_v}{3}(1 + 2.K_o) \quad (2.22)$$

As can be seen from Figure 2.6 (b) there was a linear relationship between  $Q_b$  and  $p'$  which continued through the origin. The initial value of  $\sigma'_h$  was obtained from pressure-meter data. Changes in  $\sigma'_h$  were calculated using isotropic elastic theory discussed in section 2.2.3 and Eqn. 2.20. The ultimate pile base capacity was found to be:

$$P_b = A_b Q_b = A_b N_q^* p' \quad (2.23)$$

where  $A_b$  - Pile base area  
 $N_q^*$  - Bearing capacity factor on  $p'$

The results demonstrate that simplified elastic theory provided a good tool with which pile behaviour in dense sand can be predicted. There is, however, no reason as yet why foundation in clay should behave in such a linear fashion when subjected to large reductions of effective overburden pressure, especially if all time low vertical effective stresses are reached.

#### 2.3.4 Simpson et al. (1987 and 1989): CIRIA SP69

In 1989 the Construction Industry Research and Information Association published a specially commissioned report concerning the implications of a rising groundwater level beneath London (Simpson et al., 1989). The report gave an historical overview of the events leading up to the then present situation and indicated areas of London most at risk from the rising groundwater level. The potential effects on different types of foundations, tunnels and shafts caused by the groundwater level rise were considered.

Of particular relevance to the work being carried out are the conclusions concerning shallow and piled foundations:

**Shallow foundations:**

For shallow foundations located on the tertiary clays and surrounded by a perched water table the effects of a rising groundwater level in the deep aquifer will be nominal. This is due to a majority of the pore pressure change in the tertiary clays (London clay and Woolwich and Reading clay) occurring beneath the surface zone where pore water pressures are primarily controlled by the perched water table. For shallow foundations in fill or terrace sands and gravels which are in direct contact with the deep aquifer there will be some loss in bearing capacity and additional settlement as the groundwater level rises.

**Piled foundations:**

A distinction is made between straight shafted predominantly friction piles and under-reamed piles in which both shaft friction and end bearing contribute to the load carrying capacity. It is recognised that there will be some loss in load carrying capacity although this is not likely to lead to actual pile failure. Calculations relating shaft friction to horizontal effective stress (Burland, 1973, Burland and Twine, 1988) predict a loss of between 16% and 0% for an increase in pore pressure of 50% of hydrostatic at depth reducing to 0% pore water pressure change at the surface. Loss in design end bearing capacity is related to the loss in available undrained shear strength as a result of reducing effective stresses and soil swelling. The second, and possibly the more important, effect on piles is the settlement that will occur as a result of increasing base load, reducing soil stiffness and soil swelling passed the piled foundation. The anticipated modes of behaviour for deep and shallow foundations in clay are shown in Figure 2.7.

**2.3.5 Kulhawy and Beech (1987): The effect of recovering water levels on foundation side resistance**

Kulhawy and Beech (1987) demonstrated the effect of fluctuations in

groundwater level on foundation side resistance. While Kulhawy and Beech were principally dealing with a normally consolidated deposit they demonstrated indirectly that on recovery of groundwater level there is a reduction in foundation side resistance where stress change is calculated using an expression such as equation 2.17. In reviewing this paper Steenfelt (1987) warned that minor movements caused during foundation installation will result in stress relief and may cause a reduction in horizontal effective stress. The work of Burland and Twine (1988) and Anderson et al. (1985), while not contradicting Steenfelt's comment, does suggest that foundation side resistance may be calculated using an approach such as that described by Kulhawy and Beech.

### **2.3.6 Andersen (1990): An initial series of centrifuge tests modelling rising groundwater in clay**

As part of a pilot study for the present project three centrifuge tests were carried out by Andersen (1990). The project was carried out to assess the ease of centrifuge modelling for examining the effects of a rising groundwater table on foundations in clay.

The tests were carried out using dead weights to model the foundation loads. The model foundations correspond to a 1.3m pile 15m long and a 3.8m diameter pad at prototype scale. Figure 2.8 shows the model configuration.

In the three tests carried out the results showed that it was possible to measure soil and surface movements due to rising groundwater and that piles settled relative to the soil surface. The results were of a qualitative form and were useful in preparing the initial centrifuge tests reported herein.

### **2.3.7 Challa and Poulos (1992): Model tests of piles in swelling clay**

A series of model scale tests was carried out to investigate the behaviour of driven piles in clay subjected to increasing pore water pressure. The tests used a 25mm diameter pile 230mm long in a

pressurised test container some 380mm in diameter. The clay body was produced by compacting clay at the optimum moisture content into the test container. The clay surface was surcharged prior to driven pile installation. The sample was then inundated with water from the top and bottom. During the period of clay swelling measurements of pile stresses and soil and pile movements were recorded. No measurement of pore water pressure in the soil was made and hence it was not possible to correlate pile to soil surface relative displacement and pile load capacity loss with change in soil effective stress.

However, the tests showed that:

- o There was a significant loss in pile load capacity resulting from an increase in soil moisture content (equivalent to a reduction in effective stress level) as shown in Figure 2.9;
- o Soil swelling around a floating unloaded pile caused tensile stresses in the pile as shown in Figure 2.10;
- o Movement of a floating unloaded pile increased as the soil heave increases (tests T04 and T05). However, for a pile socketed in a stable sand layer pile movement would be controlled by the anchoring stress and would tend towards a limiting value (tests T06 and T07). Figure 2.11 shows the results of four piles, two floating and two with bases in sand.

#### 2.4 A simple "by hand" settlement calculation

The previous sections in this Chapter have summarised foundation behaviour in ground with a stable pore water pressure regime and outlined foundation behaviour in ground with a changing pore water pressure regime. Prediction of foundation settlement during a rising groundwater event requires knowledge of foundation load transfer to the ground and changes in soil strength and stiffness which result in reduced pile capacity, pile settlement and ground heave.

Calculation of foundation settlement due to rising groundwater must consider the dominant method of load transfer in friction and end bearing piles.

#### 2.4.1 Friction piles

Piles in which shaft friction dominates will ultimately be partially in tension as the soil swells around a rigid pile, as demonstrated by Challa and Poulos (1992) for driven piles. Pile settlement will result from soil swelling passed the pile shaft which experiences zero pile to soil relative movement at the neutral point as defined by Fleming and Powderham (1989) and O'Reilly and Al-Tabbaa (1990). Reduction of pile shaft friction, for bored piles, in which  $K_s$  is approximately equal to  $K_o$ , may be obtained approximately using formulae such as Eqns. 2.4 and 2.20 assuming that appreciable plastic deformation of the soil does not occur. Soil heave above the new pile neutral point may be assessed using suitable soil deformation moduli. In estimation of the neutral point a balance is made between pile head load, shaft friction carrying the load and shaft friction anchoring the pile. If conservative assumptions are made concerning pile settlement the neutral point will move down the pile shaft and the surface pile settlement will be an upper bound. These assumptions, however, will lead to non conservative estimates of pile tension which should be assessed independently. A schematic diagram of friction pile settlement, Figure 2.12., shows initial and final profiles of stress in the pile shaft and defines the neutral point (level of zero pile soil displacement and also where tensile forces will be maximum) demonstrating the depth of soil causing pile settlement relative to the surface.

#### 2.4.2 End bearing piles

Piles which mobilise appreciable end bearing resistance during initial loading will also mobilise full shaft friction during the initial loading stage. In this case bored pile settlement is a function of pile settlement relative to the soil at pile base level and soil heave above the pile base level. Pile settlement relative to stationary ground may be assessed using a procedure such as that presented by Fleming (1992) and outlined in Section 2.1.2.3. Two calculations would be carried out, one before and one after the rising groundwater event, the difference being pile settlement during the event. Loss in pile shaft capacity would be calculated using the same method as friction piles while base

capacity would be in terms of ultimate drained strength in order to assess long-term settlement as suggested in Section 2.1.1.2. Calculation of soil heave contributing to pile settlement would be from the level of the pile base after settlement due to the rising groundwater event. A schematic of end bearing pile settlement is shown in Figure 2.13 indicating pile settlement at the surface and at the base which is in contrast to the movements for friction piles presented in Figure 2.12.

## 2.5 Summary

The first section of this literature survey outlines current hand calculation design methods for calculation of foundation ultimate load capacity and foundation displacement response to loading. Attention has been paid to drained foundation capacity as it is this that will determine foundation behaviour during a long-term rising groundwater event.

In the second section of the review in-situ soil stresses during one dimensional deposition and erosion were summarised. Assumptions and calculation of horizontal effective stress change during a rising groundwater event were presented.

In the third section CIRIA SP69 and a selection of case histories where foundations were subjected to fluctuations in pore water pressure were presented. In all reported cases loss in foundation base capacity was found to be less than the loss in vertical effective stress at foundation base level. For a pile test in sand the reduction in base resistance was found to be proportional to the mean normal effective stress. Reduction in pile shaft resistance has been reported to be comparable to the loss in far field horizontal effective stress.

The final section draws together the observation of foundation behaviour and proposes a simple method of foundation settlement prediction during a rising groundwater event.

## CHAPTER 3 CRITICAL STATE SOIL MODELS AND TRIAXIAL TESTING

### 3.1 Introduction

This chapter consists of two distinct parts. In the first part two soil models, the Schofield model (Schofield, 1980) and a three surface kinematic hardening model (Stallebrass, 1990) are introduced. The models are used in the finite element analyses presented in Chapter 6. In the second part a short series of triaxial tests is presented. The tests were designed to provide the basic soil parameters required in the finite element analyses and to investigate the effects of changing pore water pressure on coefficient of earth pressure ( $K_0$ ) under one dimensional conditions. The parameters used in the finite element modelling are presented in Chapter 6.

### 3.2 Introduction to Critical state soil mechanics

The concepts of critical state soil mechanics, that the ultimate shear strength ( $M.p'$ ) at critical state of soil is solely dependant on specific volume; and that on reaching the critical state strength during plastic shearing there is no further volume change or generation of excess pore water pressure, have become widely accepted. These concepts have been incorporated into critical state soil models such as the original Cam-Clay model described in Schofield and Wroth (1968). This model allowed realistic prediction of soil behaviour during plastic yielding for soil in a normally consolidated or lightly overconsolidated state. Within the yield locus overconsolidated behaviour was based on isotropic elasticity theory where:

$$\begin{pmatrix} \delta \epsilon_v \\ \delta \epsilon_s \end{pmatrix} = \begin{pmatrix} 1/K' & 0 \\ 0 & 1/3G' \end{pmatrix} \begin{pmatrix} \delta p' \\ \delta q \end{pmatrix} \quad (3.1)$$

$$K' = \frac{v p'}{\kappa} \quad (3.2)$$

$$G = K' \frac{3(1-2\nu')}{2(1+\nu')} = \frac{3(1-2\nu')}{2(1+\nu')} \frac{v p'}{\kappa} \quad (3.3)$$

The original Cam clay model has given rise to altered and often more sophisticated versions. The Schofield model (Schofield, 1980) incorporates a rupture and a fracture surface as part of the Cam clay yield locus and assumes isotropic elasticity within the yield locus. A three surface kinematic hardening model (Stallebrass, 1990 and 1991) models the effects of recent stress history and incorporated within the modified Cam clay state boundary surface. Overconsolidated behaviour incorporates the effects of recent stress history within an elasto-plastic framework. Britto and Gunn (1987) used some of these soil models in the finite element program CRISP and provided the opportunity for other users to implement different models into the same basic program (Stallebrass, 1992).

### 3.3 Schofield Model

The layout of the Schofield model is shown in Figure 3.1. The model differs slightly from the original version proposed by Schofield (1980) in geometry but the essential features are the similar. The model implemented in CRISP (Britto and Gunn, 1990) has the same state boundary surface as the original Cam clay for soil in a normally consolidated or lightly overconsolidated state ( $p' > p'_o$ ). For heavily overconsolidated soils peak stress ratios have been reduced so that yield occurs on the no tension cut off or the Hvorslev surface. The three parts of the state boundary surface are shown in Figure 3.1 (a). The equations for the state boundary surface are:

No tension cut-off:

$$q = 3p' \quad (3.4)$$

Hvorslev surface:

$$q = (M - H) p'_o \left[ \frac{p'}{p'_o} \right]^{\kappa/\lambda} + H p' \quad (3.5)$$

Cam clay surface:

$$q = M p' \ln \left[ \frac{p'_c}{p'} \right] \quad (3.6)$$

Yield on any part of the state boundary surface obeys the normality condition. For a stress state dry of critical ( $p' < p'_c$  as labelled on Figure 3.1b) negative volumetric strain increments are calculated and contraction of the state boundary surface occurs with strain softening until a critical state is reached. Shear and volumetric strains inside the state boundary surface may be calculated using equation 3.1 above.

The model in CRISP allows specification of either a drained Poisson's ratio ( $\nu'$ ) or a constant value of shear stiffness ( $G$ ) from which elastic shear strains are calculated. By specifying Poisson's ratio shear stiffness is calculated using equation 3.3 above, this then varies with mean normal effective stress and specific volume.

### 3.4 Three surface kinematic hardening model: Stallebrass model

The advantages of Cam clay and associated soil models lie in the prediction of plastic strains which occur as soil yields and strain hardens on the state boundary surface for states wet of critical. The behaviour of soil in an overconsolidated state is reduced to isotropic elastic behaviour as mentioned in section 3.2 above. The increased awareness that overconsolidated clays are non-linear (Jardine et al., 1984, Stallebrass, 1990) has led to soil models that are capable of modelling overconsolidated soil behaviour incorporating the non-linear aspects of soil behaviour prior to major plastic shearing.

The model formulated by Stallebrass (1990) is shown in Figure 3.2. It consists of the outer ellipse of the modified Cam clay model (Roscoe and Burland, 1968) which is renamed as the Bounding surface. Inside this bounding surface there are two kinematic yield surfaces. The smaller surface is the new yield surface inside which strains increments are elastic (ostensibly the region where  $G_0$  exists). Outside this lies the history surface, which when in line with the stress increment and tangential to with the inner (yield) surface defines the limit of recent stress history effects. The soil stress state is restrained to lie on or inside all three surfaces which expand and contract during loading and unloading. The three surfaces have the same shape (that of the bounding surface) and have sizes that are related to the bounding surface by fixed

ratios. The model will revert back to modified Cam clay behaviour when the soil state is on the bounding surface.

Parameters for use in the finite element modelling are presented in Chapter 6.

### 3.4.1 State boundary surface

The state boundary surface, named the 'bounding surface' is an ellipse in the  $q - p'$  space with formula:

$$\frac{p'}{p_0} = \frac{M^2}{M^2 + \eta^2} \quad (3.7a)$$

where  $\eta$  = stress ratio  $q/p'$

$$q = \sqrt{(\sigma'_1 - \sigma'_2)^2 + (\sigma'_2 - \sigma'_3)^2 + (\sigma'_1 - \sigma'_3)^2} \quad (3.7b)$$

$$p' = \frac{\sigma'_1 + \sigma'_2 + \sigma'_3}{3} \quad (3.7c)$$

Stress changes which enlarge the bounding surface obey the normality condition in keeping with the family of Cam clay models where

$$\frac{\delta \epsilon_v^p}{\delta \epsilon_s^p} = \frac{M^2 - \eta^2}{2 \eta} \quad (3.8)$$

The volumetric state on a normally consolidated soil is defined in  $\ln v - \ln p'$  space where:

$$\ln v = N - \lambda^* \cdot \ln p' \quad (3.9)$$

Where  $\lambda^*$  = Slope of compression line in  $\ln v - \ln p'$  space.

A full description of plastic yielding on the state boundary surface is included in Wood (1992) and will not be reproduced here.

### 3.4.2 Overconsolidated behaviour

The description of soil behaviour within the state boundary surface is an extension a two-surface model proposed by Al-Tabbaa (1987) and is based on observations of laboratory tests carried out by Richardson

(1988) and Stallebrass (1990) in which the effects of recent stress history were investigated.

Observations from triaxial tests showed that soil stiffness was a function of change in direction of load path and length of load path, the combined effects of which are called 'recent stress history'. The effects of stress path rotation are shown on Figure 3.3 and Figure 3.4 which are taken from Stallebrass (1990). Figure 3.3 shows the effect of shearing a sample, initially isotropically consolidated to  $p_c' = 720 \text{ kN/m}^2$ , along a constant  $p'$  stress path after approaching  $p' = 300 \text{ kN/m}^2$ ,  $q = 0 \text{ kN/m}^2$  from four different directions as indicated on Figure 3.4. In these figures two distinct features of behaviour are seen that are not modelled in modified Cam clay. Firstly, by rotating stress path direction the shear stiffness changes as seen in Figure 3.3 where the line for  $\theta = 180^\circ$  has a larger shear modulus than the two shearing stages after rotations through  $\theta = 90^\circ$  and  $-90^\circ$ . The stress increment which has not been rotated  $\theta = 0^\circ$  has the lowest stiffness. All four tests had the same overconsolidation ratio and similar specific volumes prior to shearing. Secondly, the effect of changing stress state inside the bounding surface is seen on Figure 3.4. Stress increments, which move any of the surfaces, within the bounding surface result in elastoplastic strains. This is seen in Figure 3.4 (a) where the dilatant behaviour of an overconsolidated sample causes a reduction in the size of bounding surface. If the sample were on the wet side of critical as in Figure 3.4 (c) volumetric strains would be positive resulting in an expansion of the bounding surface.

The reduction in size of the bounding surface when samples are sheared on the dry side of critical as a result of dilatant behaviour has an important effects not modelled in modified Cam clay by acting to restrict the size of stress ratio ( $q/p'$ ) prior to reaching the bounding surface. As with modified Cam clay if a soil element is sheared enough the dilatant behaviour will bring the sample to critical state at which point volumetric straining ceases.

### 3.5 Triaxial testing

A limited number of stress path triaxial tests were carried out to provide data for finite element analysis input and on  $K_0$  behaviour for soil stress paths in normally and over consolidated states.

#### 3.5.1 Triaxial apparatus

The triaxial testing was carried out in a Bishop and Wesley (1975) type hydraulic triaxial cell . The cells were set up to test soil samples with nominal dimensions of 38mm diameter and 76mm height. The cells were connected to a mains air supply with a constant minimum pressure of  $800\text{kN/m}^2$  which defines the upper bound of cell pressure (the cell is capable of withstanding higher pressures). Higher axial pressures were possible due to the area ratio between axial ram and sample. The cell was controlled using a micro-computer and dedicated software similar to that described by Atkinson et al. (1985b). The equipment is described briefly below.

#### 3.5.2 Controlling software

A modified version of the program TRILOG3 (Stallebrass, 1990 and Richardson, 1988) was used to control the stress and strain increments. TRILOG3 has the following features:

- o Control of axial and radial strain paths
- o Logging and recording of data
- o Procedure for reducing effect of voltage fluctuation to transducers
- o Area correction for calculation of axial stress.

Axial ram control using a stepper motor driven Bishop ram and clicker box providing axial strain control was also possible.

Several important variations to the original program were made to provide better quality results for the non-standard range of stress or strain paths followed:

A compliance correction for axial load cell compression has been applied to axial displacement measurement. The correction allows more accurate calculation of axial strain (Atkinson and Evans, 1985a). The compliance correction is based on the axial load. This correction is important when simulation of  $K_0$  conditions is being carried out. The compliance was seen to be non-linear and has been modelled using a second order polynomial fit. Axial strain corrections for a deviator stress of  $300\text{kN/m}^2$  (deviator load of  $0.34\text{kN}$ ) were in the region of 0.2%.

A compliance correction was applied to the volume gauge. When pore pressures in the volume gauge remain constant during a test this correction is not needed. However, when pore pressures change, for instance when simulating a changing groundwater table, applying a compliance correction to the volume gauge will improve accuracy. The compliance measured was reproducible and recoverable on a complete loop of back pressure. Richardson (1988) reported that the flexibility of the volume gauge (as measured here) was large compared to that of the drainage leads and of the pore pressure transducer.

An extra procedure allowing shearing at constant mean normal total stress (or, if pore pressure is kept constant, mean normal effective stress) was added to the program. The procedure controls radial stress during strain controlled axial shearing.

During radial strain controlled  $K_0$  stages the frequency of cell pressure updating was reduced by a factor of 10 to 20 compared to the rate of updating axial stresses and pore water pressure. This addition to the program reduces the amount of radial stress hunting for the stress corresponding to the required radial strain producing a smoother stress path. However, even with this program change there was significant oscillation of the cell pressure at changes of stress path (eg  $K_0$  loading to  $K_0$  unloading) where the soil stiffness is relatively high.

### 3.5.3 Controlling hardware

A schematic of the connections between the micro-computer (a BBC micro-computer), the interface unit (Spectra ms-interface), relays and triaxial

cell is shown in Figure 3.5. The computer, using the control program described above receives data from the cell transducers via the interface unit. The information is processed and the required stress changes are calculated. Movements of the stepper motors controlling the manostats are calculated and relayed to their destination.

#### 3.5.4 Instrumentation:

The work being carried out in this series of tests requires large stress changes and correspondingly large strains. While the incorporation of internal strain transducers (both axial and radial) often provides higher quality data it was not considered necessary in this work. The instrumentation used consisted of:

- o Internal axial load cell (Surrey University type, Wykeham Farrence)
- o Druck 10 bar pressure transducers for back pressure and cell (radial) pressure
- o Imperial College type volume change gauge equipped with a RDP displacement transducer
- o MPE or RDP displacement transducers for measuring axial strain.

During the series of tests back pressure and cell pressure transducers behaved satisfactorily with steady calibration constants and offsets. Displacement transducers for axial and volume strain measurement also performed well. Drift of the load cells during the period of a test (approximately 1 month) was recorded at the ends of some tests. The drift corresponded to an error of up to  $10\text{kN/m}^2$  resulting in less reliable data.

Calibration of transducers took place through the test set up within a temperature controlled environment. Calibration constants for load and pressure transducers were taken from the best fit line over the anticipated pressure/load range. Calibration constants for the displacement transducers have been taken from their linear range. All the instrumentation used gave linear responses over the range of operation for the tests carried out.

A detailed description of the instrumentation, signal conditioning and logging system used have been given by Richardson (1988) and Stallebrass (1990) and will not be reproduced here.

### 3.6 Testing and test results

#### 3.6.1 Sample and cell preparation

The samples were consolidated from a clay slurry with a nominal moisture content of 120%. Two methods were used for preparation of the samples:

A floating wall consolidometer was used for preparation of single samples to a vertical effective stress of 100–200kN/m<sup>2</sup>. The floating wall consolidometer used has a length of 200mm and an internal diameter of 38mm. Frictionless top and bottom pistons ensure that the stress passes through the sample rather than through the floating ring;

Stiff overconsolidated clay samples were obtained from a large clay specimen consolidated in a centrifuge tub. The samples were brought to a maximum preconsolidation pressure of  $\sigma_v' = 1250\text{kN/m}^2$  before controlled swelling to  $\sigma_v' = 200\text{kN/m}^2$  and final rapid unloading before sampling. 38mm samples were taken in thin walled stainless tubes which were wax sealed for storage prior to testing.

Prior to mounting a sample zero outputs from the transducers were recorded with the cell full of water but open to atmospheric pressure. The sample was then mounted on the triaxial pedestal and surrounded by a side drain prior to fitting the membrane. The side drains were used to reduce drainage path lengths and consolidation times and were similar to those used by Stallebrass (1990). The cell was then filled with water and sealed, the sample was then allowed to come into equilibrium with the drainage shut. Once the pore pressure had stabilised the drainage leads were flushed whilst pore pressure and cell pressure were controlled. Saturation was then checked by measuring the B value (the change in sample pore pressure divided by the change in cell pressure under undrained conditions); a value of over 0.95 (absolute minimum) was required before testing commenced. If the B value was not satisfactory

at the required back pressure, drainage was allowed under controlled conditions to saturate the sample. The B value was then rechecked prior to connection of the suction top cap.

### 3.6.2 $K_0$ effective stress paths

Most of the tests were carried out under one dimensional conditions to simulate the geological history of the ground. Figure 3.6 shows the normally consolidated behaviour (with intermediate unload reload loops removed) of five tests in the vertical effective stress to horizontal (radial) effective stress plane. The five tests show good agreement giving a value of the coefficient of earth pressure at rest in the normally consolidated state ( $K_{onc}$ ) of 0.65.

This values lies within the reported experimental range of 0.62 from Equation 2.12 and 0.69 found by Al-Tabbaa (1987) using an instrumented oedometer. The value of 0.65 has been adopted for  $K_{onc}$ .

On unloading, the stress paths were somewhat ragged due to the initial stiffness of the soil on stress reversal and the hunting process of the radial stress to maintain zero radial strain. Five traces on unload stress path are shown in Figure 3.7(a), (b) and (c) and are grouped together according to the common stress paths and the maximum stress reached in each test. Averaging of the results about common points has been carried out. The results have been correlated by plotting the coefficient of earth pressure ( $K_{ou}$ ) against the overconsolidation ratio calculated using vertical effective stress ( $R$ ) as shown in Figure 3.8. An average line through the points suggests that for initial loading and unloading:

$$K_{ou} = 0.65 R^{0.44} \quad (3.10)$$

At the end of the unloading stress path, cycles of pore water pressure were carried out to measure the effective stress path obtained due to changing pore water pressure under one-dimensional conditions. The results of these stress paths are shown in Figures 3.9(a) to (d). Test L3 shown in Figure 3.9(d) was sampled from a tub with  $\sigma'_{vmax}=1250\text{kN/m}^2$ , the other three samples were brought to their highest

effective stress conditions in the triaxial cell. All four tests have been plotted as change in vertical effective stress against change of horizontal effective stress in Figure 3.10. The tests all show similar hysteretic stress path loops. All four tests show closure of the stress path loop and where second loops are started a strong degree of reproducibility. The average change of stress in the four tests was:

$$\frac{\Delta\sigma'_h}{\Delta\sigma'_v} = 0.49 \quad (3.11)$$

In section 2.2.4 it was suggested that closed cycles of pore water pressure could be approximated using equation 2.20. For a Poisson's ratio of 0.3 (reported by Al-Tabbaa, 1987) and the assumptions of linear elasticity:

$$\epsilon_1 = \frac{1}{E'}(\sigma'_1 - \nu'(\sigma'_2 + \sigma'_3)) \quad \text{etc.} \quad (3.12)$$

the value in the change of horizontal to vertical effective stresses in Eqn. 3.11 would be 0.43. The tests were carried out at  $K_0$  values somewhat lower than exist in the upper layers of an overconsolidated clay deposit and are more appropriate to stress changes at depth than at levels close to the surface.

The stress loops show the difficulty the cell had in changing stress path direction under strain control as seen by an initial drop in horizontal effective stress on the initial increase in vertical effective stress (drop in pore water pressure).

### 3.6.3 Volumetric conditions during $K_0$ stress paths

In the presentation of the critical state soil models given above the relationship between specific volume, mean normal effective stress and stress ratio ( $\eta = q/p'$ ) is defined for both models by relating the intercept of the current swelling line and the state boundary surface to  $p'_c$ . Therefore if the position of any constant stress ratio plane can be found the behaviour of the soil can be fixed in volumetric-stress space. The relationship between specific volume and mean normal effective stress

for the tests presented in Figure 3.6 has been plotted in  $\ln v - \ln p'$  space in Figure 3.11 as required for the Stallebrass model. The average measured value for  $N_0$  (the interception of the one dimensional compression with  $p' = 1 \text{ kN/m}^2$  in  $v/\ln p'$  space) is 3.03 and for the slope of the one-dimensional normal consolidation line  $\lambda$  is 0.18 and  $\lambda^*$  is 0.083.

During unloading from the maximum pressure the swelling line has a continuously increasing slope as seen in Figure 3.11. This change in slope is not considered in the Schofield model for which  $\kappa$  is taken to be constant. Figure 3.12 shows the back pressure cycles for tests T8, T9 and L1 all of which had the same maximum preconsolidation pressure of  $\sigma_v' = 600 \text{ kN/m}^2$  under one-dimensional conditions. The results show the open loops associated with an elasto-plastic material as described in the Stallebrass model with average slope of  $\kappa = -\delta v / \delta \ln(p') = 0.04$ .

Values for  $\kappa$  and  $\kappa^*$ , under one-dimensional and isotropic conditions, have been obtained from Al-Tabbaa (1987) and reproduced in Figure 3.13 and Figure 3.14 for unloading and reloading respectively. The results show that the tangent values of  $\kappa$  and  $\kappa^*$  vary considerably with the length of stress path with increasing values, or reducing stiffness, as the length of stress path increases.

#### 3.6.4 Shearing

At the end of several of the tests the samples were sheared in drained compression along a constant  $p'$  path. The results of three such tests (ultimate stress ratio and where appropriate peak stress ratio) are shown in Figure 3.15 plotted in  $p' - q$  space. The design line for the projected Critical State Line is shown with a slope of  $M = 0.85$ . The volumetric strain is plotted against triaxial shear strain in Figure 3.16. Tests T1 and T3 show positive volumetric strains as would be expected for lightly overconsolidated samples. Neither sample reaches a constant volume state as seen by the ever increasing volumetric strain even though both samples ultimate stress ratios during axial strain controlled shearing. The heavily overconsolidated sample, L1, shows a more unique volumetric state at high shear strain levels.

## CHAPTER 4 CENTRIFUGE MODELLING AND THE MODEL TEST PROCEDURE

### 4.1 Introduction

The use of centrifuge model testing for investigation of geotechnical situations started in Russia between the First and Second World Wars for the examination of mining related situations (Schofield, 1980). Since then geotechnical centrifuge testing has become used extensively as demonstrated by contributions to specialist and general soil mechanics related conferences.

Before describing the equipment used in the series of centrifuge tests the basic scaling laws relevant to the centrifuge testing will be described. The different models used will be described and errors inherent in centrifuge modelling assessed. The chapter ends with a description of the instrumentation and equipment used in the model tests.

### 4.2 Centrifuge scaling laws

When a mass is rotated about a fixed point it experiences an acceleration as it is constantly pulled out of a straight line. The inertial acceleration ( $a$ ) directed towards the axis of rotation generated in this way is

$$a = \omega^2 r \quad (4.1)$$

where

$a$	-	centrifuge acceleration ( $m/s^2$ )
$\omega$	-	angular velocity (rad/s)
$r$	-	radius of centre of gravity of mass (m)

However, if the model is considered independently the direction of the acceleration is reversed so that it acts towards the base of the model. This component of the acceleration is used in centrifuge modelling. The direction of acceleration is perpendicular to the model surface in the same manner that Earth's gravity is perpendicular to level ground. When comparing the model in a centrifugal acceleration field with one where the dominant acceleration is due to the attraction of the Earth's mass ( $g$ ), the ratio of accelerations ( $n$ ) is:

$$n = \frac{a}{g} = \frac{\omega^2 r}{9.81} \quad (4.2)$$

All scaling relationships are calculated using the factor 'n'.

#### 4.2.1 Stress and dimensions

Soil behaviour (in drained and undrained conditions) is dominated by the frictional forces between particles and their relationship with the volumetric state of the soil (usually expressed as voids ratio or specific volume for clays). To enable a centrifuge model and a prototype to be compared, the soil, at similar positions in the model and the prototype, must be at the same stress level. To achieve this model dimensions must be reduced by the same ratio that stress gradients increase:

$$\sigma_m - \sigma_p = d_m \rho n g - d_p \rho g \quad \therefore d_m = \frac{d_p}{n} \quad (4.3)$$

where	d	-	depth
	$\sigma$	-	stress in model
	$\rho$	-	soil density
subscript	m	-	model
subscript	p	-	prototype

Secondly, the soil must be prepared to the correct volumetric state either before the centrifuge test starts or on the centrifuge arm during the test. In this way soil strength (including dilation for heavily overconsolidated samples) and stiffness will be modelled correctly.

#### 4.2.2 Time

In soil mechanics, time is important when considering the shearing of soil and the rate of diffusion processes. In this project the rate of excess pore water pressure dissipation is to great advantage.

In consolidation theory the rate of pore pressure change is dependent on the soil consolidation (or swelling) properties and the drainage path length. Assuming that the soil properties are the same in model and

prototype (which requires similar stress histories as pointed out by Goodings, 1985) diffusion processes, will take place in a time of  $1/n^2$  in the model compared to the prototype as in one dimensional consolidation theory:

$$\frac{\delta u}{\delta t} = c_v \frac{\delta^2 u}{\delta d^2} \quad (2.4)$$

where  $c_v$  - coefficient of consolidation  
 $u$  - pore pressure  
 $t$  - time  
 $d$  - drainage path length

This condition requires that both model boundary conditions and drainage path length are scaled properly.

#### 4.2.3 Mass

The effect that a mass (eg. kilogrammes) has on a model is a combination of the increase in force (Newtons) it exerts due to the increase in acceleration level ( $n$ ) and the reduction in soil or foundation area on which it acts ( $1/n^2$ ). These combine to create to give an effective scale factor for mass of  $1/n^3$ .

#### 4.2.4 Summary

The combination of the scaling laws described above provides a powerful tool for examining foundation behaviour in clay. In the tests carried out the centrifuge acceleration was held constant at 100g during the test. Table 4.1 shows the model to prototype relationships for a typical test. Further scaling relationships are presented in Taylor (1987).

### 4.3 Centrifuge model and preparation

Prior to commencing the centrifuge test the overconsolidated clay sample (Speswhite Kaolin) had to be prepared. This was carried out by consolidation of a clay slurry with an initial moisture content of 120-130%. Consolidation took place in a computer controlled hydraulic press schematically shown in Figure 4.1(a). The press was controlled by a desk

top computer fitted with a multi-function PC super card by CIL (1989). The computer program combined with the interface card processed data from the instrumentation marked on Figure 4.1(a) and updated voltage output to the convertors controlling air pressure to the air-water interface and hydraulic pump. The elevated pressures required for consolidation of centrifuge samples are obtained by use of an on-line pump which converts and amplifies (a factor of 36) the air pressure into oil pressure. Using this method centrifuge size soil samples can be consolidated to  $1500\text{kN/m}^2$  (21 tonne load) with the existing set-up.

The clay was mixed from either a powder or recycled clay mixed with distilled de-aired water. In most tests the final consolidation pressures were  $1250\text{kN/m}^2$ ; full details are given in chapter 5. On achieving full consolidation at the maximum pressure the clay samples were swelled back to a typical vertical pressure that would be experienced (around  $220\text{kN/m}^2$ ) during the centrifuge test at 100g. When equilibrium was reached at this lower pressure pore water pressure transducers were installed in the clay through ports mounted in the centrifuge tub sides. The holes, in which the transducers were inserted, were formed using a guided auger. Prior to inserting the transducer a small amount of de-aired clay slurry was placed in the end of the hole to create an air free interface between soil and transducer. The holes were then backfilled with slurry prior to sealing the transducer cable at the port.

In most tests final model preparation in the press used a downward hydraulic gradient technique (Zelikson, 1969) to create an effective stress distribution in the model similar to the one that would be achieved after equilibrium is achieved on the centrifuge. Figure 4.1(b) shows a schematic of the stresses generated using the downward hydraulic gradient technique. Further comments on the benefits of using the downward hydraulic gradient technique are given in Section 4.6.

Shortly (three to four hours) before the centrifuge test was planned to start the clay sample was removed from the press. Swelling of the clay was reduced by closing the tap on the base drain inlet at the base of the model (this reduces dissipation of negative pore water pressures) and by

removing all traces of free water from the surface of the clay. Model foundations were then installed in preformed holes. The holes were excavated using a thin walled tube which was guided so that the holes were vertical (parallel to the tub sides) and not oversized as shown in Figure 4.2. A small amount of de-aired slurry was placed at the base of the hole prior to placing the foundations. When an under-reamed pile was being modelled the under-ream was excavated from the base of the shaft using a custom made tool. The under-ream void was filled with a quick setting resin prior to placing of the straight shafted part of the pile.

A dry sand layer was then placed on the clay surface before placement of the displacement transducers and loading of the tub onto the centrifuge arm as seen in Figure 4.3a. A typical model set up with two similar piles is shown in Figure 4.3b.

#### 4.3.1 Soil stress errors

In the preparation of the overconsolidated layer of soil a maximum preconsolidation pressure ( $p'_{max}$ ) was applied to the top of the sample. When primary consolidation had finished the pressure was reduced leaving the soil layer with a constant  $p'_c$  with depth. This is somewhat different to the prototype situation where  $p'_c$  will increase with depth. If it is assumed that the top of the clay layer has the correct stress history the differences between model and prototype are:

##### Stiffness:

The reduction in maximum preconsolidation pressure at the base of the model compared to the prototype will result in a higher specific volume than expected. Research by Stallebrass (1990) showed that the soil bulk modulus and probably its shear modulus were dependent on mean normal effective stress and overconsolidation ratio ( $p'$  and  $R$  which together specify the current specific volume). While the vertical effective stress will be similar in model and prototype  $R$  and therefore  $p'$  will be lower in the model than the prototype leading to reduced soil stiffness.

##### Strength:

There will be a lower gradient of undrained strength with depth in the

model (when scaled to the corresponding prototype) than in the prototype situation as predicted using critical state soil mechanics for failure on the critical state line:

$$S_u = \frac{M}{2} \exp\left(\frac{\Gamma - v}{\lambda}\right) \quad (4.4)$$

The specific volume will be higher in the model than the prototype due to the reduced preconsolidation pressure and slightly lower mean normal effective stresses.

This reduction in undrained shear strength is confirmed by Stewart (1989) who compiled undrained strength data from laboratory and centrifuge tests using Speswhite Kaolin clay and determined:

$$S_u = 0.22 \sigma'_v R^{0.57} \quad (4.5)$$

#### Permeability:

Al-Tabbaa (1987) showed that for Speswhite Kaolin permeability was a function of voids ratio where the vertical and horizontal permeabilities ( $K_v$  and  $K_h$ ) could be calculated using:

$$k_v = 0.5 (v - 1)^{3.25} \times 10^{-6} \text{ mm/sec} \quad (4.6)$$

$$k_h = 1.43 (v - 1)^{2.09} \times 10^{-6} \text{ mm/sec} \quad (4.7)$$

Hence, the reduction in permeability with depth will not be as rapid in the model as in the prototype (assuming it were made of Kaolin) due the more uniform specific volume with depth. This leads to a flatter pore water pressure profile when downward seepage is being modelled as shown in Figure 4.4. Consequently, in the model, lower initial pore water pressures were achieved at equilibrium prior to groundwater level rise than would be expected in the prototype. Similar trends will be seen for models and prototypes which are formed of different types of clay.

Bromhead (1994), using finite element calculations and an idealised layered deposit, commented on the effects of variation of permeability with depth. He found that naturally occurring reductions in permeability with depth resulted in only small reductions in pore pressure in the upper part of a clay deposit when subjected to downward seepage and under drainage. Pore water pressure profiles measured in the London area,

reported by Simpson et al. (1989), show that the reductions in pore pressure at the top of natural clay deposits are reasonably small when subjected to downward seepage and under drainage. It was reported that the non-linear link between the pore pressures at the top and base of the clay layer could be a result either incomplete consolidation (Simpson et al., 1989) or non constant permeability with depth (Bromhead, 1994).

#### 4.4 Centrifuge modelling errors

In the ideal prototype situation a foundation will be installed in a bed of clay homogenous in the horizontal plane and with a near linearly varying total stress with depth. The clay layer will at some depth below the surface have a horizontal base and will be infinite in the horizontal direction or at least have vertical boundaries at some distance from the foundation to cause no interference with the foundation. Foundation loads will be in line with the foundation centre line which itself will be vertical. In a centrifuge model the effect of changing radius through the model (Eqn. 4.1) will result in model geometry moving away from this ideal situation. Also, the necessity to have models of finite size will inevitably result in some boundary effects.

##### 4.4.1 Vertical acceleration field

Eqn. 4.1 shows that as the increase of acceleration level is linear with model depth resulting in soil with higher stress gradients at the base of the model than at the surface. It has been shown that to minimise this error the required 'g' level should be calculated for a point at one third of the model depth. This results in the correct average vertical stress down the centre line of the model. The total stress at any point down the model centre line can be expressed as:

$$\sigma_{vt} = \int_{z_0}^{z_0+d} \rho D \omega^2 dD \quad (4.8)$$

giving:

$$\sigma_{vt} = \frac{\rho \omega^2}{2} (2Z_0 d + d^2) \quad (4.9)$$

where  $Z_0$ , and  $d$  are defined on Figure 4.5.

Figure 4.6 shows the total vertical stress distribution for prototype and centrifuge model situations for a 25m deep layer at prototype scale.

#### 4.4.2 Radial acceleration error

Eqns. 4.9 and 4.10 assume that the model is not offset from the centre line extending diametrically from the centrifuge axis. For points off this line eqn 4.10 becomes:

$$\sigma_{vt} = \frac{\rho\omega^2}{2}(2xy+y^2) \quad (4.10)$$

Where:

$$x = \left( z_o^2 + \left( \frac{O_{c1} z_o}{z_o + d} \right)^2 \right)^{0.5} \quad (4.11a)$$

$$y = ((z_o + d)^2 + O_{c1}^2)^{0.5} - x \quad (4.11b)$$

The symbol  $O_{c1}$  (offset from centre line) is defined in Figure 4.5. When  $O_{c1}$  is made equal to zero Eqn. 4.10 reduces to Eqn. 4.9.

Figure 4.7 shows the prototype stress variation with depth at ' $O_{c1} = 0.18m$ ' model scale, which represents a line of points close to the edge tub. At the base of the model there is a stress 3.7% greater than the equivalent point in the prototype situation when 'd' is assumed to be a third of the full depth of clay in the calculation of  $\omega$  ( $[(gn/(z_o+d))^{\frac{1}{2}}]$ ). This compares to 2.6% in Figure 4.6 along the model centre line. The average stress error in the whole sample is +0.5% compared to the prototype situation.

#### 4.4.3 Model foundation orientation in gravity field

Due to the geometry of the centrifuge swing it was necessary to place the model foundations offset from the model centre line. The axis of each foundation was offset by 0.08m from the centre line. This results in an average foundation inclination of 1 in 20 to the resultant acceleration direction. This inclination is significantly larger than a typically

recommended bored pile vertical tolerance of 1 in 75 (Fleming et al., 1992). However, the effects of this are somewhat mitigated by the direction of foundation loading which is kept fully in line with the foundation axis. The non-axial component of foundation load results from the net weight of the pile which is small compared to the magnitude of axially imposed foundation load. It was not possible to incline the model foundations so that they were parallel to the resultant acceleration direction due to the orientation of the tub sides. The tub sides are orthogonal to its base allowing the soil to swell uniformly. If the foundations were inclined to the tub sides they would also be inclined to the principal direction of soil swelling and consolidation.

#### 4.4.4 Coriolis acceleration errors

Coriolis acceleration errors resulting from particles moving from one radius of gyration to another are small in the tests being carried out due to the low permeability of the soil and the small foundation movements during loading and unloading. For the piezocone tests where the rate of penetration in test RW16 was 2.0mm/sec the Coriolis acceleration ( $a_c$ ) error is:

$$\frac{a_c}{a} = \frac{2 \frac{dr}{dt} \cdot \frac{d\theta}{dt}}{\frac{d\theta^2}{dt} \cdot r} = \frac{2 \cdot \frac{dr}{dt}}{r \cdot \frac{d\theta}{dt}} = \frac{2 \cdot \text{velocity}}{\omega \cdot r} \quad (4.12)$$

giving a result of approximately 0.01%. This is negligible compared to the other unknowns of a piezocone test.

#### 4.5 Test equipment

In this section the equipment used for carrying out the tests is described.

##### 4.5.1 Acutronic 661 centrifuge

The Acutronic 661 centrifuge is a dedicated geotechnical centrifuge. A schematic of the important features is shown in Figure 4.8. It combines a swing radius of 1.8m (the typical radius of the point at one third clay

depth for use in eqn 4.1 is approximately 1.60m ) with a maximum acceleration of 200g and package mass of 400kg. The maximum operational capacity is 40g.tonne (either 200kg at 200g or 100kg at 400g).

The machine is situated in a aerodynamic shell which is surrounded by a sacrificial soft brick wall. This wall is in turn surrounded by a reinforced concrete containment shell. The centrifuge arm is balanced manually by moving a counter weight prior to spin up. The centrifuge pedestal has built in strain gauges which monitor the out of balance force constantly during operation. The machine will automatically shut down if the out of balance force exceeds a preset limit. This safety feature allows unsupervised running of the machine overnight.

The slip ring stack is located above the centrifuge and comprises 130 electrical rings and 5 hydraulic rings (oil, water and compressed air). Of the electrical slip rings 64 are used for relaying transducer signals from the model to the logger, the remainder are used for power supply to the arm, triggering solenoid valves and relay of closed circuit television signals.

#### 4.5.2 Data recovery

Transducer signals are amplified and filtered in the on-arm junction boxes. On-arm amplification is either 1, 10 or 100. The signals are then transferred from the junction boxes to the control room where there is further amplification (1, 2, 4 and 8 times) and filtering prior to being logged on a personnel computer. The computer is fitted with a 12 bit analogue to digital convertor data logging card manufactured by Burr Brown. The card is interfaced by a commercially available data logging program "Labtech notebook" version 4.1.

The program allows transducer signals to be logged at predetermined voltage ranges of  $\pm 0.01$  volts to  $\pm 10$  volts and an autoranging setting is available where the program selects the optimal input voltage range to use. The amplifiers on-arm and in the control room are set to provide the strongest signal being transferred across the slip rings and to fully use the logging range that has been chosen.

#### 4.5.3 Model containers

Two centrifuge tubs were used during the series of tests. Both tubs had nominal dimensions of 400mm internal height and 420mm internal diameter. The tub used in the first four tests was made of steel with painted sides. It had access ports at 5mm, 50mm, 150mm and 250mm above the base through which pore pressure probes were installed. In the remainder of the tests a polished stainless steel tub was used in which extra ports were installed at intermediate positions of 100mm and 200mm above the base. The sides of both tubs were greased with Duckhams Keenomax L3 prior to placing the base sand drainage layer and clay slurry for consolidation. Consolidation took place in one run requiring extensions to be mounted above the tubs during the initial stage of consolidation.

#### 4.5.4 Foundation types and installation

The effects of pile installation in centrifuge models has been studied by Craig (1985). The study concentrated on driven piles in sand and clay and for piles in clay, at least, the rate of driving was not seen to influence long term settlement under loading. Bored pile construction and subsequent loading during flight has not been studied.

Ideally the model pile foundations would have been installed during flight on the centrifuge. Installation would have taken place after equilibrium had been reached with a low water table and before the groundwater table was raised. This, however, was not possible due to the complexity of the procedure and was not attempted. The foundations were installed in clay at 1g prior to loading the assembled model onto the centrifuge swing. Modelling procedures were adopted to limit the effects of pile installation prior to spin-up and are discussed in section 4.6.

With the exception of the pad in test RW1 all foundations were made of aluminium and were loaded externally using loading rigs described in section 4.5.5. The foundations were installed in holes bored in the clay. The holes were excavated following the same procedure in all cases (three plugs of 50mm length with diameter equal to foundation diameter) to help ensure that foundation behaviour would be similar. Prior to

placing the foundation in the hole kaolin slurry was placed in the base of the hole. This slurry was displaced upwards between the hole sides and the foundation when the foundation was placed ensuring continuity between foundation and soil.

In the cases where an under-ream pile was being installed the pile shaft was excavated as usual. Excavation of the under-ream was carried out using a miniature tool placed down the shaft. The under-ream void was then filled with quick setting cement in test RW4 (not wholly successful) and a quick setting metal loaded epoxy resin in the remaining under-ream tests. When the under-ream material had become solid the pile was placed down the hole partially filled with kaolin slurry (in test RW4 no kaolin slurry was placed down the hole prior to pile placement resulting in a low shaft capacity).

Foundation load was measured above ground level at the pile top (typically 40mm above soil level) using a load cell. The actual total pile load was then the net weight of the pile plus the load cell reading plus the unmeasured weight of the lower part of the load cell (at 100g this corresponds to approximately 24 tonnes prototype pile load) In several tests load cells mounted in the pile bases were used to distinguish between pile shaft and base loads.

Four different foundation types were used. All had a nominal length 150mm in the clay with shaft diameters from 12.7mm to 19mm. The under-reamed piles were constructed with a 16mm diameter shaft and a 23mm diameter base. A typical pile design with under-ream and load cell is shown in Figure 4.9.

#### 4.5.5 Loading rigs

As mentioned in section 4.2.3 mass has a scale factor of  $1/n^3$  in the centrifuge compared to the prototype. This fact is utilised in providing load to the foundations. The simple loading device shown in Figure 4.10 applies the load 'vertically' (in line with foundations and tub sides) to the foundation by using an axial bearing to control the orientation of the loading pin. Foundation load is altered by removing (loading) or

adding (unloading) water to the bucket suspended on the arm. Loading is achieved by using a remote controlled solenoid valve to dump water, while unloading is carried out by inserting water through an hydraulic slip ring to the bucket. In test RW5 and onwards the loading pin and load cell were loosely suspended from the balancing lever allowing touch down of the load cell and pin, followed by the balancing lever, to be gradual resulting in a smoother initial loading of the foundation.

#### 4.5.6 Standpipe

The top and bottom boundaries of the clay layer are used to control the equilibrium pore water pressure conditions. The surface of the clay was kept either wet (surface water present) or in suction (surface sealed with liquid paraffin). The surface liquid condition did not change during any one test.

The sand layer at the base of the clay was connected to the standpipe arrangement, as shown in Figure 4.11. The arrangement allowed three different pore water pressures to be applied to the base of the clay layer creating three different equilibrium pore water pressure profiles during a test. The required level was selected by operation of solenoid valves (normally closed setting) attached to the dump and lower overflow standpipe ports.

#### 4.5.7 Instrumentation

Three different types of instrumentation were used:

- o Druck PDCR 81 miniature pressure transducers fitted with a porous ceramic front element were used to measure pore water pressures within the clay model. In each model there were between three and five transducers evenly distributed through the depth of the model. The pore pressure transducers had a pressure range of either 300 or 1000kN/m<sup>2</sup> depending on the maximum pressure they would be subjected to during the model preparation and testing. Similar transducers were also used to monitor water levels in the standpipe, loading rig water containers and the surface water level. Output from the transducers was in the order

of  $\pm 0.1V$  at full scale deflection. The output was amplified by 100 times by the on-arm junction box prior to being relayed to the logging system.

o Linearly variable differential transformers (LVDT's) were used to measure foundation and soil surface movements. In tests RW1-RW3 five LVDT's (range  $\pm 12.5mm$ ) were used, three to monitor surface movements and one on each foundation. In test RW4 - RW7 six LVDT's (range  $\pm 5mm$ ) were used, three on the surface and three distributed over the two foundations. In test RW9 onwards an extra measurement of soil surface movement close to the tub edge was taken. Output from the transducers is  $\pm 3.5V$  for both ranges of transducers used. The output was amplified by 1 prior to being relayed to the logging system. In latter tests an off-arm amplification with a gain of 2 was applied to the  $\pm 5mm$  LVDT's.

o RDP load cells were used to measure imposed foundation loads at the surface while an Entran load cell and a City University load cell were used to measure pile base load. The surface load cells had a linear range of  $\pm 2200N$  ( $\pm 500lbs$ ) while the pile base load cell had a linear range of  $\pm 500N$ . The RDP load cells have an output of  $10 \times 10^{-3} V/kN$  while the lower capacity Entran load cell outputs  $0.13V/kN$ . The output was amplified by 100 on-arm and in later tests a further amplification factor of 2 was applied.

All instrumentation was calibrated through equipment used during the tests, (arm mounted junction boxes with filters and amplification, slip rings and logging system). Pore pressure transducers were calibrated against a pressure transducer which is regularly calibrated against a dead weight system. Load cells were calibrated with hanging weights. LVDT's were calibrated against a micrometer scale. Typical calibration data from test RW15 is shown in Figure 4.12.

#### 4.5.8 Piezocone and actuator

The piezocone used in tests RW8 and RW16 was a  $60^\circ$  cone with cross sectional area of  $1cm^2$  manufactured by Fugro-McClelland of Holland. The penetrometer was fitted with a porous stone  $12.5mm$  from the cone tip or  $1mm$  from the cone shoulder and an internal pore water pressure

transducer. The influence that the pore pressure, in the internal cavity of the cone, has on the load cell reading is

$$q_t = q_c + (1 - a)u \quad (4.13)$$

where

$q_t$	-	corrected cone resistance
$q_c$	-	measured cone resistance
$a$	-	effective cone area ratio
$u$	-	pore pressure

A value of  $a=0.6$  was measured by Allman (1992a) in a calibration chamber while a value of  $a=0.71$  has been calculated from measurements from the cone geometry. The value measured by Allman has been used this work.

The piezocone is mounted on an actuator, Allman (1992b). The actuator has two degrees of freedom (one horizontal movement and vertical) and is driven by stepper motors connected to an off-arm controlling computer in the control.

The cone was disassembled prior to use and carefully de-aired prior to reassembly under fluid. In test RW8 the cone was saturated using silicon oil in an effort to prevent desaturation during in-flight moving between test locations. The use of silicon oil was reported by Meigh (1987) as a beneficial aid in preventing desaturation. However, at 100g the cone became desaturated and reduced the usefulness of the data. In test RW16 different preventative measures to stop desaturation were adopted. The cone was saturated with distilled water and the tip was always immersed in a thirty millimetre deep layer of water overlying the sand layer. The cone did not desaturate during testing giving reproducible results of pore water pressure and cone resistance measurements.

#### 4.6 Pore pressures and downward hydraulic gradient consolidation.

In modelling foundations in clay it is considered important to install the foundations in soil at the correct effective stress level. Ideally the model bored piles would be installed in flight after pore pressure equilibrium had been achieved. Pad footings are less effected by the stress condition at which they are installed. Failure to install piles

in soil with the correct effective stress regime will result in unrealistic soil structure interaction caused by soil consolidation (or swelling) resulting in down drag (or uplift) of the pile (see section 5.5.1). For instance a pile having undergone down-drag will have unrealistically high toe loads, as monitored in test RW3 and RW4. On loading the pile the base would provide a stiffer response than expected. Whilst it was not been possible to install bored piles during flight due to the complex process of excavation and pile placement steps were taken to install the pile in the clay model with the correct effective stress regime. This was carried out by using a downward hydraulic gradient (Zelikson, 1969) in the press prior to model removal providing an effective stress profile that would later be achieved after spin-up on the centrifuge, by keeping the time from removal of the model from the press to spin-up on the centrifuge to a minimum (thus reducing swelling prior to centrifuge spin-up) and by keeping water away from the clay surface. The idealised downward hydraulic gradient stress profiles obtained in the consolidometer have shown in Figure 4.1(b).

In addition to the benefit of installing the piles in soil with the correct effective stress conditions the time to pore pressure equilibrium on the centrifuge after spin-up was also reduced.

While it was not possible to get reliable readings of pore water pressures in the model prior to spin-up due to cavitation in the transducers positive excess pore water pressures were significantly reduced when downward hydraulic gradient and quick model assembly were used. In tests where the downward hydraulic gradient technique was used the excess pore pressure at the mid height pore pressure probe was typically reduced by over 50% compared to the cases where it was not used.

#### 4.7 Test procedure

##### **Spin-up:**

Immediately prior to spin up of the model the base drainage was opened. The centrifuge was then started and accelerated to the required speed during two to three minutes. During spin up excess pore water pressures

(relative to the top and base pore water pressure conditions) were created.

**Excess pore water pressure dissipation:**

These excess pore water pressures immediately start to dissipate to the boundary conditions which are set to produce one of two different initial pore pressure profiles. In a majority of the tests downward seepage was set up through the clay layer by maintaining a surface water table in the sand layer on top of the clay and by allowing free drainage at the base of the clay as shown in Figure 4.13(a). A second profile modelling a clay layer with an impermeable surface cap and a hydrostatically increasing pore pressure with depth with the upper part of the clay layer in suction was also set up as shown in Figure 4.13(b). The impermeable surface was created by covering the clay with liquid paraffin. The liquid paraffin prevented drying out of the clay surface. Dissipation of the excess pore water pressures usually took place overnight during which the centrifuge was largely left unsupervised.

**Foundation loading:**

Foundation loading was then carried out using the loading rigs mounted vertically above the foundations. During this stage some foundations were loaded to failure (a displacement of 10% of the base diameter) prior to unloading to the required working load.

**Rising groundwater event:**

The pore pressures in the clay were then raised in one or two steps by increasing the water pressure at the base of the model using the external standpipe. The final pore pressure regime was set to be close to a hydrostatic profile extending from the model surface.

**Further foundation loading:**

When the pore water pressures had established at the higher level further foundation load tests were carried out. The centrifuge was then stopped and moisture content samples taken.

**Piezocone tests:**

In the two tests where the piezocone was used the initial pore water

pressure profile shown in Figure 4.13a was created after spin-up and excess pore water pressure dissipation. Three piezocone tests were then carried out in to a clay depth of 200mm at constant rates of penetration. The centrifuge was then stopped and the actuator holding the piezocone moved to allow further tests in undisturbed soil. The centrifuge was restarted and the pore water pressure raised to a hydrostatic profile extending from the clay surface. Further piezocone tests were then carried out.

Preliminary results from several early centrifuge tests have been presented by Morrison and Taylor (1994a and 1994a).

## CHAPTER 5 CENTRIFUGE TESTS AND RESULTS

### 5.1 Introduction

A total of sixteen centrifuge tests were undertaken with up to two foundations located in each model. The general test procedure was described in section 4.7. The test configurations are presented in Tables 5.1(a), (b) and (c) where foundation geometry, clay preconsolidation pressure, initial pore water pressure profile and some general comments are given.

In the following the centrifuge tests are grouped together according to the principal objective of the particular experiment. The description commences from the point where the model had reached equilibrium with a low water level on the centrifuge.

#### Tests RW1 to RW4:

These four tests provided information on testing problems as well as basic information on foundation behaviour in a rising groundwater environment. Each test was more sophisticated than its predecessor due to improved testing procedure and loading rigs. In test RW4 the downward hydraulic gradient system was first used for final sample preparation in the press. Load tests were carried out on all foundations resulting in non standard behaviour of the foundations during the rising groundwater event. Test RW2 was unsuccessful due to variation of imposed foundation load during the rising groundwater event.

#### Tests RW5 to RW7:

In these tests the effect that initial load testing, prior to the rising groundwater event, has on foundation behaviour during a rising groundwater event was examined. Two identical piled foundations were installed in each model, one of which was load tested prior to raising the groundwater level. Test RW5 was unsuccessful due to an uncontrollable increase in foundation load during the rising groundwater level stage.

#### **Tests RW8 and RW16:**

In these tests series of piezocone penetration tests were carried out. Test RW8 was unsuccessful due to desaturation of the piezo-element and a break down in the data logging system. In test RW16 a surface water lake, deep enough to keep the cone submerged during cone movements from one testing location to another, was used to prevent drying out of the piezo element. The results of the piezocone penetrations provided data against which loss in pile base load capacity during a rising groundwater event can be compared. Pore water response in the model after removal of the cone showed no sign of hydrostatic continuity with the surface water table between tests at the low water level suggesting that the holes healed during removal of the cone over a large proportion of their depth.

#### **Test RW9:**

In this test London Clay was used instead of Speswhite Kaolin. The test was stopped twice as a result of malfunction of the slip rings. The test was not repeated due to the excessive sample preparation time required due to the low permeability of London Clay. Problems were also likely to occur during running of the centrifuge due to the excessively long testing times required.

#### **Tests RW10 and RW11:**

Data from previous loading tests was used for calculation of appropriate foundation loads for modelling the influence of factor of safety on similar foundations during a rising groundwater event. In test RW10 under-reamed piles were modelled while in test RW11 more slender straight shafted piles were used. The piles were load tested after the rising groundwater event.

#### **Tests RW12 and RW13:**

The drainage conditions were changed in these tests to assess the effect that a sealed clay surface would have on foundation settlements. The

perched water table present in all other tests was replaced with a layer of liquid paraffin which is immiscible in water. The tests used a combination of one pile and one shallow footing as used in tests RW1 to RW4. The foundations were not load tested prior to carrying out the rising groundwater event.

#### **Tests RW14 and RW15:**

These tests were carried out to assess the effects of foundation geometry on settlement during a rising groundwater event. In each tests two different piles (an under-reamed pile and a straight pile) were tested at different loads but similar factors of safety. Load tests were carried out after the rising groundwater event.

##### **5.1.1 Data obtained from tests**

The data obtained from each test commencing with model preparation and culminating with centrifuge spin-down include:

- o Stress history in consolidation press;
- o Initial excess pore water response during spin up;
- o Dissipation of excess pore water pressure generated during spin up resulting in soil and foundation movements and negative skin friction loading on pile shafts and pile base loading;
- o Model foundation load settlement relationship during loading;
- o Increase in pore water pressures (rising groundwater event) causing soil and foundation movements and redistribution of stresses in deep foundations;
- o Model foundation load-displacement relationship during load testing after rising groundwater event;
- o Generation of excess pore pressures during spin down.

The first six items are necessary for analysis of the centrifuge modelling of foundations in a rising groundwater environment. The last item gives a rough check on total vertical stress at each pore water pressure transducer level.

For the tests where piezocone penetrations were being carried out profiles of cone load and pore water pressure were obtained against a background pore water pressure profile. These tests were carried out at low and high pore water pressure profiles and require the data in the first three points above for full analysis of the soil stress state.

## 5.2 Generalised pore water pressure changes in the model

The behaviour of the clay body during the centrifuge test is controlled by the water pressure boundary conditions. These conditions allow water to leave the model (consolidation) or enter the model (swelling) resulting, when equilibrium is achieved, in the required effective stress regimes.

### 5.2.1 Spin up and subsequent dissipation

As previously stated the changes in total stress in the model cause similar changes in pore water pressure during spin up. The event is considered to be essentially undrained resulting in a zero effective stress change. Figure 5.1 from test RW10 shows a typical pore water response during spin up. As the speed increased so did the pore water pressure. There may be some lag in the pore water pressure reading possible as a result of desaturation of the pore pressure transducer and potential cavitation of the clay-water mixture due to the pore suction generated when the sample was unloaded from the press. The pore pressure transducers at the base and at the mid-height of the model (labelled Base and Mid) show a quick response while the transducers at two fifths and four fifths depth (labelled L2 and L4) show a distinct delay in response to spin up.

On reaching full speed the change in pore water pressures can be monitored as they dissipate to the imposed boundary conditions as shown on Figure 5.2(a) from test RW10. The pore water pressures dissipate to low equilibrium levels of between 20 and 50kN/m<sup>2</sup> through out the model when the imposed boundary conditions shown in Figure 4.13(a) were used. When a sealed surface was imposed the pore water pressures dissipated to a depressed hydrostatic profile as shown in Figure 5.2(b)

from test RW13 with the boundary conditions shown in Figure 4.13(b). In Figure 5.2(a) and (b) traces of net pile base load during the pore water pressure dissipation stage are shown. In Figure 5.2(a) the pile base load response reflected the pore water pressure changes in the surrounding soil showing an increase in load as the soil consolidated so dragging the pile base into the ground. In general the pile base loads were small and were later exceeded when working loads were applied reversing the direction of shear along the pile shaft in the process. In Figure 5.2(b) the pile load did not change significantly as the pore water pressure in the soil at the pile base remained fairly constant. However, the pile base load was high during the pore water pressure equilibrium stage and must be considered during the analysis of subsequent pile loading and rising groundwater events.

#### 5.2.2 Rising groundwater event

When equilibrium had been reached with the low pore water pressures indicated by the final points in Figure 5.2 the model was ready for modelling the rising groundwater event. Foundation loads were applied using either complete load tests or more frequently by applying a nominal working load. The initial vertical effective stress regimes were high for the nine tests using a surface water table and downward seepage as shown by line 'a' in Figure 5.3. The vertical effective stress profiles for the two tests using a sealed surface are presented in Figure 5.4.

For the tests where downward seepage was used, Figure 5.3, the loss in vertical effective stress in the region of the pile was of the order of 40% at all levels monitored by pore water pressure transducers. Figure 5.5 shows the increase in pore water pressure from test RW10 plotted against time. At the finish of the test pore water pressures were sub hydrostatic resulting in the vertical effective stresses being, on average, twelve percent higher than the very long term condition. Failure to reach full hydrostatic pore water pressure conditions was caused by time restraints on centrifuge access and by a modelling inconsistency. The modelling error was a result of the curved phreatic surface which exists in centrifuge testing. The base drain water level was controlled by the standpipe whose overflow level was set level with

the top of the sand surcharge. This results in a sub hydrostatic pore water distribution on the centre line where the pore water transducers were located. In the analysis, no correction to the measured pore water pressures have been made to account for the pile position offset from the centre line. The surface water table was kept close to the top of the sand layer in the centre of the model.

For the tests where the surface was sealed as shown in Figure 5.4, the pore water pressure did not get close to a long term condition as indicated on Figure 5.6 from test RW13, even though the rising groundwater stage lasted over two times longer than that shown in Figure 5.5 where downward seepage was present. The contributory reasons for the slow equilibration of pore pressures are: the lack of downward seepage which provides access to water from the surface thus reducing the drainage path length, and a rectangular excess pore water pressure distribution compared to a triangular one with water available top and bottom. There is also a possibility of unmonitored surface evaporation reducing pore water pressures near the surface.

### 5.2.3 Spin down

At the end of the test the centrifuge was brought to rest and the model returned to 1g. During this event the pore water pressures were monitored giving an estimate of the total vertical stress change and a rough indication of vertical total stress at each transducer level (some side friction on the tub sides may take up some of the total stress change). Figure 5.7 from test RW16 shows the readings of five pore water pressure transducers during spin down. The readings gave a check on total stresses calculated from transducer positions within the model (measured during model excavation) multiplied by an average bulk unit weight of the soil.

### 5.3 Moisture content at end of tests

Moisture contents were taken at the end of the test after spin down. Care was taken to prevent as much swelling as possible prior to sampling by closing the base drainage, removing any free surface water and by

taking the moisture content samples as quickly as possible. Figure 5.8 and 5.9 show the final moisture content profiles for all tests (except test RW7) where the initial preconsolidation pressure was  $1250 \text{ kN/m}^2$ . Figure 5.8 contains data from the eight tests where surface water was present during the model testing. Figure 5.9 contains the two tests where surface water was not present. In both sets of data there is a significant reduction in water content with increase of depth over the top 200mm. This trend reverses in the bottom 50 to 75mm and probably results from swelling due to water intrusion from the base drain. The scatter in data, especially in Figure 5.8 is a result of the variation in final vertical stress in the model as previously shown in Figure 5.3. In test RW11, marked with solid squares in Figure 5.8, the pore water pressure was reduced prior to spin down and this set of data forms the lower bound to the scatter of data points. All moisture content samples have liquidity indices between 0.18 and 0.27 at 50mm depth reducing to between 0.13 and 0.20 at 200mm depth. The Speswhite Kaolin used in the series of centrifuge tests had Atterberg limits of PL = 34% (Viggiani, 1992) and LL = 65% giving PI = 31%.

#### 5.4 Piezocone tests

The piezocone tests were carried out to assess the reduction in the strength of the clay due to a rising groundwater event. In centrifuge test RW16 a total of eight piezocone penetration tests were carried out to a clay depth of 190mm, typically 40mm below the base level of the model piles used in the other tests. The tests were carried out in a model with surface water and downward seepage similar to Figure 4.13 (a). Three tests were carried out with a variable depressed water table and five tests with near hydrostatic pore water pressures. The vertical effective stress conditions at the start of each test and rates of penetration are shown in Table 5.2.

Two different penetration rates were chosen,  $2.0 \text{ mm/sec}$  (tests 3,6,7 and 8) and  $0.2 \text{ mm/sec}$  (tests 1,2,4 and 5). The data provide a comparison of cone resistance at different rates of loading and shearing in soil with different effective stress regimes.

Atkinson and Salfors (1991) summarise cone penetration testing and report that cone resistance and when available sleeve friction are functions of soil strength. Correlations of cone resistance with deformation moduli are empirical and are therefore site specific.

#### 5.4.1 Piezocone test results

##### 5.4.1.1 Tests at 0.2mm/sec

In Figure 5.10(a) and (b) uncorrected cone stress and excess pore water pressure are plotted against penetrometer position below the clay surface (there was a 9mm sand surcharge on top of the clay layer). The data fall neatly into two distinct bands representing the two different effective stress conditions. Tests CPT1 and CPT2 carried out in the depressed pore water pressure regime lie above tests CPT4 and CPT5 carried out in the high pore water pressure regime in both uncorrected cone resistance and excess pore water pressure plots. The offset of the excess pore water pressure in Figure 5.10(b) is a result of the porous element of the cone being 12.5mm behind the tip of the cone which is used as the reference point. A correction of +12.5kN/m<sup>2</sup> (0.0125m by 10kN/m<sup>3</sup> by scale factor) to the excess pore water pressure would only be valid in the sand layer, where hydrostatic conditions exist, and has therefore not been applied. The pore pressure ratios ( $B_q$ ) were calculated using a formula suggested by Senneset and Janbu (1985) and supported by Atkinson and Salfors (1991):

$$B_q = \frac{u_t - u_0}{q_t - \sigma_{vt}} = \frac{\Delta u}{q_n} \quad (5.1)$$

where	$u_t$	-	measured pore water pressure
	$u_0$	-	back-ground pore water pressure
	$q_t$	-	cone resistance corrected for pore pressure in cone cavity (see Section 4.5.8)
	$\sigma_{vt}$	-	total vertical stress
	$\Delta u$	-	excess pore water pressure
	$q_n$	-	net corrected cone resistance

as shown in Figure 5.11.  $B_q$  was relatively constant for most of a penetration test and had values of approximately 0.2 for tests CPT1 and

CPT2 and 0.15 for tests CPT4 and CPT5.

Figure 5.12 shows the traces of net corrected cone resistance ( $q_n$ ) plotted against vertical effective stress for the four tests carried out at 0.2mm/sec. The four tests show that  $q_n$  has a high degree of correlation with vertical effective stress irrespective of the depth below ground level.

In Figure 5.13 the net corrected cone resistance ( $q_n$ ) is plotted against mean normal effective stress ( $p'$ ). The mean normal effective stress has been calculated using the relevant equations presented in Section 2.2 and the  $K_0$  relationships presented in section 3.5.2. The maximum and minimum vertical effective stress levels have been calculated from the stress regimes in the consolidation press and pore water pressures measured during centrifuging of the sample. These maximum and minimum vertical effective stresses allowed calculation of mean normal effective stress. The traces at the different effective stress regimes are visibly different but the trend, unlike that in Figure 5.12, does appear to pass closer to the origin. Calculation of horizontal effective stress has been carried out as carefully as possible. However, as shown by Al-Tabbaa (1987) and in Figure 3.8 the chosen line relating  $K_0$  on unloading to overconsolidation ratio is very much an average and some errors are likely.

#### 5.4.1.2 Tests at 2.0mm/sec

Figures 5.14(a) and (b) to 5.17 correspond to Figures 5.10 to 5.13 but are for piezocone tests carried out at 2.0mm/sec rather than 0.2mm/sec. Cone test CPT3 was carried out at a low water level (high effective stress regime) while cone tests CPT6, CPT7 and CPT8 were carried out at a high water level (low effective stress regime). As with the tests at the slower cone penetration rate the three tests at the high water level show good repeatability of uncorrected cone resistance and generated excess pore water pressure (see Figure 5.14(a) and (b)).

The pore pressure ratio, as in Eqn. 5.2, gave peak values of 0.5 and 0.4 for the test at low water level and high water level respectively as

shown in Figure 5.15. Again the repeatability of the tests was good.

Net corrected cone resistance ( $q_n$ ) results are plotted against vertical effective stress and mean normal effective stress in Figures 5.16 and 5.17. In both plots there is a strong degree of correlation of cone resistance with effective stress levels.

#### 5.4.2 Discussion of piezocone results

##### 5.4.2.1 Rate of penetration

Meigh (1987) reported on the effects of cone penetration rate on cone resistance and found that for a variety of both normally and overconsolidated clays, cone resistance increased with penetration rate (within the band of 1 to 20mm/sec for three different clays and 0.1 to 20mm/sec for London Clay). Almeida and Parry (1983a) found that for Kaolin, variation in penetration rate between 1 and 20mm/sec did not effect the measured cone resistance for either normally consolidated or overconsolidated deposits. The tests carried out in this research project were at 0.2 and 2.0mm/sec and demonstrated a reversal of the trend reported by Meigh. A possible explanation for this is found in a comparison of the excess pore water pressure response at the cone base shown in Figure 5.11 and Figure 5.15 in terms of pore water pressure ratio ( $B_q$ ). For the faster tests  $B_q$  averaged 0.45 while for the slower tests an average value of 0.15 was measured at depth. It seems likely that in the tests at 0.2mm/sec a combination of soil permeability (Kaolin has a relatively high permeability for a clay) and cone penetration rate has lead to partially drained conditions resulting in higher cone resistance. It may be that for Kaolin the threshold speed at which drained effects start to become apparent lies between 0.2 and 2.0mm/sec which is at the lower bound of the penetration rates investigated by Almeida and Parry (1983a).

##### 5.4.2.2 Correlation with undrained strength ( $S_u$ )

Foundations in stiff clay usually have their base resistance calculated in terms of  $S_u$  as described in section 2.1.1.2. Correlations of cone

resistance with undrained strength are not straightforward and have led to a variety of cone factors ( $N_k$ ) depending on cone resistance and plasticity. Almeida and Parry (1983a and 1983b) carried out a series of comparisons of cone penetration resistance with vane shear strength measured in calibration chambers and during centrifuge tests where cone resistance was related to the vane measured undrained shear strength by:

$$N_k = \frac{q_t}{S_u} \quad (5.2)$$

and

$$N_c = \frac{q_t - \sigma_{vt}}{S_u} = \frac{q_n}{S_u} \quad (5.3)$$

For a soil at a medium to high overconsolidation ratio (an average value of  $R = 6$  exists at the pile base level) a combination of data points from Almeida and Parry (1983a) and Francescon (1983) (after Almeida and Parry, 1983a) give values for  $N_k$  of 9.5 and  $N_c$  of 8.5. They noted that the measured cone bearing capacities were lower for reconsolidated kaolin than for naturally occurring clays which typically have values of  $N_k = 18 \pm 4$  (Meigh, 1987).

Stewart (1989) used the relationship proposed by Skempton (1954) relating undrained shear strength to plasticity index and vertical effective stress

$$\frac{S_u}{\sigma'_v} = 0.11 + 0.37 \text{ PI} \quad (5.4)$$

and the relationship linking undrained strengths for a one-dimensionally overconsolidated and normally consolidated deposits to overconsolidation ratio (Ladd et al., 1977)

$$\frac{(S_u/\sigma'_v)_{oc}}{(S_u/\sigma'_v)_{nc}} = R^m \quad (5.5)$$

to give for Speswhite and Spestone Kaolins (which are thought to have similar mechanical properties and both have a plasticity index of 31% as reported by Mair, 1979)

Using undrained strength calculated from Eqn. 5.6 and an assumed constant

$$\frac{S_u}{\sigma_v} = 0.22 R^{0.57} \quad (5.6)$$

$N_c = 8.0$  (which gives a better fit than 8.5) results in a predicted profile of cone resistance. This profile is plotted in Figure 5.18 with data from the four cone tests at 2.0mm/sec. The rapid gain in strength at low effective stress levels is predicted reasonably well. The measured cone resistance is over-predicted at intermediate stress levels corresponding to intermediate depths and converges at higher stress levels towards the base of the model for both low and high water levels. Some difference in predicted to measured results may be caused by variation in stress paths assumed in the predicted values and the stress paths actually followed by the clay sample. The results from Almeida and Parry (1983a) show that  $N_c$  was not a constant and for a particular soil type varied with overconsolidation ratio. However, at high overconsolidation ratios  $N_c$  did not vary significantly. This allowed comparisons to be made of undrained shear strength before and after a rising groundwater event using the same cone constant.

#### 5.4.2.3 Correlation with drained strength

The tests carried out at 0.2mm/sec produced a set of results which, while not consistent with fully drained conditions, as shown by the generation of excess pore pressure evident in Figure 5.11, do display some aspects of drained behaviour. In Figure 5.12 there is a strong reliance of cone resistance with vertical effective stress and which implies a cohesion intercept. In Figure 5.13 (cone resistance against mean normal effective stress) the general trend is closer to passing through the origin if the high cone resistance at low effective stress level is attributed to peak friction angles larger than  $\phi'_{cv}$  on the Hvorslev surface. The difference in the tests at low and high water table in Figure 5.13 is disappointing and may be a result of errors in the calculation of horizontal effective stress.

#### 5.4.2.4 Comparison of drained and undrained strength

The effect of the rising groundwater event on drained and undrained strength is different. If Figures 5.12 and 5.16 are compared it is

clear that the percentage reduction in the partially drained strength is significantly larger than the reduction in undrained strength, approximately 30.5% compared to 24% respectively based on the piezocone tests or 20% (undrained strength reduction) from Eqn. 5.6 at the level of the pile base in the other centrifuge tests for a 40% reduction (approximately 250 to 150kN/m<sup>2</sup>) in  $\sigma'_v$ . The results have further ramifications with respect to the foundation load tests discussed in the next section. Foundation loading took place using a constant rate of loading approach. For a typical foundation peak load was reached in 300 seconds model scale. At this rate of loading it is likely that nearly fully drained conditions existed and as such foundation base resistance measured was approaching a long-term maximum for the settlements obtained.

The penetration tests carried out by Almeida and Parry (1983a) incorporated an average shaft friction measurement. They found that shaft resistance reduced with decreasing penetration rate for a soil with overconsolidation ratio of 10. For the rate of pile penetration arising from the constant rate of loading an extrapolation of the findings of Almeida and Parry suggest the shaft resistance measured during loading will be fully drained and a minimum.

### **5.5 Piled foundation load behaviour prior to rising groundwater**

The results of the piezocone tests described in section 5.4 demonstrate that the undisturbed ground experiences a reduction in both undrained and partially drained bearing capacity during a rising groundwater event. In this section the results of piled foundation load behaviour before the rising groundwater event will be presented. This will provide an initial framework in which foundation movements during a rising groundwater event can be discussed. In Table 5.3(a), (b) and (c) the loading history of all the foundations are presented. Loads are presented in Newtons (N) and are appropriate to model scale (equivalent prototype loads can be determined by multiplying by the scale factor of  $n^2$ ). Stresses on foundation shafts and bases are reported in kilo Newtons per meter squared and are appropriate to both model and prototype alike as demonstrated in section 4.2. Foundation shaft and base loads use the

following definitions:

$$P_t = P_s + P_b = q_s A_s + q_b A_b \quad (5.7)$$

$$q_s = \frac{P_{t1} + W_p - P_{b1}}{A_s} \quad (5.8)$$

$$P_b = \frac{q_{b1} - W_s}{A_b} \quad (5.9)$$

where	p	-	Mobilised load (t = total, s = shaft, b = base)
	$P_{t1}$	-	Load registered on top load cell
	$P_{b1}$	-	Load at pile base level
	q	-	Mobilised stress (s = shaft, b = base)
	$W_p$	-	Pile self weight plus unregistered weight of load cell
	$W_s$	-	Weight of excavated soil
	A	-	Area

The load measured at the base of the pile is considered to be the gross pile base load. For calculation of the actual load mobilising base resistance the weight of excavated soil is subtracted to obtain the net pile base load. In the case of under-reamed piles a similar approach is adopted. The annulus of soil above the pile under-ream surrounding the pile shaft is not considered to act on the pile base after settlement has taken place and is therefore not included in calculation of net pile base load.

For piled foundations, shaft and base loads change during the main phases of a centrifuge test as a result of soil movements and effective stress changes. The loads at all stages of the centrifuge test are required to carry out full analysis of the test. An incorrect distribution of load (load carried by the shaft compared to load carried by the base) on a pile prior to a rising groundwater event will lead to irregular behaviour when the pore water pressure rises. Shallow foundations are assumed to interact with the ground only via their base and are not susceptible to incongruous load distributions.

### 5.5.1 Piled foundations during initial pore water pressure equilibrium stage

In section 5.2.1 of this chapter reference was made to pile bases attracting load as a result of consolidation of the surrounding soil after spin up. This problem was recognised early on in the series of tests and by the time the fourth test was attempted a downward hydraulic gradient system (described in Section 4.6) was working for the final consolidation stage in the preparation press to reduce ground movements in the vicinity of the pile during model preparation and after spin up. However, even for simple model configurations it was not possible to prevent some soil consolidation after spin up which resulted in small, but for slender piles significant, pile base loads prior to foundation loading. Previous research into load displacement response of piles has shown that pile shafts mobilise full resistance after much smaller displacements than pile bases (see Section 2.1.2). Therefore for slender, nominally friction, piles loading to working loads would not result in the mobilisation of significant base load. To find the piles which had been affected by these extra base loads the base response was monitored during foundation loading as discussed in Section 5.5.2. When there was an initial base load that did not increase during pile loading the pile base was assumed to be non-standard. This criterion for modelling prototype situations accurately suggests that only piles which mobilise end bearing resistance at working loads may be modelled correctly in the centrifuge tests. Two piles displayed no increase in base load when subjected to working loads. Pile 2 (a slender 12.7mm diameter pile) in test RW14 displayed a low mobilised shaft friction together with a high base load resistance and was clearly affected by consolidation of the surrounding soil. The movements of this pile, and other non-instrumented slender piles, must be considered to have been affected by consolidation of the ground after spin-up. Settlement behaviour during the rising groundwater event was assumed to be a lower bound to the settlement that would be measured without this initial high base load. Pile 1 in test RW6 displayed no increase in base load during loading. The fact that base load was small (net load less than zero) combined with a shaft friction approaching full capacity which suggests

that the pile was near to prototype conditions after loading and its behaviour will be compared with the remaining piles.

### 5.5.2 Initial foundation loading

Prior to the rising groundwater event foundation load tests to failure (typically a displacement of 10% foundation base diameter, section 2.1.1) were carried out in tests RW1, RW3, RW4, RW6 and RW7 as shown in Table 5.3(a) and (b). In tests RW3 and RW4 a distinction between pile shaft and base capacity was possible. In tests RW10 and RW15 where under-reamed piles were being modelled, the ultimate shaft capacity was also obtained as the settlement required to mobilise working base capacity exceeded that needed to mobilise full shaft capacity. The load-displacement response of the five piles that were loaded to failure are shown in Figure 5.19. The two piles for which there was distinction between base and shaft load measurement in Figure 5.19(a), show a relatively soft response of the base compared to the shaft, similar behaviour is displayed by prototype piles. Two of the piles in Figure 5.19(b) show a more linear increase in load with displacement after the initial stiff response of the shaft observed in the other two piles or in the piles in Figure 5.19(a). This is because the loading for these two piles continued until a displacement of 10% pile base diameter has been achieved while for the other piles some of the displacement was due to settlement at constant load. Loading of the pile in test RW4 was stopped prior to reaching a settlement of 10% pile base diameter due to the onset of large movements, possible related to cracking of the concrete under-ream noted after the test.

Calculations of the parameter  $\beta$  (Eqn. 2.2) were carried out using an average vertical effective stress for the piles where full mobilisation of skin friction was achieved. An average value of  $0.3 \pm 0.025$  was obtained from four piles at low water table where full shaft friction on initial loading was seen to be mobilised (P1 in RW3, P1 in RW7, P1 in RW10 and P1 in RW15). This combined with a pile shaft friction angle of  $16^\circ$  (this was measured during a reversal stage of a standard shear box interface test, Tahzeem 1993) gives a coefficient of earth pressure at the shaft of 1.05. The equations presented in section 2.2 predict

significantly higher values of  $K_0$ . The change in  $K_0$  is attributed to reduction in radial effective stress due to the installation procedure adopted for pile installation. Loss in prototype radial stress would be less due to the ameliorating process of placing concrete which acts to re-establish the radial stress prior to concrete curing. Finite element analyses of model and prototype pile installation processes have been carried out in Chapter 6.

When piles were unloaded after pile testing the distribution of shaft to base load was not the same at similar loads during the loading stage. The pile base unloads more slowly than the shaft, occasionally resulting in the average shaft friction acting to push the pile base into the ground as shown in Figure 5.20(a) taken from the under reamed pile in test RW4 (in Figure 5.20 overload refers to additional base, or shaft, load during unloading after load testing, compared to the load distribution during initial loading). On initial unloading, pile base and shaft load reduce. On further unloading the rate of base unloading reduces while the shaft maintains its rate of unloading. By the time that the required working load is reached the net shaft load is negative and the base is carrying all the head load and the component of negative shaft load. The straight pile in test RW3, Figure 5.20(b) shows a similar trend except that at working load the net shaft stress is still acting to carry some head load. In this case the magnitude of average shaft stress after loading is approximately 59% the maximum shaft stress that would normally be mobilised at the working load.

## 5.6 Foundation behaviour during a rising groundwater event

In the presentation of foundation behaviour during a rising groundwater event five tests will be discussed in detail. Each test demonstrates a different facet of foundation behaviour during a rising groundwater event and is typical of other tests not presented in detail. The results of all successful tests are used in providing the final picture of foundation behaviour.

Once the foundations have come into equilibrium with their working loads the pore water pressure in the base sand aquifer is increased rapidly in

one or two steps. During the following period the pore water pressure in the clay comes into equilibrium with the increased pore water pressure in the basal sand resulting in soil and foundation movements. A full set of figures and basic description for each of the eleven most successful centrifuge tests and the piezocone test (RW16) is given in Appendix A.

#### 5.6.1 Tests RW3 and RW6: Comparison of pre-loaded and non pre-loaded piles

In these tests the behaviour of a pre-loaded pile is compared with that of a non pre-loaded pile. Test RW3 provides the behaviour of a pre-load tested pile during a rising groundwater event and test RW6 allows comparison of a load tested and a non-load tested pile.

The sequence of loading and unloading to the required working load of the pile in test RW3 has already been described in section 5.5.2 and Figure 5.20 (b). At the onset of the rising groundwater event the pile had a factor of safety of 2.1 (calculated using an ultimate load from a continuous rate of loading test) and a load distribution between shaft and base of 109N and 76N respectively. This compares with the load distribution of approximately 180N and 5N (shaft and base) at the same total load of 185N on initial loading.

The pile load distribution during the rising groundwater event is shown on Figure 5.21. Vertical effective stress at 150mm clay depth (corresponding to pile base level) is plotted along the abscissa. The initial pile load distribution lies on the right hand side of the figure corresponding to initial high effective stress regime. The pile load distribution is plotted as the ordinate. During the rising water event the pile load distribution changes as the soil around the shaft swells resulting in an uplift of the pile and an unloading of the base. At the end of the rising groundwater event the shaft load has increased to 180N. This is below ultimate shaft load for the existing effective stress regime ( $P_s = 234N$  for  $\sigma'_{v, av} = 90kN/m^2$ ) as shown in Figure 5.22. Here the ultimate shaft capacity measured at three different effective stress levels at which full shaft friction was mobilised during test RW3 is plotted against average vertical effective stress along the pile shaft.

If further swelling of the soil had occurred it is anticipated that increased shaft friction would have been mobilised resulting in uplift of the pile base (and unmeasured tension in the lower part of the pile).

Test RW6 was designed to assess the effect of the redistribution in pile load during a rising groundwater event. Pile 1 was instrumented with a base load cell and was not load tested prior to raising the groundwater level. Pile 2 was not instrumented and was load tested. The pile load distributions are shown in Table 5.4 before and after the event for Pile 1 and calculated values for Pile 2. Figure 5.23 shows the pile movements during the rising groundwater event. Vertical effective stress at the pile base level is plotted on the abscissa with pile and surface movements on the ordinate. The inset figure shows the pore water pressure profiles associated with the four indicated effective stresses on the main figure. The foundation loads during the same period are shown on Figure 5.24. The two total loads remain constant during the early part of the test but Pile 2 loses load after  $\sigma'_{v150}$  decreases below  $160\text{kN/m}^2$  beyond which point test results are not reported. The signals are noisy due to interference on the centrifuge slip rings. However, it is possible to detect that Pile 1 shaft load increases during the early part of the test prior to a slight decrease towards the end of the test at which stage full shaft capacity will have been mobilised. Pile 2 will have behaved similarly to the pile in test RW3 during the rising groundwater event both having started with an overloaded pile base. The change in effective stress during this test (RW6) was larger than in test RW3 allowing larger differential settlements between pile and surface providing more opportunity for Pile 2 to re-establish a pile load distribution similar to Pile 1.

The movements associated with each pile, shown in Figure 5.23, demonstrate that the effect of pre-loading a pile is to reduce settlement relative to the surface during a rising groundwater event. Pile 2 settled less than Pile 1. Although both piles in test RW6 were not instrumented the observed behaviour of pre-loaded piles in tests RW3 and RW4 (a full record of behaviour during a rising groundwater event for each is included in Appendix A) suggests that the effect of preloading is to reduce pile base settlement relative to the ground surface during

a rising groundwater event. The base load for Pile 1 in test RW6 increased marginally during the latter part of the test suggesting a small base settlement. For Pile 2 the base settlement is likely to have been zero or possibly negative due to the pile base moving upwards relative to the surrounding soil.

The behaviour of test RW7 (reproduced in Appendix A), where two piles similar to those used in test RW6 but with lower factors of safety, reproduced a similar trend in behaviour. The piles settled more than those in test RW6 due to the smaller factor of safety and the pre-loaded pile settled less than the non pre-loaded pile.

#### 5.6.2 Test RW10: Influence of initial factor of safety on settlement

In this test the influence of initial factor of safety on pile movements during a rising groundwater event was investigated. Two under-reamed piles with base area twice that of the shaft cross-section and depth 6.5 times the base diameter were used. Neither pile was load tested prior to the rising groundwater event. The calculated initial factor of safety on ultimate load prior to the rising groundwater event was 1.8 ( $P_s + P_b/3.3$ ) for Pile 1 and 2.1 ( $P_s + P_b/5.5$ ) for Pile 2. The partial factors on pile base load are calculated assuming that on initial loading full shaft capacity is loaded and has a partial factor of 1.0.

During initial loading of Pile 1 the displacement was 0.38mm which fully mobilised the shaft friction as can be seen in Figure 5.25 where the shaft stress reaches a maximum value and then reduces to an equilibrium level as excess pore water pressures decay. Pile 2 settled by 0.1mm which when compared with the load settlement of the shaft of pile 1 was enough to fully mobilise shaft friction. During the rising groundwater event there was a measured transfer of load from the shaft to the base of Pile 1 as shown in Figure 5.26. The initial peak in total load (due to temporary malfunction of the loading mechanism) after 1000 seconds into the test is not considered to influence to overall behaviour of the pile. There is a 10% reduction in mobilised shaft stress during the rising groundwater event.

Figure 5.27 shows the displacement of the two piles and the ground surface plotted against far field vertical effective stress at the pile base level. The low factor of safety pile (Pile 1) is seen to settle 0.24mm more than the high factor of safety pile (Pile 2). Both piles are seen to settle significantly (1.28mm and 1.04mm) relative to the ground surface. At the end of the test the pore pressures were slightly sub-hydrostatic as shown in Table 5.4 where pore water pressure is quoted against clay depth measured from the sand-clay interface. Any further swelling is likely to be near to the surface and would result in ground surface swelling and a small reduction in horizontal stresses and shaft friction. This would cause an absolute downward movement of both piles; there was some evidence of this type of response towards the end of the test.

Test RW11 in which two slender piles with a length to base diameter ratio ( $L_b/D_b$ ) of 12.0 with different initial factors of safety were tested together and showed a similar result with the low factor of safety pile settling more than the high factor of safety pile. A buried plate at the same level as the pile bases showed that the lightly loaded pile did not settle significantly relative to the surrounding soil. The movement of the plate also suggests that the piles in test RW10 settled significantly compared to the surrounding soil (approximately 0.75mm and 0.5mm for Piles 1 and 2 respectively).

### 5.6.3 Test RW13: The behaviour of different foundation types (and different initial pore water pressure distributions)

In this test the displacements of a pad, a pile and the ground surface were compared during a rising groundwater event in which the pore water pressure profile was initially hydrostatic extending from a negative value at the surface. The rising groundwater stage of test RW13 lasted 43 hours during which time the pore water pressure moved half way to equilibrium in the region influencing the foundation behaviour. Figure A.RW13.1 in Appendix A shows the ever decreasing rate of increase in pore pressure with time. It was not possible to continue the test to achieve full equilibrium. The results can, however, be compared with those tests where a perched surface water table and downward seepage

existed prior to the rising groundwater event. A schematic of the different pore water pressure profiles before and after the rising groundwater event is given on Figure 4.13.

Figure 5.28 shows the foundation behaviour during the rising groundwater event. Three displacement results are presented, surface, pad and pile (the pile had a 12.7mm diameter straight shaft and was 150mm long). The first point to observe is that the magnitude of soil swelling compared to the previous tests in Figures 5.23 and 5.27 is large especially when considering that test RW13 had not reached equilibrium. The large ground heave is caused by the large percentage loss in effective stress near the soil surface which does not occur to the same extent when a perched water table exists. The second point to observe is that the pile settlement relative to the ground surface is also large (the absolute pile movement is small) compared to Pile 1 in test RW11 (reproduced in Appendix A, Figure A.RW11.3) where the pile loads were similar ( $p_w = 230-235N$ ) but test RW11 had a perched water table. The final point to observe is that of pad settlement. During pad loading to a working load of  $p_w = 150N$  a settlement of 0.12mm was observed. During the following rising groundwater event a further 0.69mm settlement occurred due to the reduction in effective stress near the surface. The pad was seated on the clay surface where at the start of the test the vertical effective stress was approximately  $90kN/m^2$  due to negative pore pressures. If the rising groundwater event had reached equilibrium the vertical effective stress would have reduced to zero. However, at the time when the test was stopped it is estimated that the vertical effective stress at the surface was approximately  $40kN/m^2$  resulting in approximately a 42% reduction in the vertical effective stress in the surrounding soil. Further swelling would have led to significantly larger pad settlement and ultimately failure of the clay foundation.

The load behaviour of the foundations is shown in Figure 5.29. The pad load remained fairly constant during the event. The initial slight increase in load during the first part of the test was due to leakage in the loading system which was corrected before the overload became large. The pile head load was constant but there was an unexpected load transfer from the pile base to the pile shaft. During initial loading a

displacement of 0.12mm occurred (the initial pile load at the start was 150N due to pile self weight) and for this displacement it appeared that full shaft capacity was mobilised. The reason for an increasing shaft capacity during the test is not clear from the results obtained but may be due to increased radial stresses acting on the pile shaft caused by a deterioration of hoop stress and a reduction in "open shaft" stability as the negative pore pressures reduce. The change in load distribution will have acted to reduce settlement of the pile during the rising groundwater event though the settlements were still large demonstrating the different mode of behaviour caused by different initial pore water pressure distributions.

In the tests modelling initial negative pore pressures at the surface downward hydraulic gradient method was not used due to experience gained by Stallebrass (1993) in a separate series of tests. This means that the soil near the surface was swelling in a primary unload stress path rather than swelling back to a previous low stress state. This will tend to exaggerate the magnitude of heave and also bearing capacity reduction due to larger horizontal effective stress changes than would otherwise be the case. However, the general trend of behaviour observed above will be unaltered.

#### 5.6.4 Test RW15: Comparison of two different geometry piles

In this test the behaviour of two different foundations were compared. Pile 1 was an under-reamed pile and Pile 2 was slender; both piles were founded at the same depth of 150mm into the clay. Full details on the foundations' geometry are included in Table 5.1. On initial loading to 290N Pile 1 settled by 0.25mm and appeared to mobilise full shaft friction as would be expected in an under-reamed pile. Pile 2 settled by approximately 0.025mm (the resolution of the LVDT was 0.004mm) on initial loading to 164N suggesting that the load increment was taken by shaft friction. A small overload (16% of  $p_w$ ) of the pile occurred during loading. This could lead to an incorrect load distribution in Pile 2 prior to the rising groundwater event, however in light of the small settlements during loading it is considered unlikely that significant base load was mobilised. Prior to the rising groundwater event Piles 1

and 2 had initial factors of safety of 2.4 and 2.0 respectively. Early on in the rising groundwater event Pile 2 suffered an increase in load to 330N corresponding to a factor of safety of 2.1 (as reported in Table 5.3c). It is estimated that this extra load will have caused 0.09mm settlement which has been removed from the displacement recorded during the rising groundwater event.

The displacement behaviour of the piles, a buried plate and the ground surface during the rising groundwater event are displayed in Figure 5.30. The results show the different magnitude of settlement associated with different pile type. The slender pile, Pile 2, settled significantly less than the under-reamed pile and was seen to move in unison with the buried plate. Pile 1 settlement is attributed to both soil swelling passed the shaft and due to settlement of the pile base. Pile base settlement is caused by transfer of load to the pile base from the shaft (this was measured in the early part of the test prior to a breakdown in the signal measurement), a reduction in soil stiffness and the necessity to mobilise a larger proportion of the drained bearing capacity (due to the larger load and reduced bearing capacity). The surface heave monitored during the test was larger than in the other tests with a perched water table. This was due to the longer swelling period (22 hours compared to other tests when the swelling stage was stopped after 11 hours) and due to the lower initial pore water pressures prior to the rising groundwater event.

In test RW14 where a similar set-up was used similar trends of behaviour were observed. The under-reamed pile (with a lower load than the corresponding pile in test RW15) which, while settling into the soil at the pile base level, resulted in significantly less settlement than the pile in test RW15 at similar values of ground surface heave. In test RW14 the base of the slender pile (Pile 2) unloaded from an initially high load (Figure A.RW14.3) suggesting pile base uplift. This was not indicated by a comparison of plate and pile displacements suggesting that the plate had experienced limited uplift due to friction on its narrow shaft.

## 5.7 Comparison of piled foundation load capacity before and after a rising groundwater event

In section 5.6.1 it was shown that load testing a foundation prior to a rising groundwater event results in non-standard behaviour during the subsequent rising groundwater event. This led to a reduction in the number of piles load tested prior to the rising groundwater event. However in several tests load capacities of the composite pile (shaft and base) or just load capacity of the shaft were obtained before and after the rising groundwater event allowing a comparison to be made.

### 5.7.1 Shaft capacity

In section 5.5.2 it was suggested that the process of pile installation caused significant reduction in radial stress acting on the pile. The actual radial stress acting on the pile is unknown. It is therefore not possible to undertake a rigorous analysis of the mechanism of loss of shaft capacity during a rising groundwater event.

However, by comparing the average shaft friction of individual piles with the change in vertical effective stress, as well as the predicted change in far field horizontal effective stress a mode of behaviour of the model pile shaft may be obtained. A summary of the results from tests RW10 and RW15 is shown in Table 5.5. In calculating horizontal effective stress the equations presented in Section 2.2 have been used taking account of stress levels generated during sample preparation and during centrifuge testing. The results confirm that loss in shaft capacity is less than loss in vertical effective stress. It also appears that for the model piles where reductions in radial stress were caused during pile installation, the percentage reduction in shaft capacity is less than the percentage reduction in calculated horizontal stress. The comparison of shaft capacity and far field horizontal effective stress is very much influenced by correct prediction of the horizontal effective stress. This must be taken into account when making any firm conclusions relating  $q_s$  to  $\sigma'_h$ .

### 5.7.2 Base capacity

During the series of tests it was noticed that if a pile was load tested before and after a rising groundwater event, failure loads were not significantly different. However, if two similar piles were tested at different ends of a rising groundwater event a loss in load capacity was obtained when comparing the two piles. A summary of measured and calculated pile base capacities is shown in Table 5.6. The seven points are plotted on Figure 5.31(a) showing a reasonable correlation of pile bearing pressure against mean normal effective stress as demonstrated by Troughton and Platis (1989) using a prototype pile test in sand. The same pile base capacities are plotted against vertical effective stress in Figure 5.31(b). The apparent cohesion intercept may in part be due to fully drained conditions not being obtained but is considered mainly to be due to the relationship between base capacity and mean normal effective stress. This result compares well with the piezocone tests at 0.2mm/sec where there was a stronger correlation of cone resistance with  $p'$  rather than  $\sigma_v'$ .

### 5.8 Factors affecting foundation movements during a rising groundwater event

In section 5.6 the results from four tests during rising groundwater events were presented. In this section the results from all the successful tests will be brought together to allow a broader picture to be drawn.

In section 5.5.1 it was suggested that the slender pile settlements were affected by initially high base loads due to negative skin friction caused during consolidation of the ground after spin-up. In section 5.6.1 it was shown that load testing a pile would reduce settlement relative to the ground surface during a rising ground water event. The data from tests RW6 and RW7 show that the effect of load testing is to reduce pile settlement during a rising groundwater by on average 1% of the pile base diameter. For the slender piles the effects of load reversal will be less due to smaller end bearing resistance mobilised (the piles were not tested to failure) and by the smaller diameter pile

base. It has therefore been decided to include these piles, in the following sections, with the other non pre-loaded piles with the understanding that settlements observed are a lower bound.

#### 5.8.1 The influence of factor of safety on pile settlement

During the series of centrifuge tests the factor of safety was varied for the three different pile geometries used. The initial factors of safety are presented in Tables 5.3 and 5.4.

In comparing the different tests it is necessary to find similar points in each test. From Table 5.4 (and Figure 5.3a where  $\sigma'_v$  is plotted against depth) it can be seen that the pore water pressures before and after the rising groundwater events were not identical. In addition, the thickness of the clay layer varied by approximately  $\pm 4\%$  from the average final thickness of 265mm (see Table 5.1) or by 9% of the thickness below pile base level. In comparing results from different tests it has been decided to compare foundation settlements at points in time when the average volumetric strain (corresponding to vertical strain for one-dimensional conditions) is the same in all models. A value for this average volumetric strain ( $\epsilon_{v, ave}$ ) of  $-0.6\%$  (i.e. swelling) was chosen. This value lies towards the end of most model rising groundwater stages. Plotting settlements at similar strain levels was chosen to overcome the differences in clay thickness which would effect the ratio of swelling above and below the pile base level if a constant magnitude of soil heave had been used. By using  $\epsilon_{v, ave}$  the magnitude of soil swelling above the pile base will be similar in all tests.

The results of ten piles used in 6 centrifuge models are shown in Figure 5.32. The piles are grouped together using straight lines to differentiate between the three slenderness ratios used. For each pile type the results follow the expected trend of increasing settlement with decreasing factor of safety. It appears that factor of safety plays a more significant role in the behaviour of the under-reamed piles than for the more slender piles as seen by the slope of the average lines through groups of different pile types.

In Figure 5.33 the approximate (upper bound) pile movement attributed to settlement of the pile base, as indicated by the buried plates (these may have moved upwards slightly as suggested in Section 5.6.4), has been isolated. The empty rectangular points are real data while the filled rectangles are taken from test RW10 where the plate settlement was estimated using data from the other three tests. The approximate results show that the slender pile settlement was dominated by heave passed the pile shaft. This is in contrast to the larger based piles which obtain a significant proportion of their settlement from base settlement.

### 5.8.2 The influence of slenderness ratio on pile settlement

The data in Figures 5.32 and 5.33 have been plotted in Figures 5.34 and 5.35 to allow examination of the effect of slenderness ratio on pile settlement. In Figure 5.34 pile settlement is plotted against slenderness ratio with average settlements for three different factors of safety shown by solid lines. The average lines show that for piles of identical length and with similar factor of safety settlement is controlled by pile geometry. The same is true for the approximate pile base settlement as shown in Figure 5.35. The piles with a higher slenderness ratio do not mobilise full shaft friction after the groundwater level rise and will experience pile base heave as suggested by the average line at  $L_s/D_p = 12$  for a pile factor of safety of 2.3.

### 5.8.3 The influence of initial pore water pressure profile on foundation movements

Data from the two piles used in tests RW12 and RW13 have been processed in the manner described in sections 5.8.1 and 5.8.2. The different initial pore water pressure profiles in Figure 4.13 result in different patterns of swelling as the groundwater level rises. For downward seepage the emphasis is on swelling near the base of the model while for a model with a depressed hydrostatic profile the emphasis is on heave in the near soil surface strata. It is therefore not strictly correct to compare swelling in models with different initial pore water pressure profiles at the same strain level since this was intended to isolate similar magnitudes of heave above pile base level in each model.

However, to demonstrate the different pattern of heave associated with a groundwater level rise originating from a depressed hydrostatic profile a comparison has been made at similar strain levels. Figure 5.36 shows data for the straight piles taken from Figure 5.32. The two piles from tests RW12 and RW13 had measured foundation settlements well in excess of the trends of pile settlement for piles where a perched water table exists.

#### 5.8.4 The influence of pile length on pile settlement

With the exception of the piles in test RW7 all piles had their bases at 150mm below the top of the clay layer. The piles in test RW7 had their bases 160mm below the top of the clay layer (this additional length was due to a failed attempt at under-ream construction after which the pile base was installed 10mm deeper). It is therefore not possible to make definitive comments on the influence of foundation length on settlement during a rising groundwater event. It is, however, clear that there are differences in behaviour between shaft dominated piles and end bearing dominated piles. The trade off between a long friction pile which will experience soil swelling past the pile base over a longer length and a pile with a large base which will suffer settlement of the base should be considered if pile settlement due to a rising groundwater event is to be minimised.

#### 5.9 Summary

Centrifuge model tests have been used to explore foundation behaviour during a rising groundwater event. The model tests have allowed observation of foundation response during simulated rising groundwater events and the performance of piezocone penetration tests before and after a rising groundwater event.

The results have shown that:

- o Pile end resistance under predominantly drained conditions is linearly related to the mean normal effective stress. Percentage loss in undrained strength, during a rising groundwater event, was

shown to be less than the percentage loss in drained strength. Pile base capacity should therefore be considered in drained strength terms for situations where effective stress reductions are anticipated.

- o For the model piles used the percentage reduction in shaft friction was less than percentage loss in calculated far field horizontal effective stress. The ultimate shaft friction stress measured during load testing was less than that calculated for a wished-in-place pile and residual strength of the clay at the interface.
  
- o Shallow foundation settlement is predominantly a function of the initial pore water profile. In situations where a perched water table exists shallow foundation settlement is limited in contrast to the case where no surface perched water table exists when significant settlements will occur.
  
- o Deep bored foundation settlement is a function of pile geometry (straight and slender or under-reamed), initial factor of safety and initial load distribution on the shaft and base. The largest settlements were measured for under-reamed piles with low initial factors of safety.

The majority of this chapter is concerned with finite element modelling of bored pile behaviour during installation and when subjected to a rising groundwater event. Modelling of pile installation and subsequent loading followed by rising groundwater sequences was carried out. A second series of finite element analyses modelled the behaviour of wished-in-place piles during a rising groundwater event. The finite element sections are followed by predictions of centrifuge model pile settlement during a rising groundwater event using the method outlined in Section 2.4.

### 6.1 Introduction: finite element modelling

A series of finite element method analyses has been carried out to predict model and prototype pile behaviour during a rising groundwater event using the Stallebrass three surface kinematic hardening model described in Section 3.4. These analyses commenced with a simplified procedure for modelling pile installation sequences relevant to the centrifuge model piles and normal prototype conditions. The pile installation analyses were successful and demonstrate different stresses in the ground around the pile due to the two different installation sequences. The analyses of the rising groundwater stages were less successful due to the connection between pile and soil elements. A possible explanation of the problem is presented together with potential modelling changes that could be used to overcome the problem.

A series of analyses following on from the end of the pile installation stage was carried out in which the pile shaft was modelled as a smooth vertical boundary. Although these analyses deviated from real conditions where the pile shaft is a friction controlled boundary (allowing slip between elements) they allowed an investigation of the effects of pile installation on stress changes during the rising groundwater event for model and prototype piles. The analyses have produced some unexpected results and highlight the stress conditions that are most likely to result in different magnitudes of pile shaft capacity change during a rising groundwater event.

The finite element analysis part of this chapter finishes with a series of analyses of wished-in-place prototype piles using the Schofield model. The analyses were carried out to assess the performance of the Schofield model for modelling piles in a rising groundwater environment.

## **6.2 Introduction to the finite element program - CRISP**

All the analyses have been carried out using the finite element program CRISP (CRITICAL State Program). The program was written in the Cambridge University Engineering Department and the basic form of the program is presented by Britto and Gunn (1987).

The program has taken on an organic form which allows users to implement different soil models within the general CRISP framework. The three surface kinematic hardening model presented in Section 3.4 has been formulated and implemented in CRISP at City University by Stallebrass (1992). The Schofield model is a standard constitutive soil model in CRISP and has not been altered for the analyses carried out.

### **6.2.1 Types of analyses**

Analyses may be carried out in axisymmetric or plane strain conditions. Drainage conditions may be undrained, consolidation or fully drained. The analyses reported in this chapter were all axisymmetric consolidation analyses. The consolidation analysis utilises theory by Biot (1941) which models the volumetric changes of a soil matrix as a function of both stress change and time change in a three dimensional framework. Analyses may be stand alone analyses or continuation analyses. The latter start from the end of a previous analysis and use the soil state at the end of the preceding analysis as the in-situ conditions.

### **6.2.2 Element types and boundary conditions**

A wide range of elements is used with the general program CRISP93, including linear and cubic strain triangles and linear strain quadrilaterals, bar and beam elements and total stress slip elements. However, in the version in which the Stallebrass model is implemented

only linear strain and cubic strain triangles are, at present, available. The boundaries of the mesh may be either displacement or stress controlled. The majority of the analyses used displacement controlled boundaries, but two investigative analyses incorporated sections of the mesh adjacent to the pile with either strain or stress controlled boundaries. The analyses using the Schofield model used linear strain quadrilaterals arranged in the same pattern as pairs of triangles used for the Stallebrass model analyses.

### 6.3 Modelling of pile installation

Two separate analyses were carried out which modelled the pile installation processes. In the first analysis (1PIEXC) a simplified prototype pile installation sequence was followed. A 15m deep 0.8m radius hole was excavated unsupported. Stresses representing hydrostatic concrete pressure, with unit weight  $24\text{kN/m}^3$ , were then placed on the shaft sides and base. The hydrostatic stresses were then replaced with solid concrete elements from the base upwards. Finally a long period was provided to allow full dissipation of excess pore water pressures generated during pile installation.

In the second analysis (1P2MOD) a pile was installed in a mesh of centrifuge model dimensions and in-situ stresses representing those after downward hydraulic gradient consolidation in the preparation press described in Sections 4.5.4 and 4.6. The pile shaft was formed at 1g prior to placing the pile elements. This was followed by a simulated acceleration of the finite element model to model centrifuge spin-up.

The sequence followed in both analyses was similar to the sequence of pile excavation steps used by Kutman (1986) and Pantelidou (1994) where the effects of diaphragm wall installation was being examined in a plane strain environment.

The two analyses allow comparison of model and prototype pile installation sequences and resultant stress fields around the piles. A summary of the two analyses is included in Table 6.1.

### 6.3.1 Mesh and material properties

The mesh used in the these analyses is shown in Figure 6.1. It comprises 316 vertex nodes and 616 elements of which 568 have soil properties and 48 concrete properties. The mesh is fixed in space using roller bearings on both vertical sides and full fixity along the base. The axis of symmetry is the left boundary of the mesh. A large number of elements were concentrated around the left side of the mesh in the zone where the pile was installed and where stress gradients were highest. The remainder of the mesh has reasonably fine elements in the vertical direction to enable the rising groundwater event to be modelled. The dimensions of the prototype scale mesh are 18m radius and 25.5m depth for analysis 1PIEXC. The model scale mesh for analysis 1P2MOD has dimensions of 1/100 that of the prototype scale mesh. The dimensions were chosen to be compatible with the centrifuge models in which the pile position was off centre. The material properties adopted in the analyses are presented in Table 6.2. The material properties were obtained from the triaxial tests presented in Chapter 3, Stallebrass (1990), Viggiani (1992) and Al-Tabbaa (1987).

### 6.3.2 In-situ stress conditions

The analyses require the input of a set of in-situ effective stresses and boundary loads in equilibrium with each other and the unit weight of the soil prior to the start of the analysis. When using the Stallebrass model, in which current soil behaviour is influenced by both recent and long term stress history, it is necessary to model the last major event that the soil was subjected to prior to pile installation and to specify the bounding surface size, which for an overconsolidated soil will have decreased from a previous maximum value. Figure 6.2 shows the variation of  $p_c'$  (defined in Figure 3.2) with vertical effective stress on unloading from 1250kN/m<sup>2</sup> obtained from a two element one-dimensional test analysis. At the start of the analysis the surfaces are centred around the specified stress state. By modelling the last major event(s) the two kinematic yield surfaces described in section 3.4 are arranged correctly prior to modelling the operations under investigation. Initial horizontal effective stresses were calculated using Equation 3.10.

In analysis 1PIEXC the stiff clay being modelled was assumed to have been subjected to recent under-drainage and it was therefore necessary to model both overburden removal, which influences near surface behaviour, and pore water pressure reduction at the base of the model which influences behaviour at depth more than at the surface. Figure 6.3 shows the three vertical effective stress profiles in-situ, after overburden removal and after pore water pressure reduction. The clay was assumed to have constant permeability with depth and would not produce a non-linear pore pressure profile at equilibrium as discussed in section 4.3.1. This approximation did not greatly affect the pore water pressures in the region of the pile but did increase pore pressure at the base of the mesh. During a continuation analysis modelling a rising groundwater event the pore water pressure changes at the base of the model will therefore be reduced resulting in smaller deep seated heave.

In analysis 1P2MOD the clay being modelled started in the consolidation press, described in section 4.3, under a total vertical stress of  $200\text{kN/m}^2$ . The model was then brought into equilibrium with a downward hydraulic gradient stress field in the manner shown in Figure 4.1(b). Removal of the model from the press was assumed to result in no change in effective stress and the pile was installed in soil with this effective stress regime.

### 6.3.3 Soil stress state before pile installation

The soil stress state before pile installation was influenced by both overburden removal and under drainage. During the overburden removal pore water pressure was fixed at the top and base of the mesh at  $-5\text{kN/m}^2$  and  $250\text{kN/m}^2$  respectively. At the end of this event pore water pressure was reduced to  $72\text{kN/m}^2$  at the base of the mesh resulting in a sub-hydrostatic pore water pressure profile. The vertical and horizontal ( $\sigma_r' = \sigma_\theta'$ ) effective stress distributions after these operations are shown in Figure 6.4. The constitutive model does not restrict the stress state to passive pressure conditions as seen near the surface where high horizontal effective stresses can exist in a low vertical effective stress region. At increased depth the value of  $K_0$  converges with that predicted by a combination of Eqns. 3.10 and 2.20 as shown on Figure 6.5.

In analysis 1P2MOD the horizontal effective stress distribution is somewhat different from that shown in Figure 6.4 due to the different stress path followed and is shown in Figure 6.6.

#### 6.3.4 Pile installation results: 1PIEXC

The most unstable time during the pile installation process is the situation just before modelling concrete placement. Figure 6.7 shows the vertical, radial and hoop effective stress distributions in the mesh at this stage. The change in stresses from the far field conditions are localised around the open excavation. Both the vertical and the hoop effective stresses are seen to increase while the radial effective stress decreases. There is zero radial total stress acting on the inside of the pile shaft and pile shaft stability is only due to the mobilisation of temporary negative pore water pressures and hoop stresses around the open shaft. The stress path, in  $p'$ - $q$  space, followed during the excavation phase is shown on Figure 6.8 for element 336 which is located one radii from the pile shaft at 10m depth and element 497 at the same depth but 1/4 pile radii from the shaft. An increase in absolute value of deviator stress ( $q$ ) occurs for both elements during shaft excavation. The deviator stress has been assigned a negative value due to the initial stress state where  $K_0$  is greater than zero.

$$q = \frac{1}{\sqrt{2}} \sqrt{(\sigma'_r - \sigma'_v)^2 - (\sigma'_v - \sigma'_\theta)^2 - (\sigma'_r - \sigma'_\theta)^2 + 6\tau_{rv}^2} \quad (6.1)$$

The stress path is reversed when modelling concrete placement in the open excavation as seen by the reducing absolute value of deviator stress. In the long term condition (the shaft boundary is impermeable) the radial stress close to the shaft face has moved back towards far field levels as can be seen by comparing Figure 6.9(a) with 6.9(b) which show distributions of radial, vertical and hoop effective stresses for the cases when the shaft was open and long term conditions after pile elements have been placed respectively. The distributions were taken along a radius at 8m beneath the top of the mesh (approximately pile mid height). The major change is the reduction in hoop and increase in radial effective stresses. The irregularity of the lines representing effective stresses is due to the data points coming from slightly different levels as can be seen from Figure 6.1 where rows of elements radiating from the

pile are inclined.

The long term vertical, radial and hoop effective stress distributions within the mesh are shown on Figure 6.10. The change in radial effective stress is a maximum close to the ground surface and decreases with depth. This may be due to the effects of the hydrostatic concrete pressure which exert a larger stress at depth relative to the in-situ horizontal stress which is a function of  $K_0$ . The long-term hoop and vertical effective stresses have also moved back towards pre-excavation values although both are still elevated close to the pile. The average reduction in radial effective stress adjacent to the pile shaft due to pile installation was 24% (225kN/m<sup>2</sup> to 170kN/m<sup>2</sup>).

Horizontal displacements induced during excavation and concreting are shown in Figure 6.11 for depth profiles at 1.0m and 5.5m from the pile axis. For the profiles 1.0m from the pile axis the maximum displacement is at 2/3 depth due to the restraining effect of the pile shaft base. Near surface movements, during concreting, were minor in the vicinity of the pile while further down the shaft concrete pressures acted to push the shaft sides near the base back towards the pre-excavation positions. There was an overall inward movement of the soil during pile installation.

### 6.3.5 Pile installation results: 1P2MOD

The model pile was installed in ground which was very stable compared to the size of hole being constructed. The effective stresses (which contribute to stability) were high relative to the pile size at 1g due to the requirement that consolidation on the centrifuge after reaching the test acceleration should be kept to a minimum.

The processes of shaft excavation resulted in a significant loss of radial stress in the soil adjacent to the pile as can be seen in Figure 6.12(a) and a corresponding, if less marked, increase in hoop stress in Figure 6.12(b). The average reduction in radial stress is 31% resulting in an average value of 160kN/m<sup>2</sup> from 232kN/m<sup>2</sup>. The zone with reduced radial effective stress is seen in Figure 6.13 and extends for

about 8 pile radii compared to 2 pile radii for the prototype pile shown in Figure 6.9(b).

Horizontal displacements during pile excavation are shown on Figure 6.14 for profiles at the same distance (scaled at 1/100) as those shown in Figure 6.11 for the prototype pile. Displacements at 10mm from the pile axis vary almost linearly with depth increasing from the base of the pile to the surface. The overall magnitude of displacement (incorporating a scale factor of 100) was smaller than final displacements during prototype installation procedure. Displacements at 55mm from the model pile axis were relatively small as in the prototype pile analysis at the corresponding distance of 5.5m.

#### 6.3.6 Comments on prototype and model pile installations

Both prototype and model pile installation analyses have resulted in a reduction of radial effective stress and an increase of hoop effective stress in the soil around the pile shaft, the model pile experiencing the larger long-term change in stress regime around the pile. The reduction in radial effective stress will result in a reduction in pile shaft capacity when subjected to axial loading. The combined radial and hoop stress distributions around the model and prototype piles have altered significantly from the initial  $K_0$  conditions (especially the model pile).

In centrifuge model pile installation the pile was placed in a pre-formed hole with a small amount of slurry in the base. The pile displaced the slurry allowing the clay access to a small amount of water which caused swelling against the pile shaft. In the model pile installation analysis this last step was omitted and may result in a higher radial stresses than actually existed. In the prototype analyses no attempt has been made to model concrete shrinkage which would also tend to reduce radial effective stresses.

The trends, however, observed in both model and prototype analyses are reasonable. The results will allow further modelling of pile behaviour during a rising groundwater event for the real case when the pile has not been wished-in-place.

#### 6.4 Piles in a rising groundwater event after pile installation

Rising groundwater events were simulated after the prototype pile installation sequence. Problems were experienced due to the difference in vertical stiffness between the pile and the soil and due to the unavailability in the CRISP code of effective stress slip elements. Slip elements which allow differential movements have been used successfully by Desai et al. (1984) and Van Langren and Vermeer (1991) in  $S_u$  materials for modelling of interface behaviour between materials of very different properties. Britto and Gunn (1990) point out that if the user requires a limiting stress element followed by slip then interface slip elements are the only option.

In CRISP93 axisymmetric slip elements have been implemented, however these respond to changes in total stress acting on their boundary and not to changes in effective stress. In modelling a rising groundwater event the change in ultimate shear stress ( $\Delta\tau_f$ ) would be:

$$\Delta\tau_{f \text{ slip element}} = \tan\delta (\Delta u + \Delta\sigma'_x) \quad (6.2)$$

which for  $\Delta\sigma'_x/\Delta u = -0.4$  (from Eqn. 2.20) would result in an increase in  $\Delta\tau_f$  of  $60\% \Delta u \cdot \tan\delta$  rather than a reduction of  $40\% \Delta u \cdot \tan\delta$ .

In the analyses that were carried out the effect of the displacement continuity between the pile and adjacent soil led to severe problems. When the soil swelled under one dimensional conditions, shear stresses were mobilised in the elements closest to the pile where the stiffness of the pile acts to restrain swelling. The largest effect occurs near the ground surface where the soil heave would be a maximum and where pile to soil relative displacement would, in practice, also be a maximum. Figure 6.15 shows shear stress along two profiles parallel to the pile axis at 0.9m and 5.5m from the pile centre at the end of the rising groundwater event following prototype pile installation (Rising groundwater event 'A' of analysis lPIEXC). For the profile closest to the pile shaft unrealistically large shear stresses exist close to the surface which is at 25.5m above the base of the mesh. Towards the base of the pile (at 10.5m above the base of the mesh) the shear stress changes direction indicating a reversal of direction of shear between the

pile and the soil. The high shear stresses near the surface are supported by a 'membrane effect' resulting from a forced shear strain on an element. The shear stresses appear to be supported by increases in the normal effective stresses. As an example, the vertical effective stress distribution for the same elements are plotted in Figure 6.16. The profile close to the pile shaft has vertical effective stresses far in excess of those at more remote locations from the pile which approximate to far field conditions.

The combined effect of the elevated shear and normal stresses results in a stable stress state as shown in Figure 6.17 where stress ratio ( $\eta = q/p'$ ) is plotted against mesh height. All the elements adjacent to the pile lie below the critical state line ( $M = 0.85$ ) and are well within the bounding surface. The profile of stress ratios 5m from the pile axis show a more usual distribution of  $\eta$  for an overconsolidated deposit where the upper 8m have stress ratios at or in excess of the passive failure calculated from a critical state angle (the possibility of a stress ratio calculated by a model based on Cam clay exceeding passive failure was discussed in section 2.2.2).

In terms of pile to soil displacement the depth at which there was a change in sign of shear stress as indicated in Figure 6.15 can be seen in Figure 6.18 where pile to soil displacement is zero (approximately 13m from base of mesh); this is termed the neutral point. Pile to soil displacement above this level acts to pull the pile out of the ground while below, the pile is pulling the soil upwards (the soil is anchoring the pile).

A second series of exploratory analyses was carried out in which the upper two layers of soil elements were decoupled from the pile or removed and replaced with an equivalent overburden surcharge and pore water pressure fixity. The vertical sides of the elements 462 and 466 adjacent to the pile were provided with either stress or strain controlled boundaries as shown in Figure 6.19. In all cases the alterations had little beneficial effect. For the stress controlled boundary analyses and the analyses where the top two layers of elements were replaced with a surcharge, the elements immediately below 466 suffered from the

membrane effect while in the strain controlled boundary situation element 465 (adjacent to 466) acted as an anchor as the soil dragged it upwards resulting in an unrealistic negative vertical effective stress and low  $p'$ .

Within the context of this project it has not been possible to rewrite CRISP code to allow for effective stress slip elements that would, potentially, overcome some of the problems encountered. It has been possible, however, to investigate briefly the behaviour of a frictionless pile shaft during a rising groundwater event.

#### 6.4.1 Pile shaft in a rising groundwater event

In the previous section the rigid connectivity between pile and soil has led to unrealistic modelling of pile shaft-soil interaction during a rising groundwater event. To obtain an approximation of model pile shaft behaviour during a rising groundwater event, pile installation was carried out as outlined in section 6.3. However, immediately before the rising groundwater event the pile elements were removed and replaced with a strain controlled boundary with zero horizontal displacement on the vertical side and a surcharge on the elements immediately beneath the pile base. The rising groundwater event was then carried out; the soil elements surrounding the pile shaft initially had  $\sigma'_r < \sigma'_\theta$  as indicated in Section 6.3.

##### 6.4.1.1 After analysis 1PIEXC

Figure 6.20 shows the variation of radial and hoop effective stress with vertical effective stress for three elements at approximately 10m depth. The elements, 500, 321 and 47 are at 0.3, 1.8 and 19 radii from the pile shaft respectively. Elements 321 and 47 show a similar reduction of radial and hoop stress as the vertical effective stress reduces during the rising groundwater event. The ratio of the average change of horizontal to vertical effective stress, as in Eqn. 6.2 is 0.45 and 0.36 for elements 321 and 47 respectively. Element 500, closest to the shaft, experienced a large reduction in radial effective stress of 0.57 times that of the vertical effective stress while the hoop effective stress

reduced by only  $0.19 \Delta\sigma'_v$ .

#### 6.4.1.2 After analysis 1P2MOD

Figure 6.21 shows elements 500, 321 and 47 which are at the same relative position as those just described for analysis 1PIEXC in Section 6.4.1. The initial relationship between radial, hoop and vertical effective stresses is different for each element at the start of the rising groundwater event. However, during the rising groundwater event the initially low radial stress of elements 500 and 321 (lower than  $K_0$  conditions illustrated by element 47) converge with the far field radial stress resulting in a more uniform horizontal effective stress field. The average change in stress is less than would be predicted using Eqn. 2.20. Hoop stresses in elements 500 and 321 have also converged towards the far field horizontal stress level and in doing so have decreased more than the far field stresses.

During the centrifuge tests percentage reduction in shaft capacity, which is related to radial effective stress as in Eqn. 2.3, was less than the predicted percentage reduction in far field in horizontal effective stress (see Table 5.5). The results from this analysis support this observation for piles which have not had the beneficial effect (in terms of increasing radial stresses leading to increased shaft friction prior to the rising groundwater event) of hydrostatic concrete pressures prior to concrete setting.

#### 6.4.1.3 Comparison of smooth shaft analyses

The two analyses reported show very different behaviour with respect to radial effective stress change during a rising groundwater event. To investigate the differences in behaviour a third analysis was carried out (1PIMOD) using the same set of operations as the prototype analyses except that hydrostatic concrete pressures were not placed on the inside of the excavation before the concrete elements were placed. The results of this analysis showed a similar response during a simulated rising groundwater event as the model pile analysis. It appears from these results that the process of reversing the stress path direction during

concreting leads to a larger reduction in radial effective stress during the rising groundwater event.

#### 6.5 Rising groundwater event using Schofield model

Section 6.4 showed that using the Stallebrass model, problems were encountered when modelling large shear strains against a rigid boundary. As a comparison the pile behaviour during a rising groundwater event was analysed using the Schofield model (described in Section 3.3). The analyses modelled wish-in-place piles with a reduced strength soil layer adjacent to the pile shaft with  $M=0.5$  (compared to  $M=0.85$  in the main body of soil). The analyses are not directly comparable with those carried out using the Stallebrass model or the centrifuge tests since pile installation was not modelled. However, they allow an assessment of a different constitutive model for assessment of pile behaviour during a rising groundwater event.

Four analyses were carried out using the same initial soil stress conditions but with different pile head loads. The mesh and pile geometry used were similar to those in the analyses reported in section 6.3 except that one linear strain quadrilateral was substituted for two linear strain triangles. One of the runs (SCH2) was repeated using a rapid pore water pressure change similar to the centrifuge model tests rather than a gradual pore water pressure change that has been used in the other finite element analyses.

Ultimate pile load was obtained by carrying out a drained load test (analysis SCH1). The resultant ultimate pile head load was 824N (at model pile scale), 502N being carried by the shaft friction and 322N by end bearing, for a pile settlement of 10% pile base diameter in keeping with the definition used in the centrifuge tests and as described in Section 2.1. Loading of the pile becomes unstable after the reduced shear strength elements around the pile shaft reach critical state at the load quoted above. Further loading causes high shear strains in this narrow band resulting in stress ratios outside the state boundary surface. Factors of safety reported in Table 6.3 are calculated using this pile load capacity. The coupling between shear and bulk moduli

assumed in the Schofield model reduces the distinction between shaft and base loading phases seen in Figure 5.19(a) resulting in significant pile base load prior to full mobilisation of shaft capacity.

The horizontal effective stress distributions before and after the rising groundwater event are shown on Figure 6.22. During the rising groundwater event the average far field change in radial effective stress (and hoop effective stress) was approximately 0.42 that of the change in vertical effective stress over much of the pile length. This is in keeping with isotropic elasticity theory which is used for modelling overconsolidated soils with stress states not on the state boundary surface. Near the surface the ratio rises to 0.55 due to plastic yielding of the soil.

The five rising groundwater analyses are summarised in Table 6.3. The overall behaviour of the analyses show that increased axial pile load causes larger settlements relative to the surface and soil at the pile base level and increased pile base load at the end of the event, all of which are in keeping with the centrifuge test results. Figure 6.23 shows surface and pile head movements (6.23a) and pile base load (6.23b) from analysis SCH5 on the ordinates against vertical effective stress at far field pile base level on the abscissa. The change-over from unloading of the pile base to loading of the pile base is clear on both figures at  $\sigma'_v = 205\text{kN/m}^2$  resulting in a temporary increase in rate of settlement relative to vertical effective stress level. In analysis SCH4 a similar trend was observed at  $\sigma'_v = 175\text{kN/m}^2$ . In the other analyses pile base load decreased continually during the rising groundwater event as the mobilised shaft friction increased.

Analysis SCH2M which modelled the rising groundwater event with a rapid change in base drain water pressure followed by an equilibrium stage gave similar magnitudes of pile and surface movements at the end of the analysis as analysis SCH2 which modelled the rising groundwater event gradually. The pattern of movement shown on Figure 6.24 from analysis SCH2M is similar to that observed in the centrifuge tests (see Chapter 5) although foundation movements cannot be directly compared due to the difference in stress field around the pile discussed in Section 6.4.

The analyses were very sensitive to the stress state in the soil adjacent to the pile shaft resulting in large numbers of increments to model a rising groundwater event. In the analyses with high pile loads (SCH4 and SCH5) over 2000 increments were required for what appears a relatively simple analysis.

## 6.6 Conclusions from finite element analyses

It appears from the finite element analyses carried out that the adoption of a wish-in-place policy may not give realistic results when modelling model pile behaviour during a rising groundwater event due to the stress changes observed during the pile installation analyses. For prototype bored piles, in which the soil stress state is disturbed during installation, the change in radial effective stress change adjacent to the pile shaft during a rising groundwater event is closer to, but slightly higher than, the far field stress change. The continuation analyses of idealised frictionless pile shafts indicated that the differences in pile installation techniques may lead to different magnitudes of behaviour during a rising groundwater event, although the trends observed in both analyses were similar.

The Stallebrass model has demonstrated its strength in modelling complex stress paths during pile installation. However, it was not successful in modelling the rising groundwater event with a pile in place. This may in part have been due to time restraints of the number of increments needed to model a rising groundwater event (the final pile installation analyses took place in over 8000 increments requiring 4.5 days on a 486DX33 IBM compatible computer) and on the low degree of freedom type of element used. There were however, problems relating to high small strain stiffness, which is considered to be a soil constant and not dependant on stress level, which induced unrealistic stress distributions near the surface and which in turn effected soil stress states at deeper levels. Incorporation of effective stress slip-elements between pile and soil may have reduced this effect significantly. Reduction of the small strain stiffness (in effect making the soil model behaviour closer to that of Cam clay) may also have reduce the "membrane" effect. Further modelling developments including the implementation of a no tension

cut-off are being carried out and will inevitably improve the model performance at low stress levels.

The Schofield model was found to be reasonably successfully for modelling wished-in-place piles during a rising groundwater event. The trends in behaviour were similar to those observed in the centrifuge tests. If it is considered that pile installation techniques do not alter the stress state around a pile shaft then using wished-in-place pile installation and appropriate soil parameters should model pile behaviour accurately.

#### 6.7 Simple analyses ("by hand") of pile settlement during a rising groundwater event

The basic format for prediction of pile settlement during a rising groundwater event was presented in Section 2.4. The method relies on work from others (Fleming, 1992; O'Reilly and Al-Tabbaa, 1990) together with trends of behaviour seen in the centrifuge testing and finite element modelling. Using the method by Fleming (1992) requires that the stiffnesses ( $E_{25}$  for the base and  $G_{av}$  for the shaft) and pile capacity must be measured or predicted before and after the rising groundwater event. Data from pile load testing (using a method which gives drained load displacement response) allows estimation of these average soil moduli and ultimate base and shaft capacities as defined by Chin (1972). Calculation of pile capacity and appropriate moduli after the rising groundwater event require consideration:

##### File capacity:

Pile base capacity was shown to be a function of mean normal effective stress for piles in sand by Troughton and Platis (1989). For piles bases in clay the centrifuge tests have shown a similar trend seen in Figure 5.31 (a). Therefore, when the initial drained capacity is known final drained capacity may be calculated using Eqns. 2.22 and 2.23. For a model pile shaft, it appears that the reduction in capacity for bored piles whose shafts have displaced inwards during construction is less than predicted using the original far field  $K_0$  value and Eqn. 2.20 as indicated by both model centrifuge piles and the finite element analyses.

However, if it is considered that pile installation causes little soil disturbance then the use of Eqn. 2.20 for calculation of reduction in horizontal stress at the shaft face would seem appropriate where the pore water pressure change does not lead to large plastic deformation. If plastic deformation is likely (approaching the state boundary surface) then larger changes in horizontal effective stress must be allowed for.

#### Stiffness moduli:

The use of one stiffness parameter each for the pile shaft and base assumes an average soil behaviour in all zones surrounding the pile. Initial estimates of the average base stiffness parameter is available from pile loading tests as suggested by Fleming (1992). Rigorous assessment of stiffness beneath the base during a rising groundwater event would be highly complex and should include consideration of stress path direction in the zone of soil around the pile. A more simple approach would be to assume that stiffness is a function of  $p'$  and specific volume as used in the Schofield model such that:

$$E_{25} \propto 3(1 - 2\nu') \frac{v p'}{\kappa} \quad (6.3)$$

Poisson's ratio and  $\kappa$  are assumed to be constant resulting in a fairly simple relationship between  $E_{25}$ ,  $v$  and  $p'$  before and after the rising groundwater event. Similar assumptions can be made for  $G_{av}$  to assess the new parameter  $M_s$  in Eqn. 2.11.

#### 6.7.1 Prediction of centrifuge model behaviour

A series of calculations have been carried out to calculate model pile settlement (under-reamed and slender types) relative to the surface during the centrifuge tests. A sample calculation for an under-reamed pile is included in Appendix B. Figure 6.25 shows the centrifuge data points for settlement of under-reamed and slender piles (marked with symbols) previously produced as Figure 5.32 compared with the data using the above method (solid lines). The under-reamed pile calculated values agree reasonable well with the data points although at higher factors of safety there seems to be an over prediction of settlement. The agreement of the calculated values with the data points is less strong for slender

piles. These two points indicate that for piles which are predominantly friction piles that either the centrifuge tests were giving conservative movements due to initial overloading of the pile base as observed in Pile 2 in test RW14, or the method of calculation over predicts movements, (or a combination of the two). The general trends, however, agree well with the centrifuge tests. Soil heave at 150mm was calculated to be 0.7mm, the remaining foundation movement was due to pile settlement.

## 6.8 Summary

Finite element analyses have investigated pile installation effects for model and prototype bored piles and the effect that they have on pile behaviour during a rising groundwater event. Finite element analyses of wished-in-place pile behaviour during a rising groundwater event have been used to assess the applicability of a less sophisticated soil model for analysis of the problem. Simple "by hand" analyses have been used for a quick assessment of pile behaviour during a rising groundwater event without recourse to complex finite element analyses.

The pile installation analyses were undertaken to assess differences in behaviour, during a rising groundwater event, that might result from the different procedure followed during installation of centrifuge model piles compared with that normally adopted for prototype piles. The results have shown that, on a smooth pile surface, the prototype piles will suffer a larger percentage reduction in shaft capacity than the model piles. This fact should be considered, when extrapolating centrifuge model results, for analysis of prototype a bored pile during a rising groundwater event where load transfer from shaft to base may be larger than in an equivalent model pile.

The analyses of the wished-in-place piles have shown that piles in a rising groundwater environment may be studied by means of finite element analyses. The Schofield model, which was used in these analyses, simplifies overconsolidated soil behaviour to isotropic elasticity and in doing so smooths out distinct modes of shaft and base behaviour seen in model and prototype piles. Implementation of interface elements which allow a finite shaft capacity to be mobilised without the problems with

soil stress state would allow slip between pile and soil and would, it seems, provide a better predictive tool.

Finally, the "by hand" analyses have shown that quick assessment of pile settlement, in this case based on centrifuge observations, may be made that provide reasonable assessment of pile settlement during a rising groundwater event. The method relies on good prediction of soil heave and on initial pile load test data followed by assessment of pile capacity reduction and deterioration of soil stiffness.

### 7.1 Methodology

The performance of foundations in stiff clay during a rising ground water event was investigated by means of centrifuge model tests and some associated numerical modelling and triaxial testing.

In the centrifuge tests, model foundations were installed in a bed of overconsolidated Speswhite Kaolin clay at 1g prior to spin up on the centrifuge. Effective stress equilibrium was obtained during flight with the foundations subjected to working loads while the pore water pressures in the clay were controlled by a depressed water pressure in the base drainage layer. The water pressure in this drainage layer was then raised so initiating a rising groundwater event in the overlying clay layer. Observations of foundation and ground displacements, pore water pressures and foundation load distribution were made during the rising groundwater event. The effects of foundation geometry (shallow or deep, straight or under-reamed piles), initial factor of safety on load, initial load distribution between pile shaft and base and initial pore water pressure distribution in the model ground were examined. In two centrifuge tests a series of piezocone penetration tests were carried out before and after a rising groundwater event.

In the finite element analyses, model and prototype installation procedures were examined to allow comparison of the model pile installation with a prototype event. Continuation analyses modelling pile behaviour in a rising groundwater event were then carried out. A set of 'by hand' calculations were carried out to assess more simple techniques for predicting foundation settlements during a rising groundwater event.

The triaxial testing was undertaken to provide basic soil parameters for use in the numerical modelling and to examine soil stress paths during one dimensional loading, unloading and pore pressure cycles.

## 7.2 Soil in a rising groundwater environment

A series of piezocone penetration tests was carried out to investigate soil strength reduction due to a rising groundwater event. Slow tests (mobilising a large proportion of drained strength) showed an almost linear relationship of net cone resistance with mean normal effective stress. The rising groundwater event caused a reduction in cone resistance at pile base level of 30% compared to a 40% reduction in vertical effective stress. Faster tests (mobilising undrained shear strength) showed a 24% reduction in cone resistance for the same reduction in vertical effective stress, predicted undrained strength reduction was 20%.

Triaxial tests investigated the relationship between radial effective stress and change in back pressure (modelling a rising groundwater event) in overconsolidated clay constrained to deform with zero lateral strain. The tests showed that the reduction in radial effective stress was less than 50% of the change in axial effective stress but more than that predicted by isotropic elastic theory.

These two sets of different tests, together with soil heave due to the change in effective stress levels, illustrate the changes in soil state that will influence the behaviour of foundations during a rising groundwater event.

## 7.3 Foundations in a rising groundwater event

The series of centrifuge tests showed that, for similar length bored piles in stiff clay, differential settlement between the two piles during a rising groundwater event depended on:

- o Foundation geometry:

The geometry of the foundation (slender or under-reamed) and the manner by which load is transferred from pile to soil was seen to effect pile settlement relative to the ground surface during a rising groundwater event. Piles which require mobilisation of end bearing resistance at

working loads will settle due to: load transfer from the shaft to the base; reduced end bearing resistance; reduced soil stiffness; and soil heave above the pile base level. Piles which rely only on shaft friction at working loads will settle mainly due to soil swelling passed the pile shaft; the lower part of the pile will ultimately go into tension. Typically, end bearing piles will settle more than friction piles of the same length.

o Initial factor of safety:

For similar geometry piles the initial factor of safety will effect settlement during a rising groundwater event. End bearing piles with a low factor of safety will be required to mobilise a larger proportion of their ultimate end bearing capacity, as load is shed from shaft to a reduced capacity base, resulting in large pile base settlement relative to the surrounding soil. Friction piles with a low factor of safety will have their neutral point at a deep level on the pile shaft and consequently there will be significant soil heave above the neutral point level.

Pile foundation length was not varied during the centrifuge test programme. However, the centrifuge tests have shown that a large proportion of pile settlement relative to the ground surface, especially for slender piles, was due to soil heave along the pile shaft. In order to assess the effects of pile length for reduction of pile settlement relative to the ground surface a comparison should be made between settlement due to pile base behaviour for shorter piles and increased depth of neutral point for longer friction piles.

In examining differential settlement between shallow and deep foundations it was shown that a shallow foundation moved with the heaving ground surface during rising groundwater events in a soil stratum where the initial equilibrium condition was a perched water table with downward seepage. Differential settlements in this case were entirely due to pile settlement relative to the ground surface.

Where the initial pore pressure distribution was hydrostatic from a depressed surface water table, the shallow foundation, founded at the top of the clay layer, settled as effective stresses in the clay near the surface reduced. Piles in ground with negative pore water pressures near the surface prior to the rising groundwater event were subjected to large soil heave above base or neutral point level. Assessment of differential settlements, in these circumstances, must consider the behaviour of foundations at all levels.

Piled foundation load capacity was seen to reduce as a result of a rising groundwater event. Base capacity, measured under largely drained conditions, was seen to be linearly related to the mean normal effective stress in the ground in agreement with the slow piezocone tests. Contrary to normal expectations, it appeared that the percentage reductions in model pile shaft capacity were less than the percentage reduction in the predicted far field horizontal effective stress. The finite element analyses suggested that this effect was likely to be a function of the pile installation procedure for the centrifuge model and would not be applicable to prototype piles. The finite element analyses indicated that reduction in prototype pile shaft capacity is more closely linked to the reduction in far field horizontal effective stress and is likely to be larger than that predicted from isotropic elastic theory.

#### 7.4 Implications for foundation behaviour and design

Foundations which are surrounded by soil where pore pressure may rise will experience:

- o A reduction in drained end bearing resistance proportional to the change in mean normal effective stress;
- o A reduction in shaft capacity proportional to the change in radial effective stress which in turn is probably slightly higher than that predicted from elastic theory (assuming the soil stress state is inside the state boundary surface);
- o A reduction in soil stiffness;
- o Soil heave around the foundation.

These factors combine to produce highly undesirable conditions for structures, especially where there are mixed foundations. Differential settlements between shallow and deep foundations may conservatively be estimated by assuming that the shallow foundation moves with the ground surface while the piled foundation will be affected by the above criteria.

Prediction of settlement of end bearing piles will require consideration of all four criteria while conservative estimates of fully reinforced friction pile settlement may be obtained by calculation of soil heave above the pile base level.

The designer of new structures must predict settlement of individual foundations and assess the likelihood of differential settlements. Where differential settlements are inevitable design must either disassociate the structural elements or provide enough sub-structure strength to bridge the potential difference in settlements. As general rules foundation types should not be mixed; ground bearing slabs should be either suspended or have enough strength (and bending moment resistance) to support uplift pressures caused by the anchoring effects of the piled foundations; and where possible foundation length should be kept to a minimum so that the effects of rising groundwater levels, which are greatest at depth, are kept to a minimum.

#### 7.5 Limitations of the work

Relatively inexpensive centrifuge modelling of bored foundations in clay during a rising groundwater event has provided a large amount of information on model bored pile behaviour in reconstituted Speswhite Kaolin during rising groundwater events. An unsuccessful attempt to use reconstituted London Clay was made but failed due to centrifuge slip ring malfunction and was not reattempted.

Major limitations of the work carried out are:

- o Installation of the bored foundations at 1g rather than during flight at the required scale factor. The finite element analyses

of prototype and model pile installation suggested that the reduction in shaft capacity during a rising groundwater event would be less in model than prototype piles. The general modes of behaviour, however, were the same.

- o The use only of Speswhite Kaolin as the model ground. Kaolin has the very desirable property, for a clay, of high permeability which allowed a drained rising groundwater event to be modelled on the centrifuge over a two day period. The effects of rising groundwater will potentially be greater for higher plasticity clays and less for lower plasticity clays.
- o The influence of ground consolidation after spin-up resulted in negative skin friction on the piles. For slender piles, this would result in base loads that were in excess of working base loads creating a non-standard pile and non-standard behaviour during a rising groundwater event. The largest slenderness ratio used was (shaft length/base diameter) 12.0.
- o The finite element analyses were carried out with the available software. In analysis of piles during a rising groundwater event the pile shaft-soil interface was found to be very important. The software used did not incorporate the correct types of interface slip elements which may have allowed better finite element modelling of the pile behaviour in rising groundwater environment.

## 7.6 Further work

Centrifuge modelling techniques capable of carrying out pile installation during flight would allow a wider ranging investigation of bored pile behaviour during a rising groundwater event. In particular, longer more slender piles could be investigated and prototype installation procedure could be followed more closely. The complexity of the procedure prevented its attempt in this research project.

The centrifuge research programme was restricted to shallow pad foundations and bored piles. For completeness, the behaviour of

displacement piles, which subject the soil to very different stresses during installation, should be investigated to provide information allowing informed prediction of prototype behaviour during a rising groundwater event.

## REFERENCES

- Allman M.A. (1992a). Bothkennar centrifuge modelling. City University, London, Geotechnical Engineering Research Centre Report No. GE/92/07.
- Allman M.A. (1992b). Development and operation of the Centrifuge Actuator. City University, London, Geotechnical Engineering Research Centre Report No. GE/92/08.
- Almeida M.S.S. and Parry R.H.G. (1983a). Tests with centrifuge vane and penetrometer in a normal gravity field. Cambridge University, Technical Report No. CUED/D-SOILS/TR141.
- Almeida M.S.S. and Parry R.H.G. (1983b). Studies of vane and penetrometer tests during centrifuge flight. Cambridge University, Technical Report No. CUED/D-SOILS/TR142.
- Al-Tabbaa, A. (1987). Permeability and stress strain response of Speswhite Kaolin. Ph.D. Thesis, University of Cambridge.
- Andersen, E.K. (1990). Centrifuge modelling of rising groundwater. City University, London, Internal Report.
- Anderson, A.M., Yong, K.Y. and Sulaiman, J.I. (1985). Shaft adhesion on bored and cast in-situ piles. Proc. 11th International conference on soil mechanics and foundation engineering, San Francisco: 1333-1336.
- Armishaw J.W. and Cox D.W. (1979). The effects of changes in pore water pressure on the carrying capacities and settlements of driven piles in a sand and gravel deposit. Recent developments in design and construction of piles, ICE: 27-236.
- Atkinson J.H. and Evans J.S. (1985a). Discussion on Jardine et al. (1984), Geotechnique, Vol. 35.3: pp 378-380
- Atkinson J.H., Evans J.S., and Scott C.R. (1985b). Developments in micro-computer controlled stress path testing equipment for measurement of soil parameters. Ground Engineering, Vol. 18.1: 15-22.

- Atkinson J.H. and Salfors G. (1991). Experimental determination of stress-strain-time characteristics in laboratory and in-situ tests. Proc. 10<sup>th</sup> European Conf. Soil Mechanics and Foundation Engineering, Florence, pp 915-956.
- Biot M.A. (1941). General theory for three dimensional consolidation. Journal of Applied Physics, Vol. 12.2: 155-164.
- Bishop A.W. and Wesley L.D. (1975). A hydraulic triaxial apparatus for controlled stress path testing. Géotechnique, Vol. 25.4: 657-670.
- Britto A.M. and Gunn M.J. (1987). Critical state soil mechanics via finite elements. Ellis Horwood.
- Britto A.M. and Gunn M.J. (1990). CRISP90-User's and programmers guide. Cambridge University Engineering Department publication.
- Bromhead E.N. (1994). Interpretation of pore water pressure profiles in underdrained strata. Proc. Int. Conf. on groundwater problems in Urban Areas, ICE, London, pp 149-158.
- Brooker E.W. and Ireland H.O. (1965). Earth pressures at rest related to stress history. Canadian Geotechnical Journal, Vol. 2.1: 1-15.
- Burland J.B. (1973). Shaft friction of piles in clay - a simple fundamental approach. Ground Engineering, Vol. 6.5: 30-42.
- Burland J.B., Butler F.G. and Dunican P. (1966). The behaviour of large diameter bored piles in stiff clay. Proc. of Symp. on Large Bored Piles ICE: pp 51-71.
- Burland J.B. and Cooke R.W. (1974). The design of bored piles in stiff clay. Ground Engineering, Vol.7, pp 28-34.
- Burland J.B. and Hancock R.J.R. (1977). Underground car park at the House of Commons, London: Geotechnical aspects. The Structural Engineer, Vol. 55.2: 87-100.
- Burland J.B. and Twine D. (1988). The shaft friction of bored piles in terms of effective strength. Proc of Conf. on Deep Foundations on Bored and Augered Piles, Balkema: pp 411-421.

- Challa P.K. and Poulos H.G. (1992). Behaviour of single pile in expansive clay. Research Report No. R651, The University of Sydney, NSW, Australia.
- Chandler R.J. and Martins J.P. (1982). An experimental study of friction around piles in clay. *Geotechnique*, Vol. 32.2: 119-132.
- Chin K.E. (1972). The inverse slope as a prediction of ultimate bearing capacity of piles. Proc. 3rd South East Asian Conf. of Soil Engineering, Hong Kong: pp 83-91.
- CIL (1989). Manual for Multi-function PC super card. CIL Electronics Ltd.
- Craig W.H. (1985). Installation studies for model piles. Application of centrifuge testing to geotechnical design, Editor Craig W. Balkema: pp 441-456.
- Desai C.S., Zaman M.M., Lighter J.G. and Siriwardanan H.J. (1984). Thin layer elements for interfaces and joints. *Int. Journal for Numerical Methods in Geomechanics*. Vol. 8, pp 19-43.
- Fleming W.G.K. (1992). A new method for single pile settlement prediction and analysis. *Geotechnique*, Vol. 42.3: 411-425.
- Fleming W.G.K. and Powderham A.J. (1989). Introduction to soil downdrag and heave on piles. Discussion at Institution of Civil Engineers, July 1989.
- Fleming W.G.K., Weltman A.J., Randolph M.F. and Elson W.K. (1992). *Piling engineering*. Second edition. Surrey University Press, Halsted Press.
- Francescon M. (1983). Model pile tests in clay. Ph.D. Thesis, University of Cambridge.
- Goodings D.J. (1985). Relationships for modelling water effects in geotechnical centrifuge models. Application of Centrifuge Modelling to Geotechnical Design. Editor Craig W., Balkema: pp 1-24.
- Jardine R.J., Symes M.J.R.P. and Burland J.B. (1984). The measurement of soil stiffness in the triaxial apparatus. *Geotechnique*, Vol.34.3: 323-340.

- Kulhawy F.H. and Beech J.F. (1987). Groundwater influence on foundation side resistance. Proc. European Conf. Soil Mechanics and Foundation Engineering, Dublin: 707-710.
- Kutmen G. (1986). The influence of construction process on bored piles and diaphragm walls - A numerical study. M.Phil Thesis, University of Surrey.
- Ladd C.C., Foott ., Ishihara K., Schlosser F. and Poulos H.G. (1977). Stress-Deformation and Strength Characteristics. 9<sup>th</sup> Int. conf. soil mechanics and foundation engineering, Tokyo, Vol. 2: pp 421-494.
- Lopes F.R. (1979). The undrained bearing capacity of piles and plates studied by the finite element method. Ph.D. Thesis Imperial College, University of London.
- Mair R.J. (1979). Centrifuge modelling of tunnel construction in soft clay. Ph.D. Thesis, University of Cambridge.
- Martin R. and Rowthorn B. (1986). The geography of de-industrialisation. MacMillan.
- Mayne P.W. and Kulhawy F.H. (1982).  $K_0$ -OCR relationships in soil. Journal of geotechnical engineering, ASCE, Vol. 108.6: 851-872.
- Meigh A.C. (1987). Cone penetration testing, methods and interpretation. Butterworths.
- Morrison P.R.J. and Taylor R.N. (1994a). Foundations in a rising groundwater environment, Proc. Int. Conf. on Groundwater Problems in Urban Areas, ICE, London, pp 342-354.
- Morrison P.R.J. and Taylor R.N. (1994b). Modelling of foundations in a rising groundwater environment, Proc. Int. Conf. Soil Mechanics and Foundation Engineering. New Delhi, Vol. 2 pp 655-658.
- Nuttall N. (1994). Forgotten wells save London from rising risk of floods. The Times, January 8 1994.
- O'Reilly P. and Al-Tabbaa A. (1990). Heave induced pile tension: a simple one dimensional approach. Ground Engineering, June, 1990: pp 28-33.

- Padfield C.J. and Sharrock M.D. (1983). Settlement of structures on clay soils. CIRIA special publication SP27.
- Pantelidou H. (1994). Changes in soil stiffness associated with diaphragm walling. Ph.D. Thesis, University of London.
- Patel D.G. (1991). A case study of the shaft friction of bored piles in terms of total and effective stress. M.Sc. Thesis, Imperial College, University of London.
- Potts D.M. and Martins I.P. (1982). The shaft resistance of axially loaded piles in clay. *Geotechnique*, Vol.32.4: 369-386.
- Poulos H.G. (1989). Pile behaviour - theory and application. *Geotechnique*, Vol. 39.3: 365-415.
- Poulos H.G. (1993). Piled rafts in swelling or consolidating soil. *Journal of geotechnical engineering*, ASCE, Vol.119.2: 374-380.
- Poulos H.G. and Davis E.H. (1980). Pile foundation analysis and design. John Wiley and Sons.
- Randolph M.F. and Wroth C.P. (1978). Analysis and deformation of vertically loaded piles. *Journal of Geotechnical Engineering*. ASCE, Vol. 104.6: 1465-1488.
- Richardson D. (1988). Investigations of threshold effects in soil deformations. Ph.D. Thesis, The City University, London.
- Roscoe K.H. and Burland J.B. (1968). On the generalised stress-strain behaviour of "wet" clay. *Engineering Plasticity*, J. Heyman and F.A. Lekie (eds.): 535-609. Cambridge University Press.
- Schofield A.N. (1980). Cambridge geotechnical centrifuge operation. *Geotechnique*, Vol. 30.3: 227-268.
- Schofield A.N. and Wroth C.P. (1968). *Critical state soil mechanics*. McGraw Hill, New York.
- Senneset K. and Janbu N. (1985). Shear strength parameters obtained from static cone penetration tests. Paper A-84-1, Inst. of Geotechnics and Found, Eng., NGI.
- Shaw E.M. (1983). *Hydrology in practice*. Van Nostrand Reinhold (UK).

- Simpson B., Lance G.A. and Wilkinson W.B. (1987). Engineering implications of rising groundwater levels beneath London. Proc. European Conf. Soil Mechanics and Foundation Engineering, Dublin: pp 331-336.
- Simpson B., Blower T., Craig D.W. and Wilkinson W.B. (1989). The engineering implications of rising groundwater levels in the deep aquifer beneath London. CIRIA special publication, SP69.
- Skempton A.W. (1951). The bearing capacity of clays. Building research congress, London, ICE. Div. 1:180.
- Skempton A.W. (1954). Discussion of the structure of inorganic soil. Proc. ASCE, Soil Mechanics and Foundations Division, Vol. 80, pp 19-22.
- Skempton A.W. (1959). Cast in situ bored piles in London Clay. Geotechnique, Vol. 9.4: 153-173.
- Skempton A.W. (1961). Horizontal effective stresses in an overconsolidated Eocene deposit. Proc 5<sup>th</sup> Int. Conf. on Soil Mechanics and Foundation Engineering, Paris: 351-357.
- Stallebrass S.E. (1990). Modelling the effects of recent stress history on the deformation of overconsolidated soils. Ph.D. Thesis, City University, London.
- Stallebrass S.E. (1991). Modelling the deformation of overconsolidated soils using finite element analysis. Conf. on Experimental Characterization and Modelling of Soils and Soft Rocks, University of Naples, Italy.
- Stallebrass S.E. (1992). Implementation of new model in CRISP - Final report to Science and Engineering Research Council. Report No. B/90/RFH/8970.
- Stallebrass S.E. (1993). Personal communication.
- Steenfelt J.S. (1987). General report. Proc. European Conf. Soil Mechanics and Foundation Engineering, Dublin: 1285-1298
- Stewart D.I. (1989). Groundwater effects on in-situ walls in stiff clays. Ph.D. Thesis, University of Cambridge.

- Tahzeem M. (1993). The interface shearing behaviour of soils. B.Sc. report No. 2161, Engineering School, City University.
- Taylor R.N. (1987). Modelling in Ground Engineering. Chapter 58 in Ground Engineers Reference Book. Editor F.G. Bell. Butterworths.
- Troughton V.M. and Platis A. (1989). The effects of changes in effective stress on a base grouted pile in sand. Proc. Int. Conf. on Piling and Deep Foundations, Vol.2, Balkema: 445-453.
- Twine D. (1987). Shaft capacity of bored, cast-in-place piles in stiff, overconsolidated clays in terms of effective stresses. M.Sc. Thesis, Imperial College, University of London.
- Van Langren H. and Vermeer P.A. (1991). Interface elements for singular plasticity points. Int. Journal for Numerical Methods in Geomechanics. Vol 15, pp.301-315.
- Viggiani G. (1992). Small strain stiffness of fine grained soils. Ph.D. Thesis, City university, London.
- Whitaker T. and Cooke R.W. (1966). An investigation of the Shaft and Base Resistance of Large Bored Piles in London Clay. Proc. symp. on Large Bored Piles, ICE, pp 7-49.
- Wilkinson W.B. (1984). Rising groundwater levels and geotechnical consequences, discussion. Proc. Instn. of Civil Engineers, Part 1, Vol. 76: 791-793.
- Wood D.M. (1990). Soil Behaviour and Critical State Soil Mechanics. Cambridge University Press.
- Wroth C.P. (1975). In-situ measurements of initial stress and deformation characteristics. Proc. Speciality Conference on In-Situ Measurements of Soil Properties, ASCE
- Zelikson A. (1969). Geotechnical models using the hydraulic gradient similarity method. Geotechnique, Vol. 19.4: 495-508.

Quantity	Example	Scale factor	Prototype	Model
No. of g	-	-	1	100
Length	Pile diameter Clay depth	$1/n$	1.2m 25m	0.012m 0.25m
Stress	Pore pressure	1	100kN/m <sup>2</sup>	100kN/m <sup>2</sup>
Load	Imposed pile load	$1/n^3$	500 Tonne	0.5kg
Time consolidation	Groundwater rise	$1/n^2$	27 years	1 day

Table 4.1 Scale factors for centrifuge tests

Test No.	RW1	RW2	RW3	RW4	RW5
Date	26/3/92	30/4/92	16/6/92	13/7/92	16/9/92
Clay type	Speswhite Kaolin	Speswhite Kaolin	Speswhite Kaolin	Speswhite Kaolin	Speswhite Kaolin
Consolidation pressure (kPa)	800	≈ 1100	1250	1000	1250
Pile 1	150	150	150	150	150
Diameter of shaft (mm)	19.1	19.1	15.9	15.9	15.9
Diameter of base (mm)	19.1	19.1	15.9	22.4	15.9
Pile 2	10	10	10	10	150
or Pad	38.1	40	40	40	15.9
Diameter of base (mm)	38.1	40	40	40	15.9
Initial PWP profile	✓	✓	✓	✓	✓
Seepage from surface to base					
Hydrostatic, suction at surface					
Final thickness of clay (mm)	276	259	276	270	267
Comments	Low factor of safety on piled foundation, pad load due to self weight. Pile load not held in vertical position.	Foundation loads not held constant during rising groundwater event. Pre-consolidation pressure not constant through model.	Foundations loaded to failure before unloading to working loads prior to rising groundwater event.	Under-reamed pile base of concrete was found to be broken with pieces tight together. Foundation load testing at low groundwater level.	Loads increasing during the rising groundwater stage due to leakage and evaporation from loading mechanism.

Table 5.1a Summary of centrifuge tests RW1 to RW5

Test No.	RW6	RW7	RW8	RW10	RW11
Date	12/10/92	9/11/92	10/12/92	26/4/93	17/5/93
Clay type	Speswhite Kaolin	Speswhite Kaolin	Speswhite Kaolin	Speswhite Kaolin	Speswhite Kaolin
Consolidation pressure (kPa)	1250	1250	1250	1250	1250
Pile 1	Depth (mm)	160	Cone penetrometer testing at low and high pore water pressure distributions	150	150
	Diameter of shaft (mm)	15.9		15.9	12.7
	Diameter of base (mm)	15.9		24.0	12.7
Pile 2 or Pad	Depth (mm)	160	✓	150	150
	Diameter of shaft (mm)	15.9		15.9	12.7
	Diameter of base (mm)	15.9		24.0	12.7
Initial PWP profile	Seepage from surface to base	✓	✓	✓	✓
	Hydrostatic, suction at surface				
Final thickness of clay (mm)	275	270	268	255	257
Comments	One pile loaded to failure prior to rising groundwater level stage. Loads held constant during test. Moderate factors of safety.	As test RW6 with lower factors of safety.	Problems with desaturation of piezo element and with data recovery electronics during the test.	Two similar under-reamed piles with different factors of safety. No load testing prior to GWL rise.	As test RW10 but with predominantly friction piles at working loads.

Table 5.1b Summary of centrifuge tests RW6 to RW11 (test RW9 excluded)

Test No.	RW12	RW13	RW14	RW15	RW16
Date	6/9/93	27/9/93	18/10/93	9/11/93	29/11/93
Clay type	Speswhite Kaolin	Speswhite Kaolin	Speswhite Kaolin	Speswhite Kaolin	Speswhite Kaolin
Consolidation pressure (kPa)	1250	1250	1250	1250	1250
Pile 1	Depth (mm)	150	150	150	Cone penetrometer testing at low and high pore water pressure distributions
	Diameter of shaft (mm)	15.9	12.7	15.9	
	Diameter of base (mm)	15.9	12.7	24.0	
Pile 2 or Pad	Depth (mm)	10	0	150	150
	Diameter of shaft (mm)	40	40	12.7	
	Diameter of base (mm)	40	40	12.7	
Initial PWP profile	Seepage from surface to base		✓	✓	✓
	Hydrostatic, suction at surface	✓			
Final thickness of clay (mm)	264	274	265	266	268
Comment	Foundations loaded to working load prior to GWL rise. Pad load reduction due to slip ring leakage in latter part of rising groundwater level stage.	Foundation loads constant during rising GWL stage. Load tests at high water level.	Comparison of two deep foundation geometries at similar factors of safety.	Similar to test RW14.	Eight piezocene tests at low and high groundwater levels. Penetration rates of 0.2mm/sec and 2.0mm/sec used.

Table 5.1c Summary of centrifuge tests RW12 to RW16

Penetration Test No.	1	2	3	4	5	6	7	8
PWP distribution	low	low	low	high	high	high	high	high
Vertical effective stress (kPa), distance below clay surface	109	99	102	64	68	73	71	71
	202	189	189	114	118	131	124	124
	278	265	260	154	158	170	164	164
	364	353	342	193	197	208	203	203
	450	445	-	222	225	228	227	227
Penetration rate (mm/sec)	0.2	0.2	2.0	0.2	0.2	2.0	2.0	2.0

Table 5.2 Summary vertical effective stress distribution during piezocone penetration tests

Test No.	RW1	RW2	RW3	RW4	RW5
$\sigma'_v$ at 1 <sup>st</sup> loading (kPa)	50mm depth		80	77	90
	100mm depth		141	154	167
	150mm depth		202	231	245
Initial pile 1 loading	Ultimate load - top (N)	Over load of foundations during spin up	390	455	260 not maximum
	Shaft stress		S=35.1	S=21.4	B=735
	Base stress (kPa)		B=617	B=735	
Initial pile 2 or Pad loading	Displacement (mm)		1.45	1.9	
	Work load - top (N)		182	210,	240
	Shaft stress	No base load cell	S=14.4	S=-1.5	B=509
Initial pile 2 or Pad loading	Base stress (kPa)				
	Factor of safety	1.0	2.1	2.2	1.35
	Ultimate load - top (N)	Dead load	263	335	325 not maximum
$\sigma'_v$ at 2 <sup>nd</sup> loading (kPa)	Shaft stress		1.40	1.26	0.64
	Base stress (kPa)				
	Displacement (mm)				
Second pile 1 loading	Working load - top (N)		147	220	190
	Shaft stress	B=220	B=131	B=192	
	Base stress (kPa)				
Second pile 2 or Pad Loading	Factor of safety	1.1	1.8	1.5	1.7
	50mm depth		84	60	59
	100mm depth		163	96	106
Second pile 1 loading	150mm depth		239	132	152
	Ultimate load - top (N)		428	423	370
	Shaft stress		S=39.2	S=21.7	B=650
Second pile 2 or Pad Loading	Base stress (kPa)		B=662	B=650	
	Displacement (mm)		0.85	2.0	1.8
	Ultimate load - top (N)		310	405	400
Second pile 2 or Pad Loading	Shaft stress		B=230	B=353	
	Base stress (kPa)				
	Displacement (mm)		1.1	2.5	1.5

Table 5.3a Summary of foundation load tests RW1 to RW5

Test No.	RW6	RW7	RW8	RW10	RW11
$\sigma'_v$ at 1 <sup>st</sup> loading (kPa)	50mm depth	95		88	95
	100mm depth	170		169	181
	150mm depth	254		249	270
Initial pile 1 loading	Ultimate load - top (N)	(no load test)	Piezocone tests at low water level	(no load test)	(no load test)
	Shaft stress	S = 28.6		S = 37.6	
	Base stress (kPa)	0.37		0.38	0.05
Initial pile 2 loading	Work load - top (N)	280		398	235
	Shaft stress	S = 29.6		S = 37.9	B = 316
	Base stress (kPa)	B = -107			
Initial pile 1 loading	Factor of safety	2.2		1.8	1.6
	Ultimate load - top (N)	455		(no load test)	
	Shaft stress	(S = 33.2)	(B = 1047)		0.03
$\sigma'_v$ at 2 <sup>nd</sup> loading (kPa)	50mm depth	60		56	63
	100mm depth	107		100	111
	150mm depth	154		138	156
Second pile 1 loading	Ultimate load - top (N)	371		460 - not failure	335
	Shaft stress	S = 31.1	B = 679	S = 33.9	1.2
	Base stress (kPa)	1.7	B = 786	0.15	0.2
Second pile 2 loading	Ultimate load - top (N)	462		450 - not max	382
	Shaft stress	1.0		0.25	1.2
	Base stress (kPa)	1.0			1.2

Table 5.3b Summary of foundation load tests RW6 to RW11

Test No.	RW12	RW13	RW14	RW15	RW16 <sup>*1</sup>
$\sigma_v$ at 1 <sup>st</sup> loading (kPa)	50mm depth	127	85	90	116
	100mm depth	190	165	169	202
	150mm depth	231	245	260	288
Initial pile 1 loading	Ultimate load - top (N)	(no load test)	(no load test)	(no load test)	Piezocone tests at low water level
	Shaft stress	S=41.5		S=34.1	
	Displacement (mm)	0.14	0.12	0.25	
Initial pile 2 or Pad loading	Work load - top (N)	305	290	300	Piezocone tests at high water level
	Shaft stress	S=41.5    B=-30	S=29.4    B=201	S=34.1    B=146	
	Factor of safety	1.76	2.4	2.3 (2.1 in RGW)	
Initial pile 2 or Pad loading	Ultimate load - top (N)			180 (not maximum)	Piezocone tests at high water level
	Shaft stress		0.015	0.025	
	Displacement (mm)	0.1			
$\sigma_v$ at 2 <sup>nd</sup> loading (kPa)	Working load - top (N)	260	147	150	Piezocone tests at high water level
	Shaft stress	B=207	S=18.2    B=328		
	Factor of safety	1.6	2.1	2.0	
Second pile 1 loading	50mm depth	90	66	59	Piezocone tests at high water level
	100mm depth	138	105	101	
	150mm depth	168	144	144	
Second pile 2 or Pad Loading	Ultimate load - top (N)	425 no failure	550	525	Piezocone tests at high water level
	Shaft stress	S=40.5    (B=602)	S=32.0    B=782	S=29.4    B=756	
	Displacement (mm)	0.55	2.0	2.5	
Second pile 2 or Pad Loading	Ultimate load - top (N)	430 no failure	290	300	Piezocone tests at high water level
	Shaft stress	B=342	S=28.8    B=927		
	Displacement (mm)	0.35	1.2	1.15	

\*1 Water table 31mm above sand layer of 9mm thickness.

Table 5.3c Summary of foundation load tests RW12 to RW16

		RW1	RW2	RW3	RW4	RW5
PWP at start of rising groundwater stage (kPa)	50mm depth	29		28	31	18
	100mm depth	37		57	44	31
	150mm depth	44		86	57	43
PWP at end of rising groundwater stage (kPa)	50mm depth	59		41	48	49
	100mm depth	106		89	102	92
	150mm depth	152		137	156	136
Movement (mm): surface		1.42		0.60	1.62	1.60
Foundation 1						
Initial conditions	FOS	1.0		2.1	2.2	1.35
	$P_w$ (N)	480		182	210	240
	$q_u$ (kN/m <sup>2</sup> )			14.3	-1.5	-
	$q_b$ (kN/m <sup>2</sup> )			376	509	-
Final conditions	$P_w$ (N)	480		182	227	
	$q_u$ (kN/m <sup>2</sup> )			24.0	20.4	
	$q_b$ (kN/m <sup>2</sup> )			25	211	
Displacement (mm)		0.38		0.50	1.12	
Foundation 2						
Initial conditions	FOS	1.1		1.8	1.5	1.7
	$P_w$ (N)	258		147	215	190
	$q_u$ (kN/m <sup>2</sup> )	(NA)		(NA)	(NA)	-
	$q_b$ (kN/m <sup>2</sup> )	222		117	171	-
Final conditions	$P_w$ (N)	258		147	210	
	$q_u$ (kN/m <sup>2</sup> )	(NA)		(NA)	(NA)	
	$q_b$ (kN/m <sup>2</sup> )	222		117	107	
Displacement (mm)		1.19		0.60	1.50	

Table 5.4a Summary of foundation behaviour during rising groundwater event tests RW1 to RW5

		RW6	RW7	RW8	RW10	RW11
PWP at start of rising groundwater stage (kPa)	50mm depth	22	13		26	20
	100mm depth	28	24		35	24
	150mm depth	34	37		45	25
PWP at end of rising groundwater stage (kPa)	50mm depth	44	46		58	52
	100mm depth	91	90		104	94
	150mm depth	135	146		156	139
Movement (mm):						
surface		1.7	1.95		1.59	1.64
150mm depth		-	-		-	1.08
<b>Foundation 1</b>						
Initial conditions	FOS	2.2	1.6		1.8	1.6
	$P_w$ (N)	200	280		397	235
	$q_u$ (kN/m <sup>2</sup> )	29.6	28.6		37.5	-
	$q_b$ (kN/m <sup>2</sup> )	-107	248		320	-
Final conditions	$P_w$ (N)	210	285		397	235
	$q_u$ (kN/m <sup>2</sup> )	30.3	28.6		33.4	-
	$q_b$ (kN/m <sup>2</sup> )	-104	273		390	-
Displacement (mm)		1.03	0.70		0.31	0.86
<b>Foundation 2</b>						
Initial conditions	FOS	2.2	1.6		2.1	2.1
	$P_w$ (N)	206	280		346	182
	$q_u$ (kN/m <sup>2</sup> )	-	-		(37.5)	-
	$q_b$ (kN/m <sup>2</sup> )	-	-		(197)	-
Final conditions	$P_w$ (N)	210	275		352	185
	$q_u$ (kN/m <sup>2</sup> )	-	-		(33.4)	-
	$q_b$ (kN/m <sup>2</sup> )	-	-		(282)	-
Displacement (mm)		1.20	0.94		0.55	1.04

Table 5.4b Summary of foundation behaviour during rising groundwater event tests RW6 to RW11

		RW12	RW13	RW14	RW15	RW16 <sup>*1</sup>
PWP at start of rising groundwater stage (kPa)	50mm depth	-34	-37	24	11	21
	100mm depth	-11	-10	34	22	25
	150mm depth	42	39	43	21	29
PWP at end of rising groundwater stage (kPa)	50mm depth	0	0	43	42	69
	100mm depth	42	55	94	90	113
	150mm depth	102	105	144	137	160
Movement (mm)						
surface		1.80	2.25	1.63	2.95	
150mm depth (mm)		-	0.77	1.26	1.48	
Foundation 1						
Initial conditions	FOS	1.7	1.4	2.4	2.1	
	$P_w$ (N)	295	232	292	320	
	$q_b$ (kN/m <sup>2</sup> )	41.5	29.2	29.8	34.1	
	$q_b$ (kN/m <sup>2</sup> )	-30	452	197	193	
Final conditions	$P_w$ (N)	300	248	300	327	
	$q_b$ (kN/m <sup>2</sup> )	38.8	34.6	30.7	29.1	
	$q_b$ (kN/m <sup>2</sup> )	39	324	202	292	
Displacement (mm)		0.34	0.46	0.91	0.5	
Foundation 2						
Initial conditions	FOS	≈ 1.6	≈ 2.1	2.1	2.0	
	$P_w$ (N)	260	150	147	164	
	$q_b$ (kN/m <sup>2</sup> )	(NA)	(NA)	18.2	-	
	$q_b$ (kN/m <sup>2</sup> )	207	119	328	-	
Final conditions	$P_w$ (N)	165	166	154	164	
	$q_b$ (kN/m <sup>2</sup> )	(NA)	(NA)	24.2	-	
	$q_b$ (kN/m <sup>2</sup> )	131	132	55	-	
Displacement (mm)		1.27	1.56	1.18	1.48	

\*1 Water table 31mm above sand layer of 9mm thickness.

Table 5.4c Summary of foundation behaviour during rising groundwater event tests RW12 to RW16

Test No.		RW10	RW15
Pile No.		Pile 1	Pile 1
Low water level	$\sigma'_{v\ ave}$ (kN/m <sup>2</sup> )	120.5	130.8
	$\sigma'_{h\ ave}$ (kN/m <sup>2</sup> )	182.9	204.9
	Load $P_s$ (N)	265	240
	Stress $Q_{s\ ave}$	37.7	34.1
	$\beta$	0.313	0.261
High water level	$\sigma'_{v\ ave}$ (kN/m <sup>2</sup> )	71.4	80.0
	$\sigma'_{h\ ave}$ (kN/m <sup>2</sup> )	140.1	153.4
	Load $P_s$ (N)	239	207
	Stress $Q_{s\ ave}$	34.0	29.4
	$\beta$	0.476	0.493
Change	$\Delta Q_{s\ ave}$ (%)	9.8	13.8
	$\Delta \sigma'_{v\ ave}$ (%)	40.7	38.8
	$\Delta \sigma'_{h\ ave}$ (%)	23.4	25.1

Table 5.5 Shaft capacity before and after a rising groundwater event

Test No.		RW6	RW7	RW14	RW14	RW15
Pile No.		Pile 2	Pile 2			
Slenderness ratio		9.5	10.0			
Low water table stresses at 150mm depth (160mm in RW7)	$\sigma'_v$ (kN/m <sup>2</sup> )	255	261			
	$\sigma'_h$ (kN/m <sup>2</sup> )	312	312			
	$p'$ (kN/m <sup>2</sup> )	293	295			
	Load $P_b$ (N)	257	274			
	$Q_b$ (kN/m <sup>2</sup> )	1047	1094			
Pile No.		Pile 1	Pile 1	Pile 1	Pile 2	Pile 1
Slenderness ratio		9.5	10.0	6.5	12.0	6.5
High water table stresses at 150mm depth (160mm in RW7)	$\sigma'_v$ (kN/m <sup>2</sup> )	156	146	146	146	146
	$\sigma'_h$ (kN/m <sup>2</sup> )	253	244	244	244	246
	$p'$ (kN/m <sup>2</sup> )	221	211	211	211	212
	Load $P_b$ (N)	193	216	390	140	365
	$Q_b$ (kN/m <sup>2</sup> )	679	786	782	927	756

Table 5.6 Base capacity before and after a rising groundwater event

Analysis		1PIEXC	1P2MOD
Mesh scale		Prototype	Model
Dimensions (m)	radius	18.0	0.18
	height	25.5	0.255
Initial stresses	Surface	100	200
	PWP	Hydrostatic	zero
	Scale factor n	1	1
Stresses before pile excavation	Surface	0	0
	PWP	-8 top to 68 base	-8 top to -390 base
	Scale factor n	1	1
Use of liquid concrete		Yes	No
Place pile elements		Replace concrete	Fill open hole
Scale factor increment		0	99
Rising water event			
A		Pile in place	
B		Frictionless shaft	Frictionless shaft

Table 6.1 Pile instalation analyses summary

Symbol	Parameter	Value	
<b>Stallebrass Model - Speswhite Kaolin</b>			
$G_s$ kPa	Elastic shear stiffness	60000	
$\kappa^*$	Elastic kappa in $Lnv-Lnp'$ space	0.007	
$M$	Stress ratio at critical state $q/p'$	0.85	
$\lambda^*$	Lambda in $Lnv-Lnp'$ space	0.0838	
$\Gamma$	Specific volume of CSL at $p' = 1$ kPa	3.0	
$K_v$ m/sec	Vertical permeability	1.11E-9	
$K_h$ m/sec	Horizontal permeability	0.2E-9	
$T$	Ratio of history to bounding surface size	0.25	
$S$	Ratio of elastic to history surface size	0.08	
$H$	Hardening factor	2.5	
$\gamma_w$ kN/m <sup>3</sup>	Unit weight of water	10	
$\gamma_s$ kN/m <sup>3</sup>	Unit weight of saturated soil	18	
<b>Schofield Model - Speswhite Kaolin</b>			
		Main body of ground	Elements close to pile
$\kappa$	Average kappa in $v-Lnp'$ space	0.035	0.035
$\lambda$	Lambda inv- $Lnp'$ space	0.18	0.18
$e_{cs}$	Voids ratio on CSL at $p' = 1$ kPa	1.97	1.97
$M$	Slope of CLS	0.85	0.5
$\nu'$	Drained Poisson's ratio	0.3	0.3
$H$	Slope of Hvorslev surface in $q-p'$ space	0.5	0.25
$S$	Slope of no ternion cut off in $q-p'$ space	3.0	3.0
$K_v$ m/sec	Vertical permeability	1.11E-9	1.11E-9
$K_h$ m/sec	Horizontal permeability	0.3E-9	0.3E-9
$\gamma_w$ kN/m <sup>3</sup>	Unit weight of water	10	10
$\gamma_s$ kN/m <sup>3</sup>	Unit saturated weight of soil	18	18
<b>Elastic - Concrete</b>			
$E$ kPa	Young's modulus	63E6	
$\nu$	Poisson's ratio	0.25	
$G$ kPa	Shear stiffness	25E6	
$\gamma$ kN/m <sup>3</sup>	Unit weight	8 or 24	

Table 6.2 Summary of material properties for finite element modelling

Analysis		SCH2	SCH3	SCH4	SCH5	SCH2M
Pile loading	Pile head load (N)	301	402	503	603	301
	Initial factor of safety	2.7	2.1	1.6	1.4	2.7
	Pile settlement on loading (mm)	0.15	0.20	0.26	0.34	0.15
Rising groundwater event	PWP change at base	Gradual	Gradual	Gradual	Gradual	Rapid
	Surface heave (mm)	1.19	1.19	1.19	1.19	1.18
	Pile settlement wrt surface (mm)	0.47	0.51	0.60	0.66	0.45
	Pile settlement wrt base (mm)	-0.11 (heave)	-0.07 (heave)	0.01 (settle)	0.08 (settle)	-0.12 (heave)
	Initial pile base load (N)	121	143	165	197	121
	Final Pile base load (N)	5	45	124 (97 min)	190 (166 min)	3

Table 6.3 Summary of rising groundwater event analyses using Schofield model (model scale)

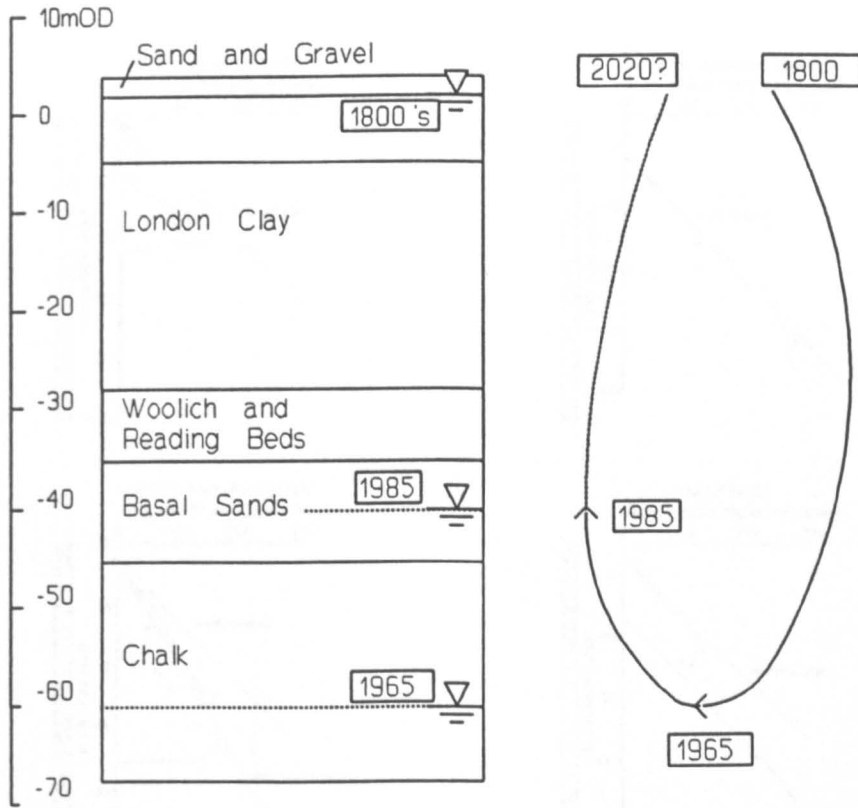


Figure 1.1 Schematic of groundwater levels beneath London

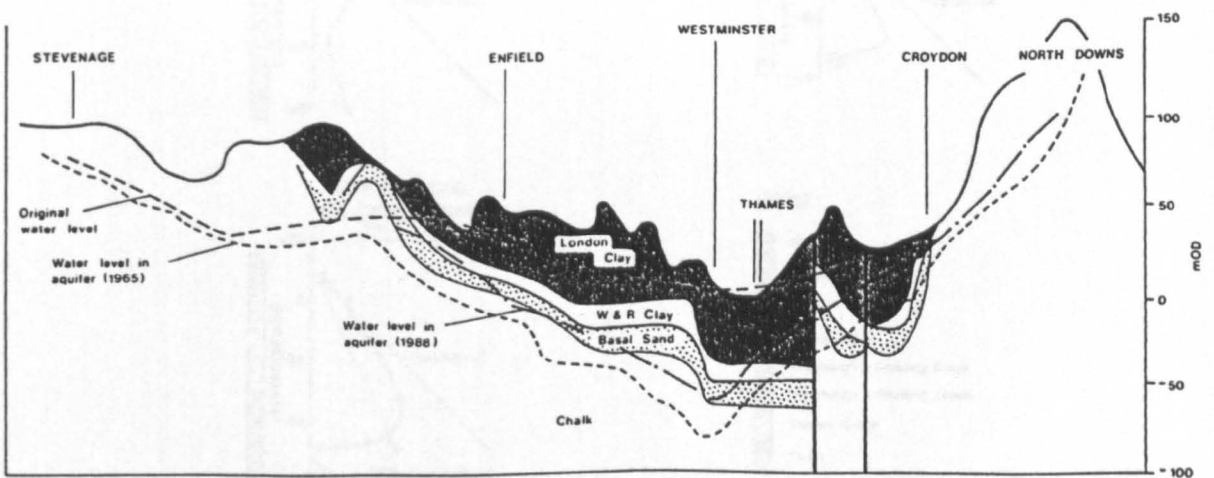


Figure 1.2 Geology of the London basin

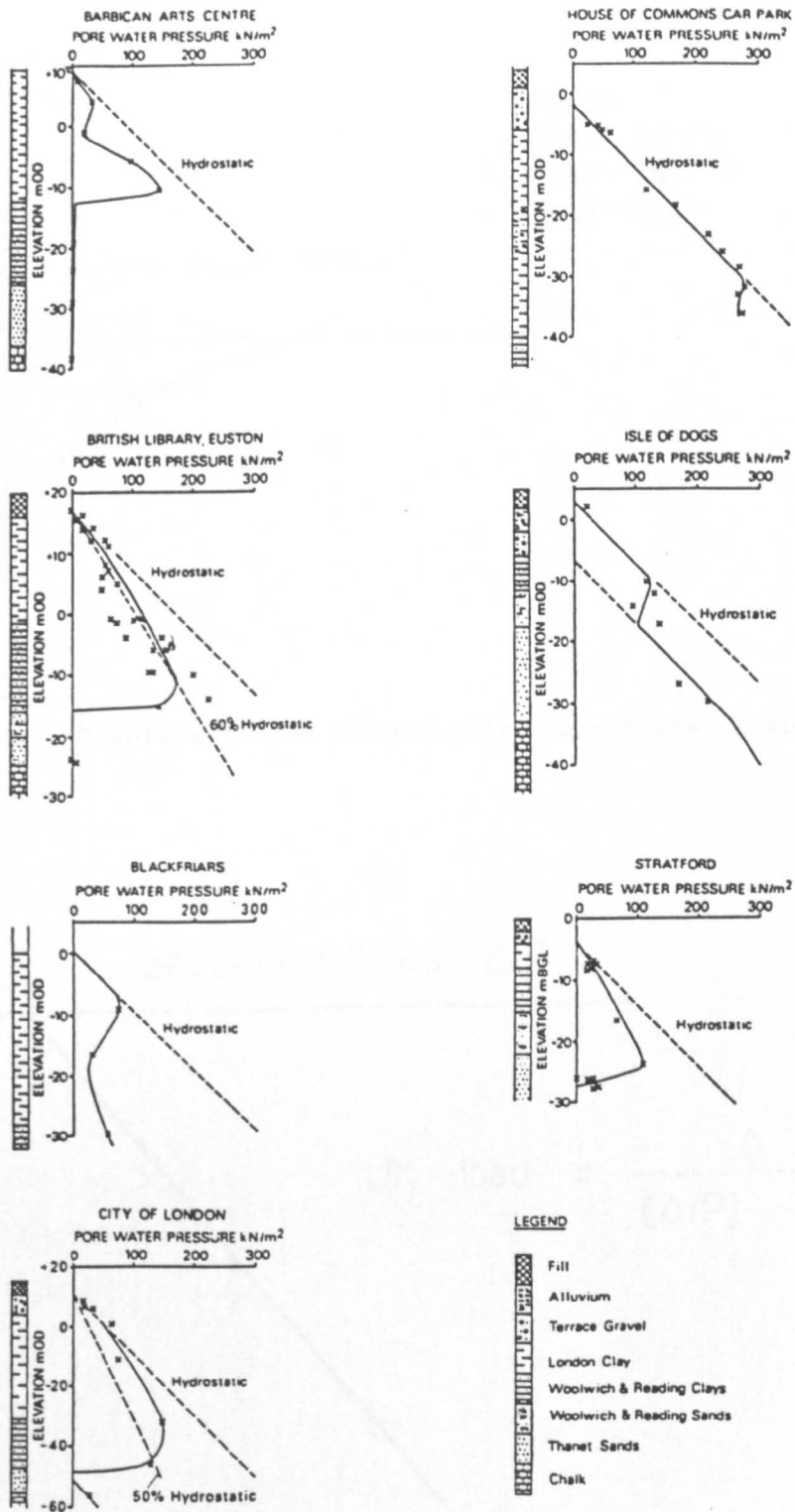


Figure 1.3 Pore water pressure profiles through London Clay (After Simpson et al., 1989)

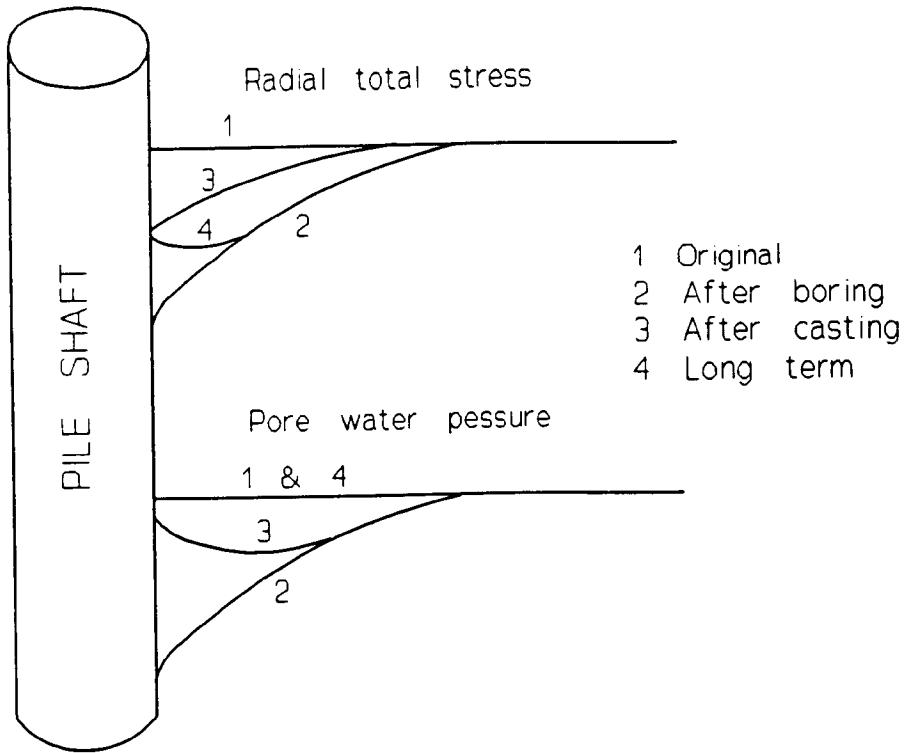


Figure 2.1 Stresses around a bored pile shaft (After Lopes, 1979)

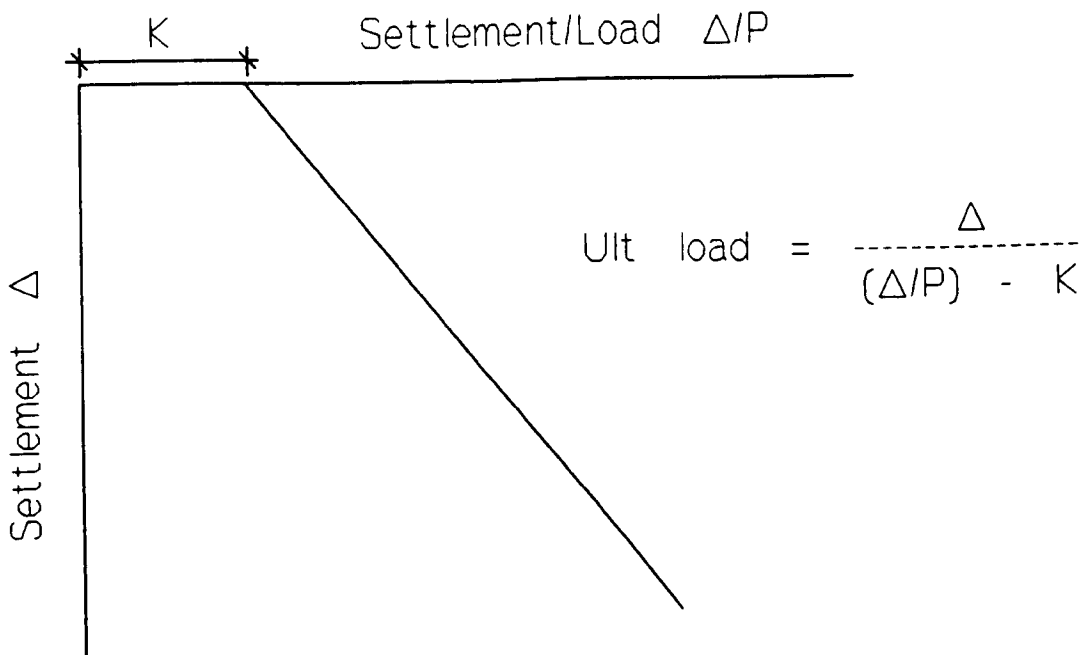


Figure 2.2 Hyperbolic function applied to pile settlement (After Chin, 1972)

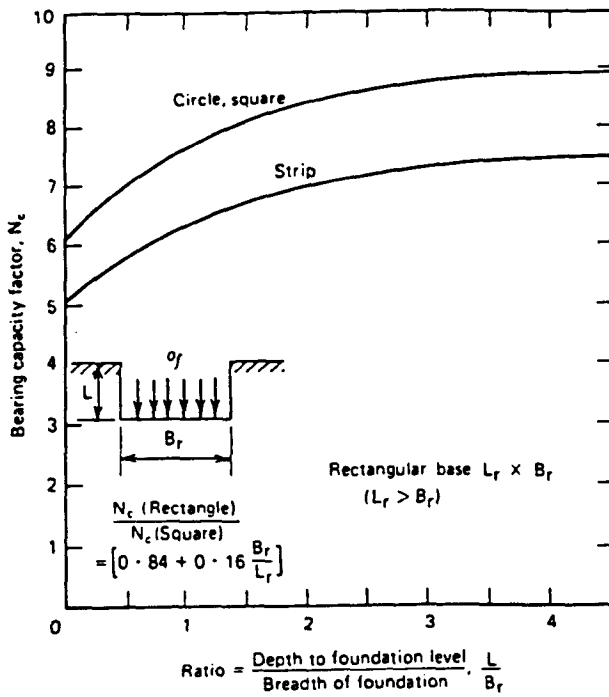


Figure 2.3 Undrained bearing capacity factor (After Skempton, 1951)

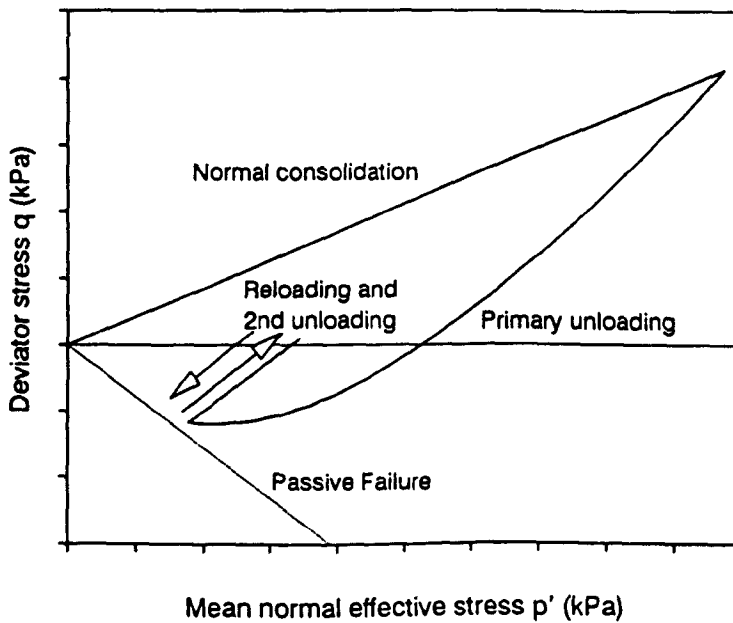
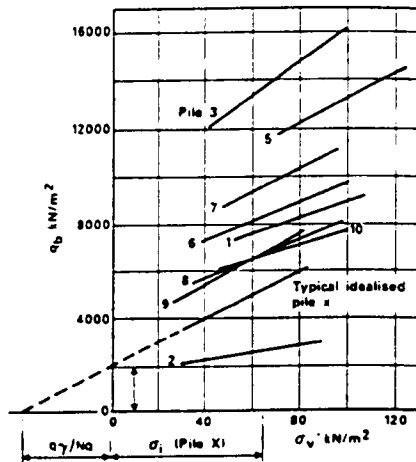
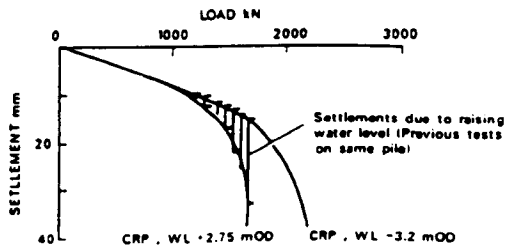


Figure 2.4 Schematic of one-dimensional stress history



a) Graph of ultimate end bearing pressure,  $q_b$ , versus effective overburden pressure,  $\sigma_v'$ , at the level of the base of the pile during testing



b) Load - settlement relationship, Pile 3

Figure 2.5 Driven pile (in terrace gravel deposit) end bearing capacity against vertical effective stress (After Armishaw and Cox, 1979)

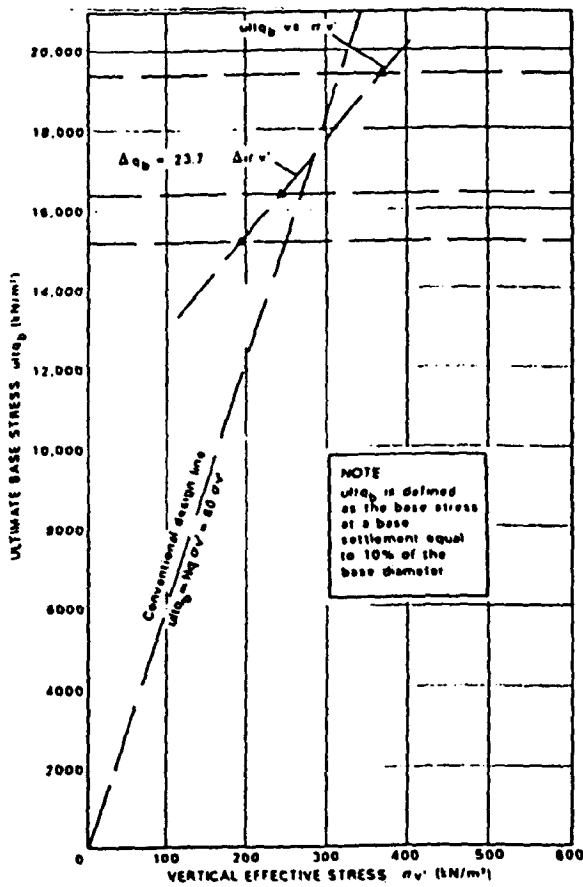


Figure 2.6a Bored pile (in Thanet sand deposit) end bearing resistance against vertical effective stress (after Troughton and Platis, 1989)

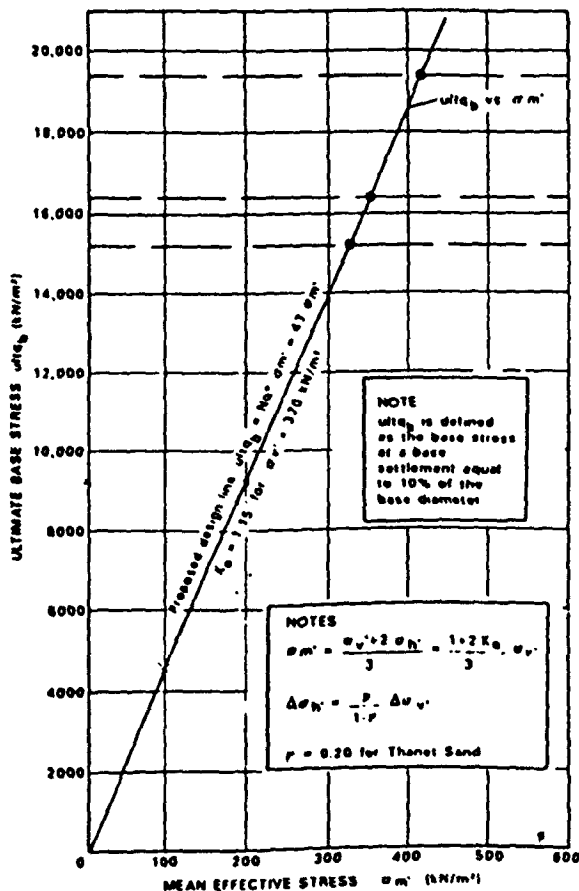


Figure 2.6b Bored pile (in Thanet sand deposit) end bearing resistance against mean normal effective stress (after Troughton and Platis, 1989)

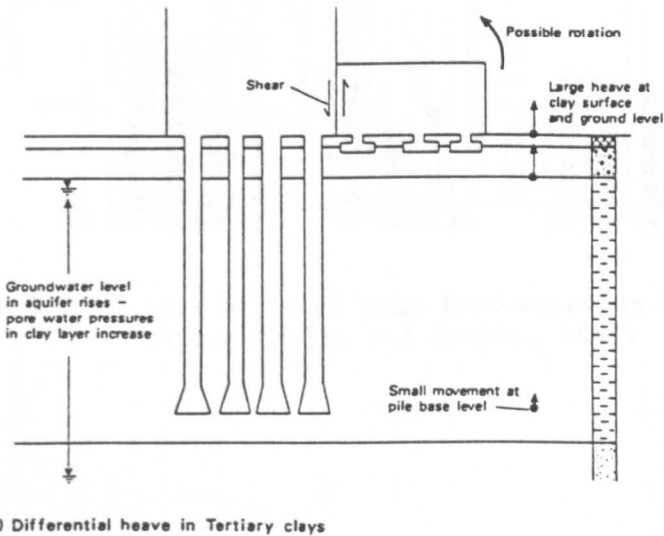
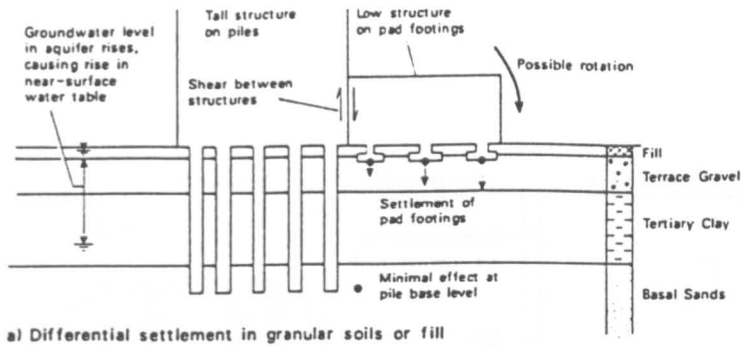


Figure 2.7 Anticipated modes of behaviour of shallow and deep foundations in clay during a rising groundwater event (After Simpson et al. 1989)

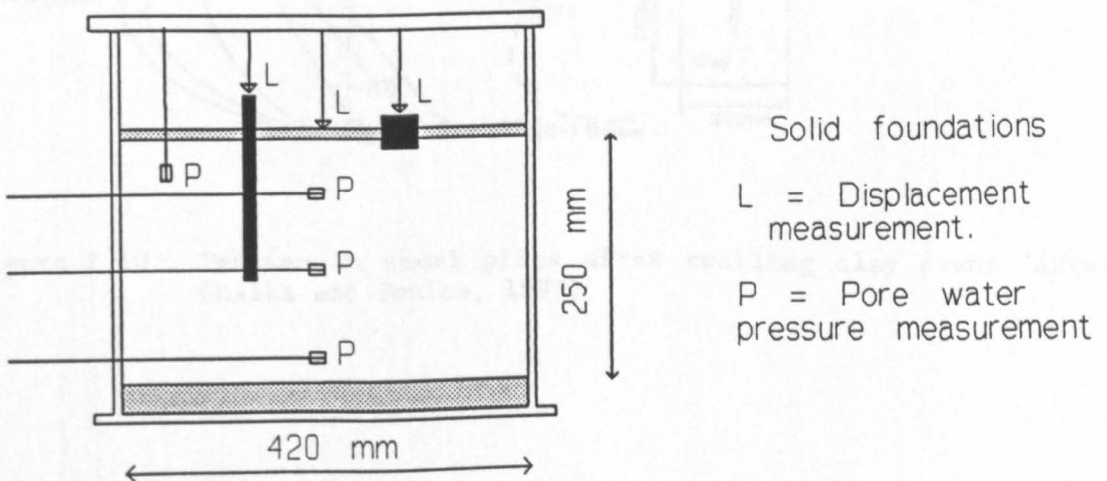


Figure 2.8 Centrifuge model set up (After Andersen 1990)

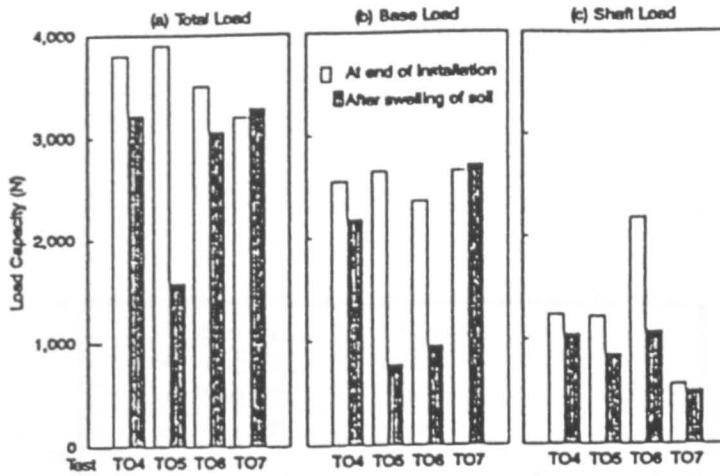


Figure 2.9 Loss of model pile load capacity after swelling clay event (After Challa and Poulos, 1993)

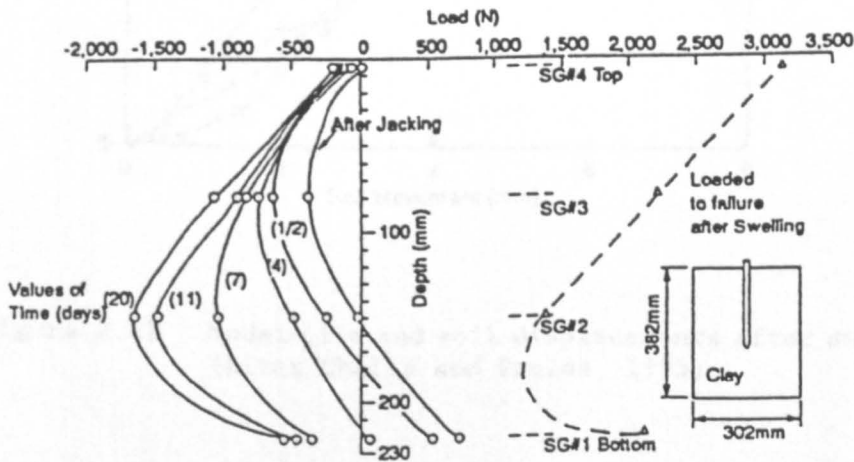


Figure 2.10 Tension in model piles after swelling clay event (After Challa and Poulos, 1993)

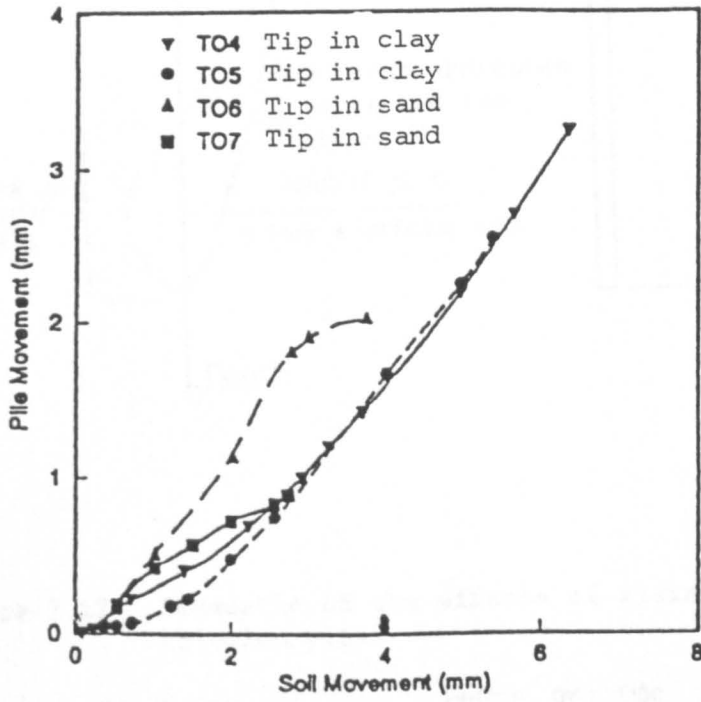


Figure 2.11 Model pile and soil displacements after swelling clay event (After Challa and Poulos, 1993)

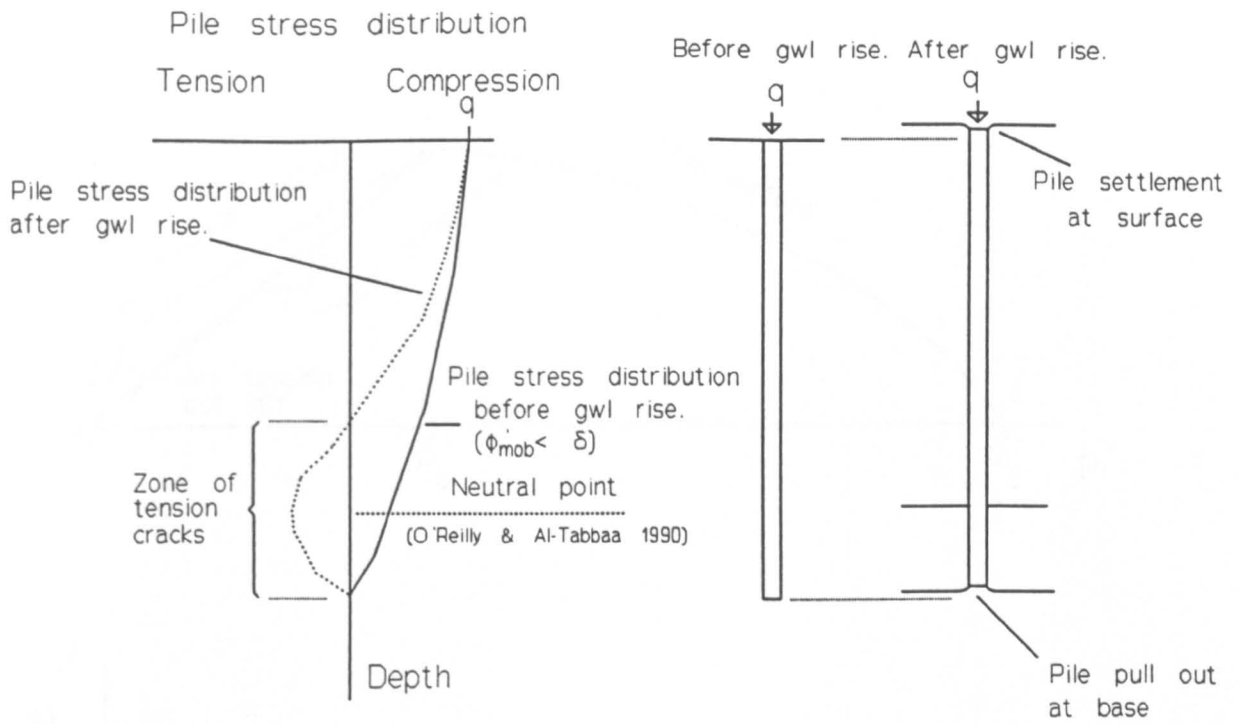


Figure 2.12 Schematic of the effects of rising groundwater levels on friction piles

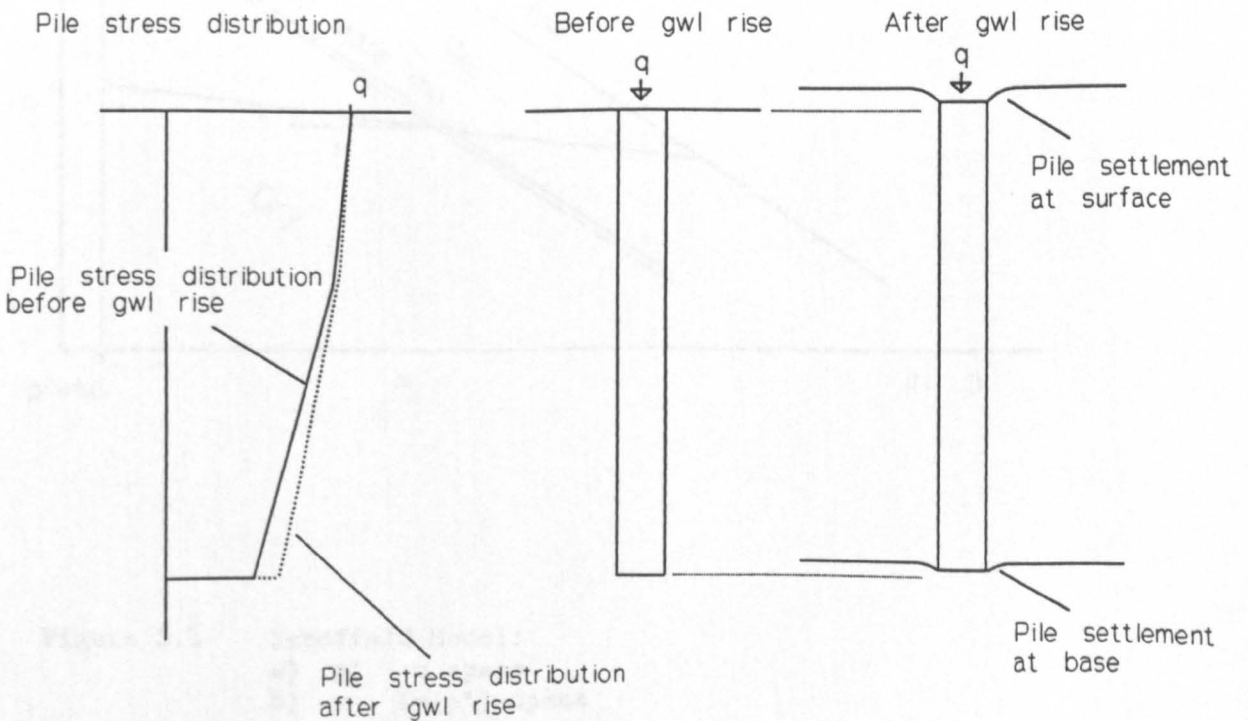
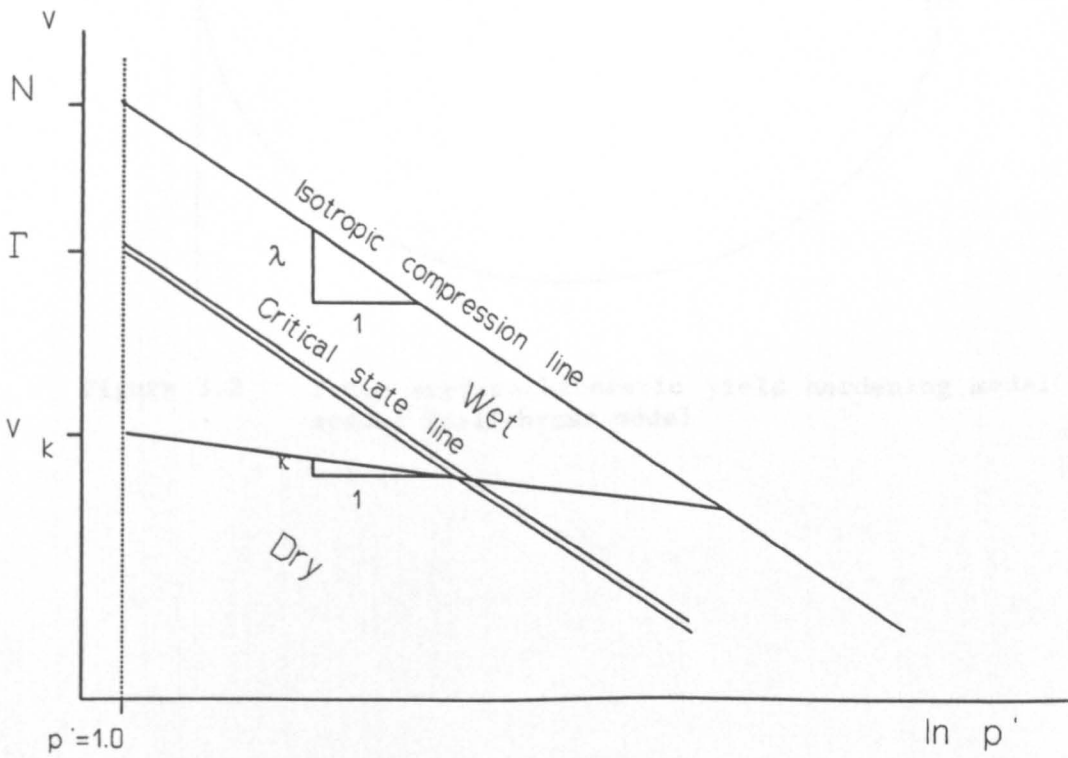
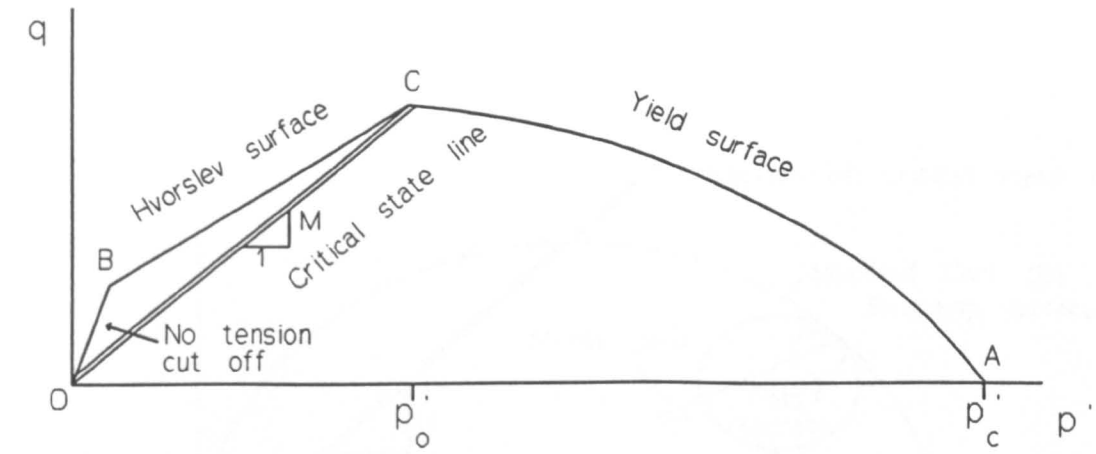


Figure 2.13 Schematic of the effects of rising groundwater levels on end bearing piles



**Figure 3.1** Schofield Model:  
 a)  $p' - q$  space  
 b)  $v - \ln(p')$  space

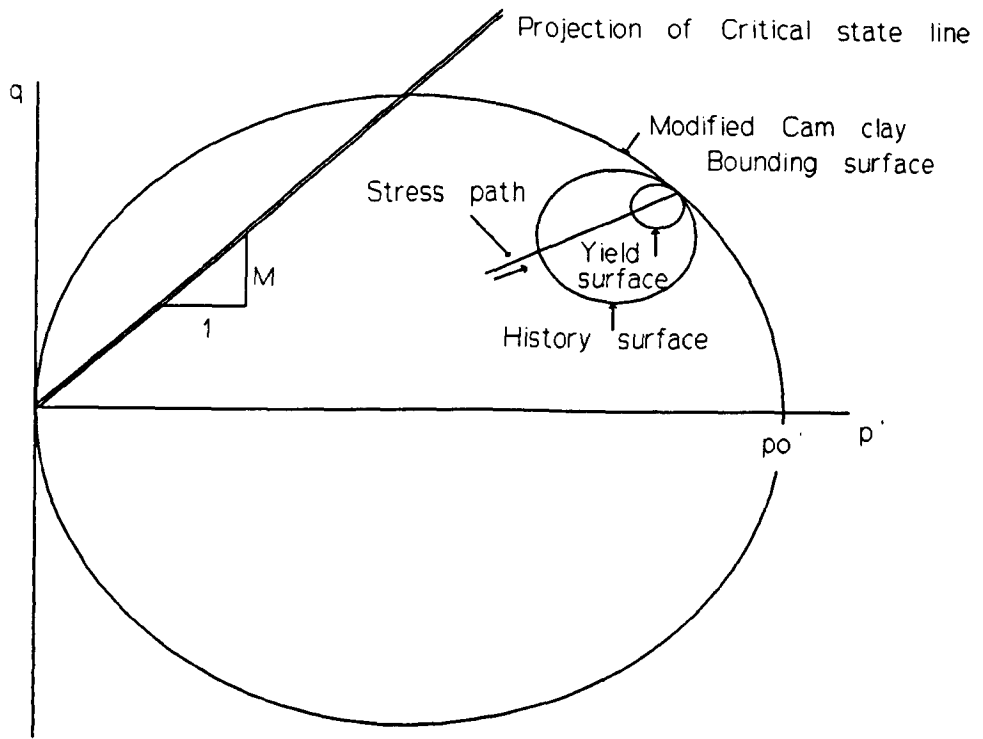
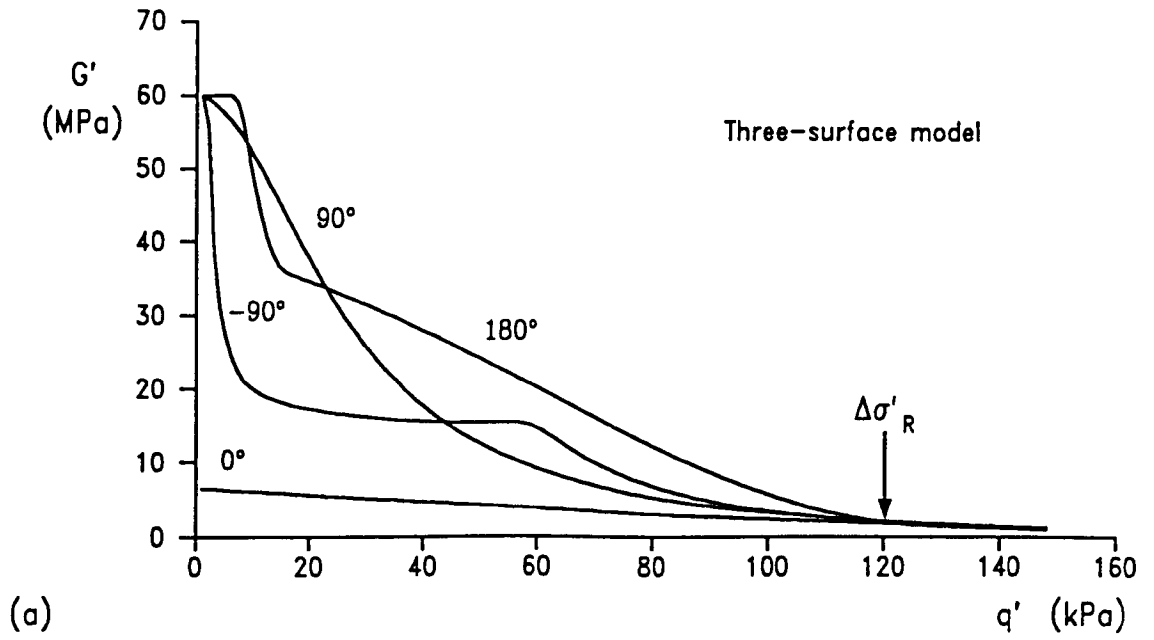
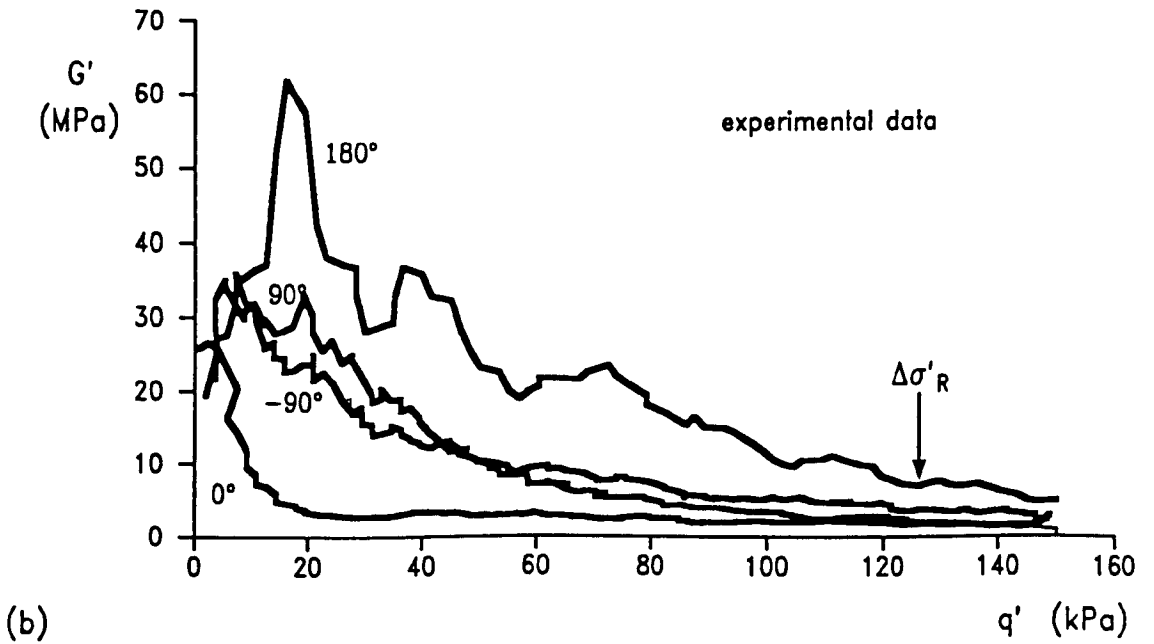


Figure 3.2 Three surface kinematic yield hardening model in  $p'$  -  $q$  space: Stallebrass model



(a)



(b)

Figure 3.3 Stiffness with shear stress for different stress path rotations (After Stallebrass, 1990)

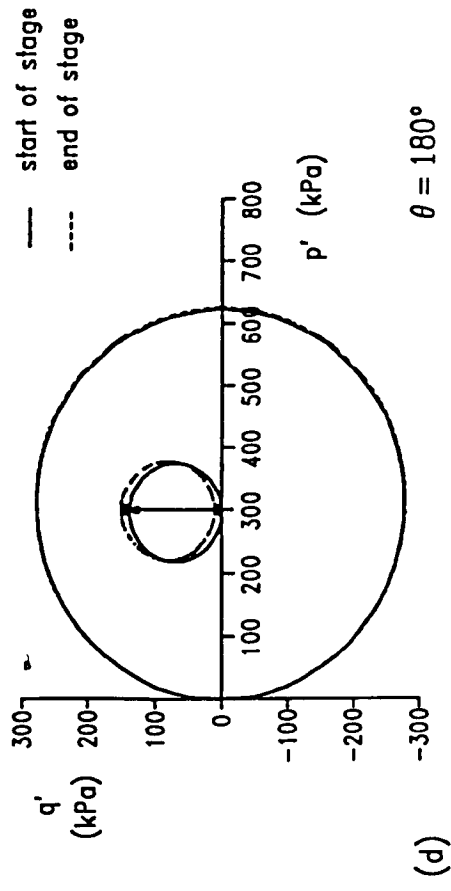
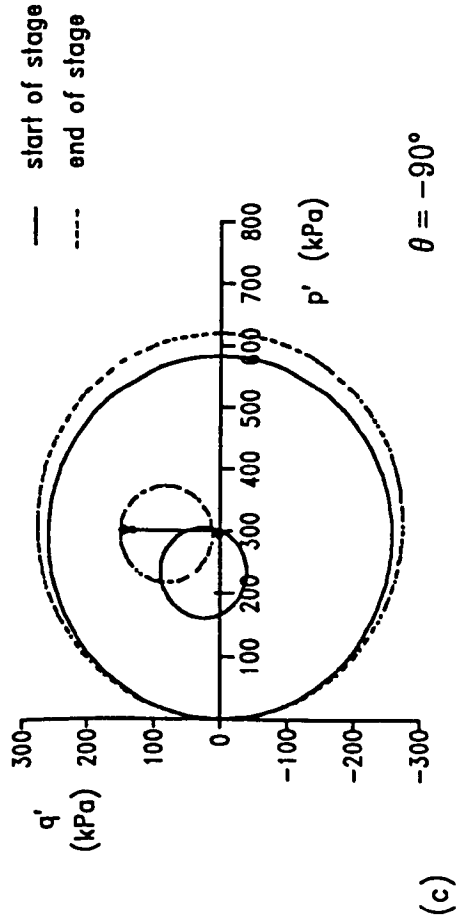
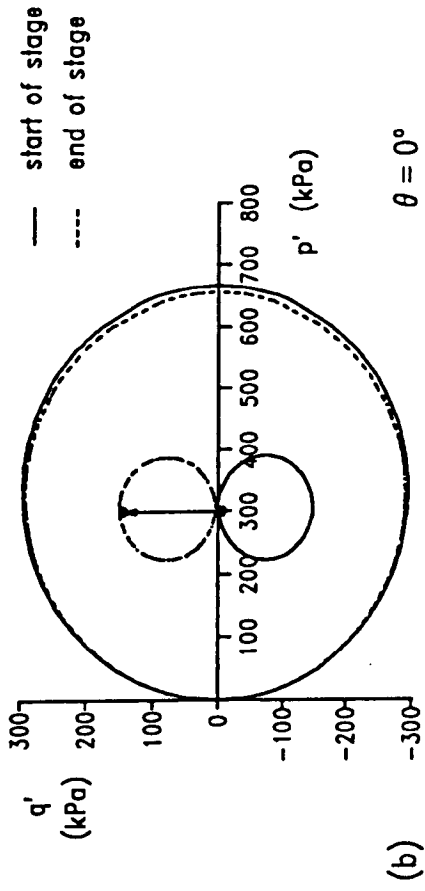
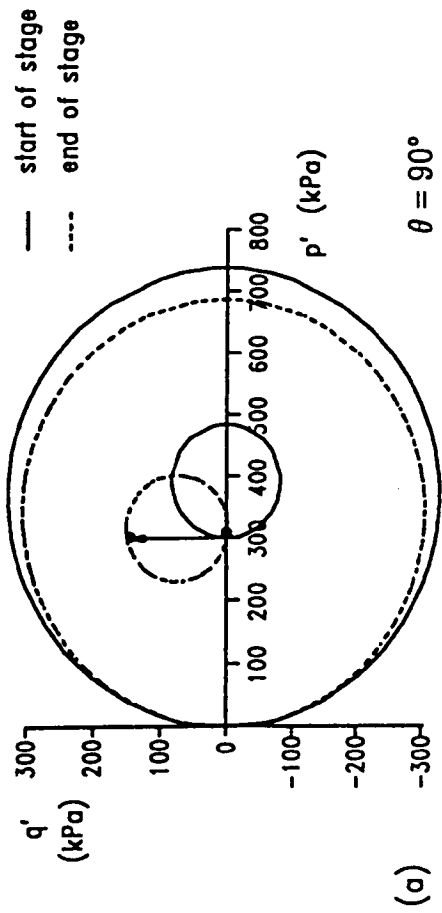
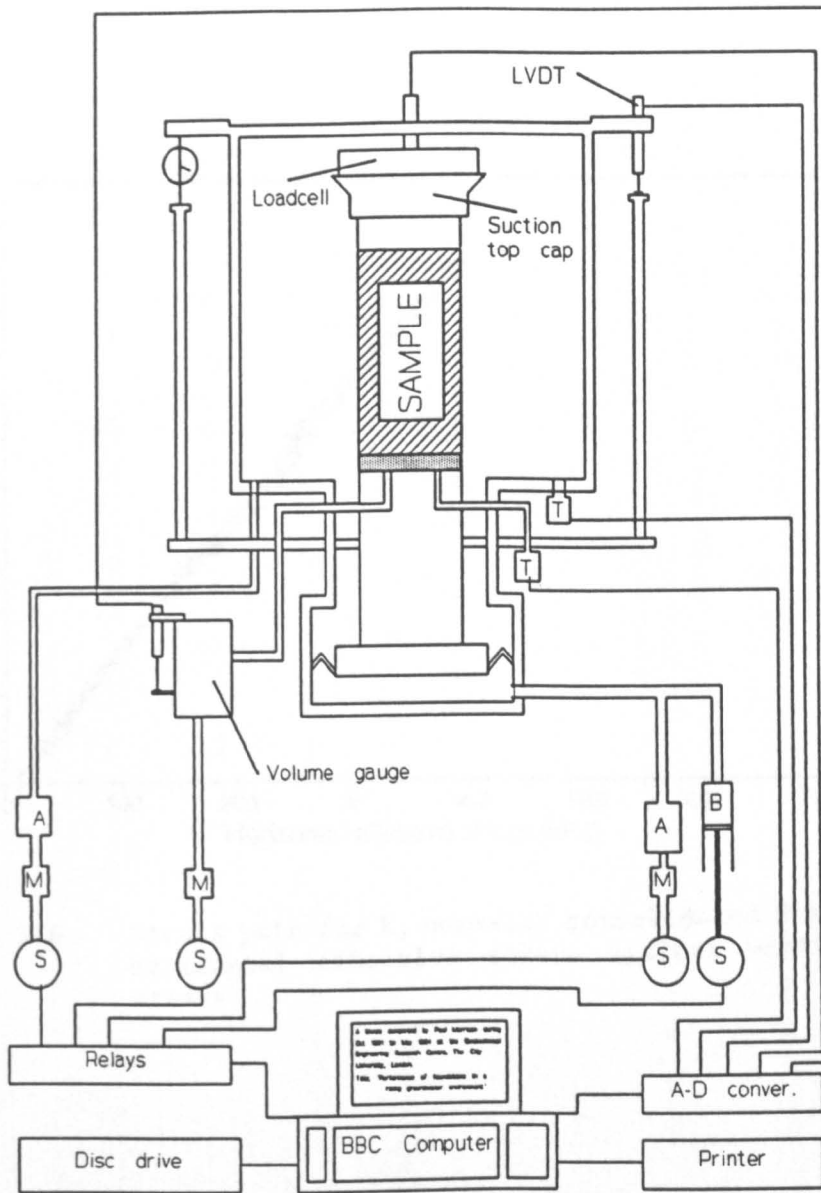


Figure 3.4 Stress path rotation for Figure 3.3 (After Stallebrass, 1990)



Key:

- M = Manostat
- A = Air/water interface
- S = Stepper motor
- B = Bishop ram
- T = Pressure transducer

Figure 3.5 Layout of triaxial stress path cell

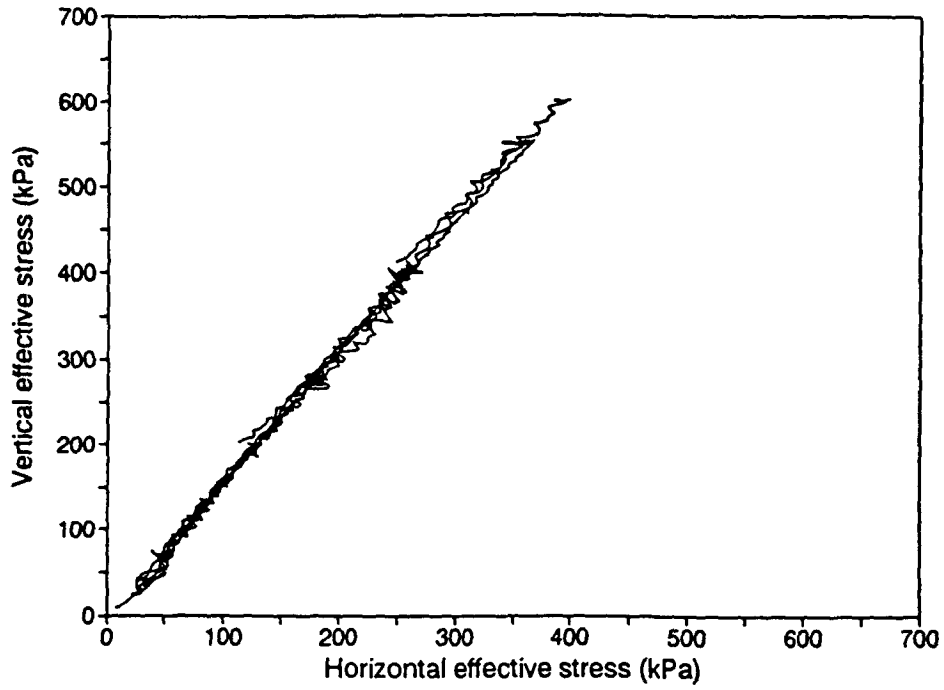


Figure 3.6 Stress path for  $K_0$  normally consolidated Speswhite Kaolin, horizontal effective stress against vertical effective stress

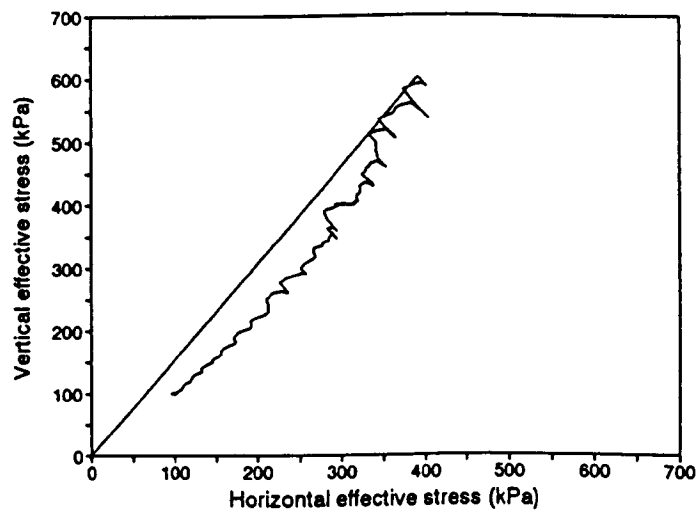
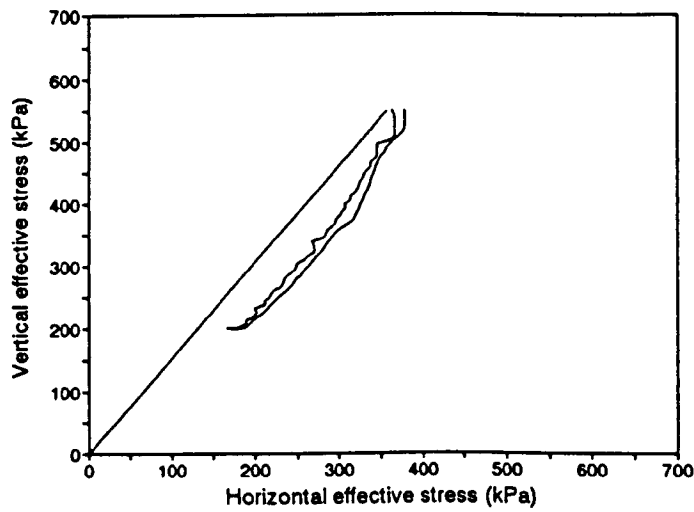
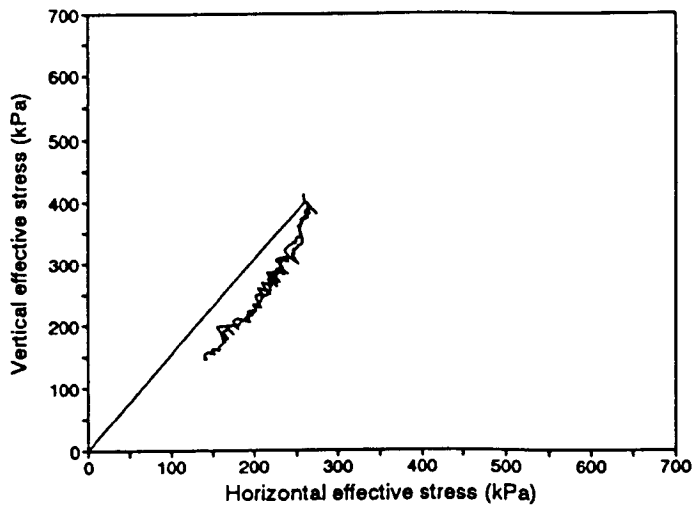


Figure 3.7 Stress path for  $K_0$  unloading of Speswhite Kaolin, horizontal effective stress against vertical effective stress:

- a) Tests 7S and 10S
- b) Tests T8 and T9
- c) Test L1

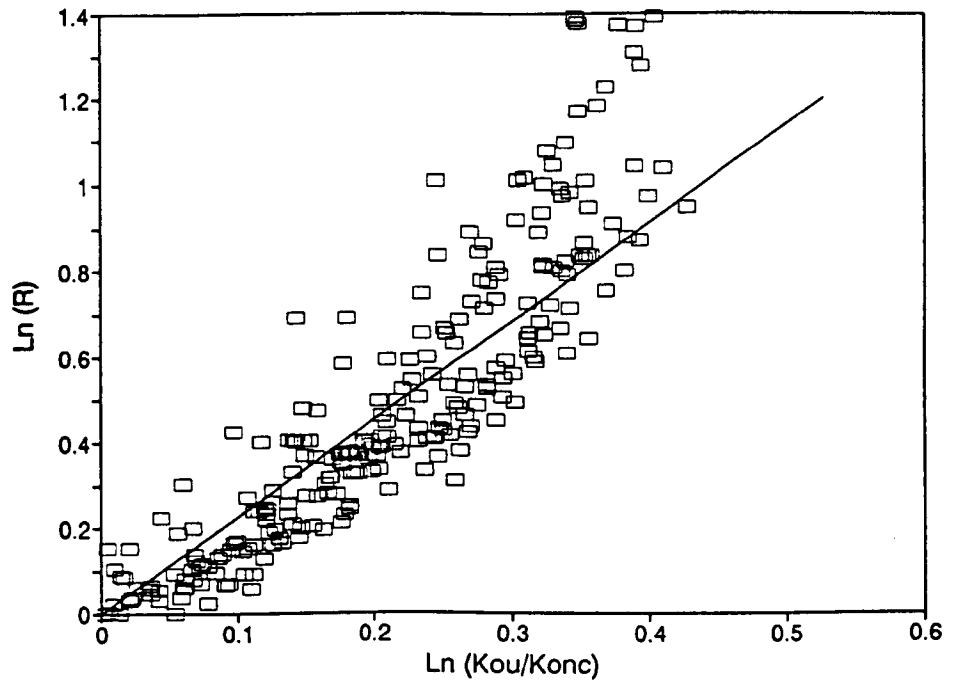


Figure 3.8 Variation of  $K_{ou}/K_{onc}$  with overconsolidation ratio

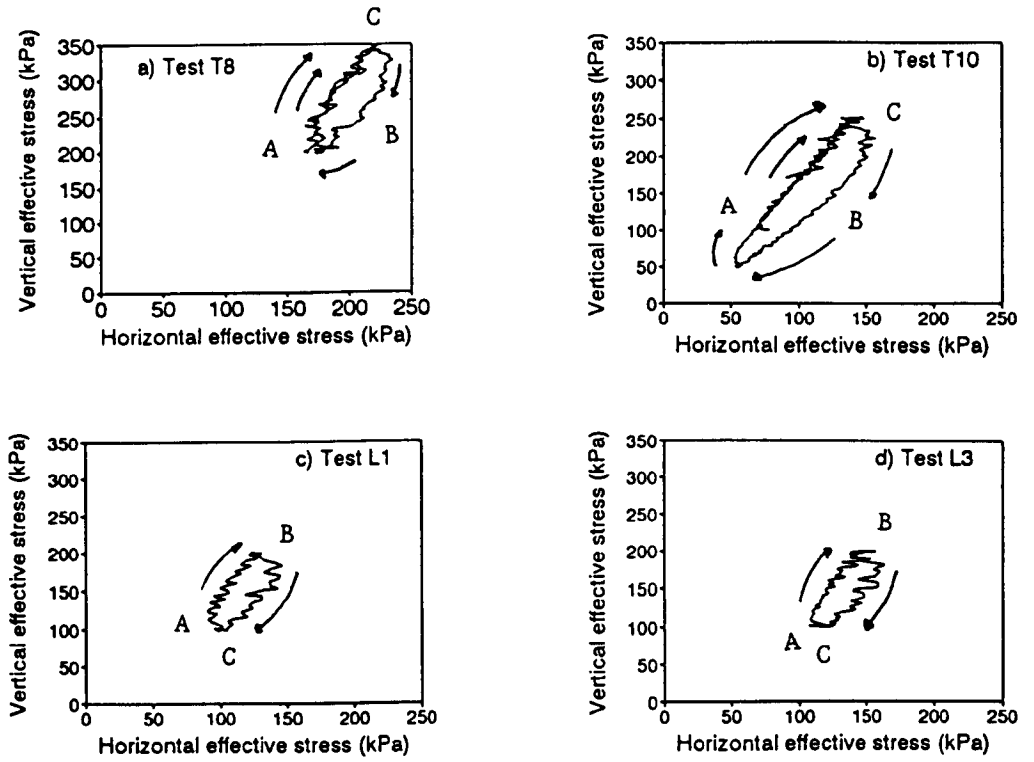


Figure 3.9 Cycles of pore water pressure under  $K_0$  conditions, horizontal effective stress against vertical effective stress, stress path from A to B to C:  
 a) Test T8                      b) Test T10  
 c) Test L1                      d) Test L3

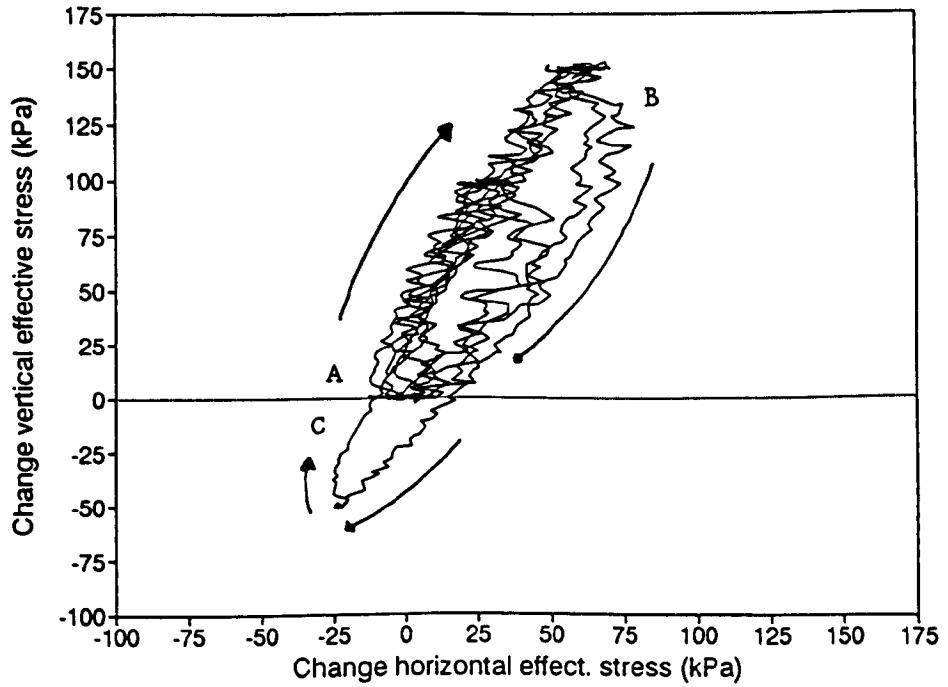


Figure 3.10 Change in horizontal effective stress with change in vertical effective stress during pore water pressure cycles, stress path from A to B to C

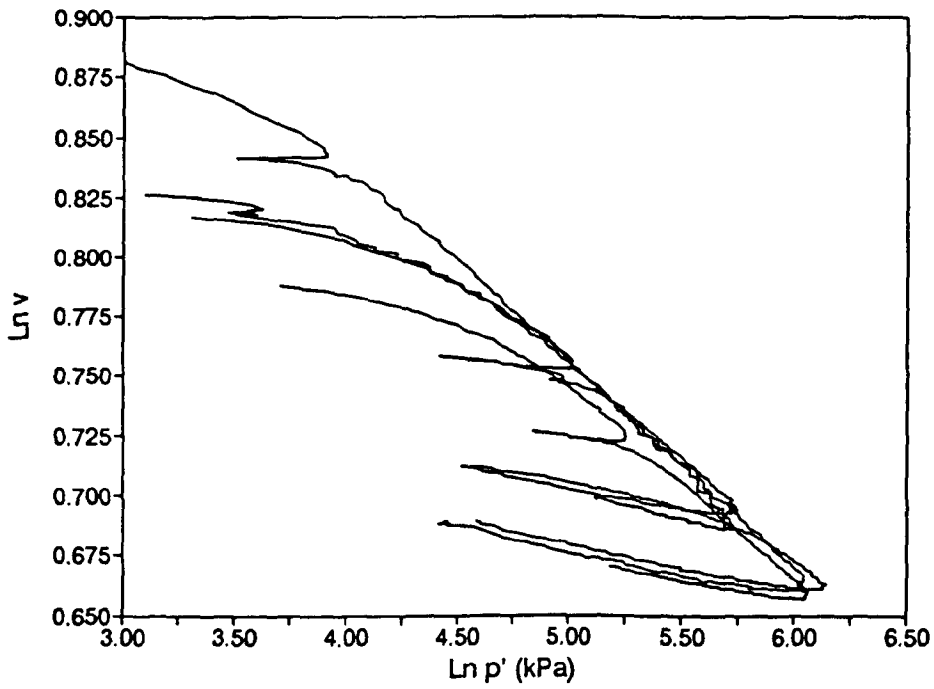


Figure 3.11  $K_0$  compression data,  $\ln(v)$  against  $\ln(p')$  for tests in Figure 3.6

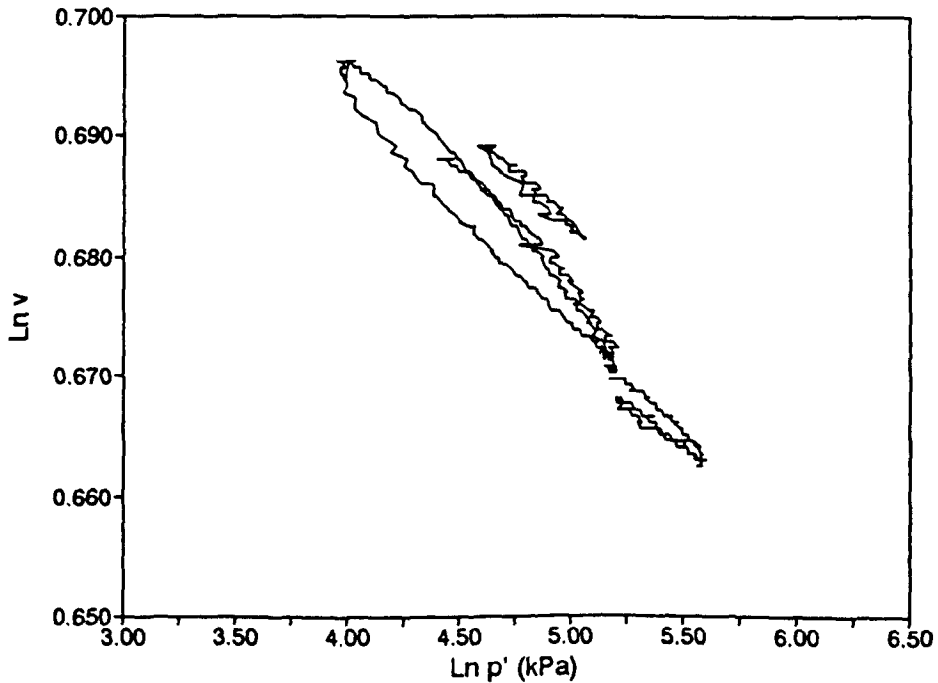


Figure 3.12  $K_0$  compression and swelling data for samples compressed to  $\sigma'_{vmax} = 600 \text{ kPa}$  during pore water pressure cycles in  $\ln(v) - \ln(p')$  space

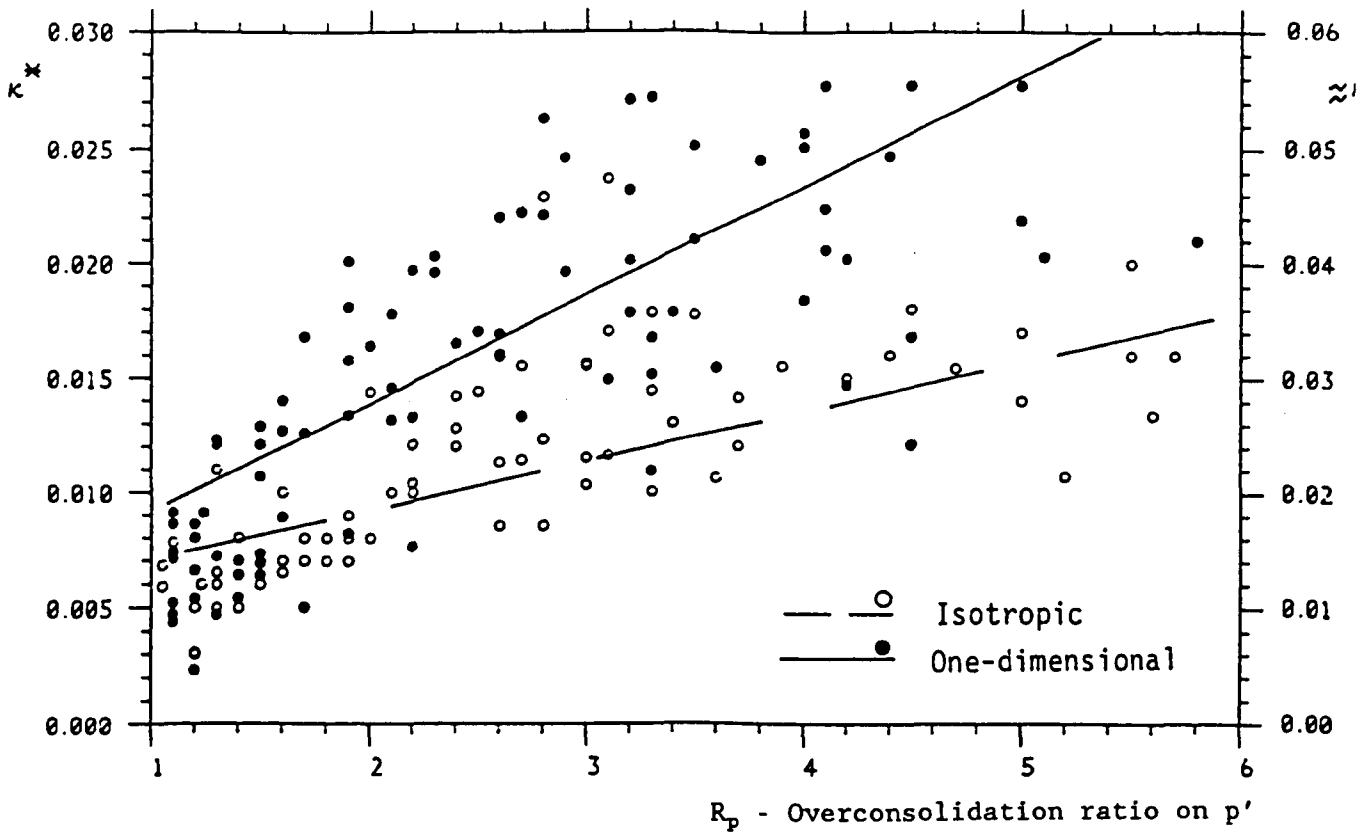


Figure 3.13 Variation of  $\kappa^*$  with overconsolidation ratio during primary unloading (After Al-Tabbaa, 1988)

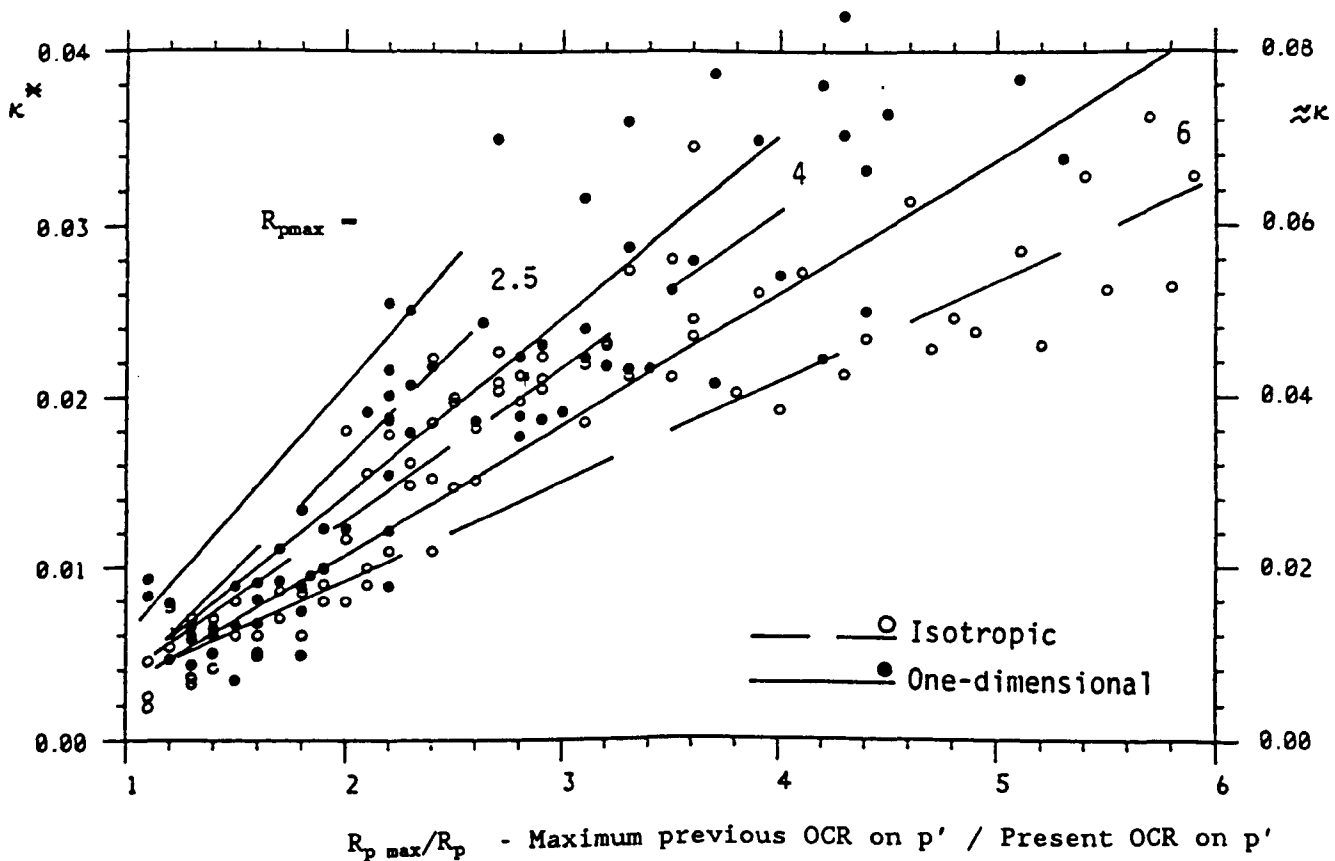


Figure 3.14 Variation of  $\kappa^*$  with overconsolidation ratio during reloading (After Al-Tabbaa, 1988)

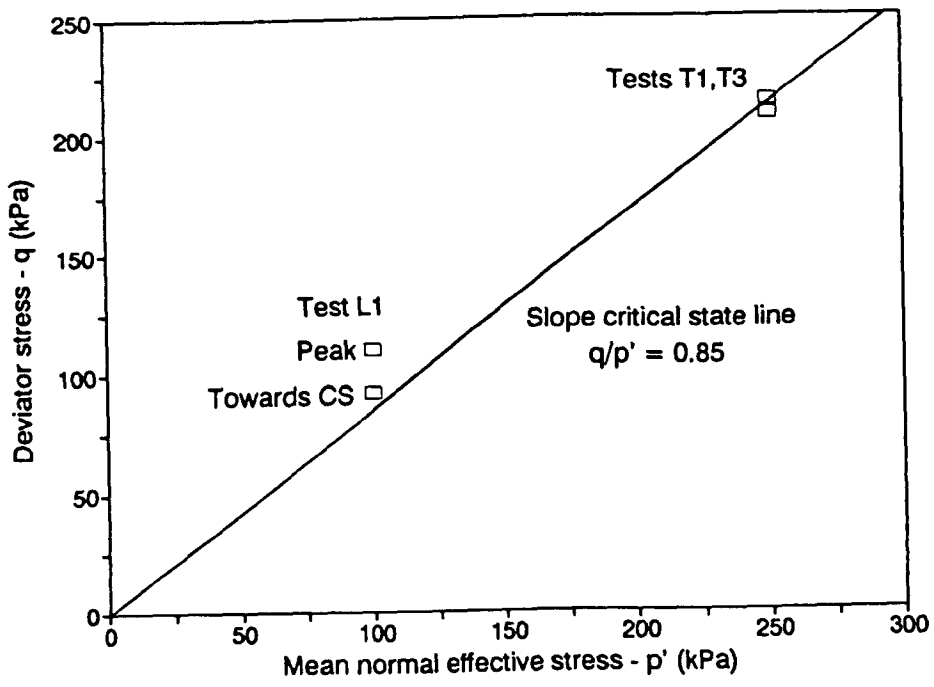


Figure 3.15 Ultimate stress states for constant  $p'$  shearing in compression

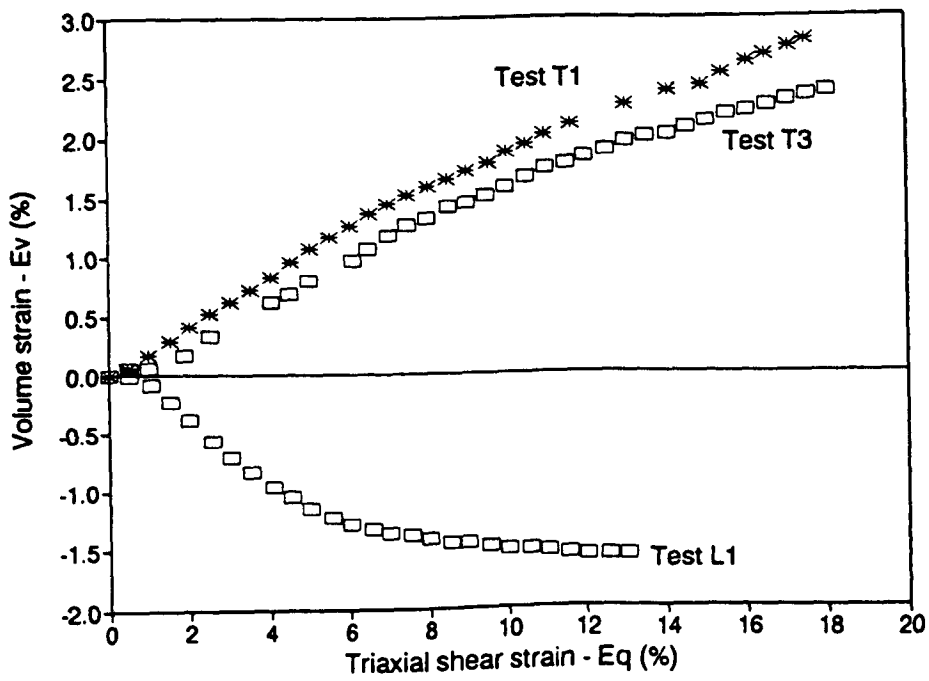


Figure 3.16 Comparison of volumetric and shear strain during constant  $p'$  shearing in compression

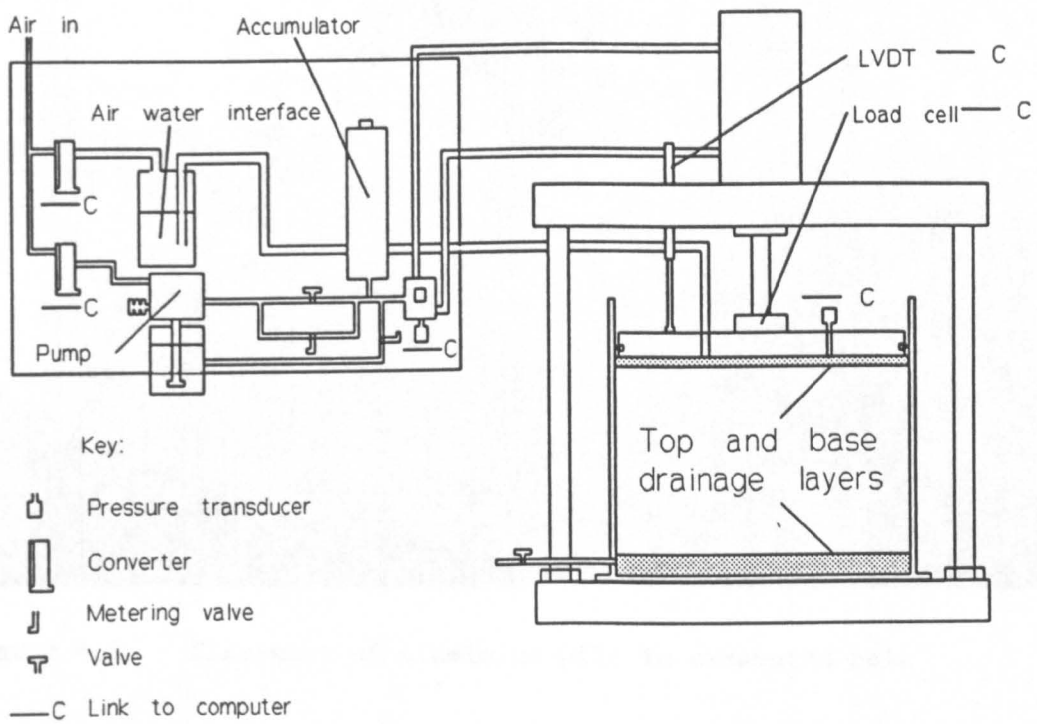


Figure 4.1a Lay out of computer controlled hydraulic consolidometer

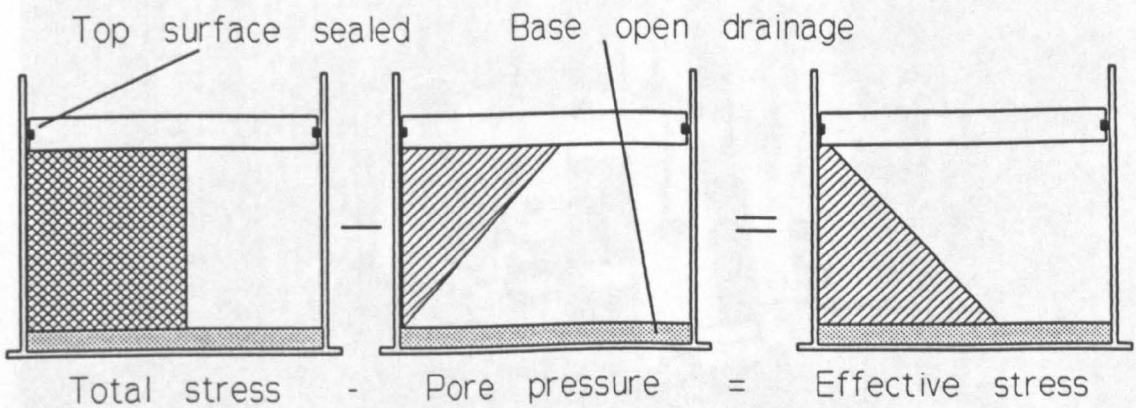


Figure 4.1b Stress states in sample using downward hydraulic gradient technique

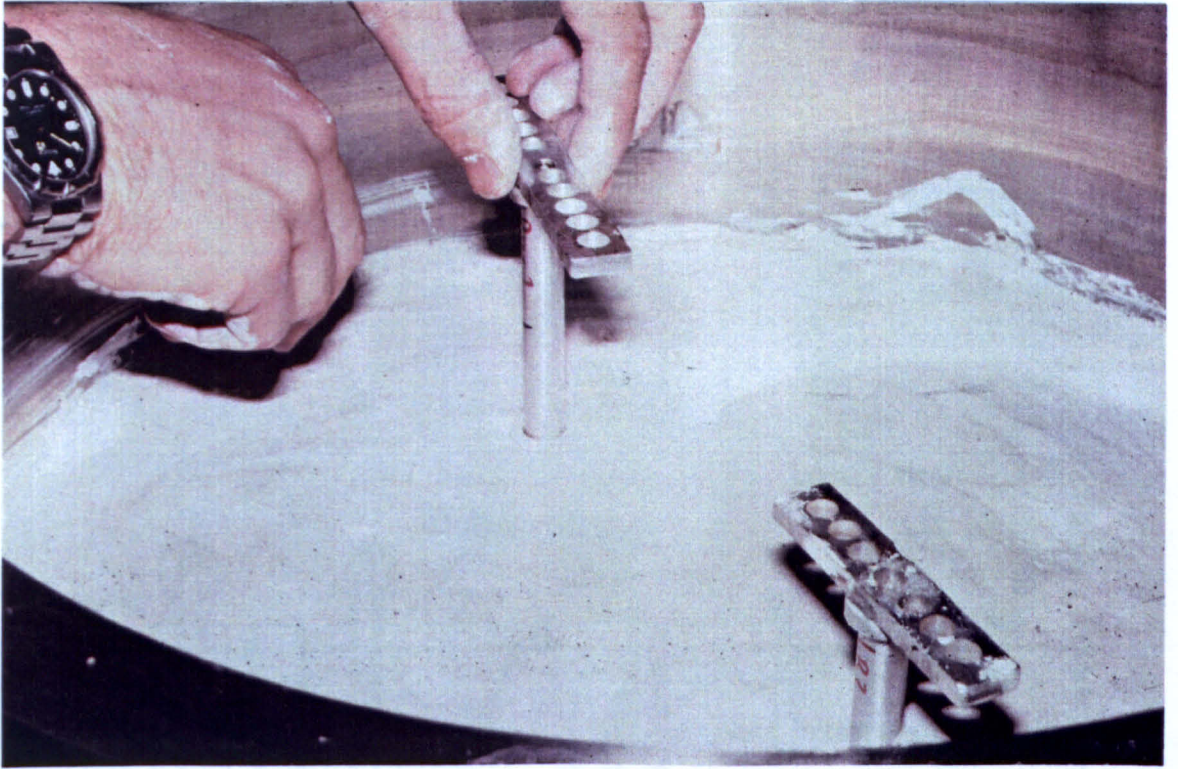


Figure 4.2 Placement of aluminium pile in excavated hole

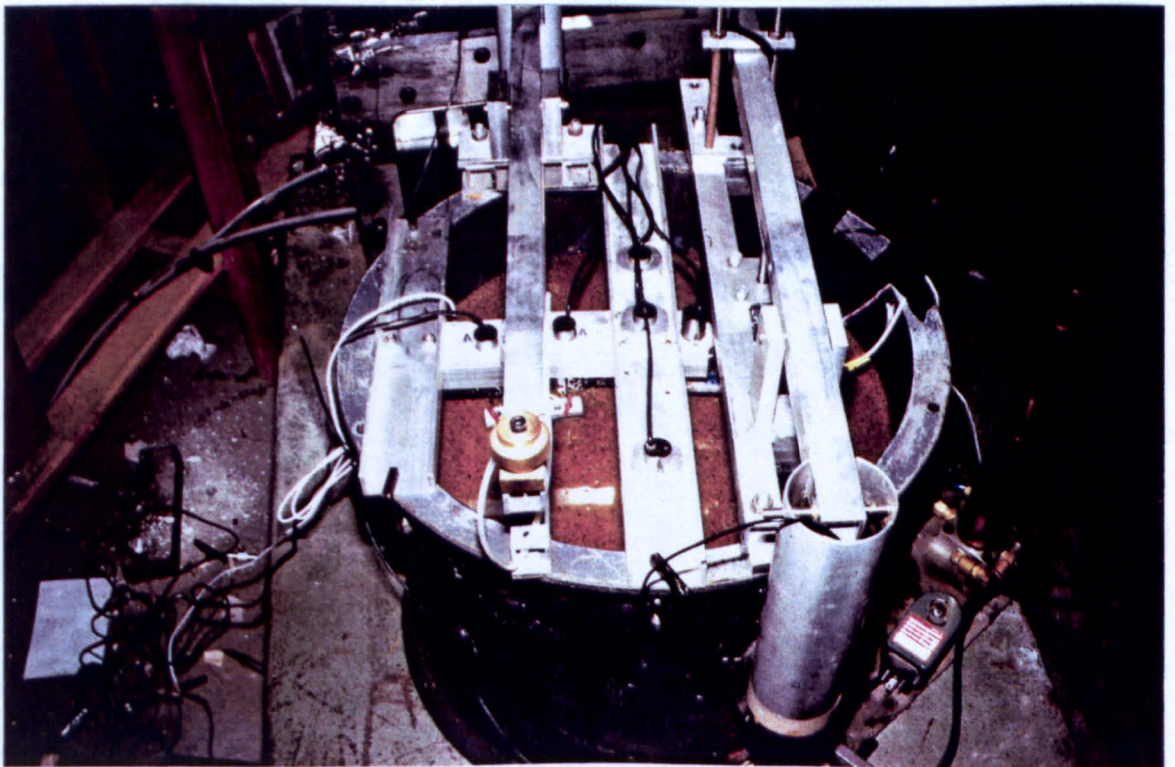


Figure 4.3a View of typical centrifuge model prior to loading onto centrifuge swing

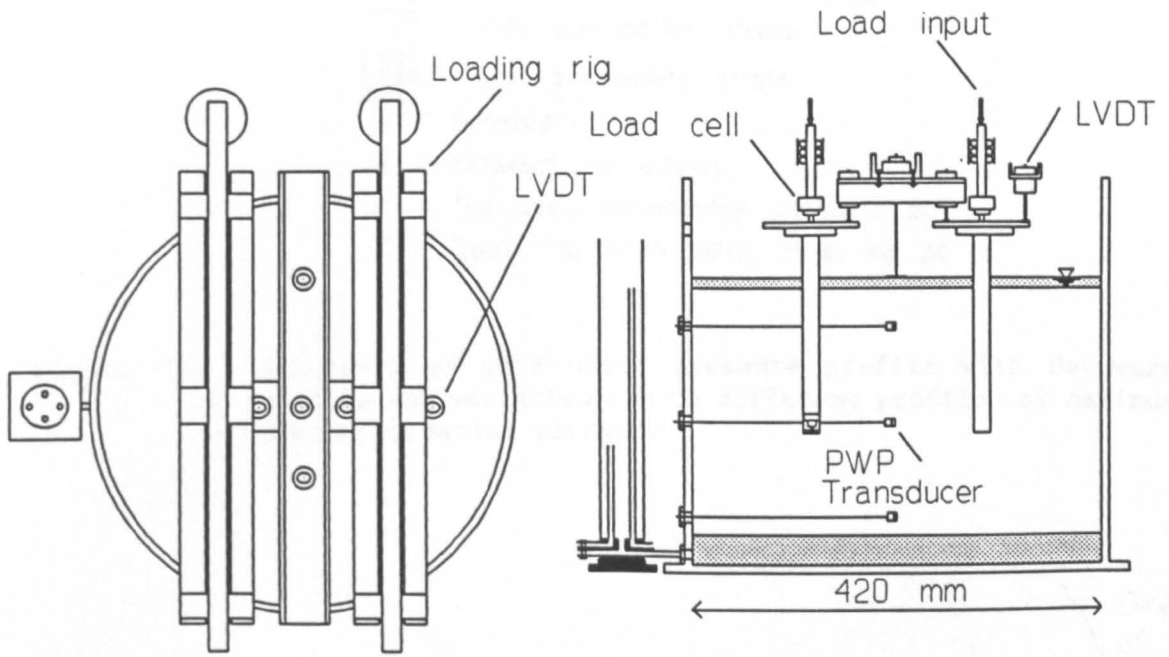


Figure 4.3b Set up of a typical centrifuge model with two similar piles

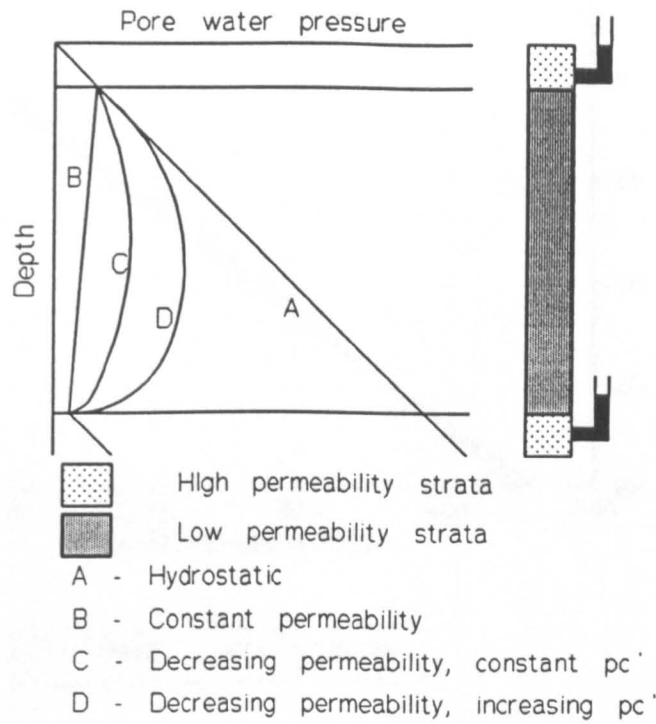


Figure 4.4 Schematic of pore water pressure profile with downward seepage and variation due to different profiles of maximum preconsolidation pressure

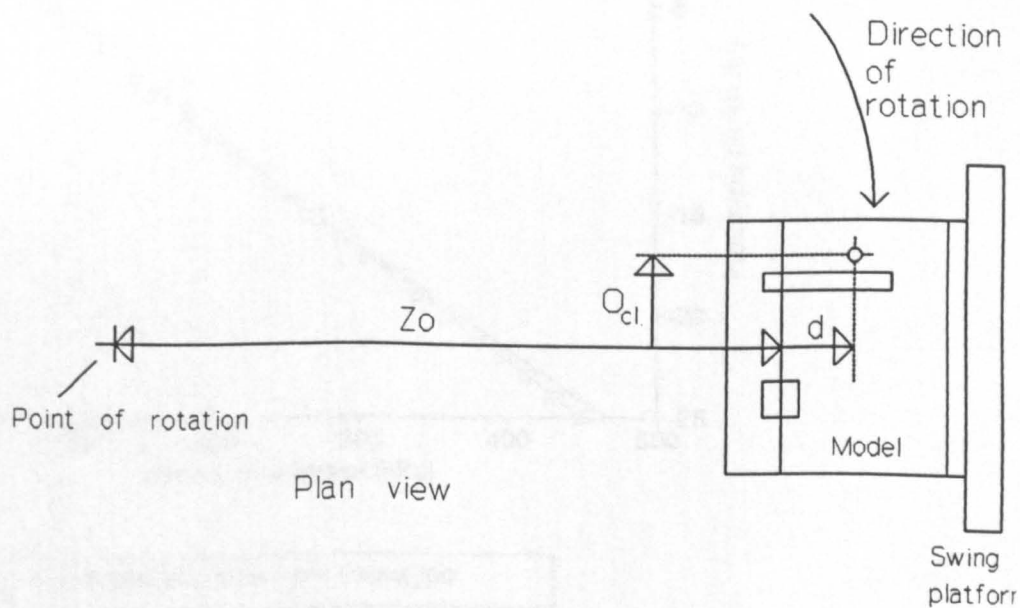


Figure 4.5 Swing and centrifuge arm geometry for calculation of acceleration errors

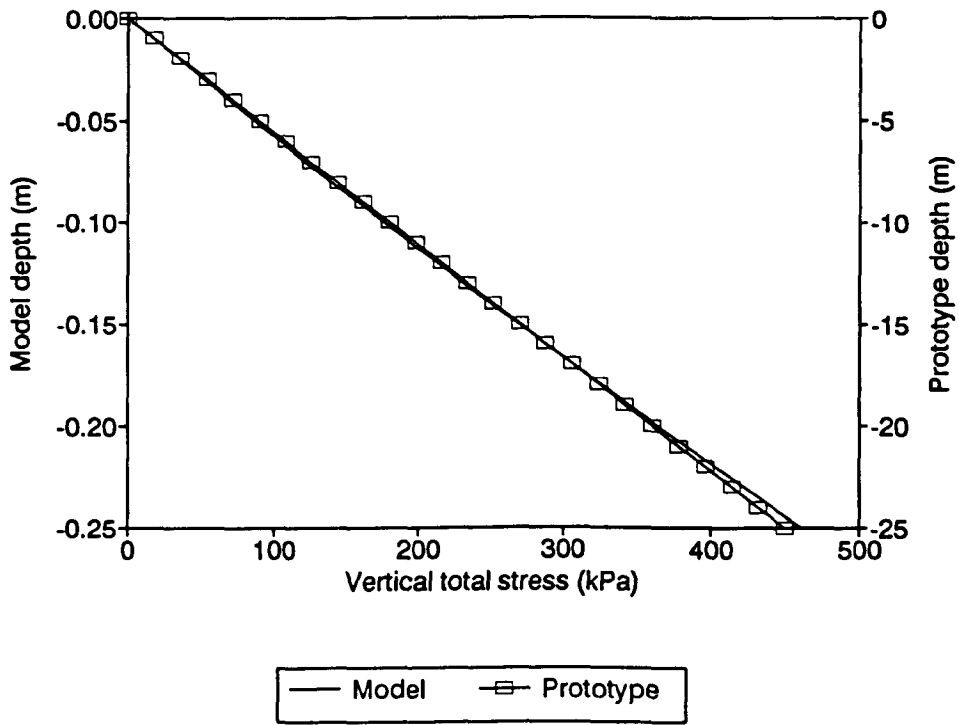


Figure 4.6 Comparison of model and prototype total stress profiles along centre line of model

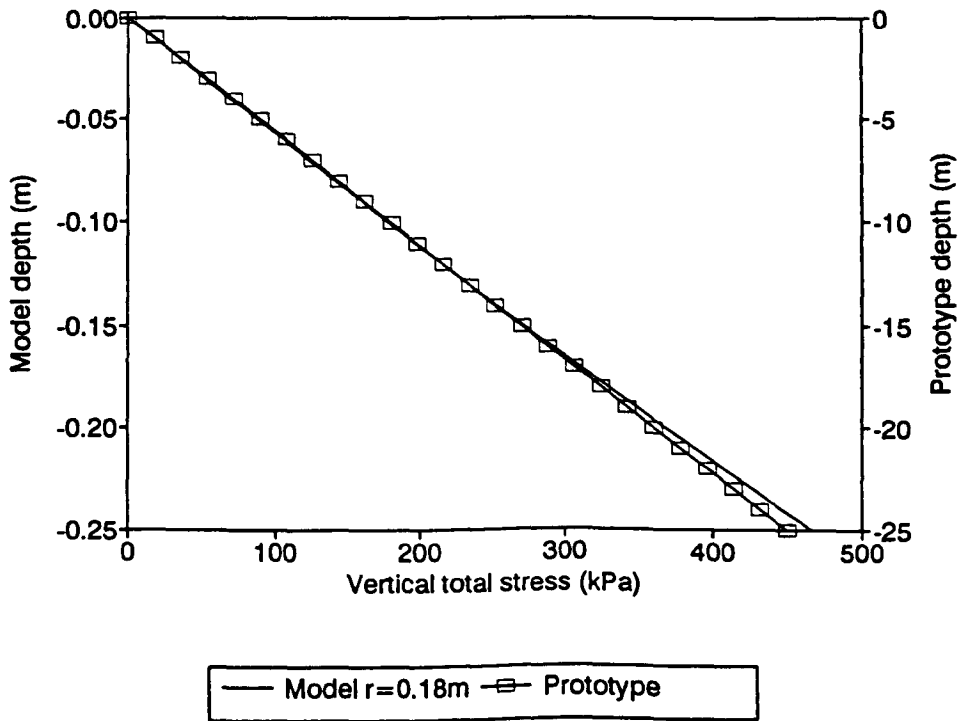


Figure 4.7 Comparison of model and prototype total stress profiles along line offset by 0.18m (model scale) from centre line of model

Centrifuge: Acutronic 661, 1.8m radius to swing base, 40g tonne capacity

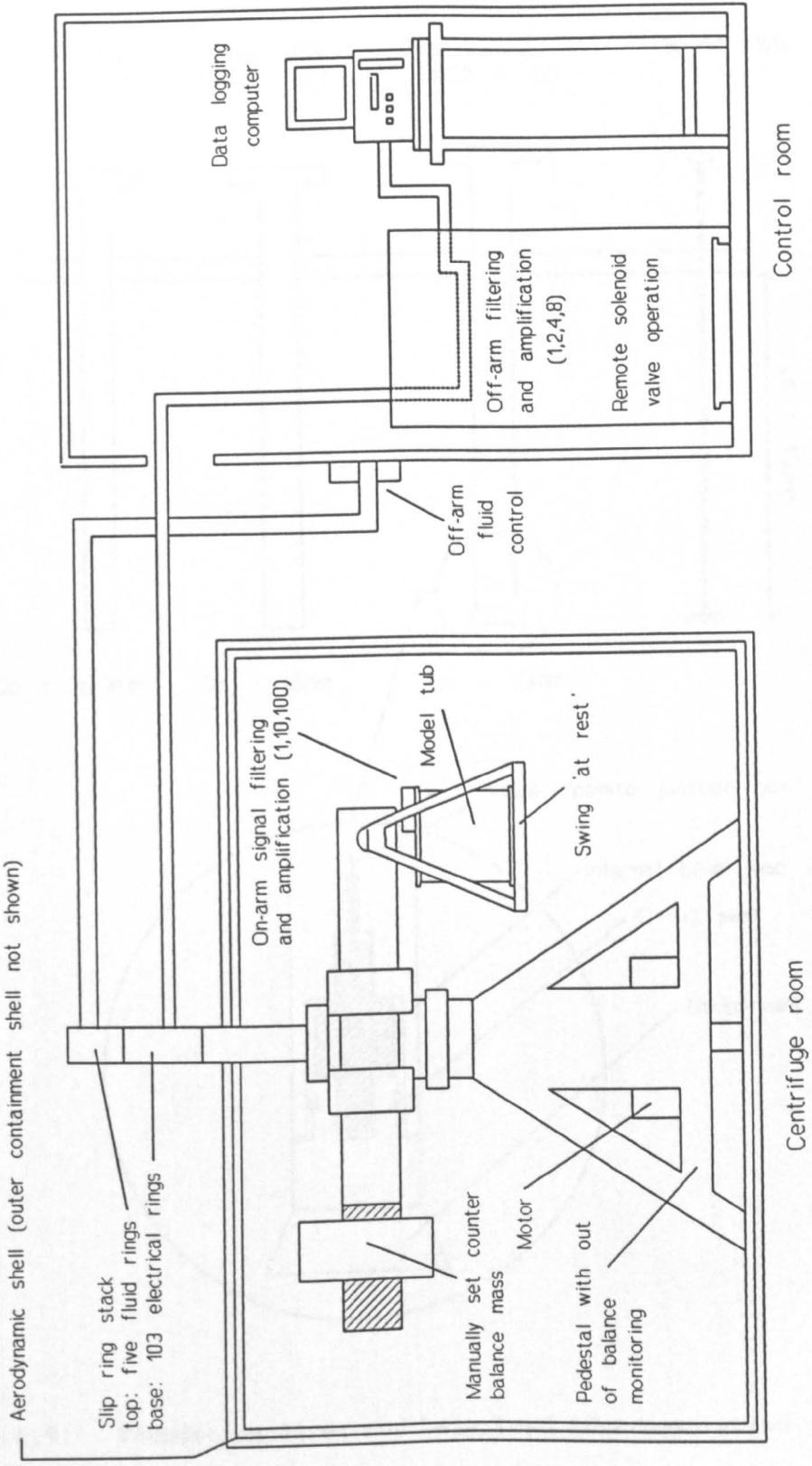


Figure 4.8 Schematic of Acutronic 661 centrifuge and testing facility

Slender pile  
 $L_s/D_b = 12.0$

Straight pile  
 $L_s/D_b = 9.5$

Under-reamed pile  
 $L_s/D_b = 6.5$

Buried plate

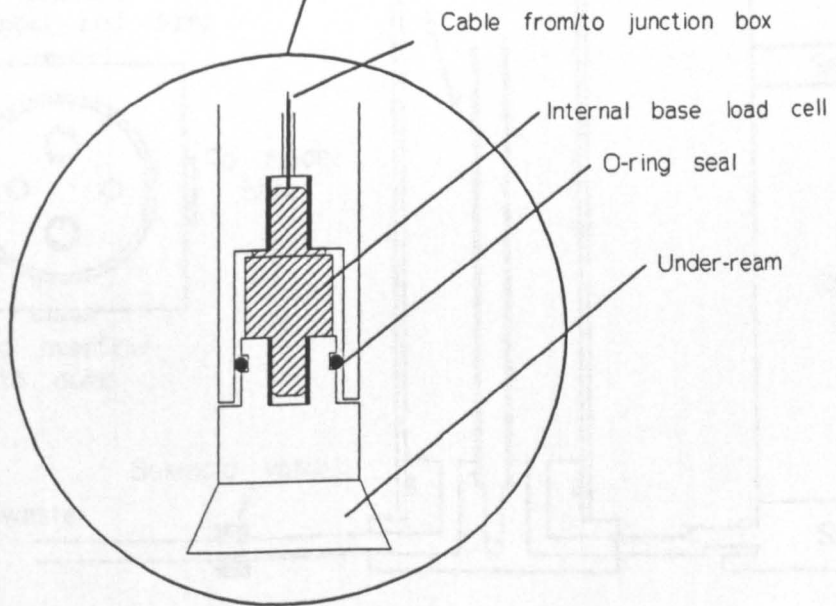
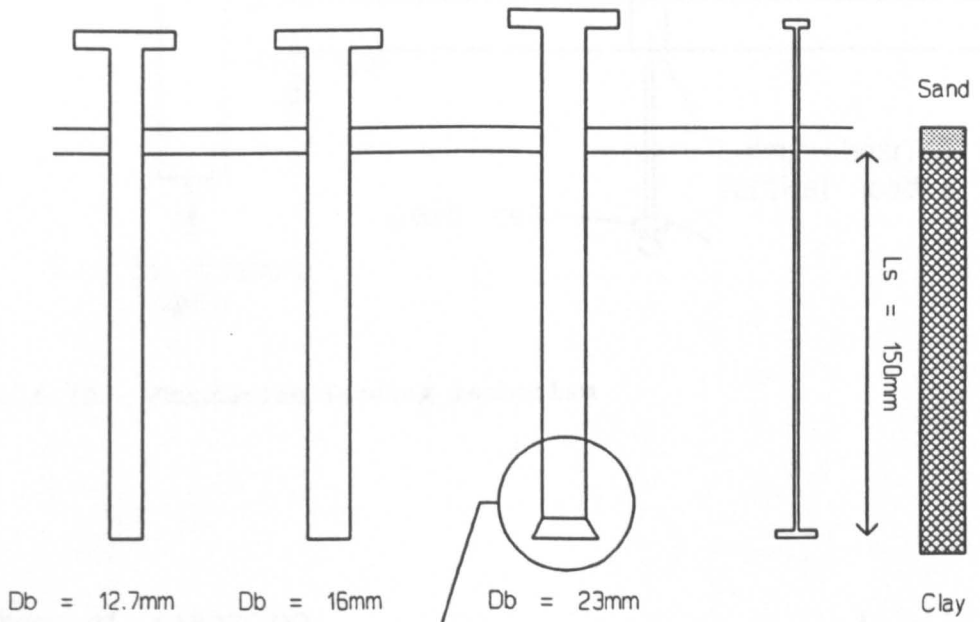


Figure 4.9 Foundation sizes and base load instrumentation

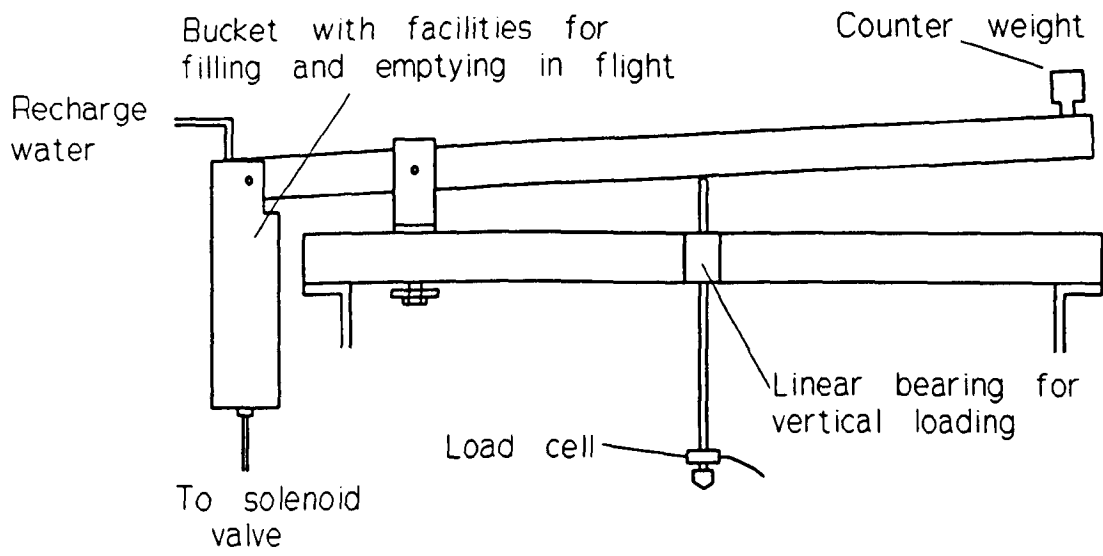


Figure 4.10 Foundation loading mechanism

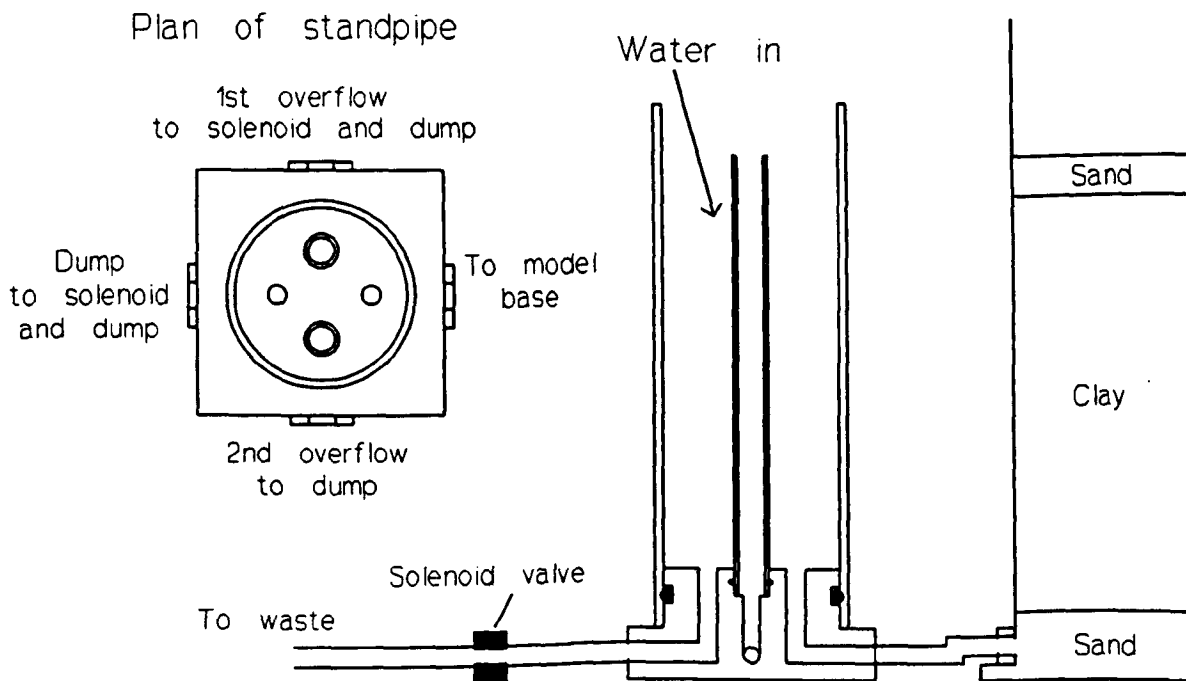


Figure 4.11 Basal aquifer pore water pressure control mechanism

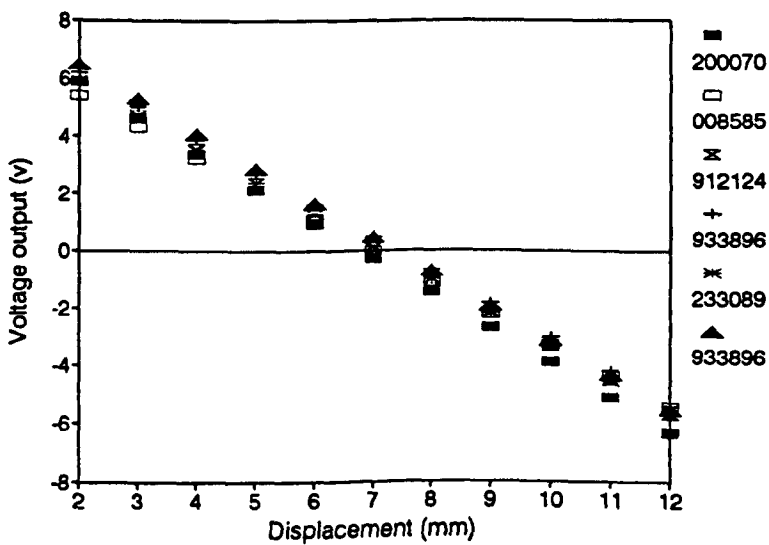
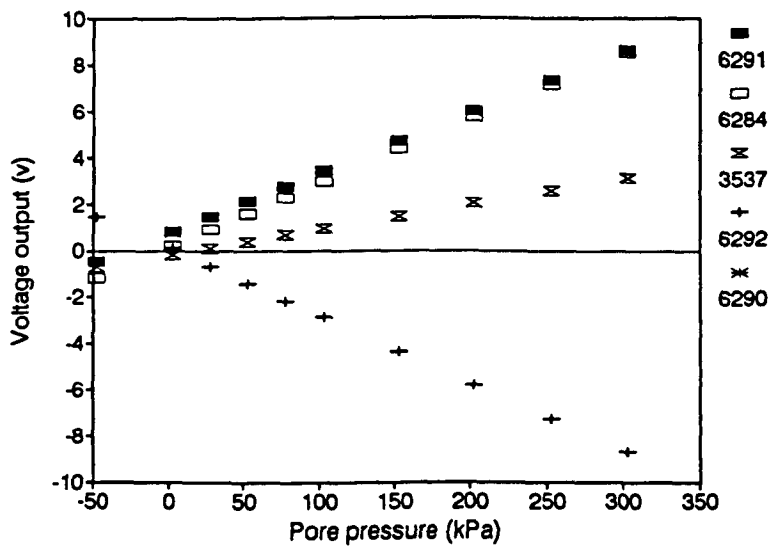
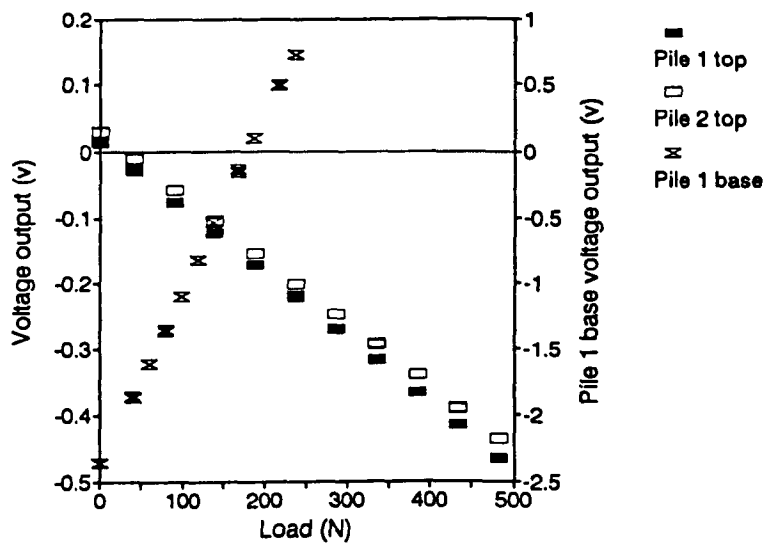


Figure 4.12 Calibration data for transducers used in test RW15:  
 a) Displacement transducers, gain = 2  
 b) Pore pressure transducers, gain = 100  
 c) Load cells, gain = 200

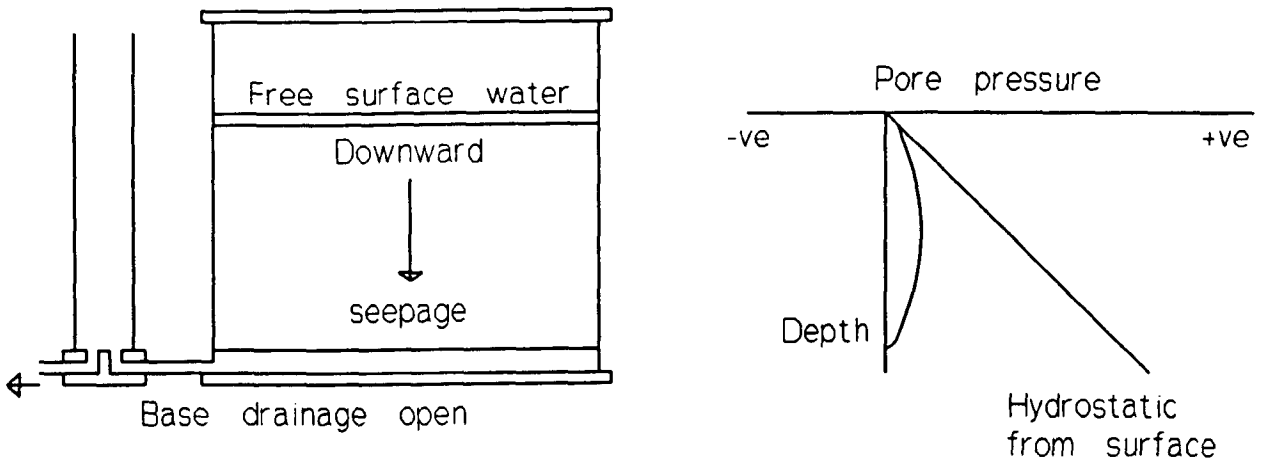


Figure 4.13a Schematic of pore water pressure profile with downward seepage and a perched water table before groundwater rising event

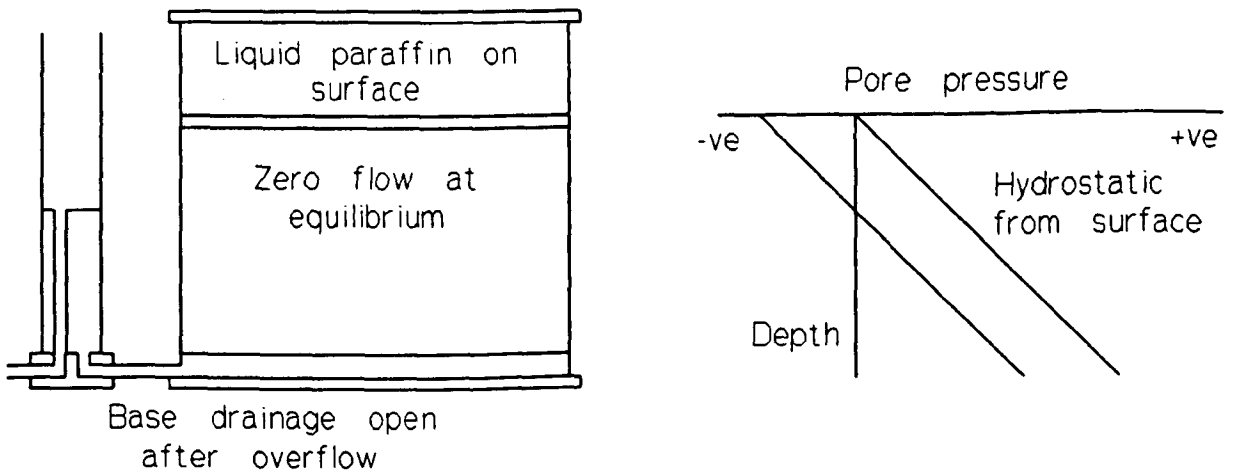


Figure 4.13b Schematic of pore water profile pressure with sealed top surface before groundwater rising event

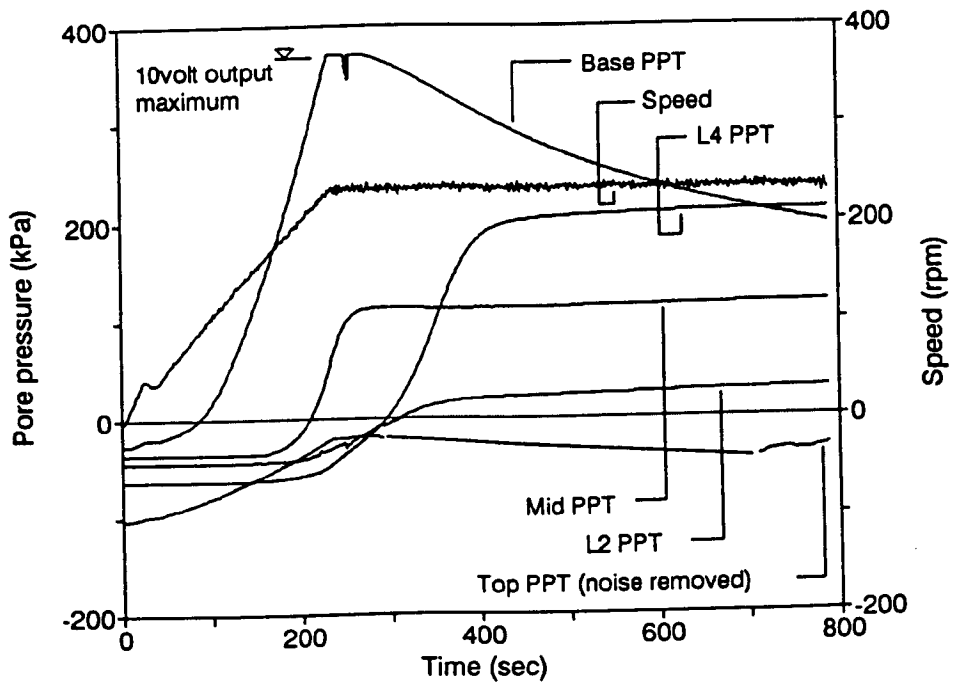


Figure 5.1 Pore water pressure response during spin-up from test RW10

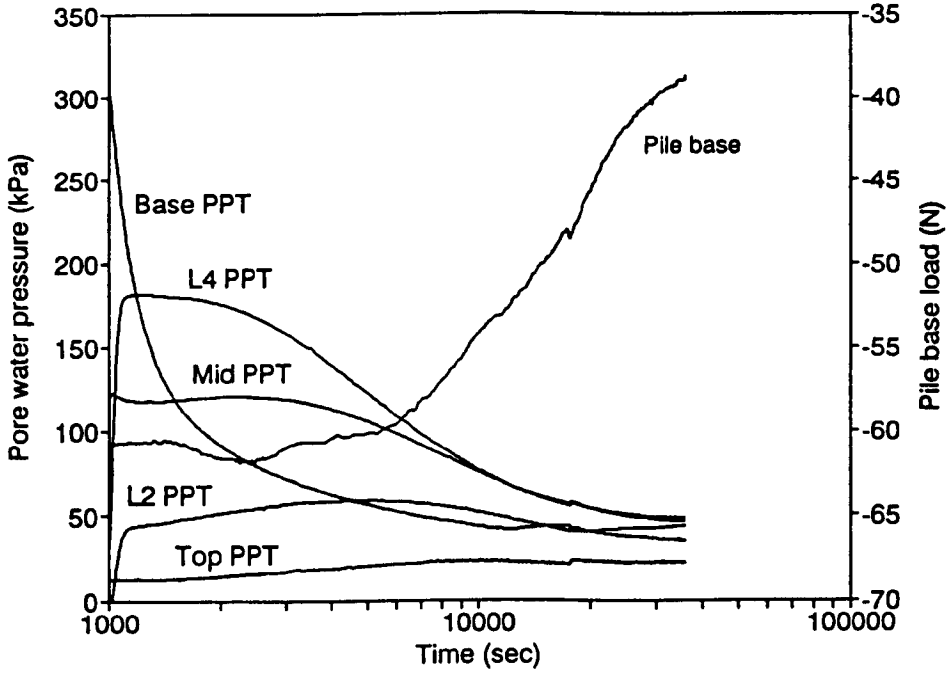


Figure 5.2a Dissipation of pore water pressure after spin-up from test RW10 with perched water table

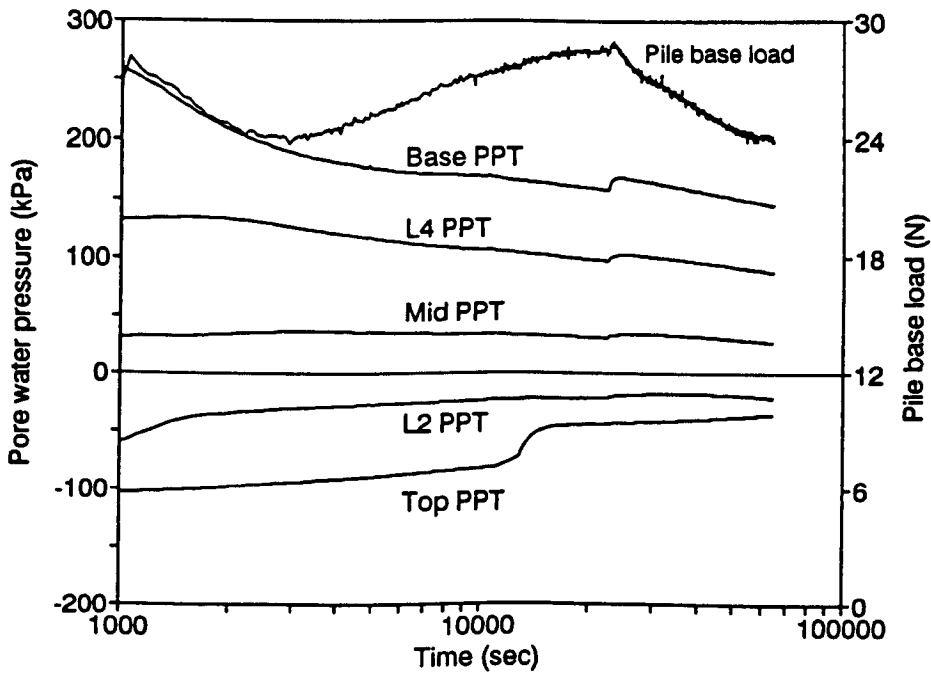


Figure 5.2b Dissipation of pore water pressure after spin-up from test RW13 with sealed surface

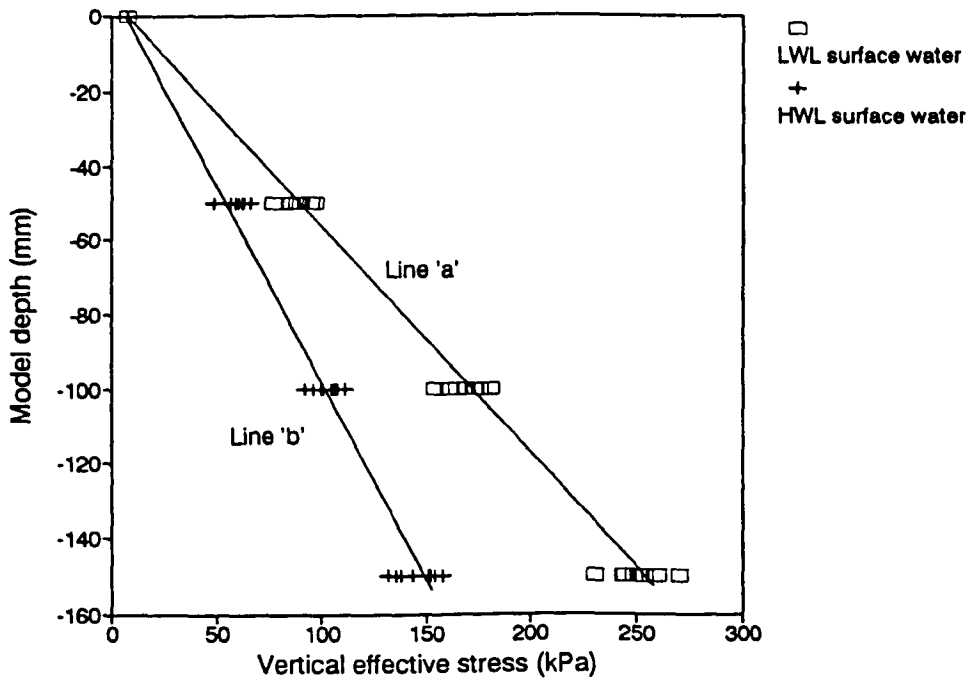


Figure 5.3 Vertical effective stress profiles before (line 'a') and after (line 'b') rising groundwater event for nine tests with a perched water table

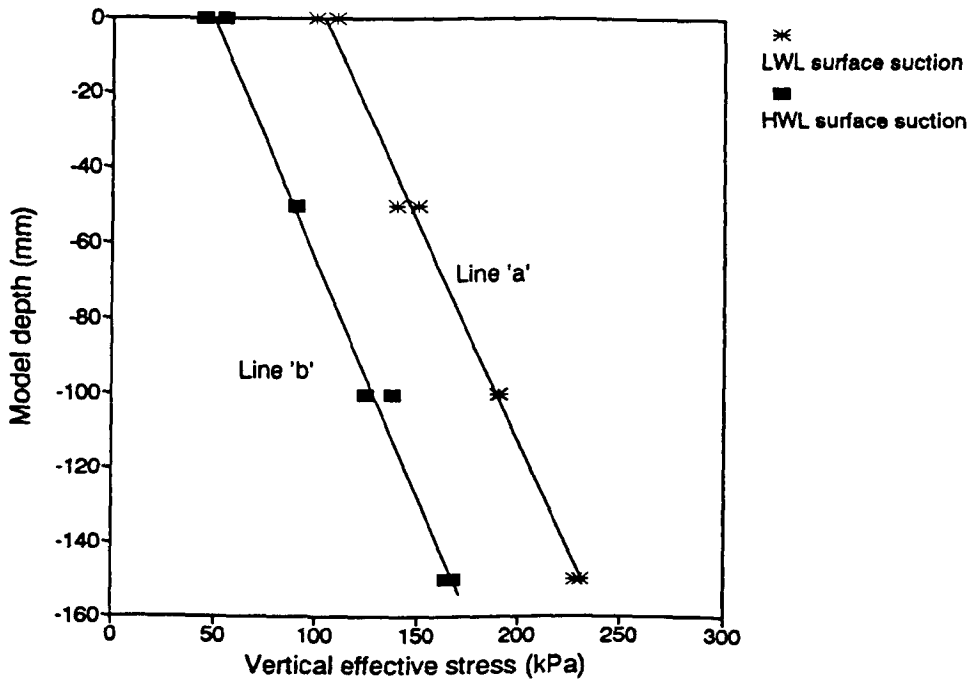


Figure 5.4 Vertical effective stress profiles before (line 'a') and after (line 'b') rising groundwater event for two tests with a sealed surface

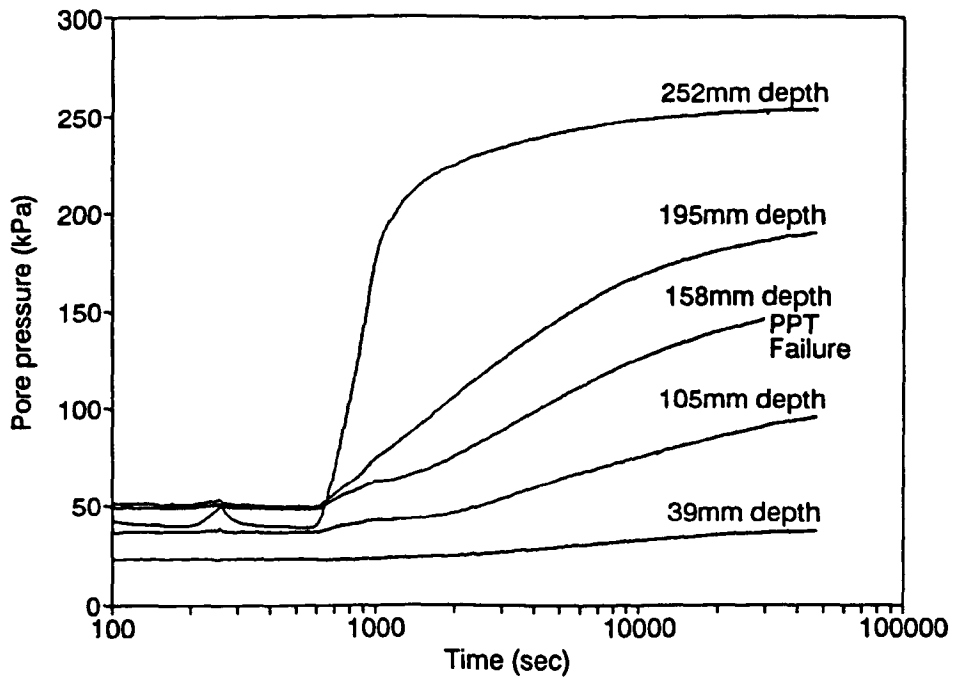


Figure 5.5 Increase in pore water pressure with time during a model rising groundwater event from test RW10 with a perched water table

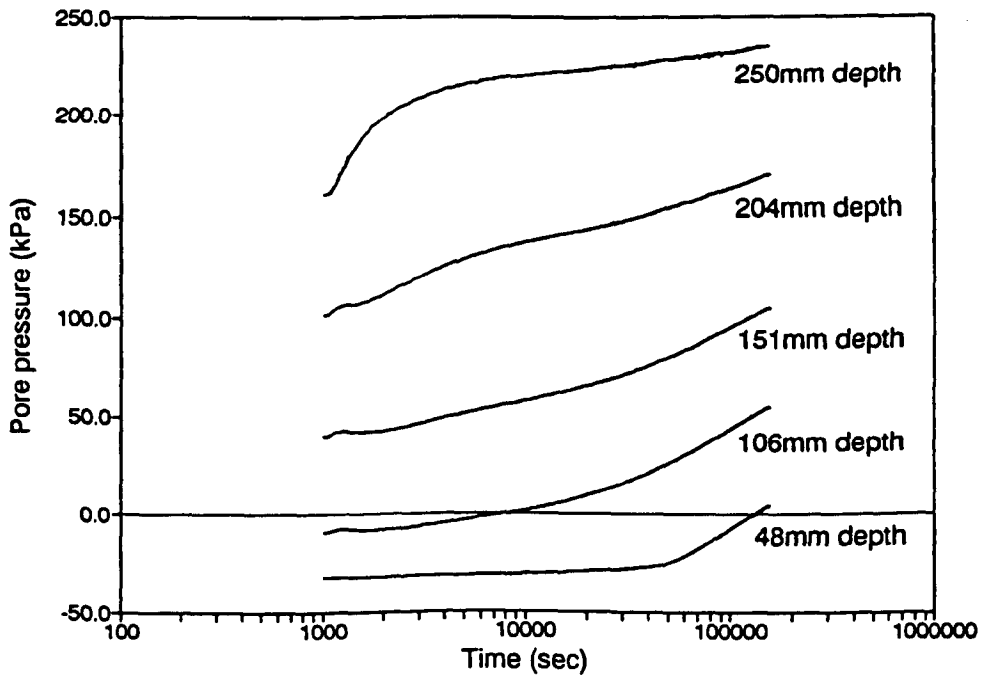


Figure 5.6 Increase in pore water pressure with time during a rising groundwater event with a sealed surface, test RW13

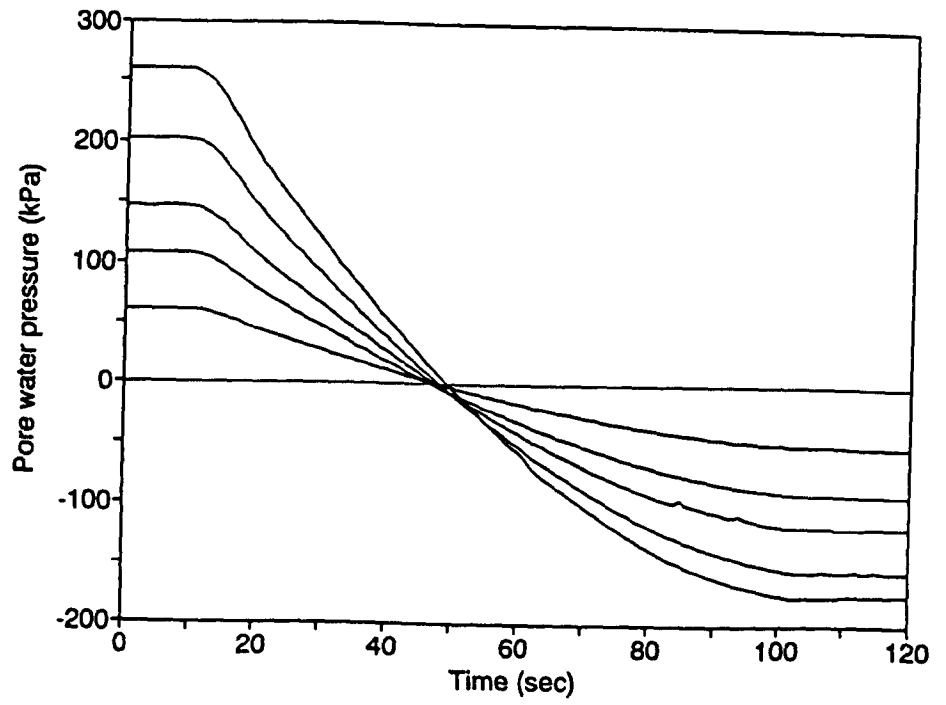


Figure 5.7 Pore water pressure response during spin-down from test RW16

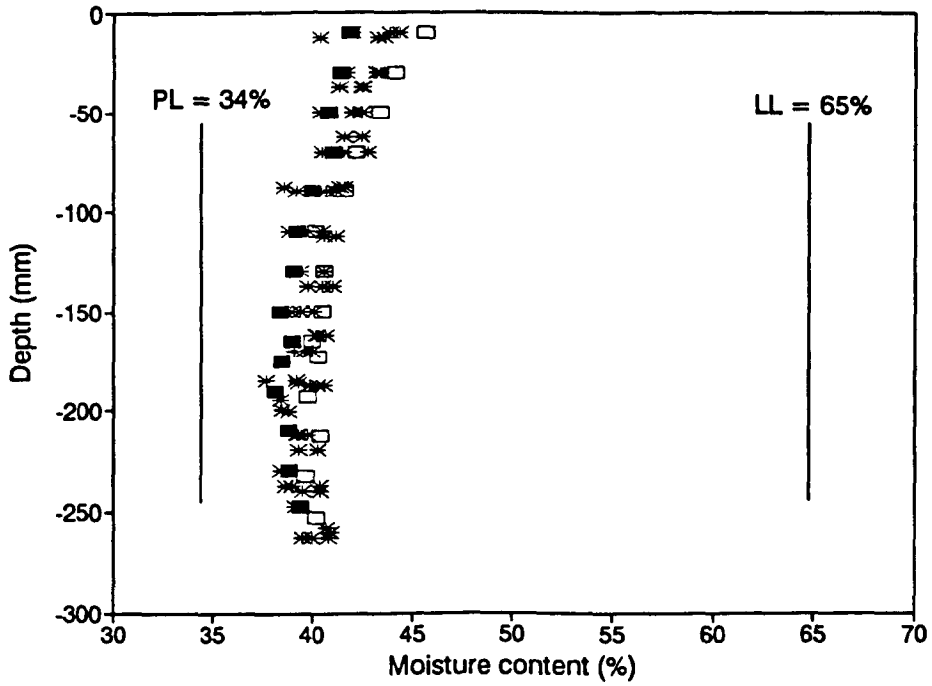


Figure 5.8 Final moisture contents for tests with downward seepage

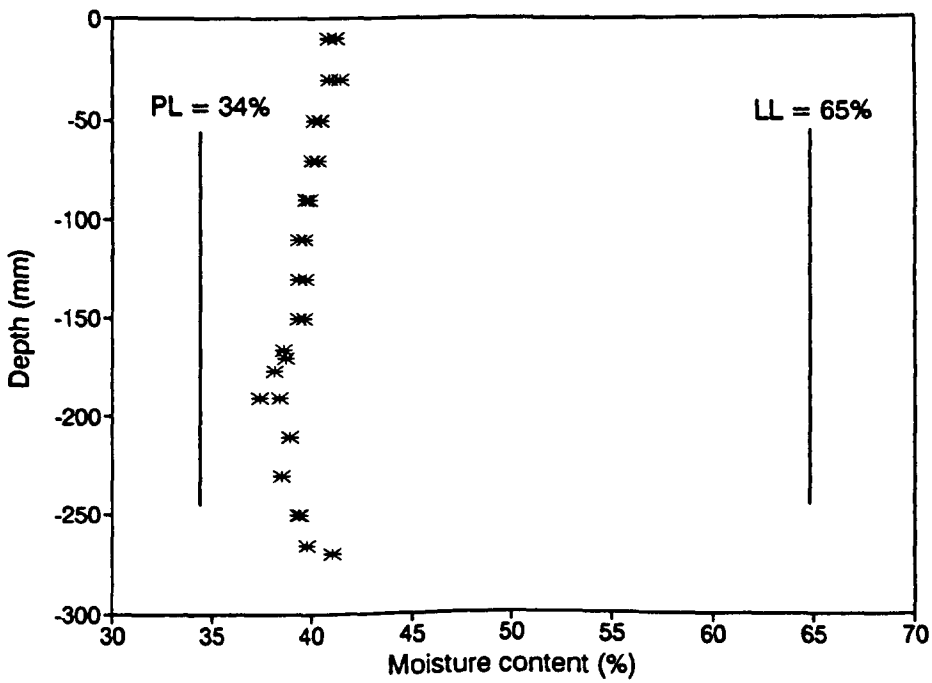


Figure 5.9 Final moisture contents for tests with a sealed surface

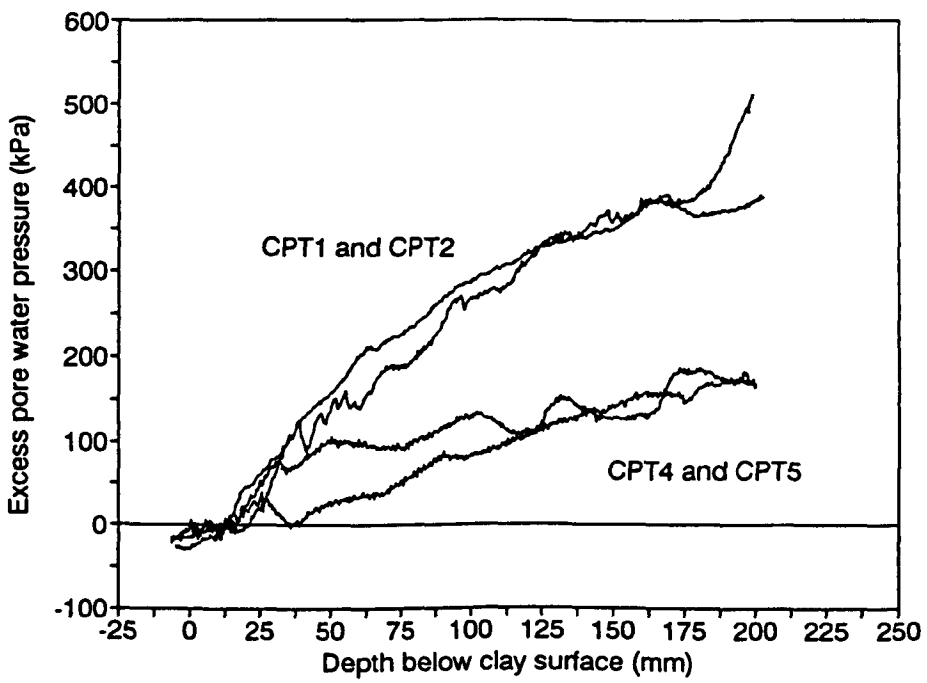
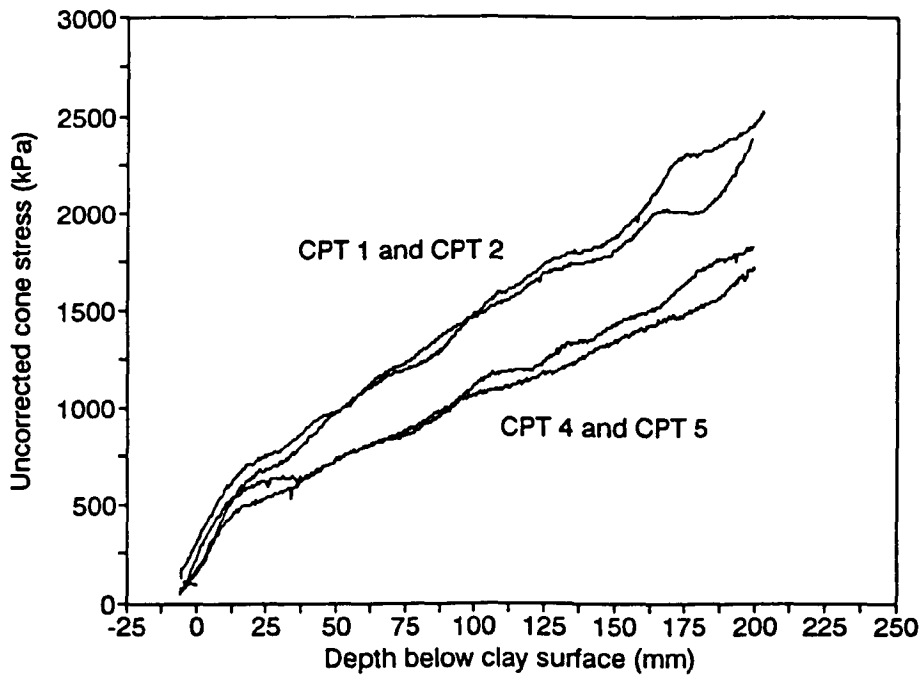


Figure 5.10 Piezocone tests at 0.2mm/sec:  
 a) Uncorrected cone resistance -  $q_c$   
 b) Excess pore water pressure -  $u_e$

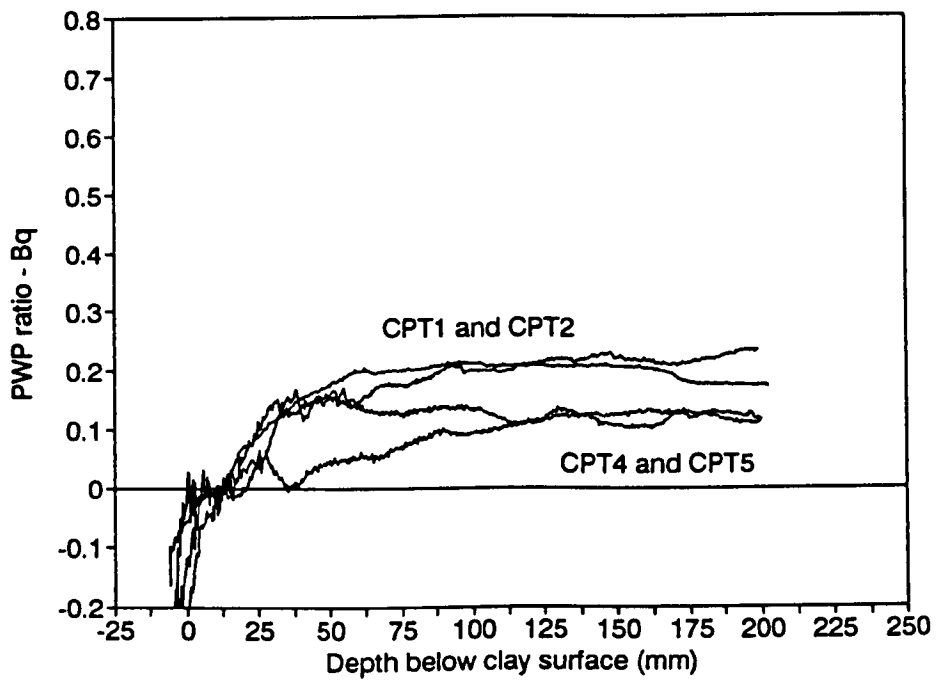


Figure 5.11 Pore water pressure ratio for tests at 0.2mm/sec

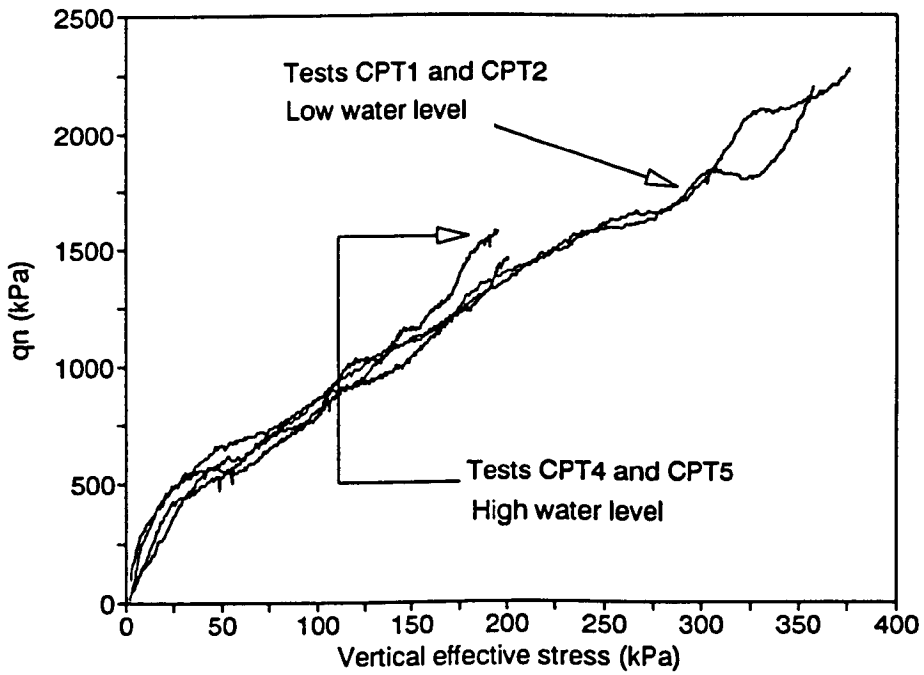


Figure 5.12 Corrected cone resistance ( $q_n$ ) against vertical effective stress at 0.2mm/sec

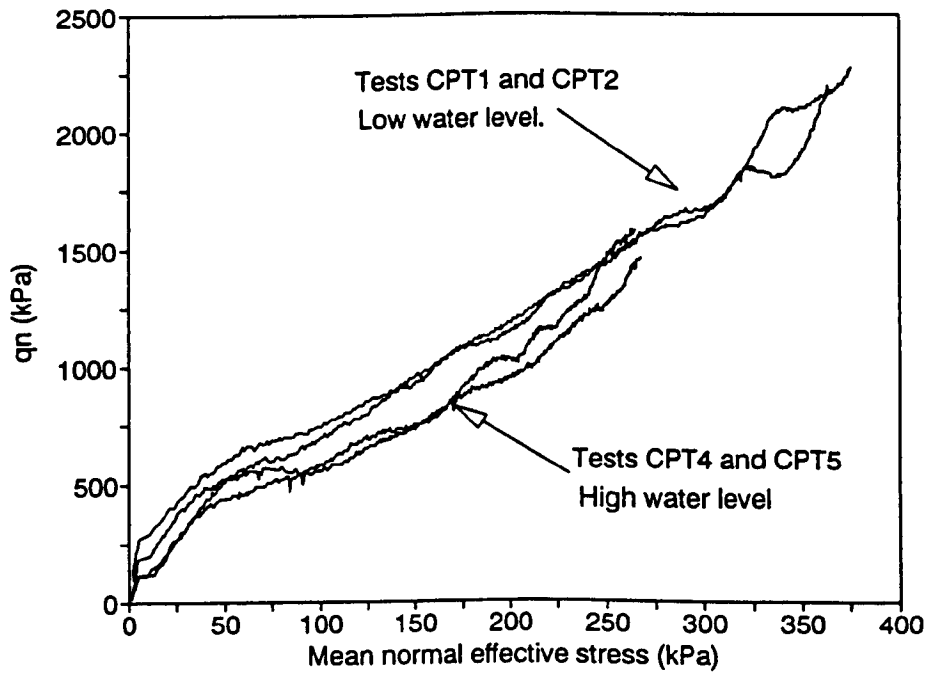


Figure 5.13 Corrected cone resistance ( $q_n$ ) against mean normal effective stress at 0.2mm/sec

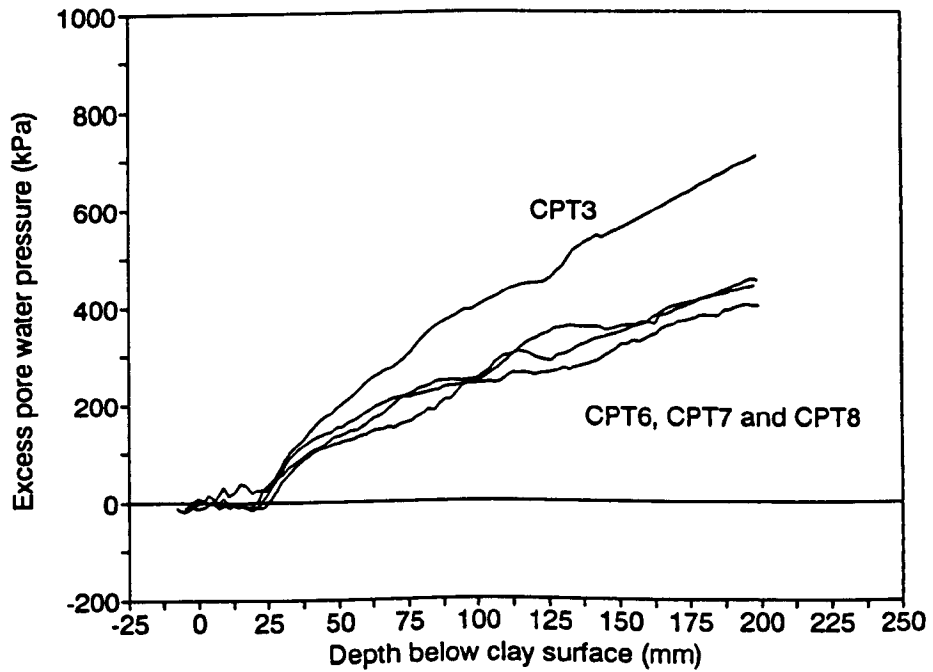
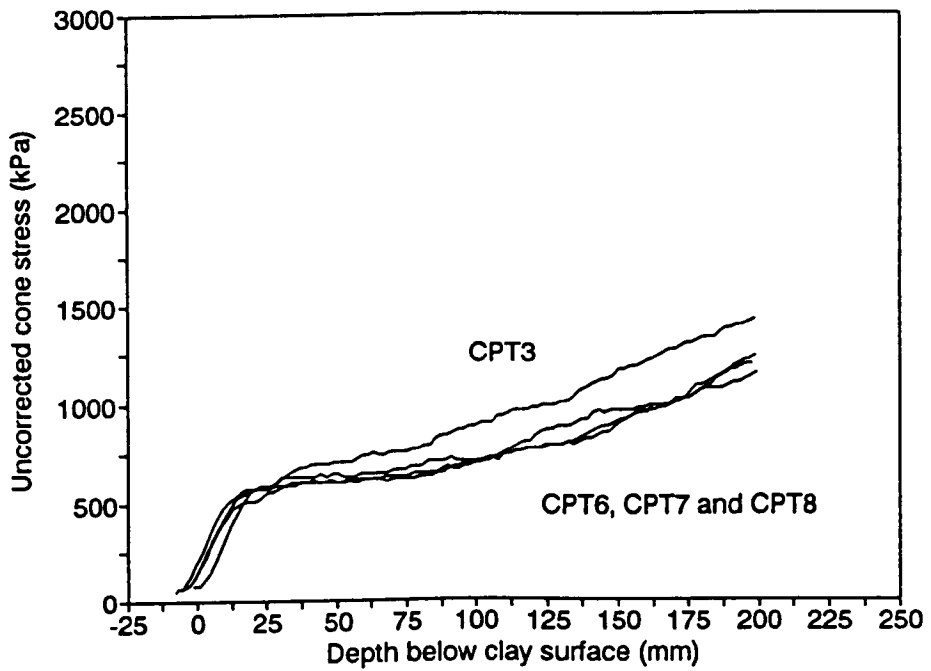


Figure 5.14 Piezocone tests at 2.0mm/sec:  
 a) Uncorrected cone resistance -  $q_c$   
 b) Excess pore water pressure -  $u_e$

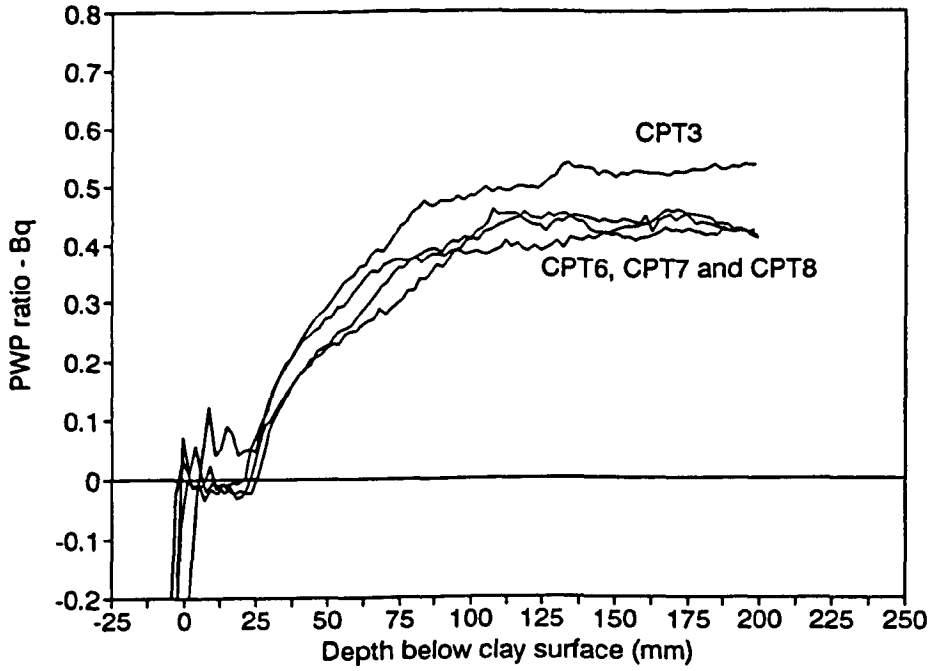


Figure 5.15 Pore water pressure ratio for tests at 2.0mm/sec

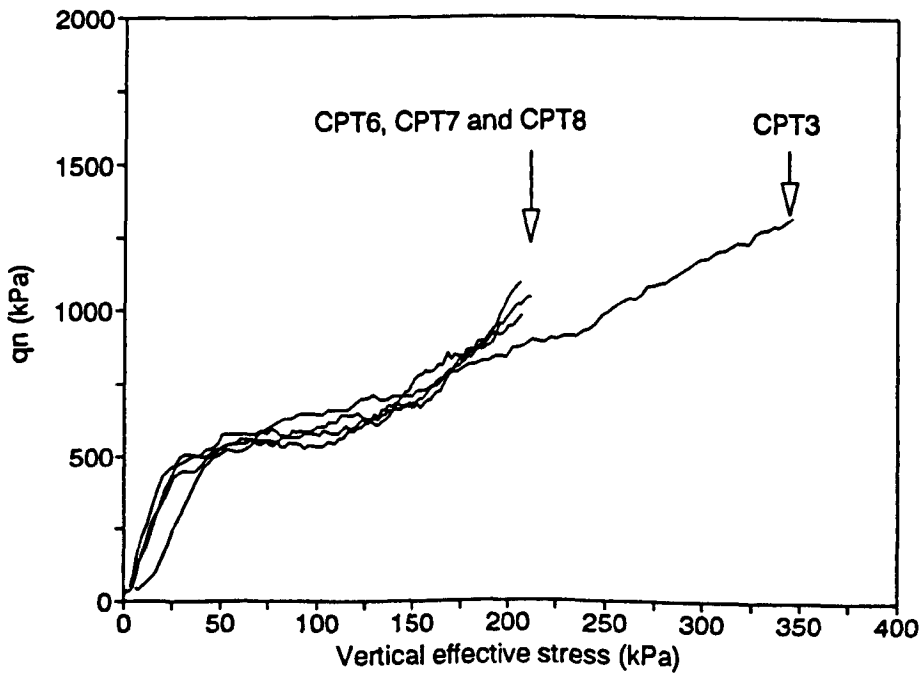


Figure 5.16 Corrected cone resistance ( $q_n$ ) against vertical effective stress at 2.0mm/sec

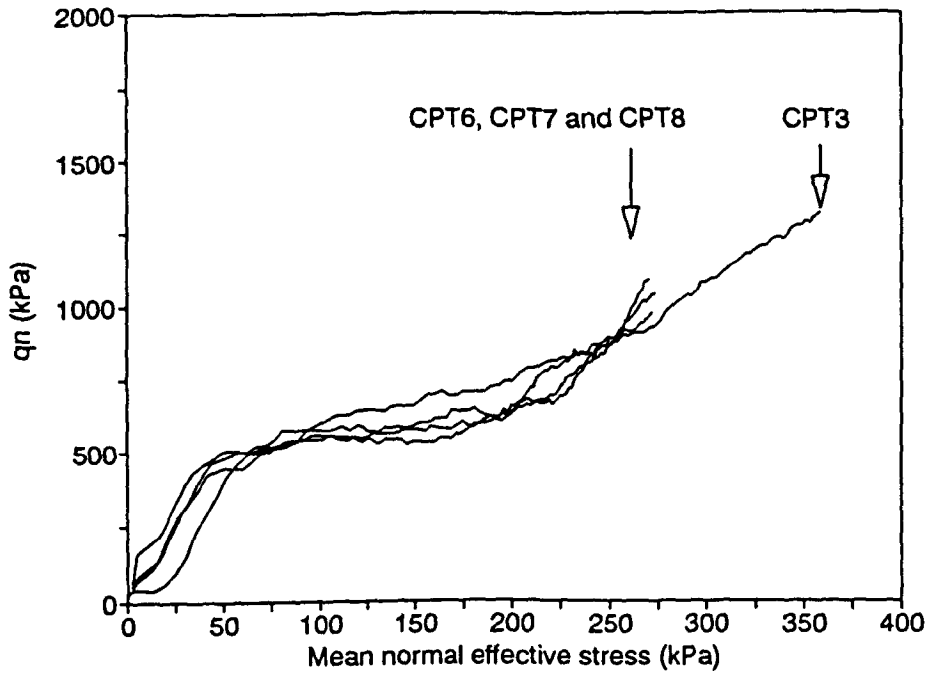


Figure 5.17 Corrected cone resistance ( $q_n$ ) against mean normal effective stress at 2.0mm/sec

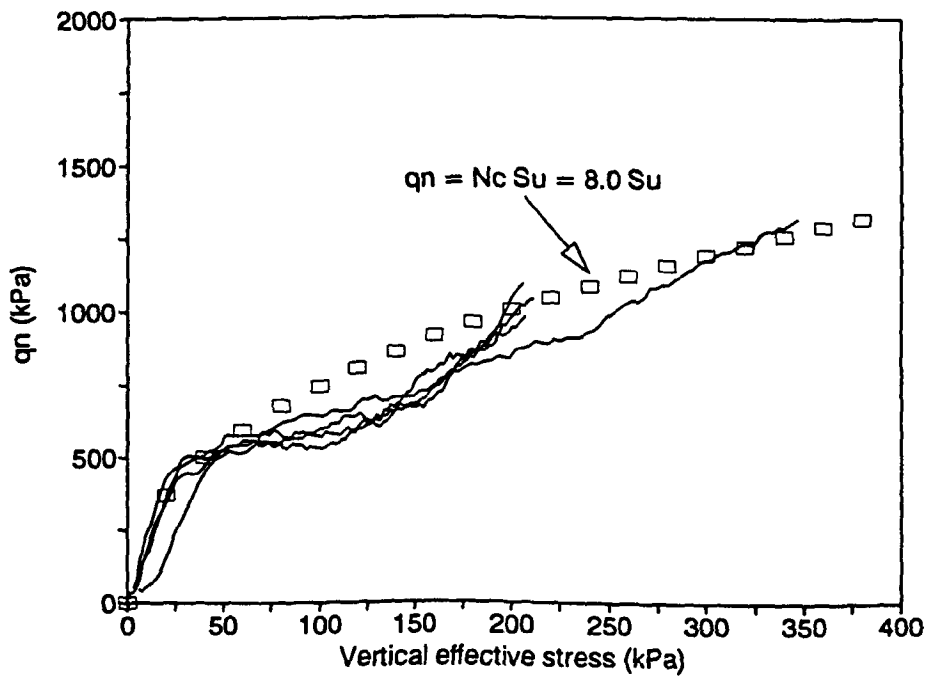


Figure 5.18 Comparison of corrected cone resistance for test at 2.0mm/sec against with calculated cone resistance ( $N_c = 8.0$ )

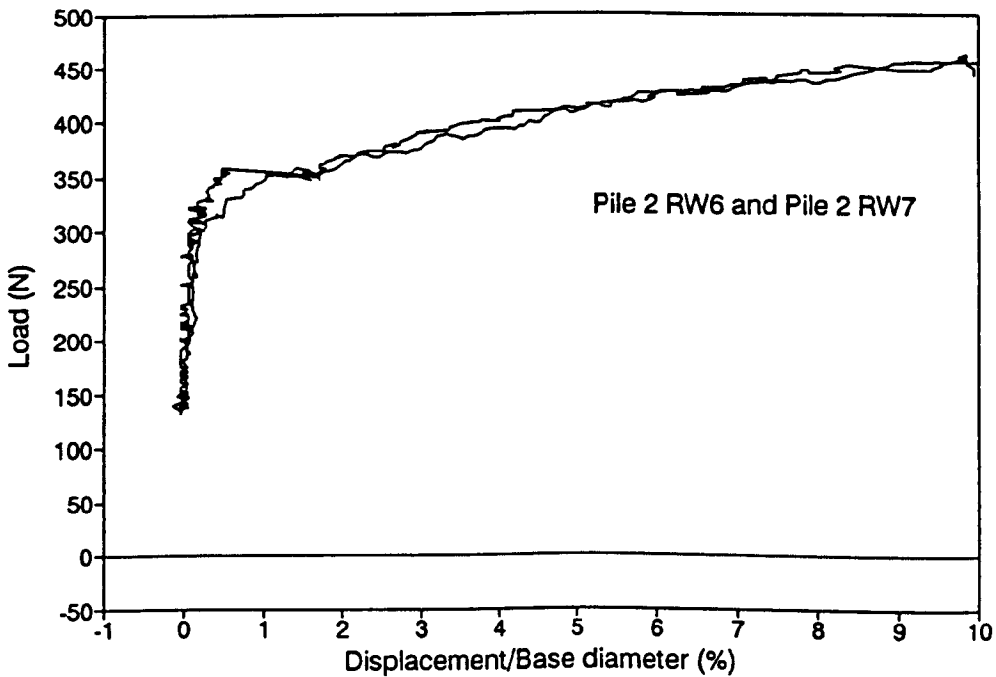
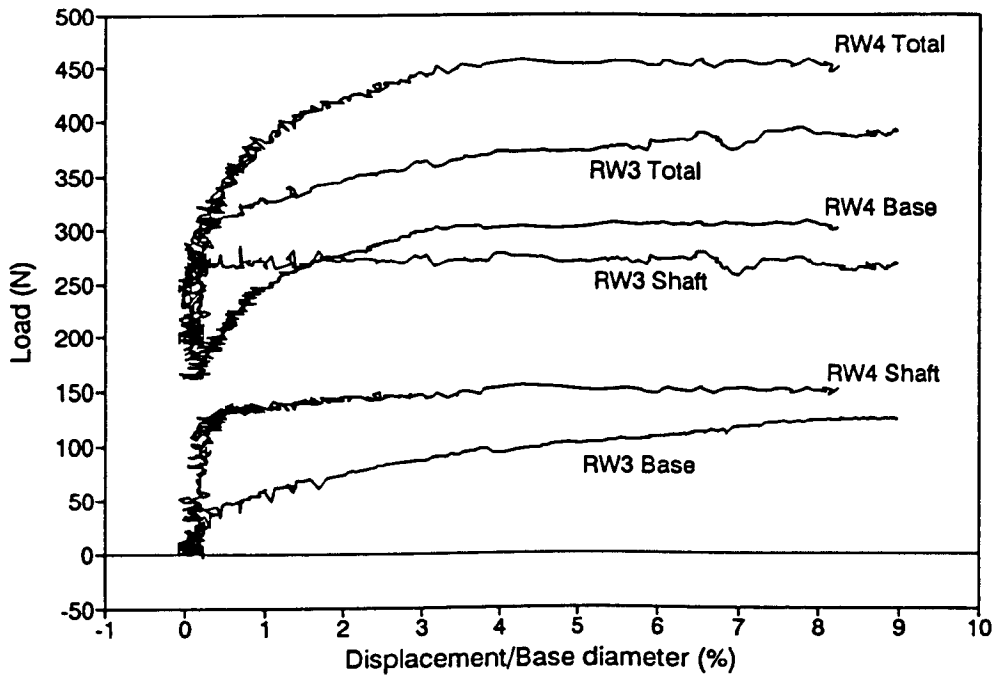


Figure 5.19 Load displacement results for pile loading prior to rising groundwater event:  
 a) Piles with top and base load measurement  
 b) Piles with only top load measurement

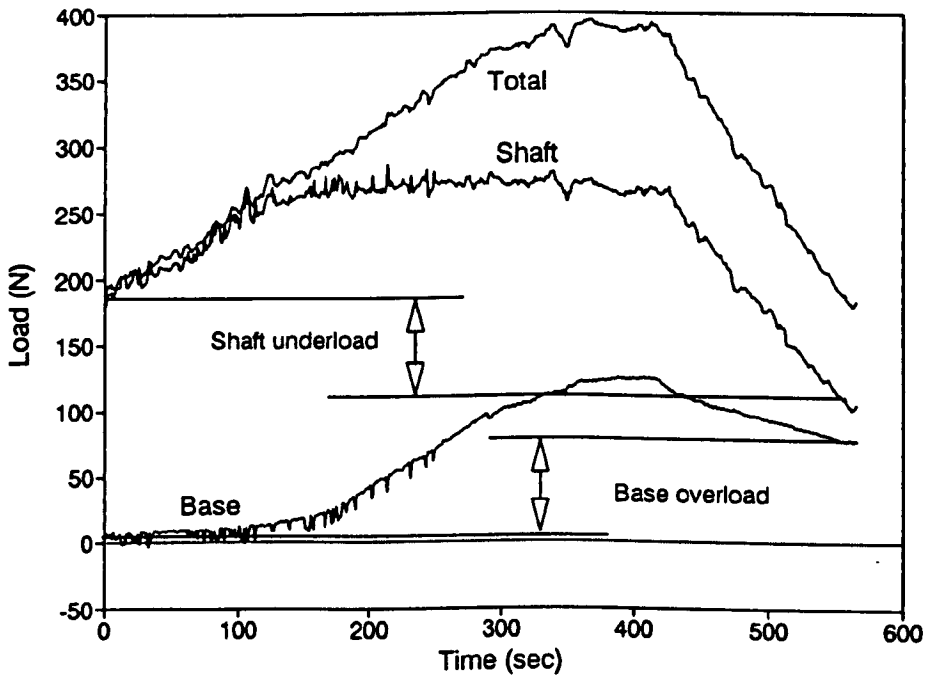
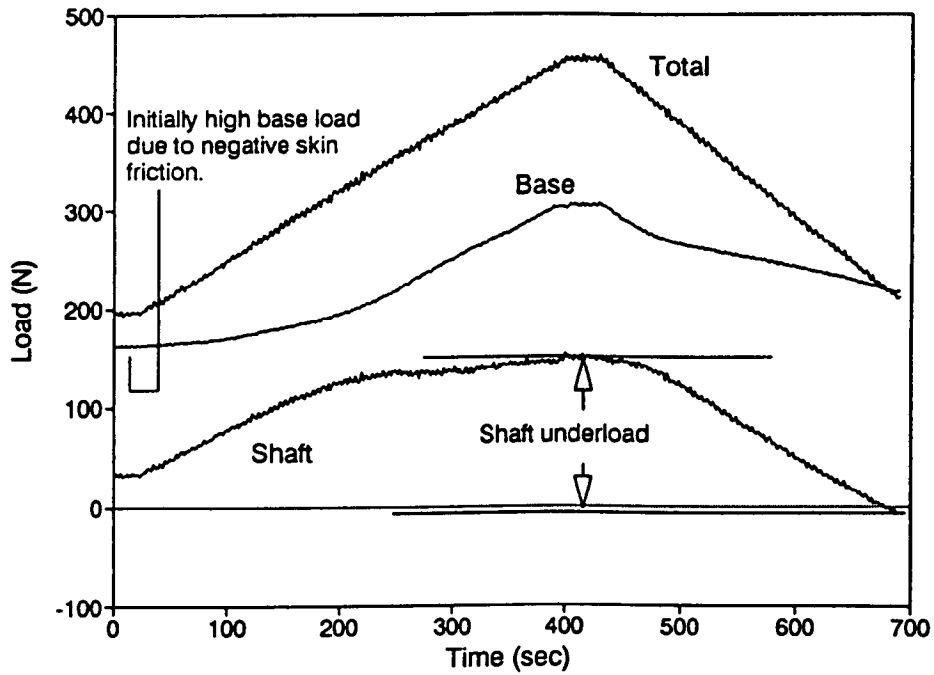


Figure 5.20 Pile load distribution during loading to failure and subsequent unloading:  
 a) Pile in test RW4, under-reamed  
 b) Pile in test RW3, straight 16mm diameter

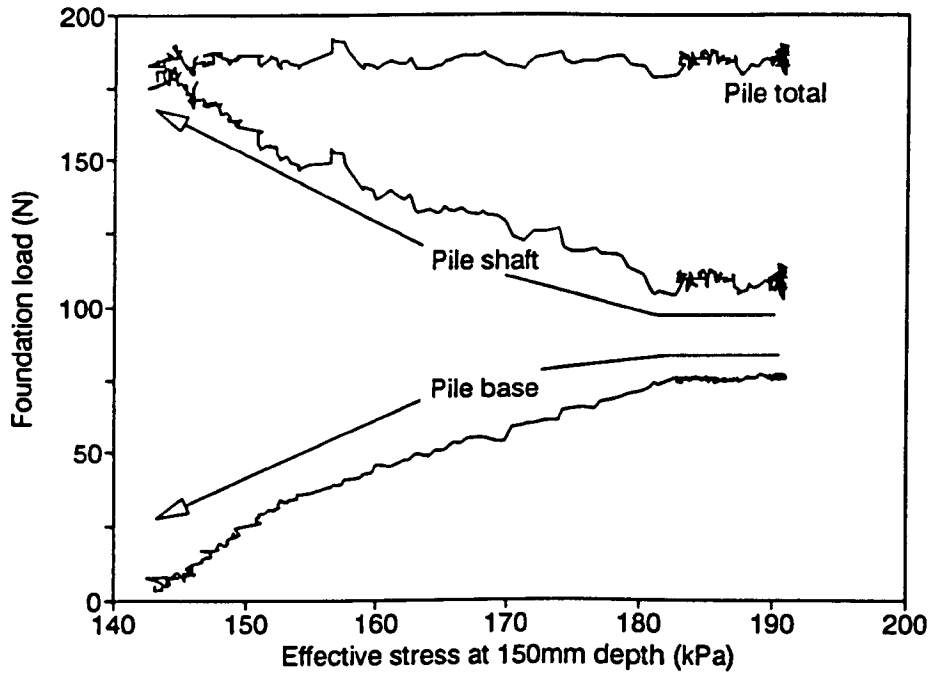


Figure 5.21 Changing pile load distribution during a rising groundwater event against vertical effective stress at 150mm clay depth, test RW3

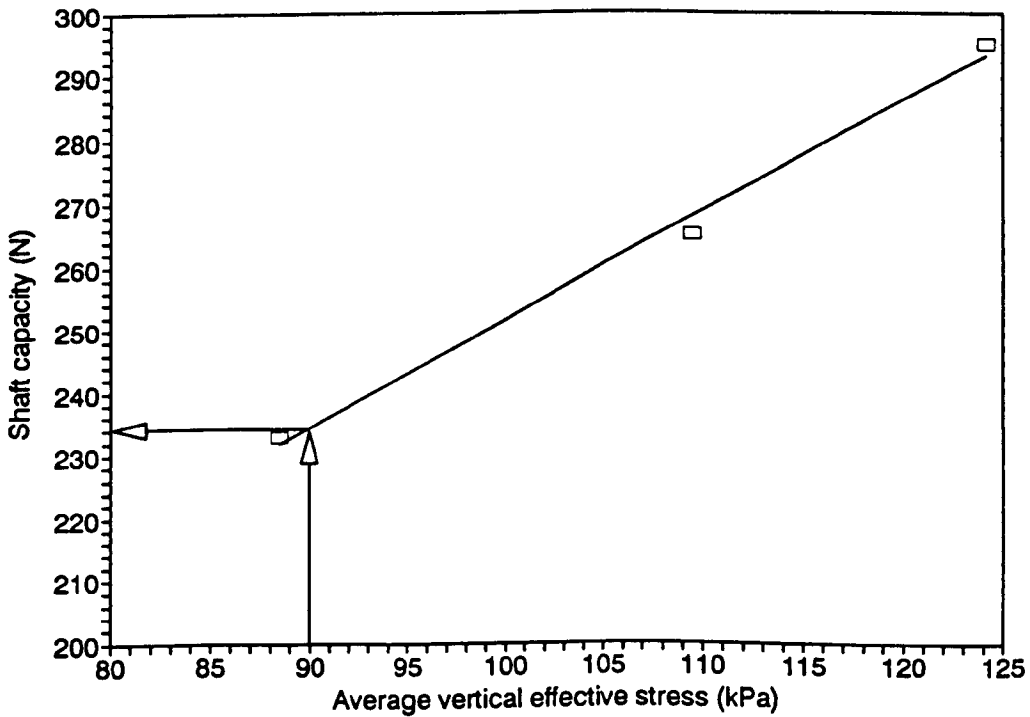


Figure 5.22 Ultimate shaft stress against average vertical effective stress at pile shaft face, test RW3

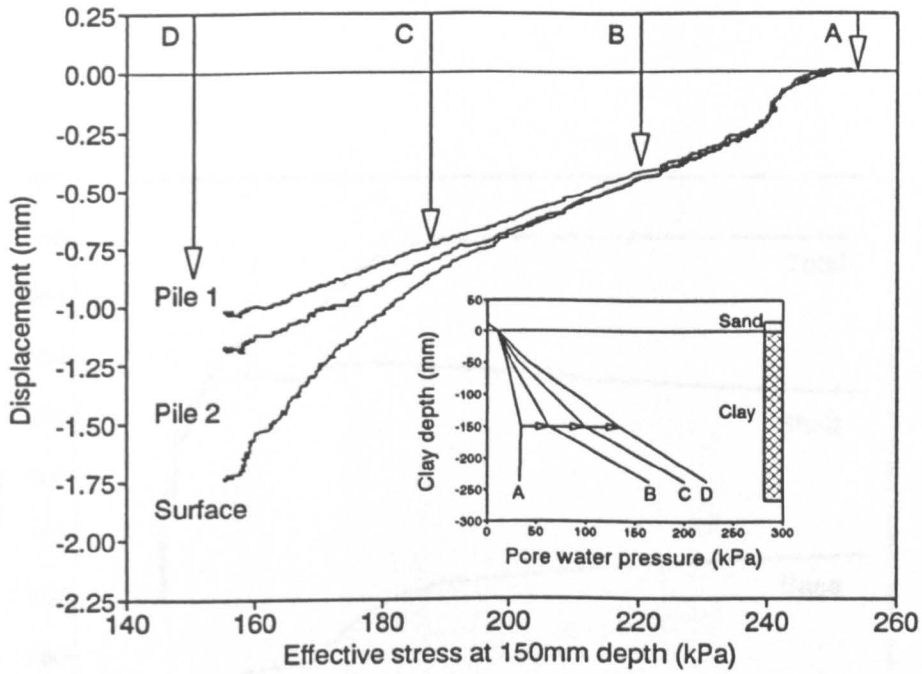


Figure 5.23 Foundation and surface movements during rising groundwater event against vertical effective stress at 150mm clay depth, test RW6  
 Inset: Pore pressure profiles at four marked stages during rising groundwater event

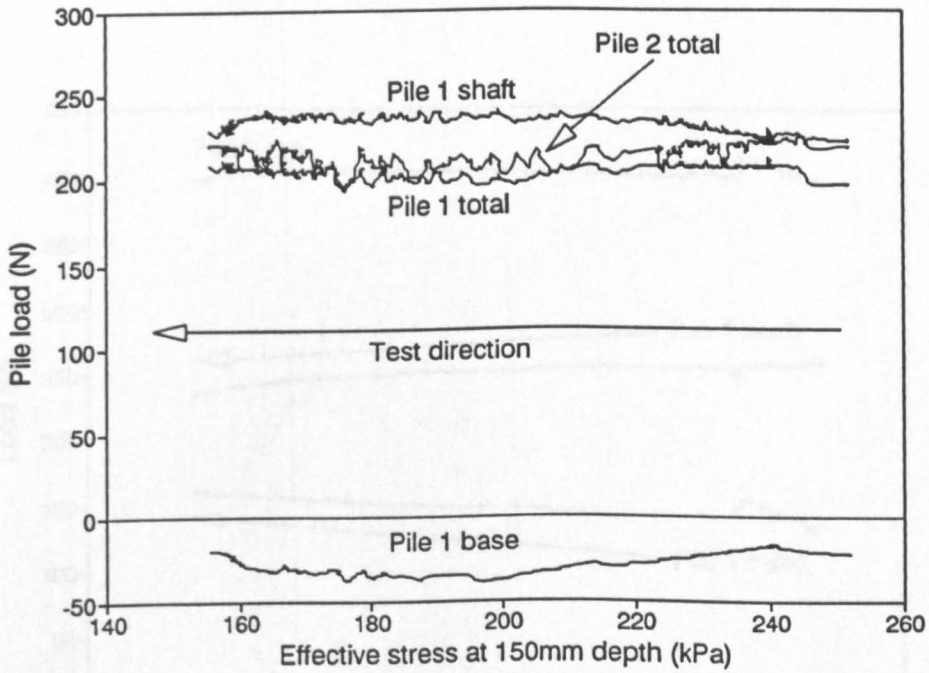


Figure 5.24 Foundation loads during rising groundwater event, test RW6

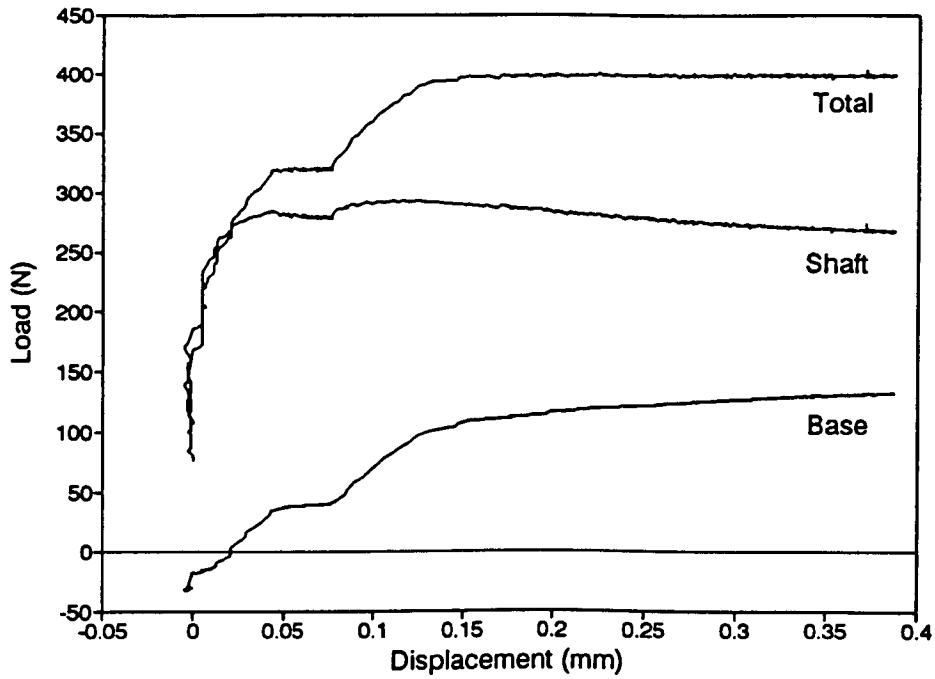


Figure 5.25 Loading of Pile 1 prior to rising groundwater event, test RW10

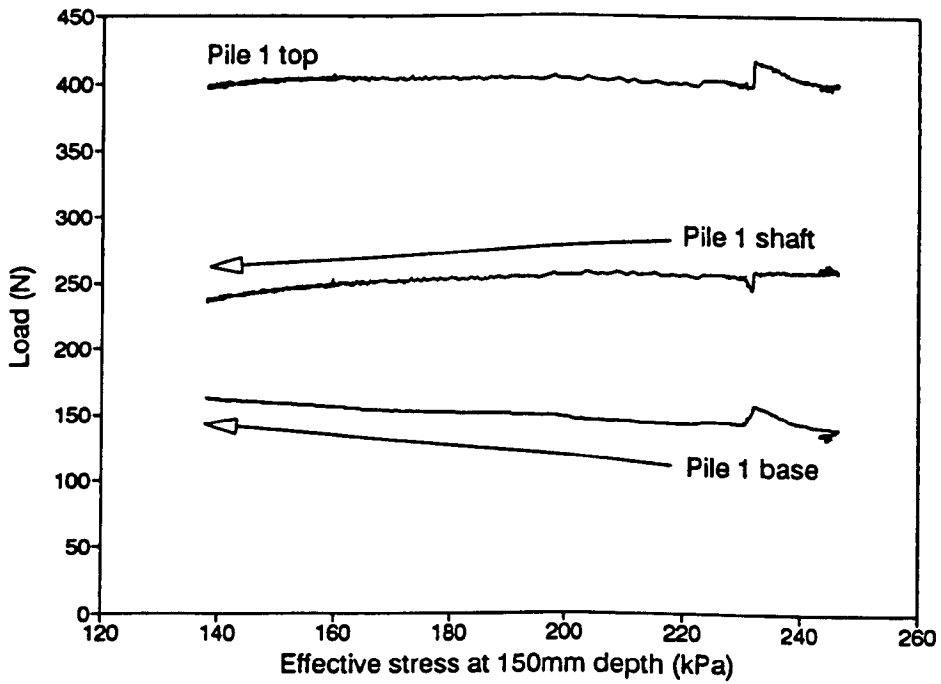


Figure 5.26 Load distribution during rising groundwater event for Pile 1, test RW10

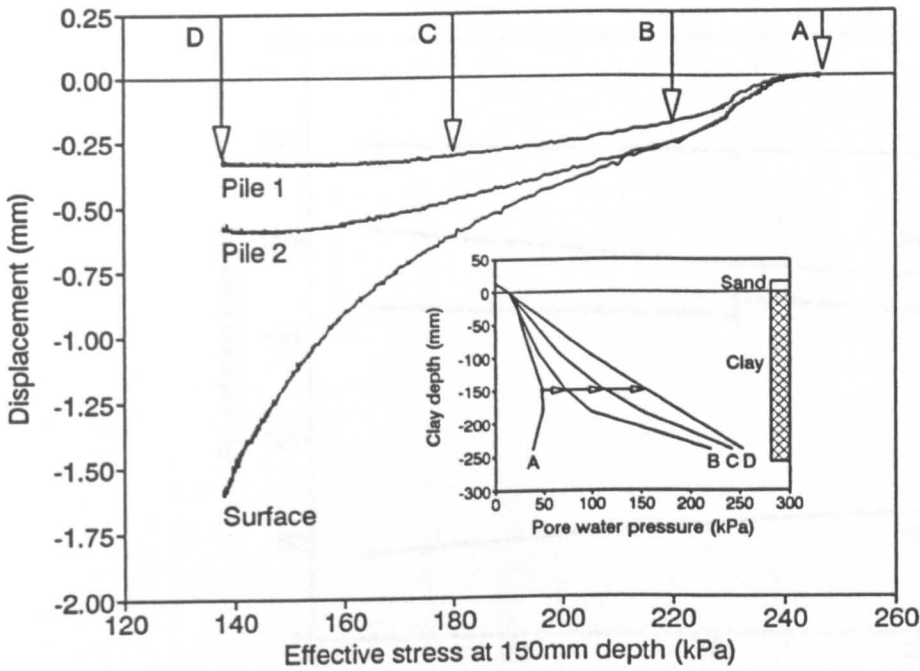


Figure 5.27 Foundation and surface movements during rising groundwater event against vertical effective stress at 150mm clay depth, test RW10  
 Inset: Pore pressure profiles at four marked stages during rising groundwater event

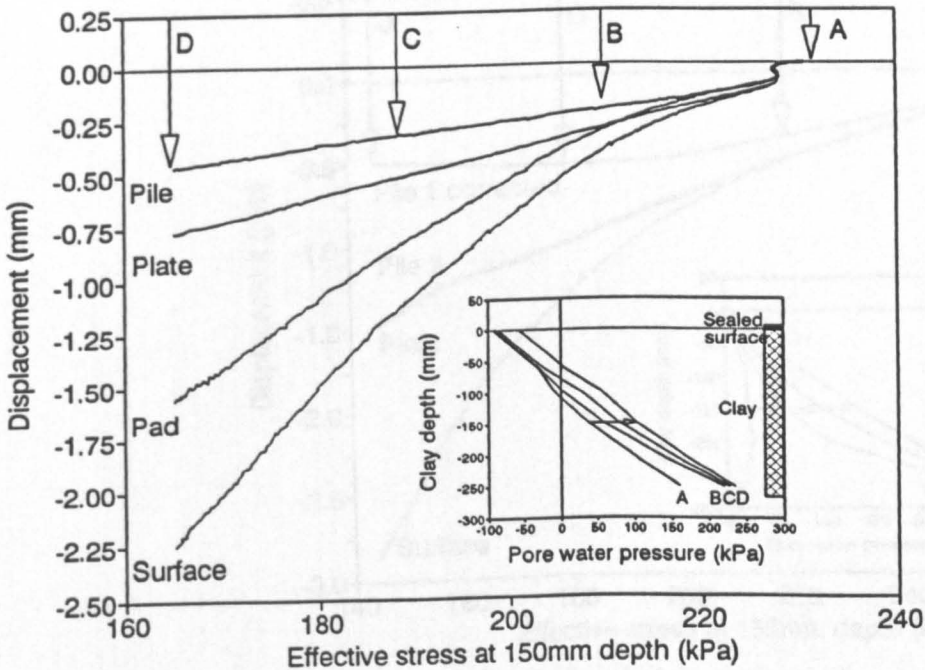


Figure 5.28 Foundation, buried plate and surface movements during rising groundwater event against vertical effective stress at 150mm clay depth, test RW13  
 Inset: Pore pressure profiles at four marked stages during rising groundwater event

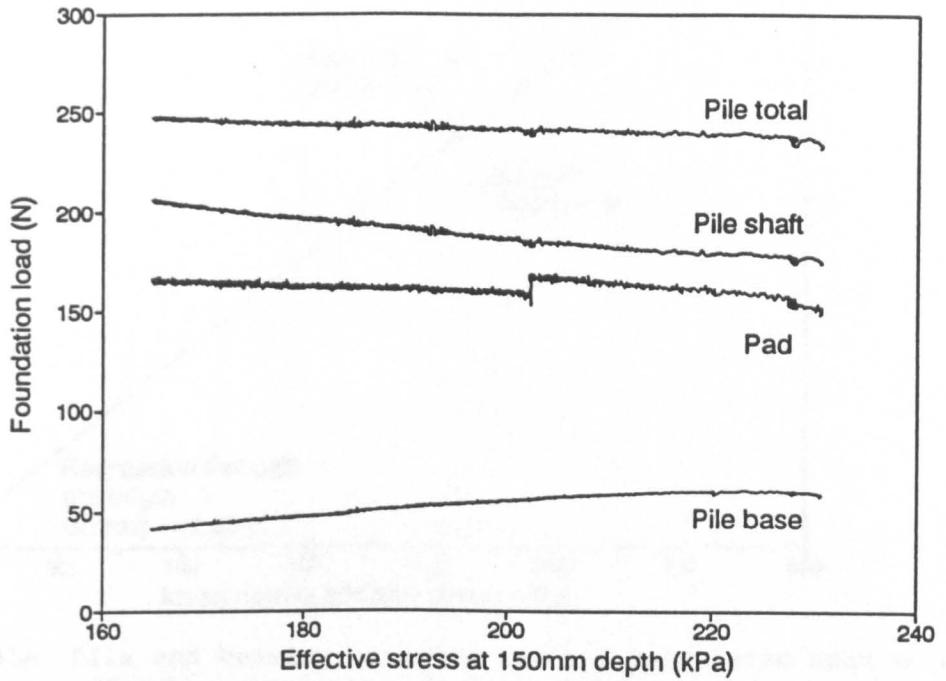


Figure 5.29 Load distribution during rising groundwater event for pile and pad, test RW13

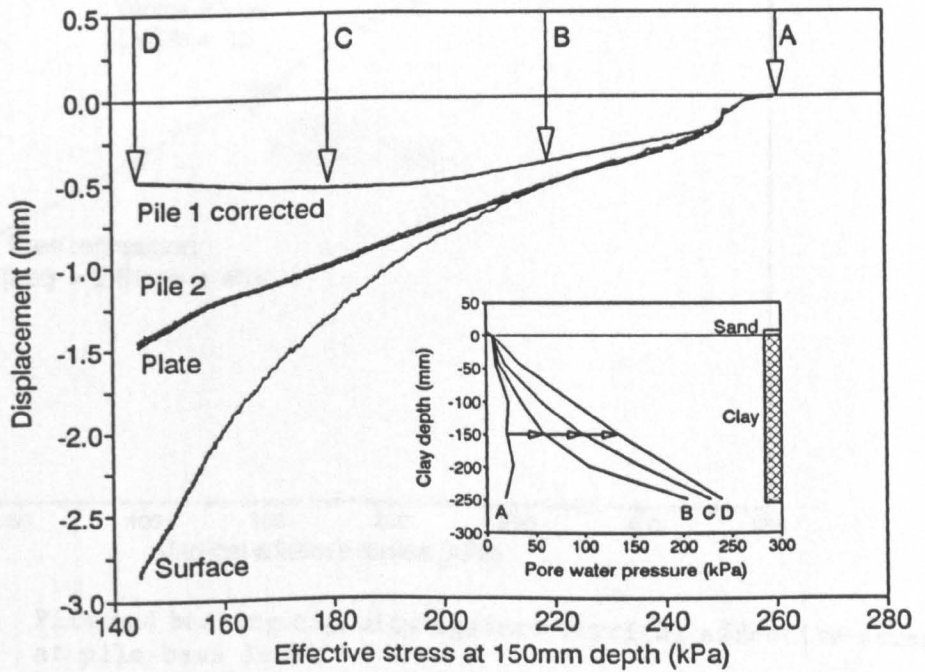


Figure 5.30 Foundation, buried plate and surface movements during rising groundwater event against vertical effective stress at 150mm clay depth, test RW15  
 Inset: Pore pressure profiles at four marked stages during rising groundwater event

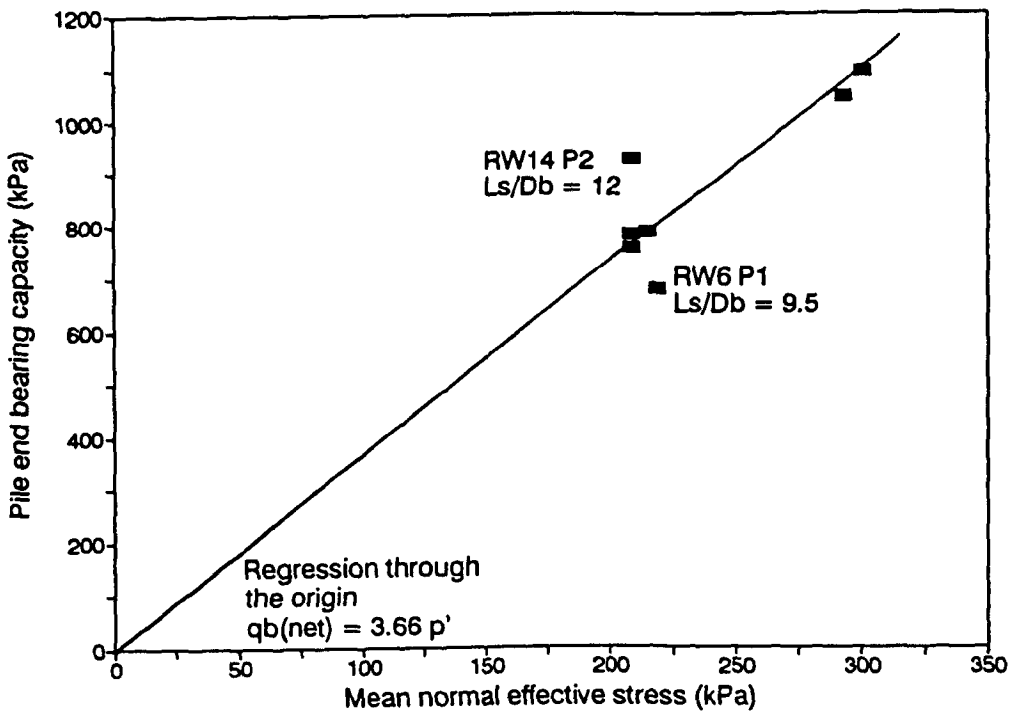


Figure 5.31a Pile end bearing capacity against calculated mean normal effective stress at pile base level

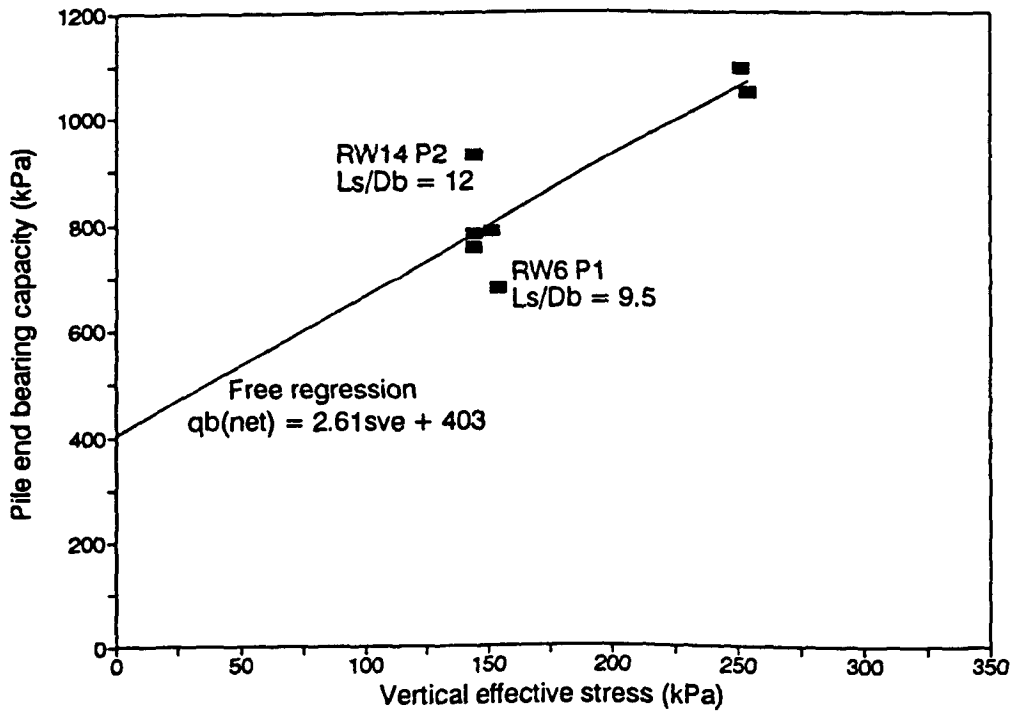


Figure 5.31b Pile end bearing capacity against vertical effective stress at pile base level

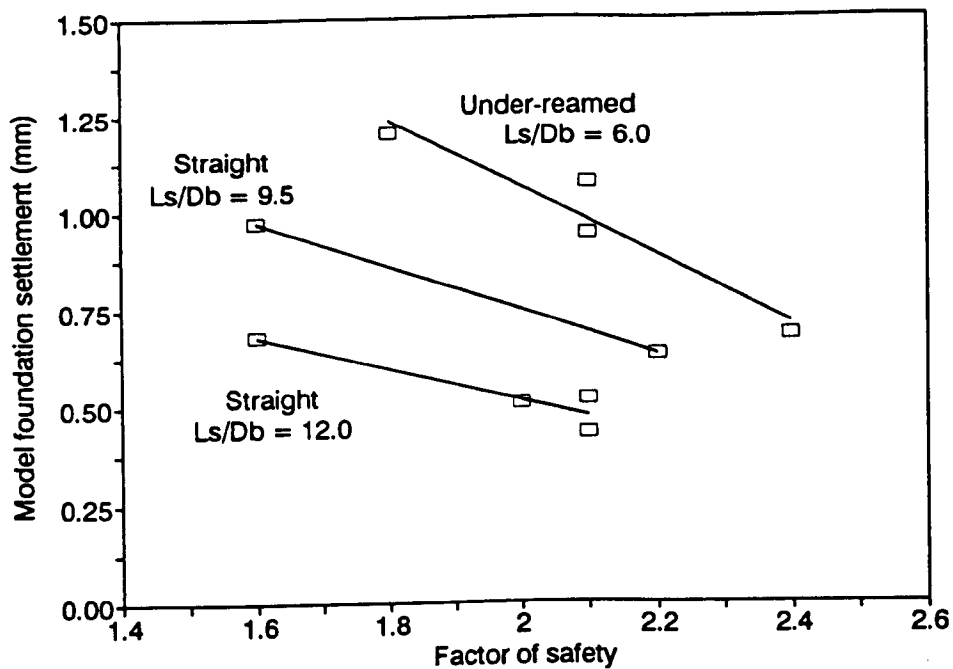


Figure 5.32 Correlation of pile initial factor of safety with settlement relative to soil surface during rising groundwater event for three pile geometries

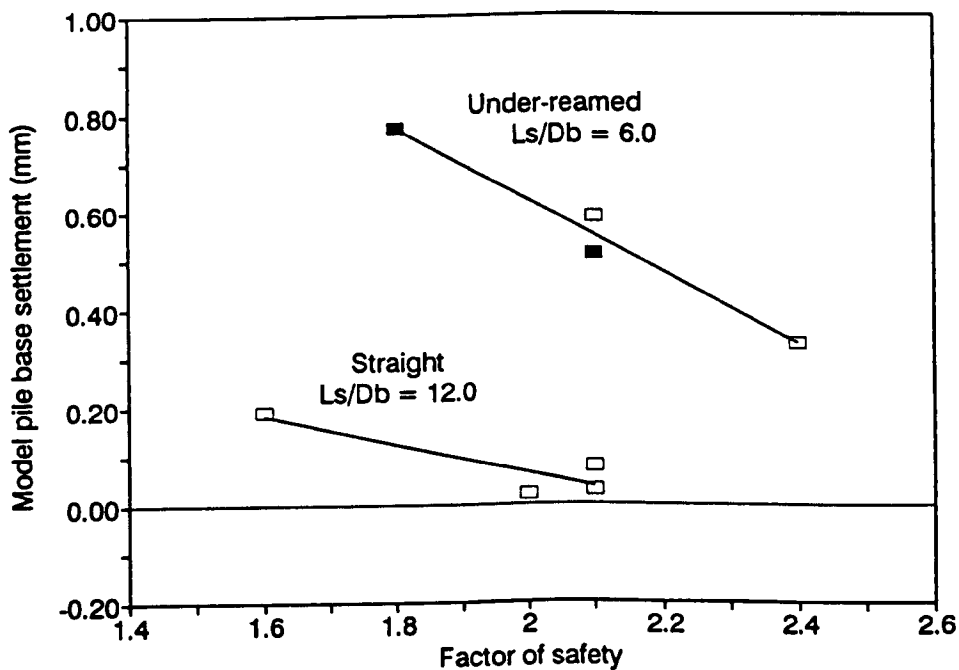


Figure 5.33 Correlation of pile initial factor of safety with settlement relative to soil at pile base level during rising groundwater event for three pile geometries

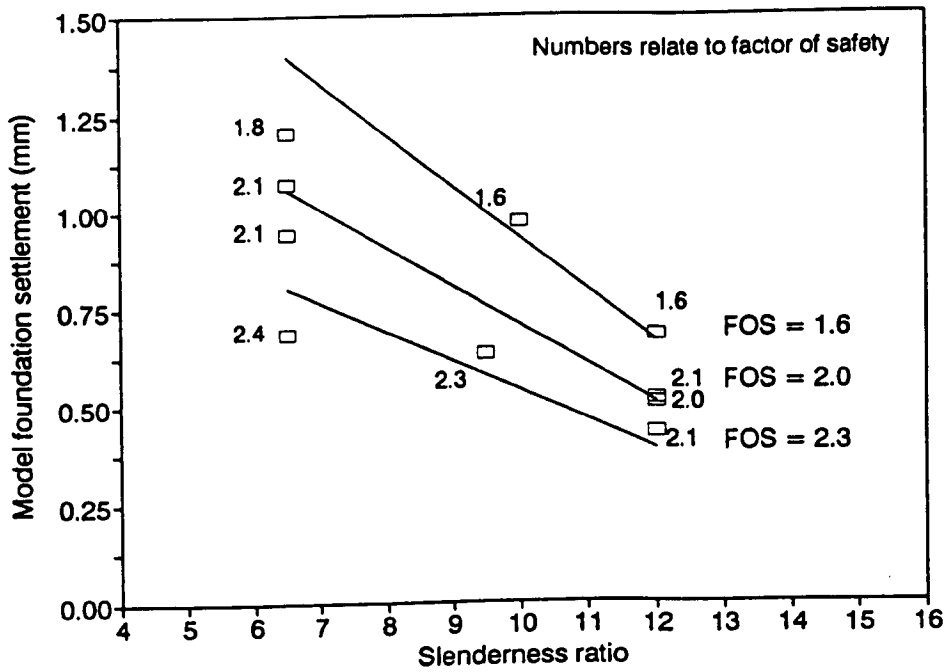


Figure 5.34 Correlation of pile slenderness ratio (pile length -  $L_p/D_p$  -pile base diameter) with settlement relative to the ground surface, with general trends for different initial factors of safety

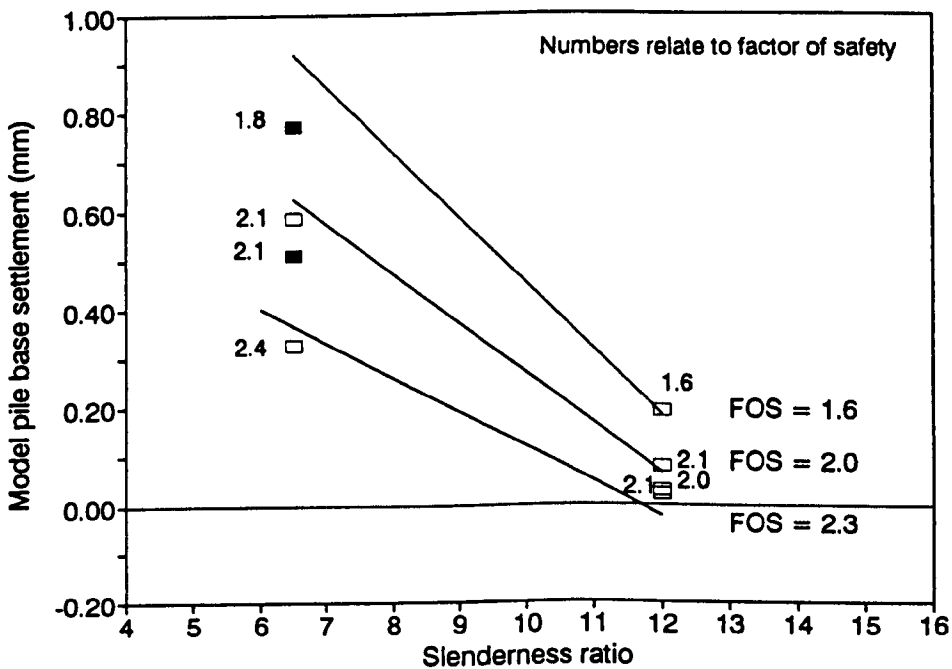


Figure 5.35 Correlation of pile slenderness ratio (pile length -  $L_p/D_p$  -pile base diameter) with settlement relative to soil at pile base level, with general trends for different initial factors of safety

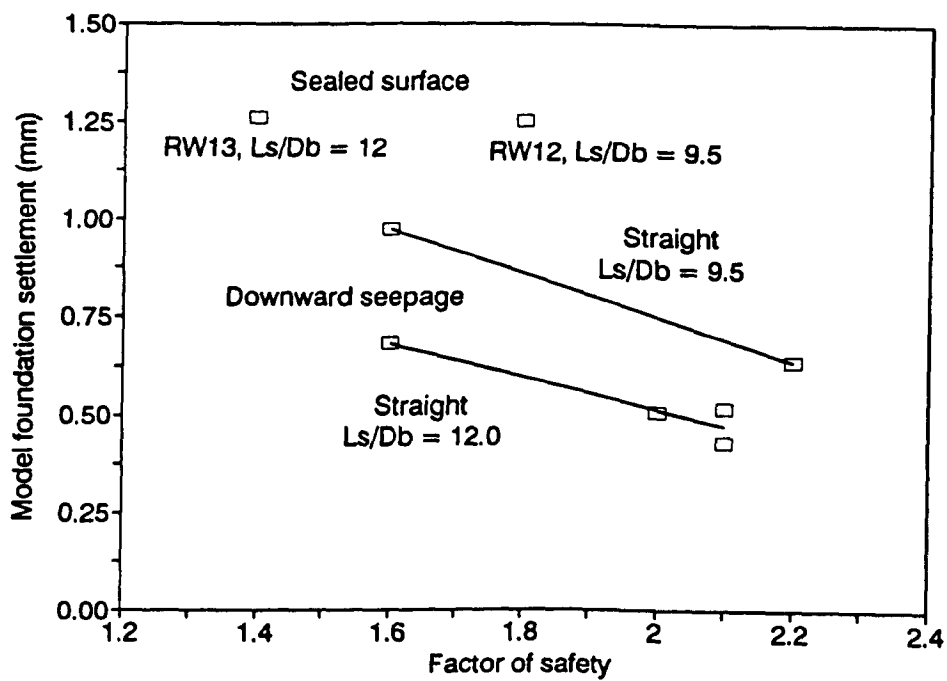


Figure 5.36 Comparison of settlement of straight piles for different initial pore pressure profiles

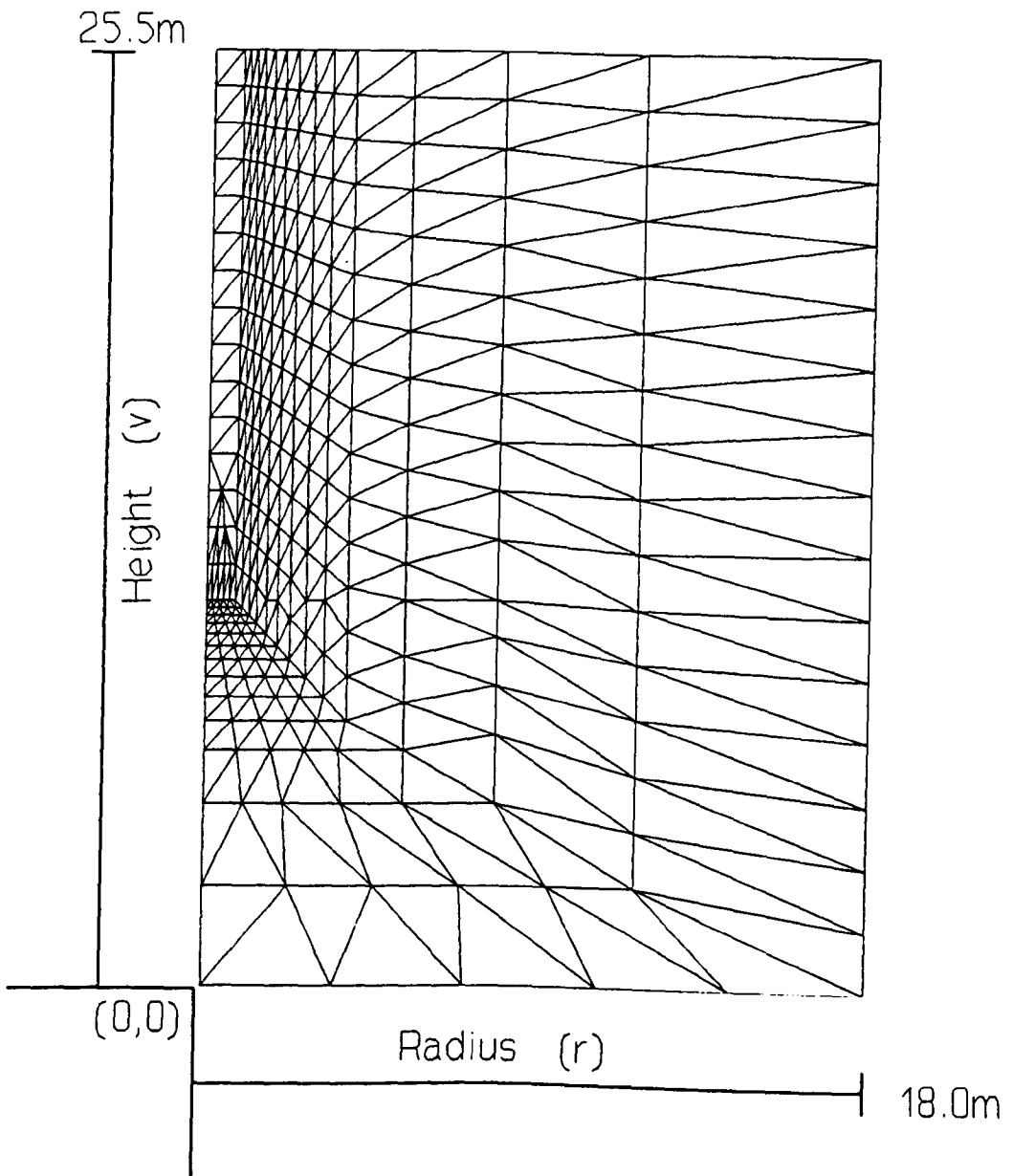


Figure 6.1 Mesh used for pile installation and rising groundwater analyses with Stallebrass model

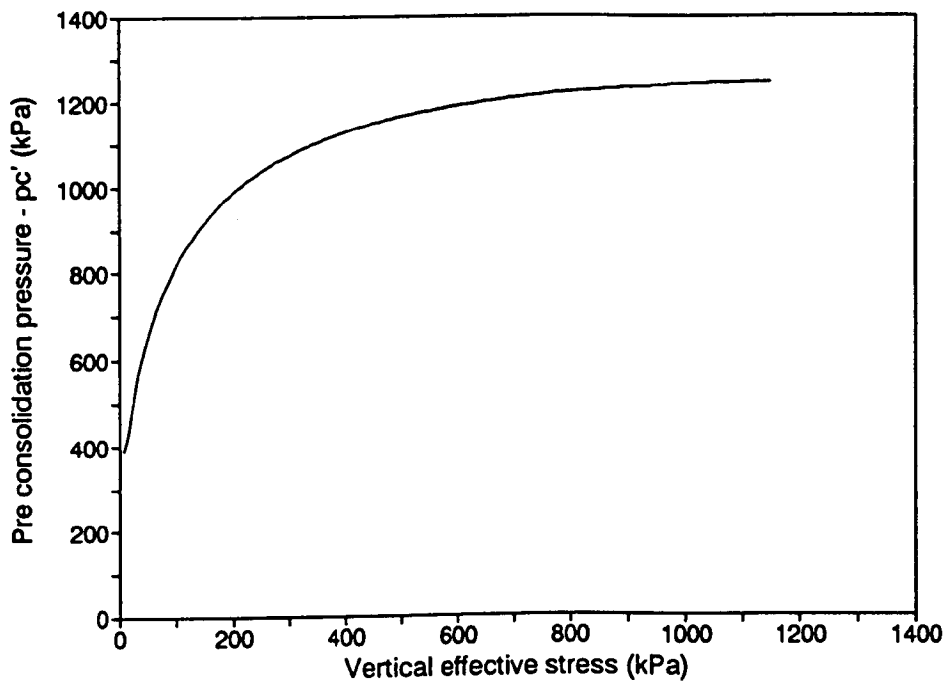


Figure 6.2 Variation of  $p'_c$  with  $\sigma'_v$  during one dimensional unloading from  $\sigma'_v = 1250\text{kPa}$

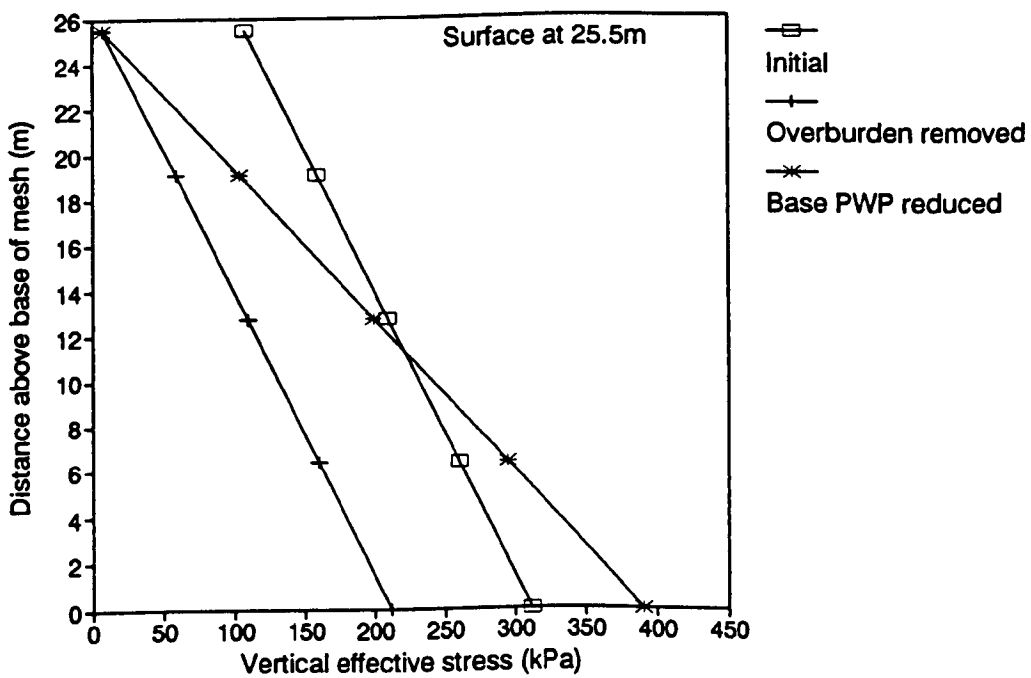


Figure 6.3 Vertical effective stress profiles before, during and after modelling effects of recent stress history, analysis 1PIEXC

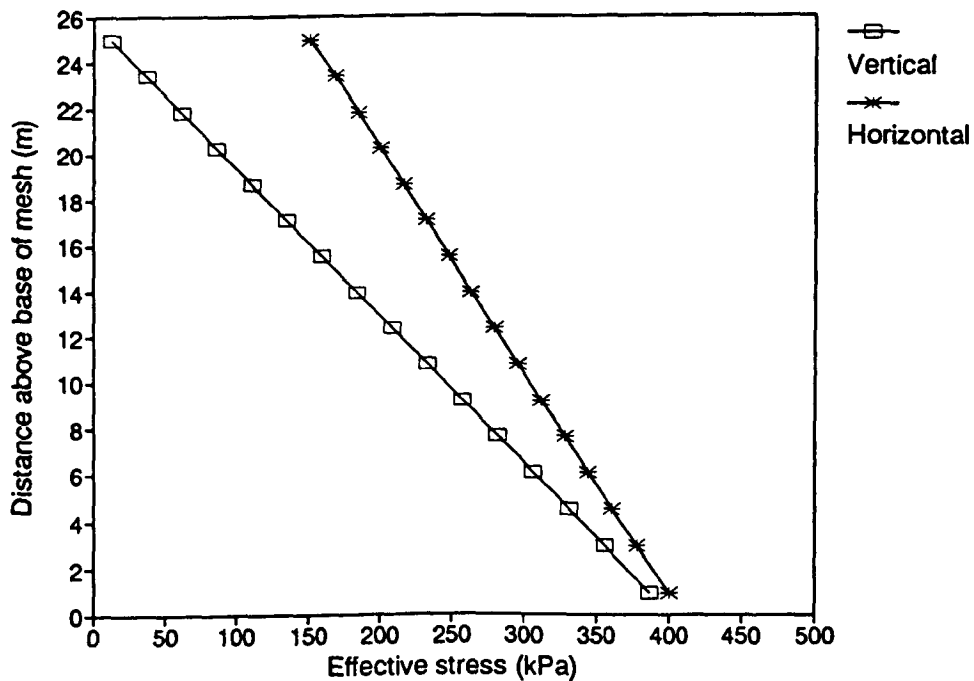


Figure 6.4 Vertical and horizontal effective stress profiles after modelling effects of recent stress history, analysis 1PIEXC

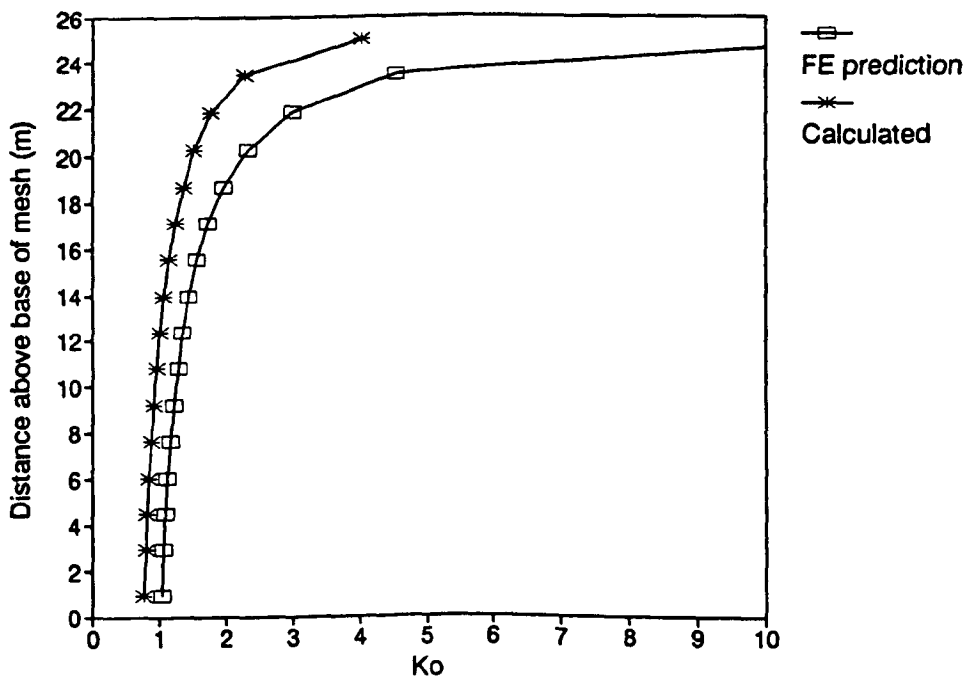


Figure 6.5 Comparison of  $K_0$  profile from Figure 6.4 and calculated profile from Eqn 3.8 and 2.20

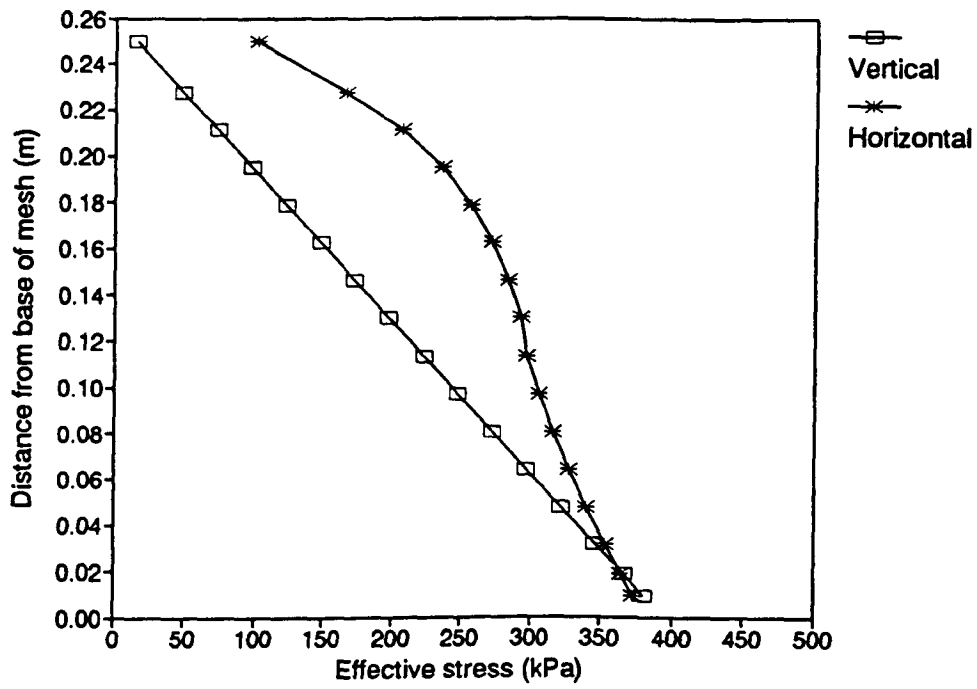


Figure 6.6 Vertical and horizontal effective stress profiles after modelling effects of recent stress history, analysis 1P2MOD

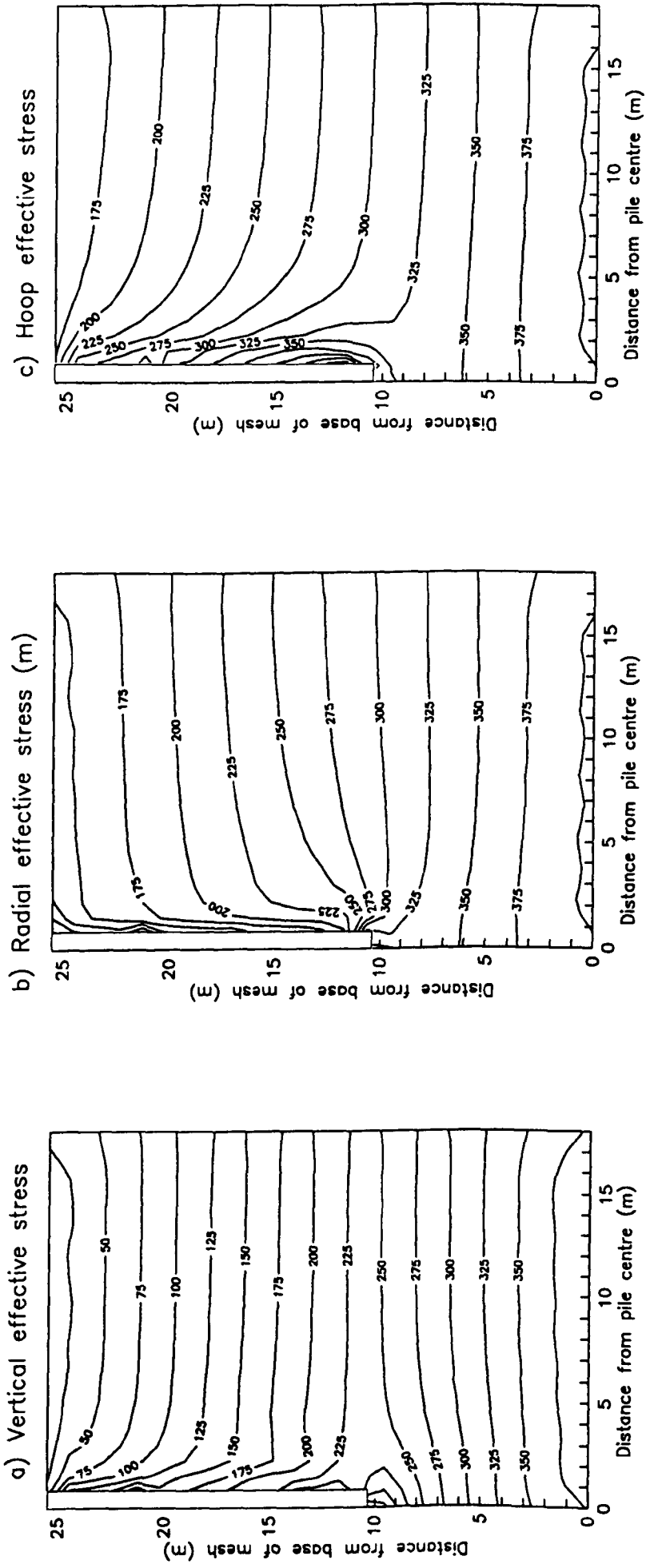


Figure 6.7 Stress distributions with open excavation, analysis IPIEXC:

- a) Vertical effective stress
- b) Radial effective stress
- c) Hoop effective stress

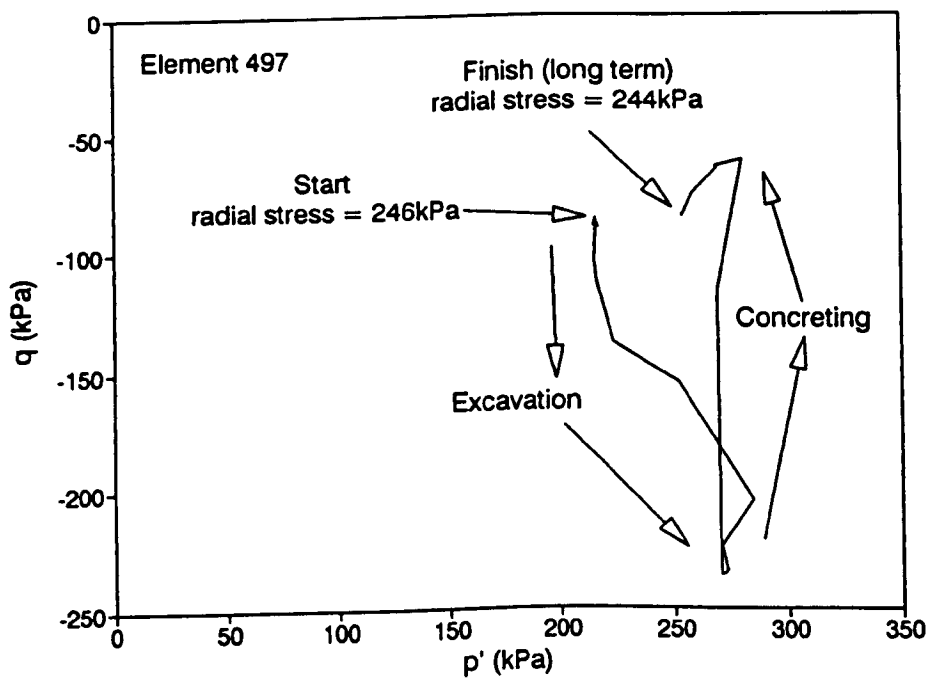
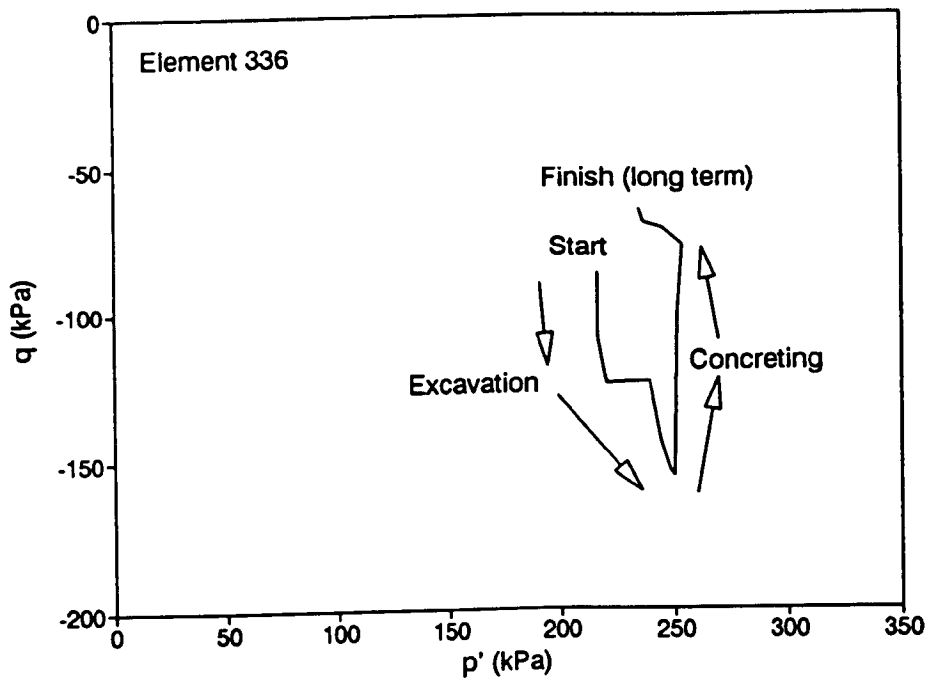


Figure 6.8 Stress path during pile installation, analysis lPIEXC:  
 a) Element 336, 10m depth 0.8m from shaft  
 b) Element 497, 10m depth 0.15m from shaft

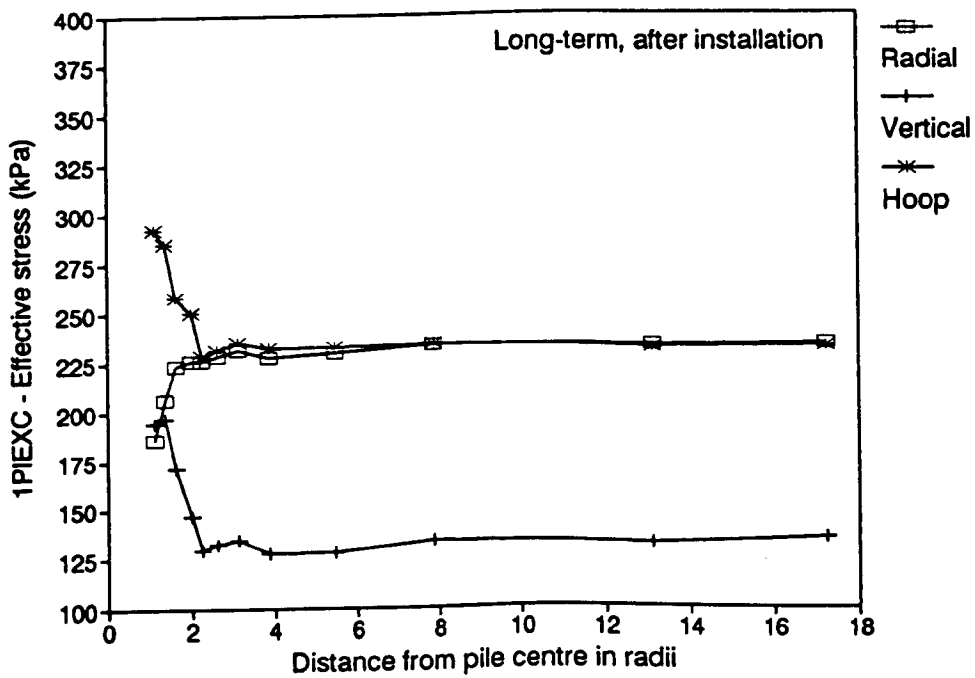
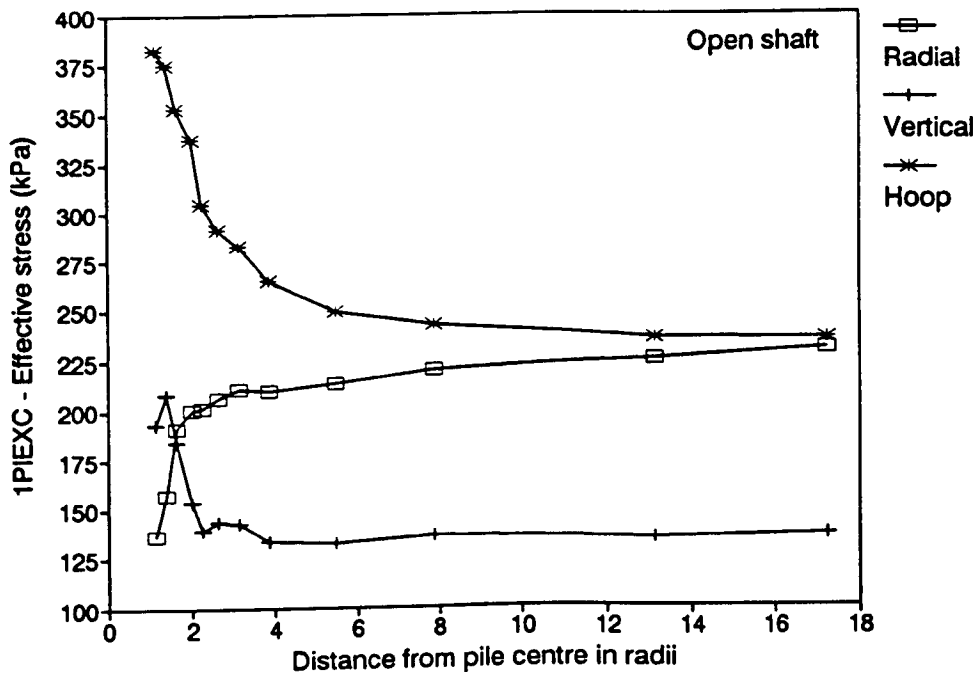


Figure 6.9 Vertical, radial and hoop effective stress distributions at 10m depth, analysis 1PIEXC:  
 a) Open shaft  
 b) After installation

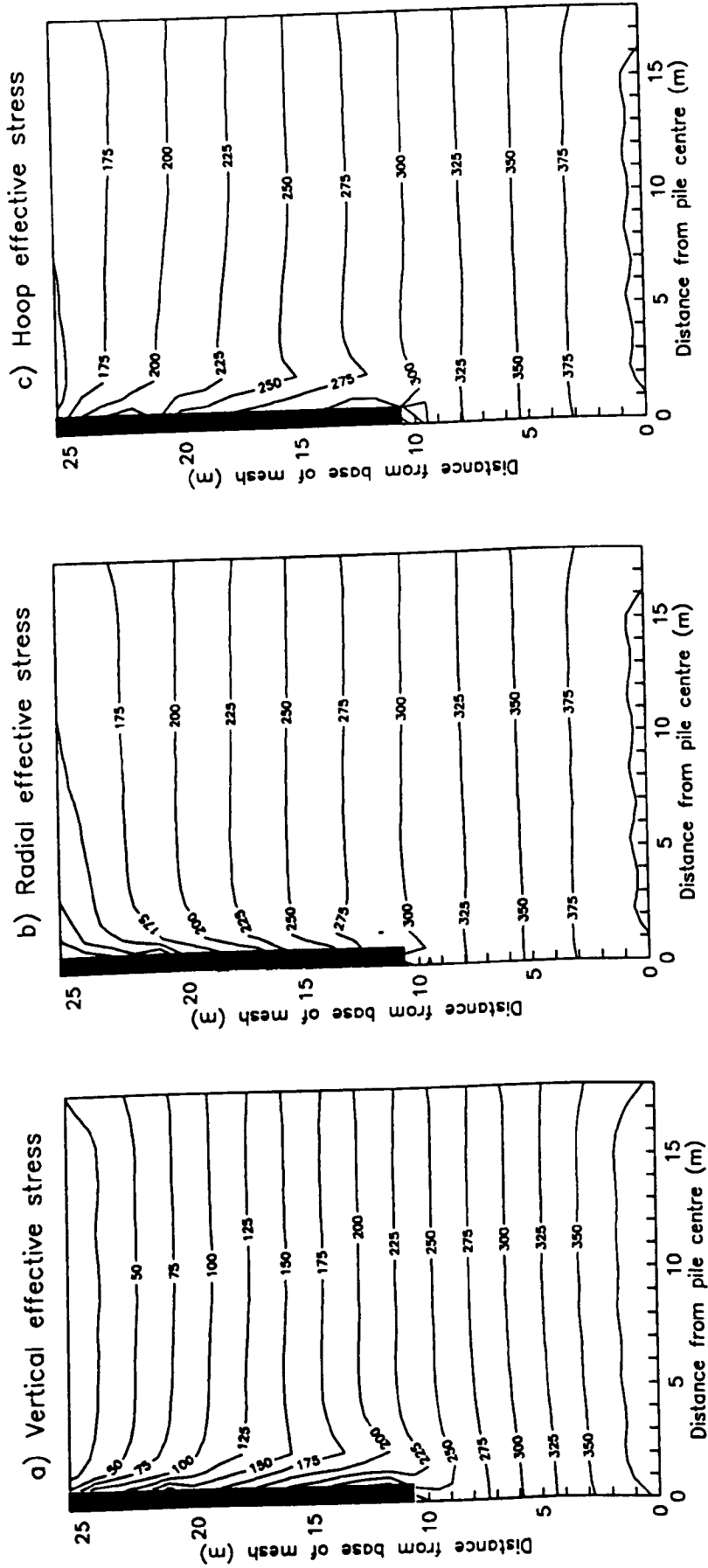


Figure 6.10 Stress distributions after pile installation, analysis

1PIEXC:

- a) Vertical effective stress
- b) Radial effective stress
- c) Hoop effective stress

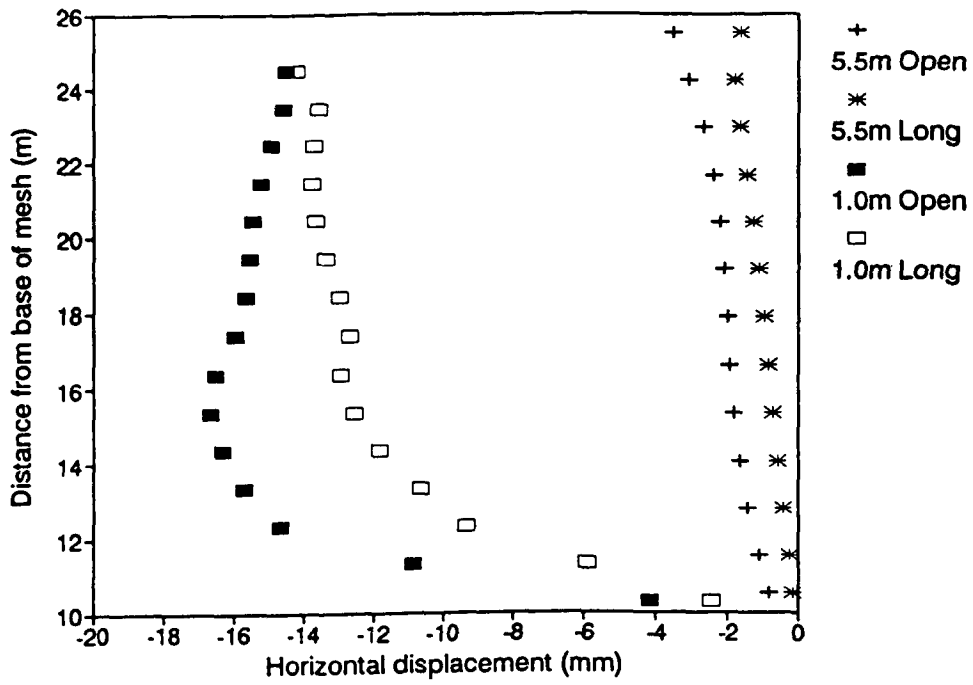


Figure 6.11 Horizontal displacements during pile installation at 1.0m and 5.5m from pile axis, analysis 1PIEXC

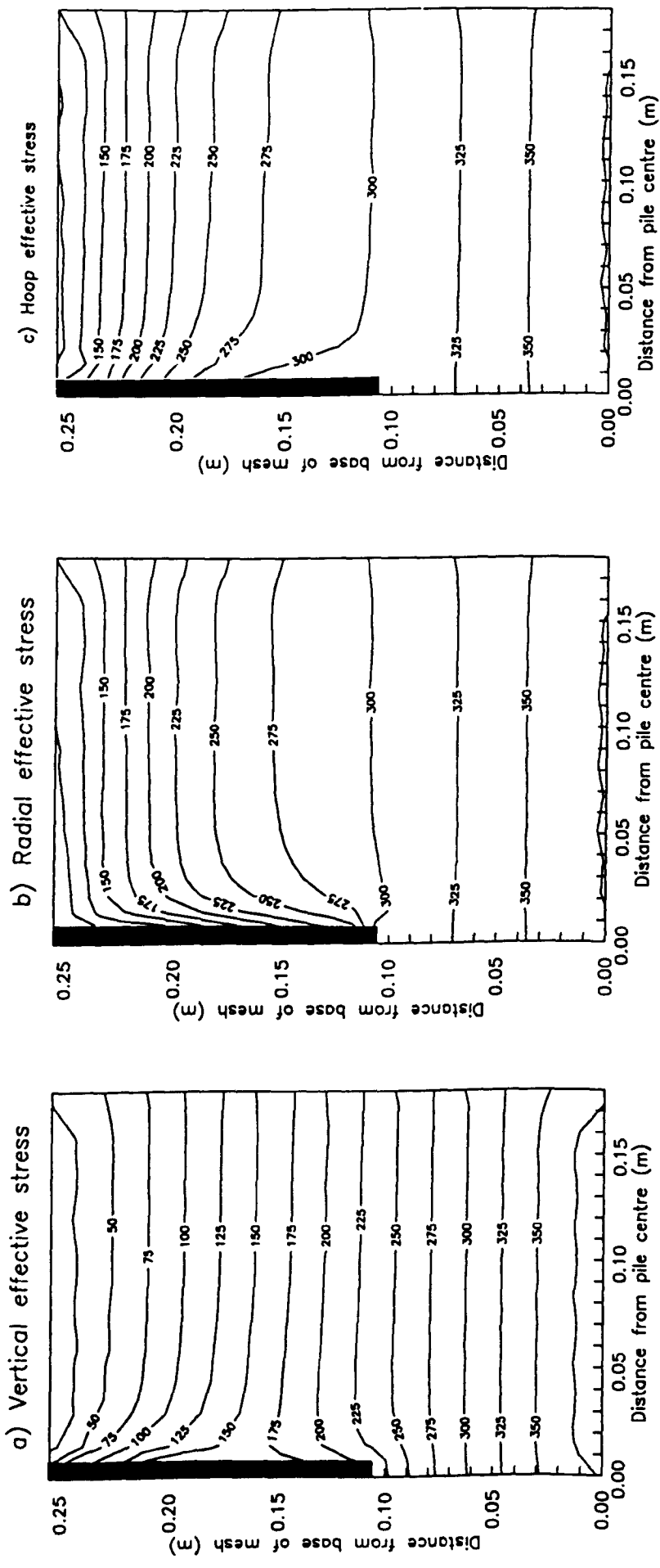


Figure 6.12 Stress distributions after pile installation, analysis IP2MOD:

- a) Vertical effective stress
- b) Radial effective stress
- c) Hoop effective stress

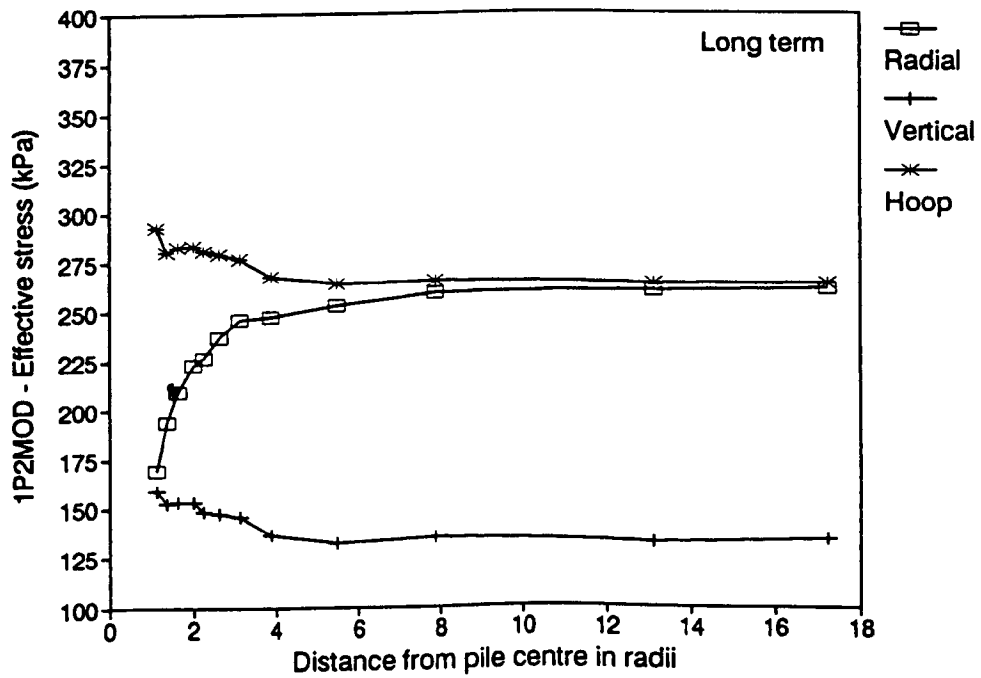
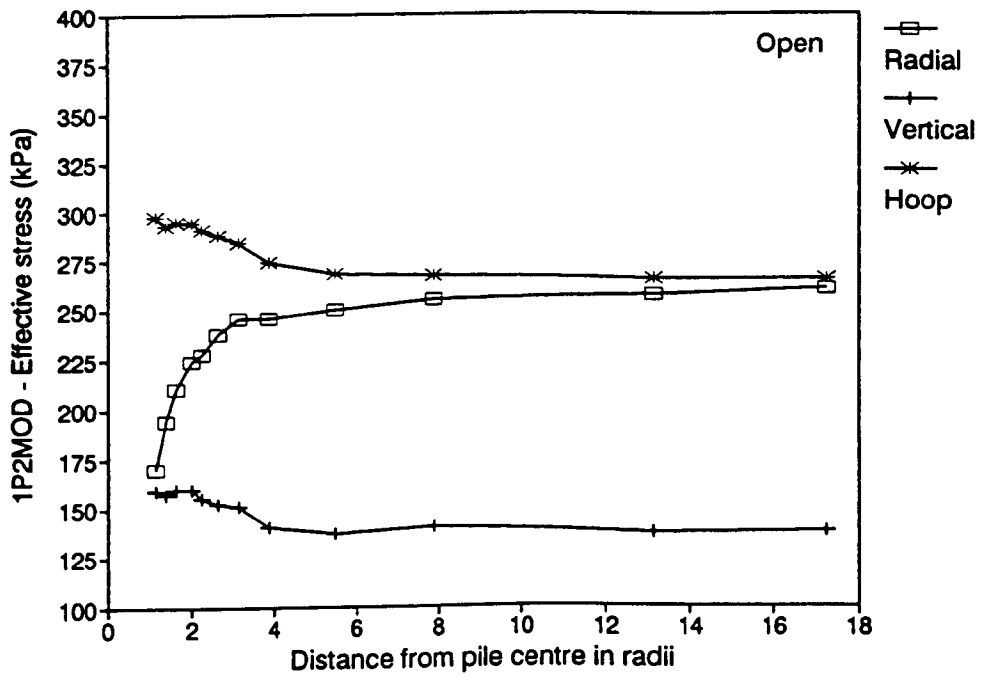


Figure 6.13 Vertical, radial and hoop effective stress distributions at 0.10 depth, analysis 1P2MOD:  
 a) Open shaft  
 b) After installation

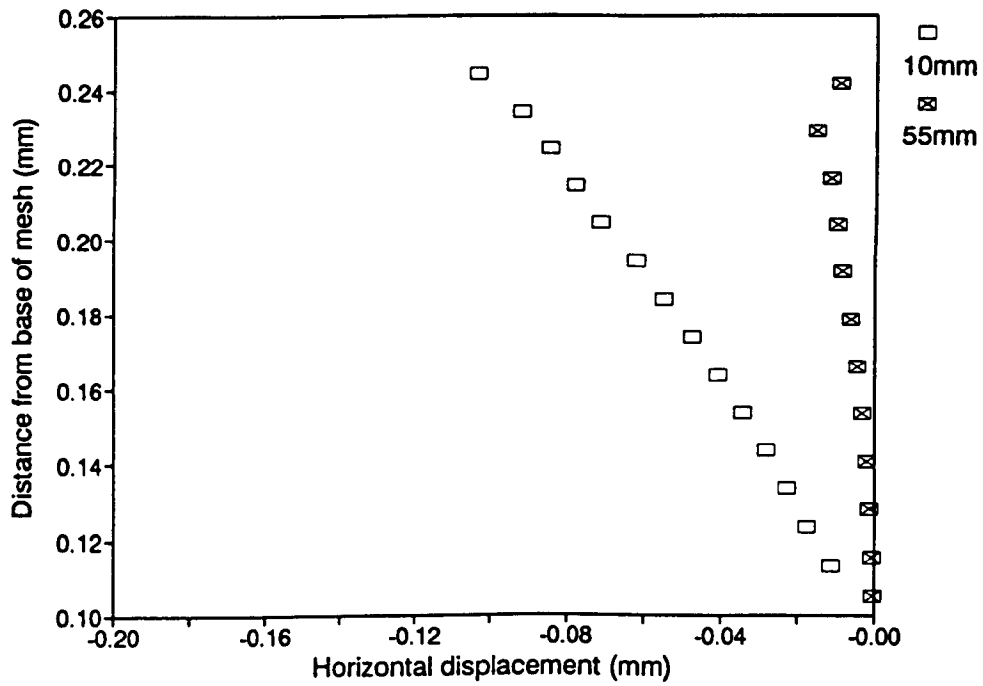


Figure 6.14 Horizontal displacements during pile installation at 0.01 and 0.055m from pile axis, analysis 1P2MOD

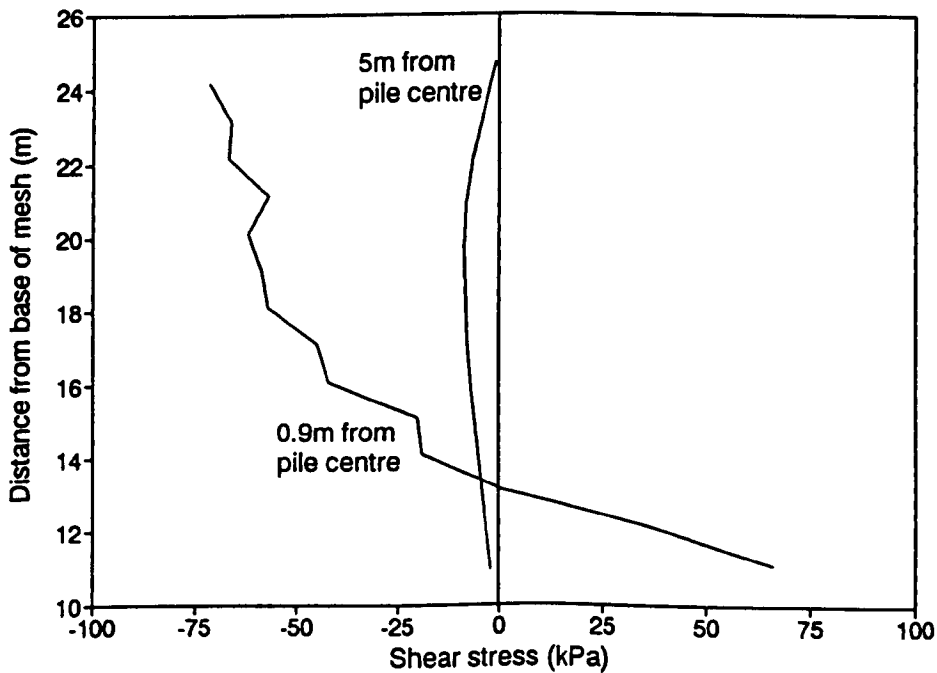


Figure 6.15 Shear stress at 0.9m and 5.5m from pile axis after rising groundwater event, analysis 1PIEXC

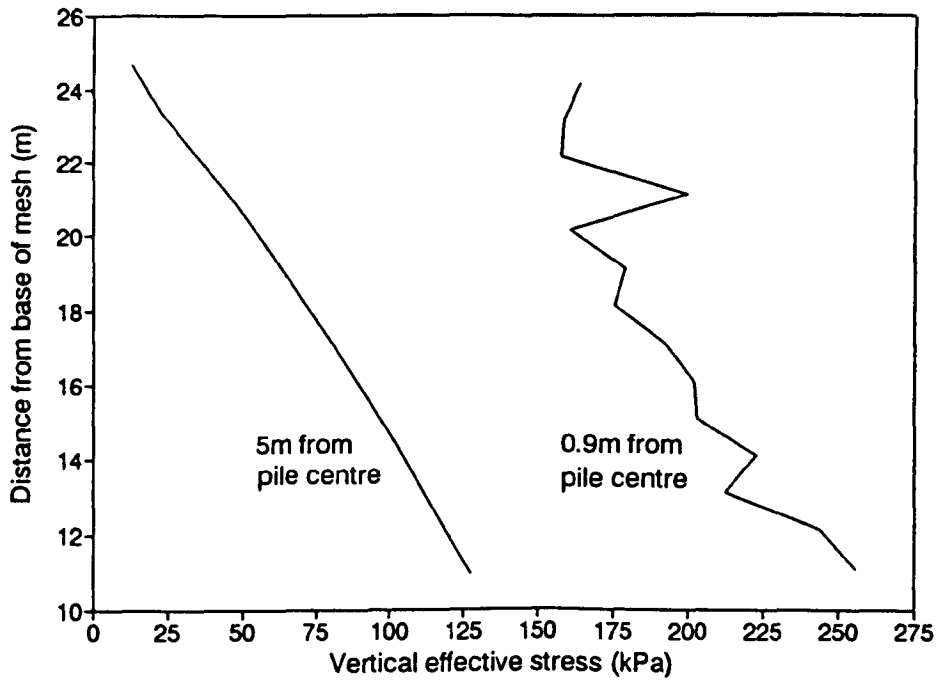


Figure 6.16 Vertical effective stress at 0.1 and 5.5m from shaft after rising groundwater event, analysis 1PIEXC

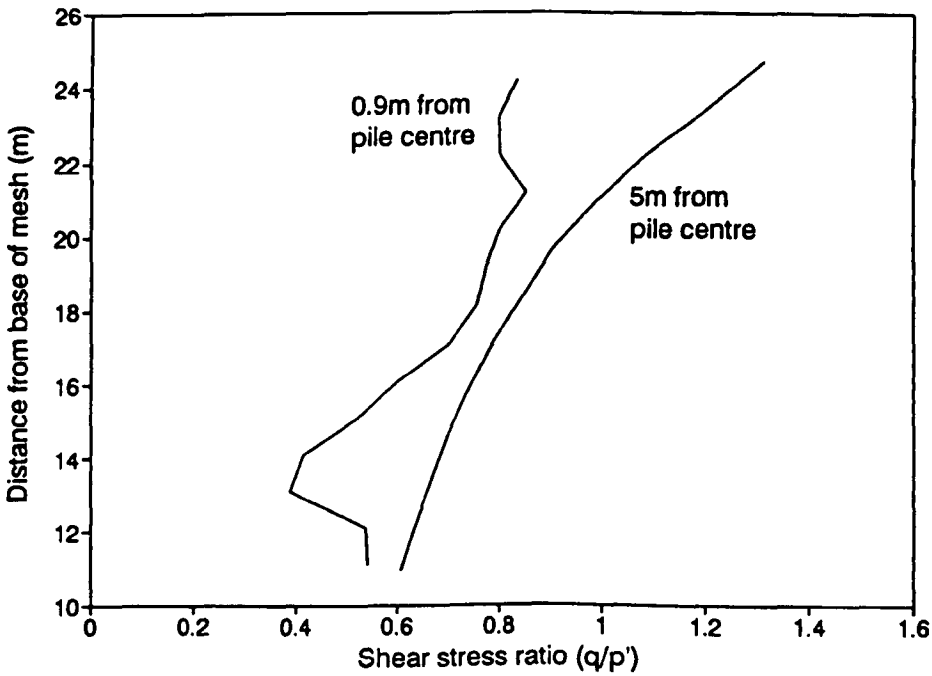


Figure 6.17 Stress ratio  $\eta$  at 0.1 and 5.5m from shaft after rising groundwater event, analysis 1PIEXC

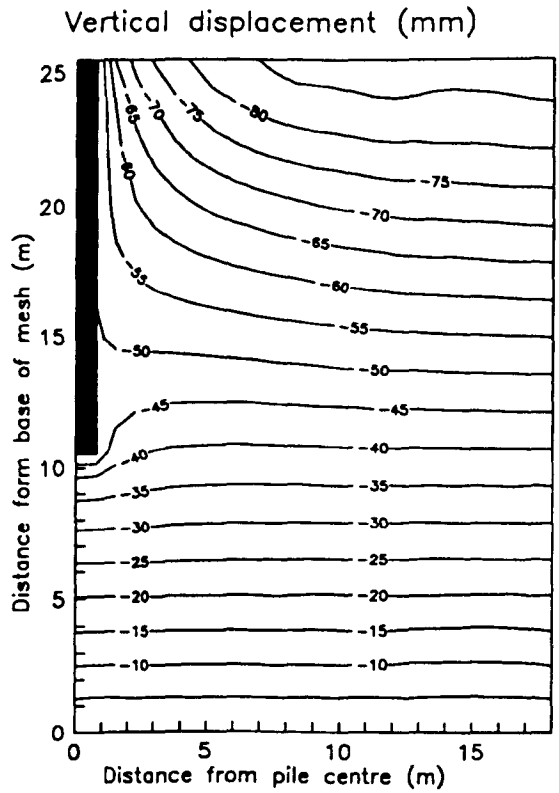


Figure 6.18 Displacement due to rising groundwater event, analysis 1PIEXC

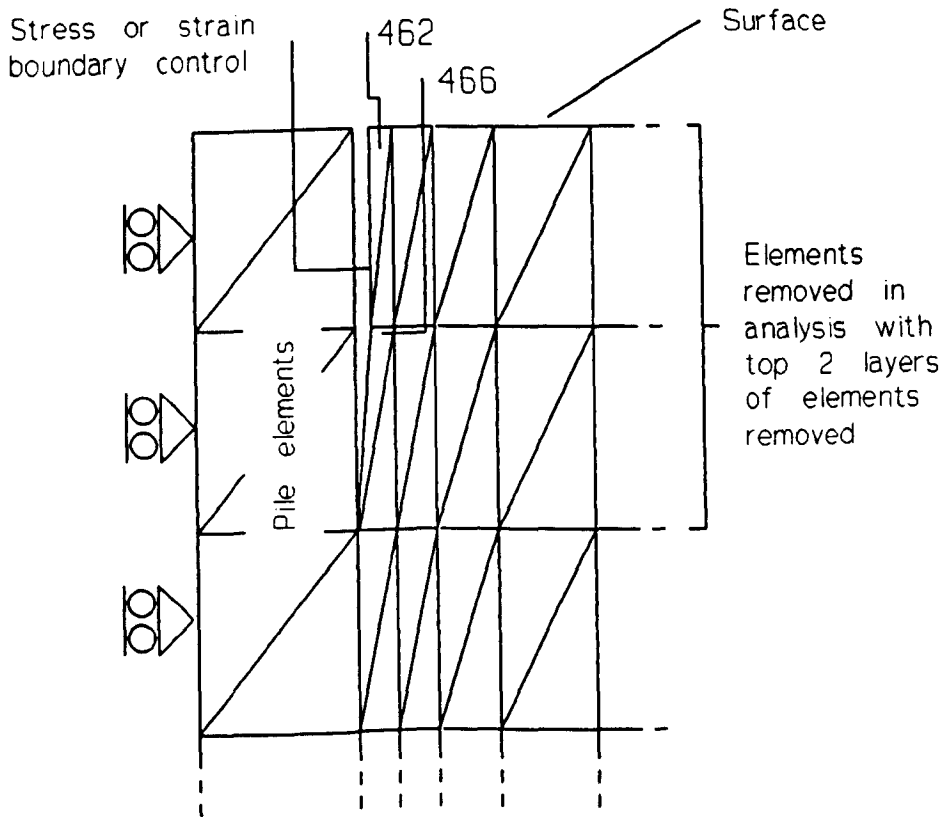


Figure 6.19 Detail of mesh with stress and strain controlled elements

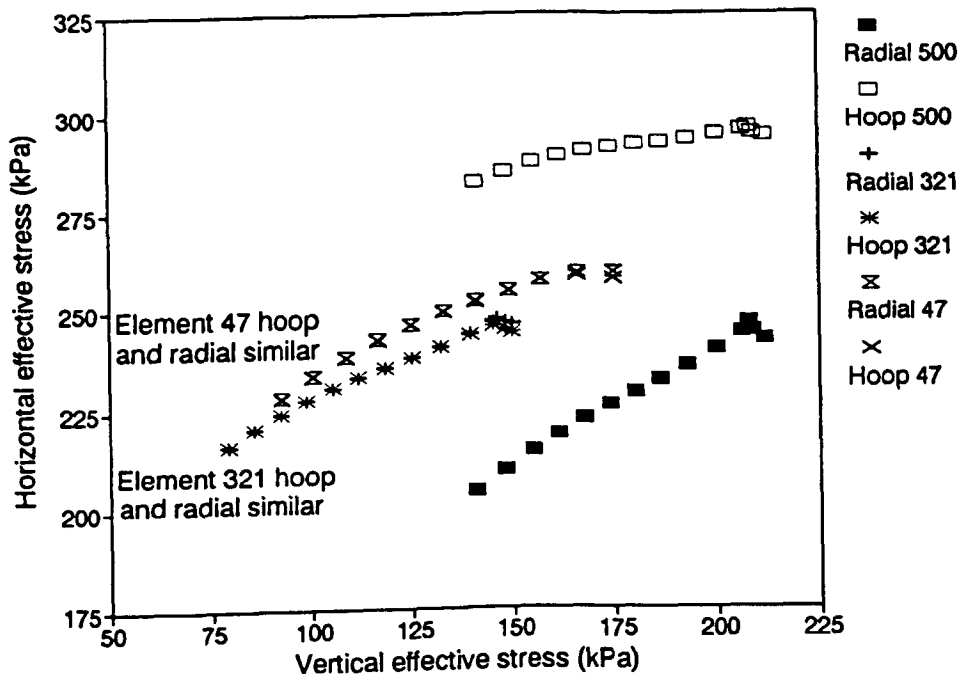


Figure 6.20 Variation of radial and hoop effective stresses with vertical effective stress during rising groundwater event with smooth pile shaft, analysis 1PIEXC

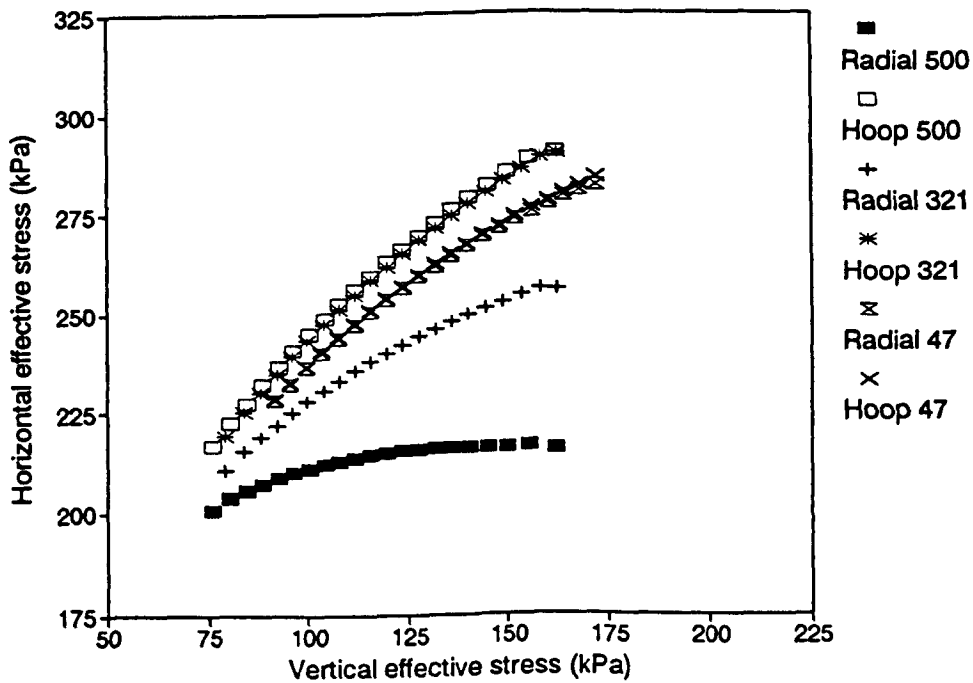


Figure 6.21 Variation of radial and hoop effective stresses with vertical effective stress during rising groundwater event with smooth pile shaft, analysis 1P2MOD

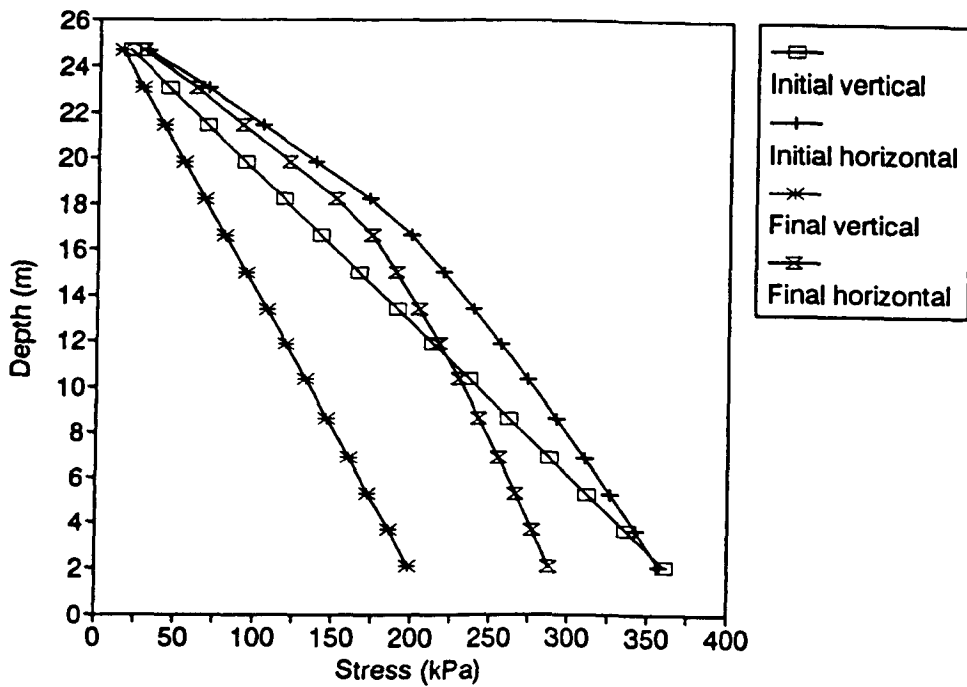


Figure 6.22 Vertical and horizontal effective stress distributions before and after rising groundwater event using Schofield model

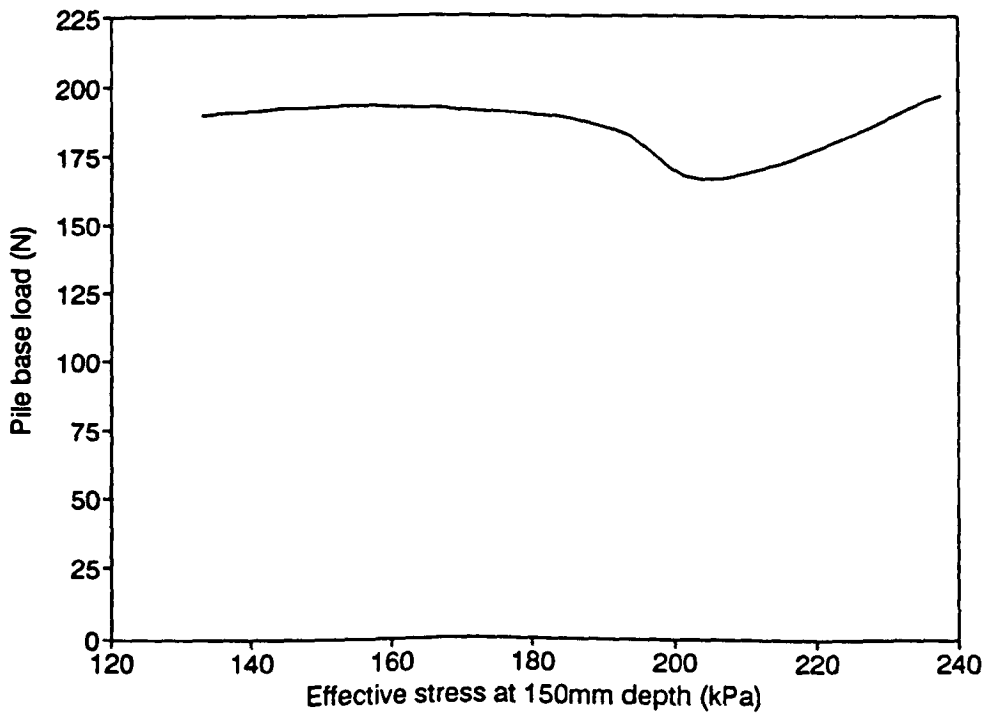
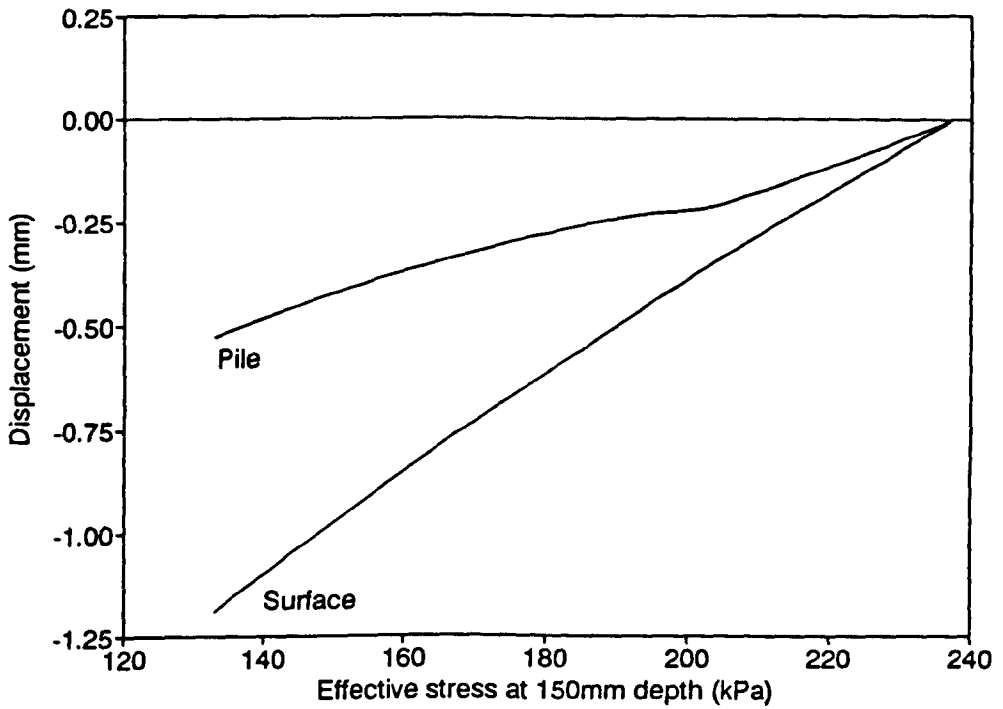


Figure 6.23 Rising groundwater event, analysis SCH5  
 a) Surface and pile displacement  
 b) Pile base load

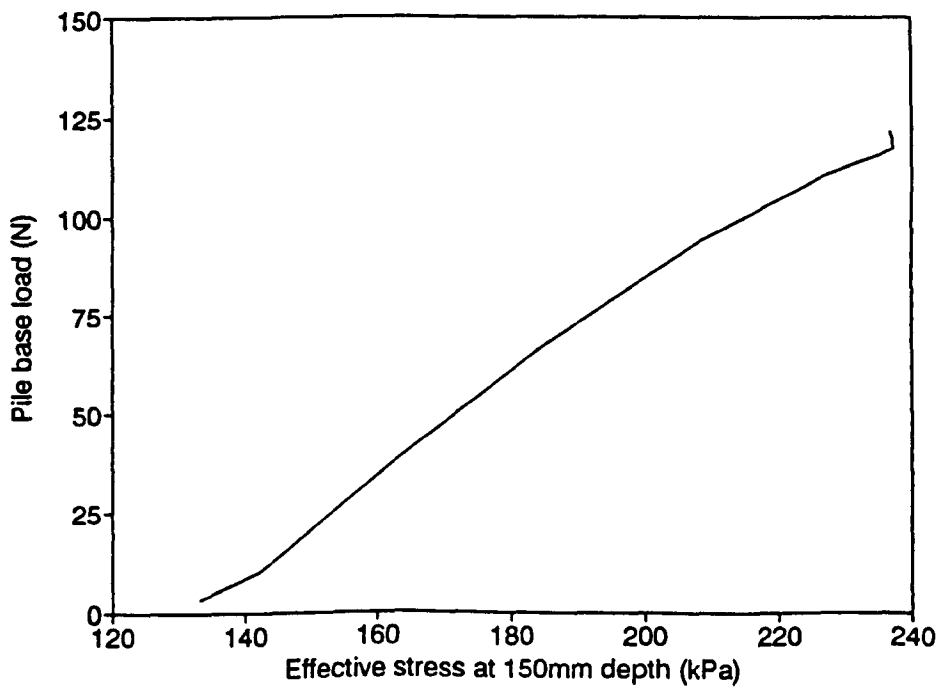
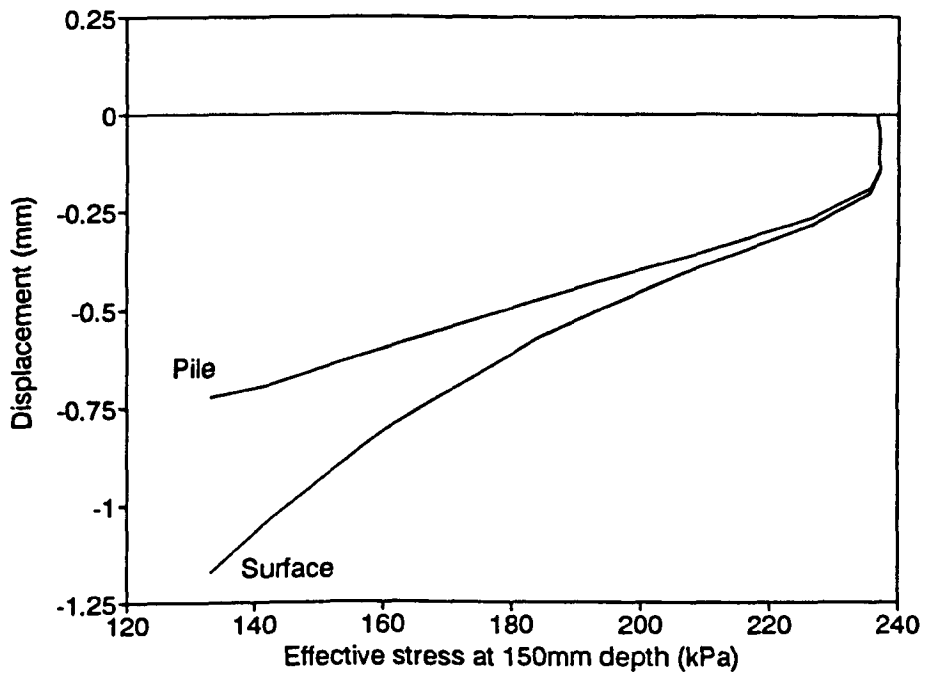


Figure 6.24 Rising groundwater event, analysis SCH2M  
 a) Surface and pile displacement  
 b) Pile base load

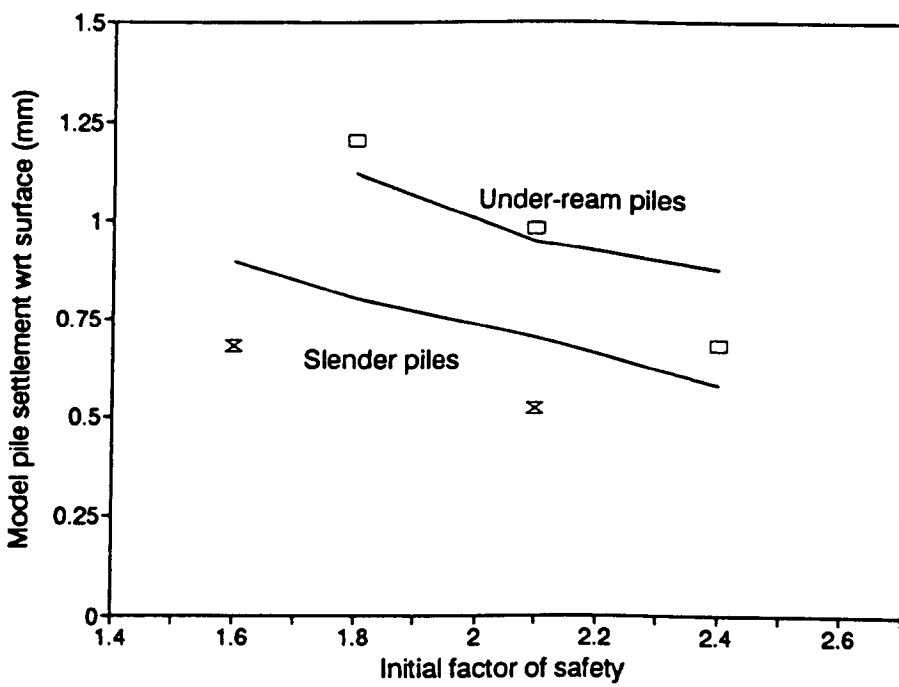


Figure 6.25 Comparison of predicted (simple "by hand" method) pile settlements with centrifuge test results

The information given in this appendix comprises a full description of the eleven most successful centrifuge tests (RW3, RW4, RW6, RW7, RW10, RW11, RW12, RW13, RW14, RW15 and RW16). The following results are presented in graphical format and are at model scale:

- 1) Pore water pressure against time during the rising groundwater event. The pore water pressure responds to a rapid change in water pressure in the base drainage layer of the model at time = 0 hours.
- 2) Displacement with time of soil surface, foundations and where present the buried plate.
- 3) Foundation loads, including (when data were available) a distinction between pile shaft and base loads against vertical effective stress at the pile base level of 150mm below clay surface.
- 4) Displacement of soil surface, foundations and where present the buried plate against vertical effective stress at pile base level of 150mm below clay surface.

Figures (1) and (2) and Figures (3) and (4) are plotted together allowing a direct comparison of displacement and pore water pressure change and displacement, effective stress and foundation load distribution.

Calculation of shaft load assumed a linear distribution of shaft capacity with depth and therefore multiplied the measured shaft load by the ratio of shaft length to length over which shaft load was determined to obtain total shaft load as shown in Table A.1.

File type	Straight	Straight	Under-reamed
Slenderness ratio	12	9.5	6.5
Length of shaft (mm)	150	150	142
Length of shaft above measurement level (mm)	149	140	132
Length of base (mm)	1	10	10
Shaft multiplication ratio	150/149	150/140	142/132

Table A.1 Pile shaft geometry.

Test RW3:

A 16mm diameter straight pile and a 40mm diameter pad were compared in this test in a bed of clay preconsolidated to 1250kPa. The pile had a base load cell which differentiated between the upper 140mm of shaft and lower 10mm of shaft and end bearing load as described above. Both foundations were load tested to find their ultimate load capacity prior to the rising groundwater event. After load testing, the foundations were subjected to working loads resulting in factors of safety on ultimate load of 2.1 and 1.8 for the pile and pad respectively.

During excess pore water pressure dissipation following spin-up the solenoid valve controlling the standpipe dump failed resulting in a build up in pore water pressure as indicated in Figure A.RW3.1 by the high pore water pressures at the start of the rising groundwater event.

During the rising groundwater event surface and foundation heave were smaller than in other tests due to the smaller pore water pressure rise as shown in Figures A.RW3.1 and A.RW3.2. The pad was seen to move closely with the ground surface while the pile lagged behind by about 0.15mm at the end of the test.

The small pile settlement (relative to the ground surface) was partially a result of the load redistribution from the pile base to the shaft seen in Figure A.RW3.3 where foundation loads are plotted against vertical effective stress at pile base level. It appeared that at the end of the stage that full redistribution of load to the shaft had yet to occur.

**Principal observations from test RW3:**

- a) Pad foundations settle only slightly were a perched water table exists to dominate near surface pore water pressures.
- b) Redistribution of load occurs from pile base to shaft during a rising groundwater event for pre-loaded piles.

**Test RW4:**

The first attempt of modelling an under-ream pile was carried out in this test. The under-ream was formed of quick setting portland cement and was not completely successful. However, the test was completed and provided useful information on the behaviour of piles with expanded bases. As in test RW3 both pile and pad foundations were load-tested prior to the rising groundwater event. After load capacity testing, working loads corresponding to factors of safety of 2.2 and  $\approx 1.5$  respectively were applied.

The load displacement response of the pile appeared to be between that of a straight shafted pile and that of a competent under-reamed pile. This observation, based on load capacity response, was confirmed by the fractured state of the under-ream on examination of the pile after the test.

Full consolidation of the clay took place prior to the rising groundwater event as indicated by the low initial pore water pressure seen in Figure A.RW4.1 compared to Figure A.RW3.1. Surface and foundation displacements were larger than in test RW3 as a result of the complete reduction in pore water pressure prior to the rising groundwater event.

The initial load test on the pile resulted in the shaft friction working to load the base at working load as seen on Figure A.RW4.3, at  $\sigma_{v150}'=230\text{kPa}$  there was a small net shaft load. During the rising groundwater event load was transferred from the base to the shaft as in test RW3.

Differential displacements between the foundations and ground surface were larger in this test than in test RW3. From Figure A.RW4.4 it can be seen that the pad settled approximately 0.125mm while the pile settled 0.5mm. Pile settlement is solely a result of soil swelling passed the pile and not due to pile base settlement as confirmed by an ever decreasing pile base load in Figure A.RW4.3.

**Principal observations from test RW4:**

- a) The pad with a low factor of safety settled slightly relative to the ground surface during the rising groundwater event.
- b) The pile behaviour during the rising groundwater event was influenced by the initial load test resulting in unloading of pile base during. The pile settlement at prototype scale of 50mm resulted from soil swelling passed the pile shaft tending to pull the pile base upwards.

**Test RW6:**

In this test a typical working pile (i.e. not previously load tested) was successfully subjected to a rising groundwater event. The test was a repeat of the unsuccessful test RW5. Two piles were tested together. Pile 1 had a base load cell and was not load tested prior to the rising groundwater event, while Pile 2 with no base load cell was pre-load tested. The combination of the two piles in one test provided data on initial load capacity and allowed a comparison of movements associated with the two different pile load conditions to be made. It also allowed a comparison of pile load capacity before and after a rising groundwater event.

Initial consolidation of the clay after spin-up resulted in low pore pressures throughout the clay body as shown in Figure A.RW6.1 at the start of the rising groundwater event.

The piles were both loaded to have a factor of safety of 2.2 on ultimate capacity. A combination of data from the two piles showed that this load represented partial factors of safety of  $Q_s/1 + Q_b/10$  for Pile 1. During the rising groundwater event pile head loads remained constant until  $\sigma_{v150}'$  dropped below 160kPa at which stage Pile 2 unloaded as seen in Figure A.RW6.3 due to a slip-ring malfunction. The movements in Figure A.RW6.4 show that Pile 1 which was not pre-load tested settled relative to the ground surface more than Pile 2. This is attributed to the different distribution of load between shaft and base at the beginning and during the rising groundwater event. By comparing the load behaviour of Pile 1 in Figure A.RW6.3 with either Figure A.RW3.3 or A.RW4.3 the difference between a pre-load tested and a typical working pile is evident. The load cell output in Figure A.RW6.3 was quite noisy. However, the results show a small initial load transfer from the pile base to the shaft which is followed by a slight reloading of the pile base for Pile 1. The displacement during initial loading of Pile 1 was 0.035mm (0.2% pile shaft diameter, from Table 5.3b) and it is therefore not surprising that full friction was not mobilised at the working load.

Figure A.RW6.5 shows a comparison of pile load capacity before (Pile 2) and after (Pile 1) the rising groundwater event. The loss in total load capacity is apparent and is approximately 19% for an average reduction in vertical effective stress over the length of the pile of 36%.

**Principal observations from test RW6:**

- a) The load testing of a pile will act to reduce settlements during a rising groundwater event. The pile was load tested to failure, this is unlikely for a working pile which will usually be proof load tested to 1.5 or 2.0 times working load. The mechanism, however, will be similar for typical prototype proof tested piles which will have overloaded bases at the start of a rising groundwater event.

- b) Both piles settled significantly relative to the ground surface, Pile 1 by 0.67mm at model scale and Pile 2 by 0.5mm at model scale as seen in Figure A.RW6.4 at  $\sigma_{v150}' = 155\text{kPa}$
- c) The reduction in load capacity was less than the loss in vertical effective stress. Base load capacity loss was approximately 25% for a reduction in vertical effective stress at pile base level of 39%. Shaft load capacity loss was approximately 10% for an average reduction in vertical effective stress over the length of the pile of 36%.

#### Test RW7:

Test RW7 had similar objectives to test RW6. Two similar geometry piles were tested together at the same working load. One pile was load tested prior to and the other after the rising groundwater event. The working loads applied resulted in a factor of safety of 1.6 or Pile 1 with partial factors on the shaft of 1.0 and on the base 2.7.

The results are presented in the same format as those in test RW6 and will not be discussed in detail.

#### Principal observations from test RW7:

- a) Both piles settled significantly relative to the ground surface, Pile 1 by 0.97mm and Pile 2 by 0.76mm at an average model vertical strain of 0.6% as seen in Figure A.RW7.4. A settlement of 1mm at model scale corresponds to 100mm at prototype scale and is likely to result in significant distress to a structure.
- b) Total load capacity loss of 14% was less than the reduction in average vertical effective stress of 35%. Base load capacity loss was approximately 21% for a reduction in vertical effective stress at pile base level of 40%. Only slight loss in shaft load capacity was measured during the rising groundwater event as indicated by the relatively flat shaft load measurements in Figure A.RW7.3.

- c) The settlements in this test were larger than those in test RW6 and were a result of the lower initial factors of safety.

0

#### Test RW10:

The results of tests RW6 and RW7 showed that factor of safety effects settlement of foundations in a rising groundwater environment. In this test two similar under-reamed foundations with different factors were compared in a rising groundwater event. Pile 1 was subjected to a load of 400N representing a calculated factor of safety of 1.8 while Pile 2 had values of 345N and 2.2 respectively. The under-ream material used was a quick-setting metal loaded epoxy (No. 551-075 from Radio Spares components UK). The resin was proof tested under unconfined compression and was seen to have satisfactory shear strength and creep properties. Behaviour of the under-ream was satisfactory in this and succeeding under-reamed piles tested.

Pore water pressures at the start of the rising groundwater test were on average 30% hydrostatic over the length of the pile. At the end of the test they had risen to 87% of hydrostatic values (Figure A.RW10.1). Foundation settlements during the rising groundwater event were large (Figures A.RW10.2 and A.RW10.4) and for most of the test the foundations remained stationary as the soil swelled both below and above the pile base level as indicated by the changes in pore water pressure in Figure A.RW10.1 at all depths. Settlements relative to ground level were 1.2mm for Pile 1 and 0.94mm for Pile 2 at an average vertical strain in the sample of 0.6%. The settlements monitored in Pile 2 of this test were similar to those in Pile 1 of test RW15 which had the same length and factor of safety.

Foundation load distribution was monitored in Pile 1 (Figure A.RW10.3). Clearly load is transferred from the shaft to the base. During initial loading of Pile 1 shaft load capacity peaked at a displacement of 0.1mm. On a continuation of loading the shaft capacity reduced, possible due to a combination of dissipation of excess pore water pressures and reduction in  $\delta$  (Eqn. 2.3). Pile 2 settlement on initial loading was 0.1mm. During

the rising groundwater event there was a load transfer of from the shaft to the base in Pile 1 (Figure A.RW10.3) of approximately 10% initial shaft capacity. Pile 2, which is thought to have mobilised full shaft capacity during initial loading, would also have experienced a similar reduction in shaft capacity.

**Principal observations from test RW10:**

- a) As previously seen in tests RW6 and RW7 piles with higher factors of safety settle less than those with lower factors.
- b) Settlements for under-reamed piles are larger than those from straight shaft piles of similar lengths and similar factors of safety.
- c) For piles which fully mobilise shaft friction during initial loading the rising groundwater event will result in a one way load transfer from the shaft to the base.

**Test RW11:**

This test was similar to test RW10 except that two straight shaft piles with slenderness ratios of 12 were tested together. Foundation loads were 235N and 182N representing calculated factors of safety of 1.6 and 2.1 for Piles 1 and 2 respectively. Neither pile had base load measurement capability. An additional displacement transducer was placed on top of a rod connected to a buried plate at pile base level allowing the pile settlement a ground level to be separated into components of soil heave passed the pile base and settlement of the pile base relative to the surrounding soil.

Pile settlement during the pore water pressure rise from 24% hydrostatic to 82% hydrostatic resulted in both piles settling relative to the buried plate. Pile 2, with the lower of the loads, settled very slightly compared to the plate and significantly less than Pile 1 in this test and 48% less than under-reamed Pile 2 in test RW10 which had a similar factor

of safety.

Principal observations from test RW11:

- a) As with the under-reamed piles in test RW10, slender piles were seen to settle more as the factor of safety reduced.

Test RW12:

Test RW12 was the first of two tests examining the result of raising the pore water pressure from a depressed hydrostatic profile. The test set up reverted back to that used in tests RW3 and RW4 where a pad and a pile were tested together. The test was carried out to assess the effects of a different initial pore water pressure profile that might occur in situations of long-term under drainage in the absence of a perched surface water table.

Figure A.RW12.1 shows the initial pore water pressures in the sample. At the start of the test pore suctions were estimated to be -34kPa at 50mm clay depth. At the end of the test this pore pressure had risen to approximately 0kPa. The rising groundwater stage of the tests lasted over 21 hours model time, twice as long as the previous tests. The time to achieve near hydrostatic pore water pressures in the clay was prohibitively long resulting in a full rising groundwater not being undertaken. The loss in control of the pad loading rig can be seen from Figure A.RW12.3 when at  $\sigma_{v150}' = 205\text{kPa}$  a sharp reduction in load occurred. The settlement of the pad will have been reduced by this unloading. However, the pad settled significantly relative to the ground surface even for the uncompleted pore water pressure rise as seen on Figure A.RW12.4.

The pile shaft load remained fairly constant during the rising groundwater event which may be a result of not being fully mobilised during initial loading to a displacement of 0.8% pile shaft diameter (initially a slight increase in shaft load was seen followed by a small decrease). The pile settlement relative to the ground surface was quite

large and was due to the small reduction in effective stress below pile base level and the large reduction above base level compatible with the initial depressed hydrostatic pore pressure profile.

Further comments on this test are combined with those on test RW13.

#### Test RW13:

This test was similar to test RW12 but incorporated a buried plate for measurement of ground heave at pile base level.

The rising groundwater stage of the test lasted 43 hours during which time the pore water pressure at 50mm clay depth rose from approximately -37kPa to 0kPa. The pore water pressures were still rising at the time the test was stopped as can be seen on Figure A.RW13.1.

Displacement measurements showed that the pad settled significantly relative to the ground surface and that the pile, a slender pile with initial factor of safety of 1.4, settled relative to the buried plate. The pad was seated on the clay surface which was covered with liquid paraffin. The initial vertical effective stress (from  $\sigma_{vt} - u$ ) close to the surface appears to be incorrect as it appears that the top pore water pressure transducer (48mm depth) had cavitated as indicated by the sharp change in pore water pressure gradient at time = 13 hours on Figure A.RW13.1. However, data from the remaining pore pressure transducers indicate that surface vertical effective stress reduced from approximately -110kPa to -40kPa. The vertical effective stress at the surface at the end of the test represents a surcharge of over two metres of overburden at prototype scale and as such was at a higher vertical effective stress than for the pads in tests RW3 and RW4 where vertical effective stress at the pad base level at the end of the tests was approximately 16kPa. From this comparison it appears that for pad and pile alike settlement due to rising groundwater beneath a depressed hydrostatic pore water pressure profile will result in larger settlements than for a similar pore water pressure increase at depth below a downward seepage pore pressure profile.

During initial loading the piles in tests RW12 and RW13 both piles settled by approximately 1% pile diameter and appeared to mobilise full shaft friction. In both tests RW12 and RW13 pile shaft load was not seen to degenerate significantly due to the rising ground water. There are no data to explain this, however, the stability of the pile shaft during construction and after spin-up, when pore pressures remained negative, is likely to have led to low radial stresses against the pile. As the pore water pressures rose the soil around the shaft would have swelled possibly resulting in higher radial effective stresses than before the rising groundwater event.

Principal observations from tests RW12 and RW13:

- a) Shallow pad foundations will settle relative to the ground surface when there is a pore water pressure increase below a depressed hydrostatic profile.
- b) Pile foundations will settle relative to the surface more in the case of pore water pressure rising below a depressed hydrostatic profile compared to an initial pore water pressure profile generated through downward seepage. The magnitude of effective stress reduction in the former case above pile base level is much larger than the latter case and causes the extra pile settlement relative to the heaving ground surface.

#### Test RW14:

Tests RW14 and RW15 completed the series of tests looking at foundation behaviour during a rising groundwater event. In both tests an under-reamed pile was compared with a slender pile. Both tests were carried out with an initial pore water pressure profile generated through downward seepage.

In test RW14 initial pile factors of safety were 2.5 on the under-ream pile (Pile 1) and 2.1 on the slender pile (Pile 2). Pore water pressure increased from 33% hydrostatic to 84% hydrostatic resulting in a average

loss in vertical effective stress of 34% over the length of the piles, and a 41% loss at pile base level.

Pile settlements relative to the surface were larger for the under-reamed pile even though it had the larger factor of safety as seen in Figures A.RW14.2 and 4. This might partly be caused by an unloading of the Pile 2 base during the rising groundwater stage.

Both piles settled relative to the buried plate which in this case appears to be due to the plate being dragged upwards, the result of which should be questioned. This is consistent with the behaviour of the base of Pile 2 which unloaded suggesting some base heave.

Further comments on this test are combined with those on test RW15.

#### Test RW15:

In this test initial pile factors of safety were 2.2 on the under-ream pile (Pile 1) and 2.0 on the slender pile (Pile 2). Pore water pressure increased from 19% hydrostatic to 81% hydrostatic resulting in an average loss in vertical effective stress of 40% over the length of the piles and a 45% loss at pile base level.

The under-reamed pile settled relative to the plate and the slender pile which was seen to move almost exactly with the plate. The larger surface heave seen in this test compared to the other tests with downward seepage is a result of the low initial pore water pressure achieved at the start of the test. This was due to the existence of small negative pore water pressures after spin up which then rose to the low equilibrium pore water pressure profile.

The slender pile was seen to move in unison with the buried plate. However, it seemed from differential movement between plate and ground surface that the plate (as in test RW14) has been dragged upwards by comparing movements with pore water pressure change in Figure A.RW15.4. It seems that the plate readings can be taken as an upper bound of soil

heave at pile base level and as such Pile 2 will have heaved slightly relative to the soil at pile base level.

Principal observations from tests RW14 and RW15 and others:

- a) This test and test RW14 confirm the influence of pile geometry on foundation settlement suggested by comparing pile settlement results from previous tests: foundations, of the same length, which mobilise base capacity at working load settle relative to the ground surface more than those which do not.
- b) A significant proportion of under-reamed pile settlement is due to settlement of the pile base due to increased pile base load (measured), reduced pile base load capacity (measured) and reduced soil stiffness (known from laboratory test results). The remaining settlement is due to all the vertical straining of soil above pile base level contributing to the pile settlement.
- c) Slender pile settlement is due almost solely to soil swelling passed the pile shaft which will result in either unloading of the pile base where a pre-load exists and/or the creation of tensile forces in the pile at the soil attempts to stretch the pile.

#### Test RW16:

This test comprised eight cone penetration tests using a Fugro miniature piezocone penetrometer. The analysed results of the tests have been presented in section 5.4 of the main text.

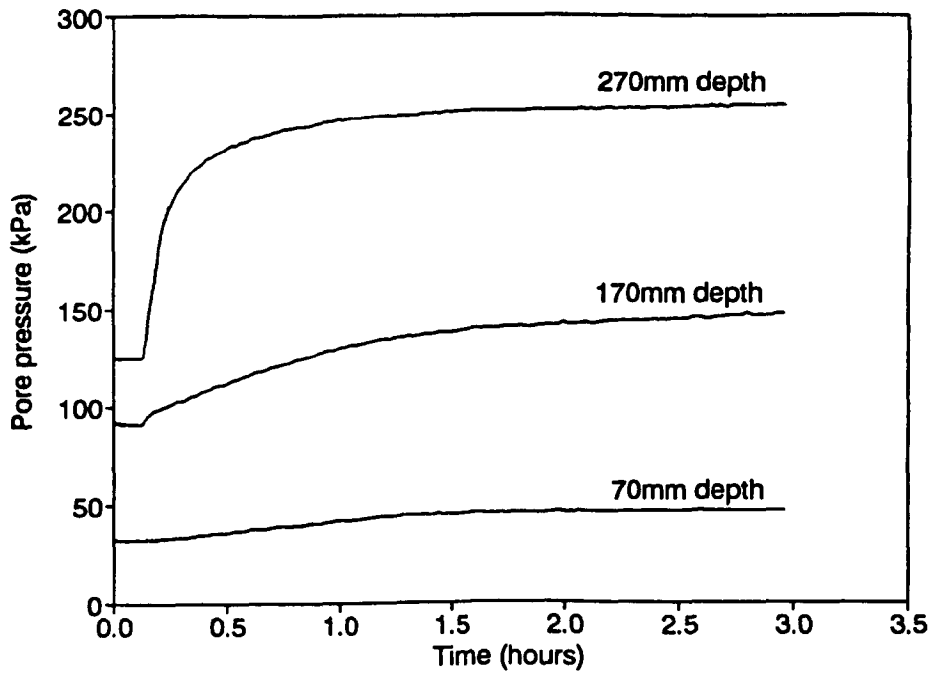


Figure A.RW3.1 Pore water pressure increase against time during rising groundwater event, test RW3

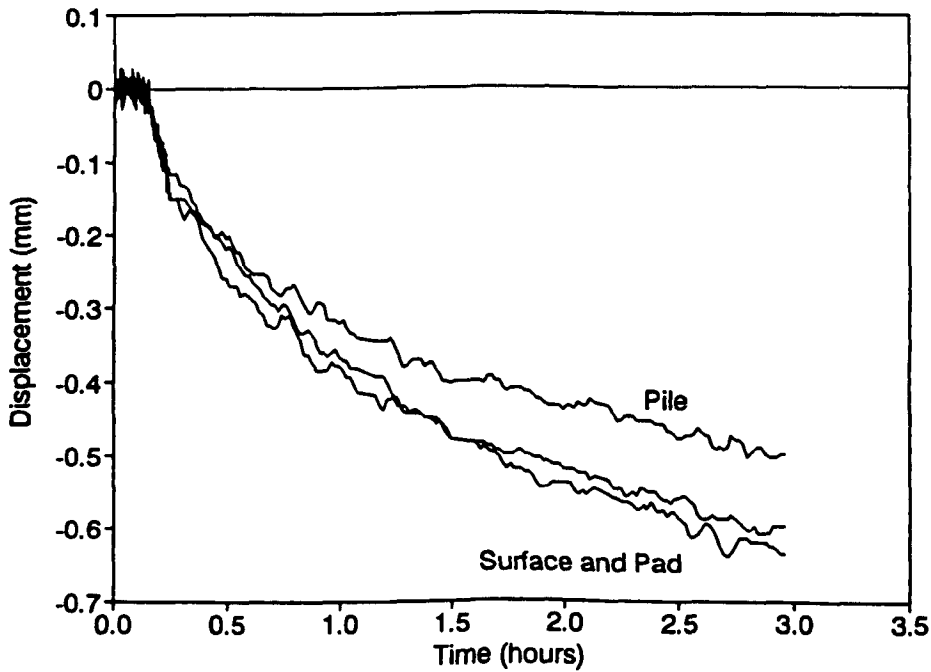


Figure A.RW3.2 Displacement against time during rising groundwater event, test RW3

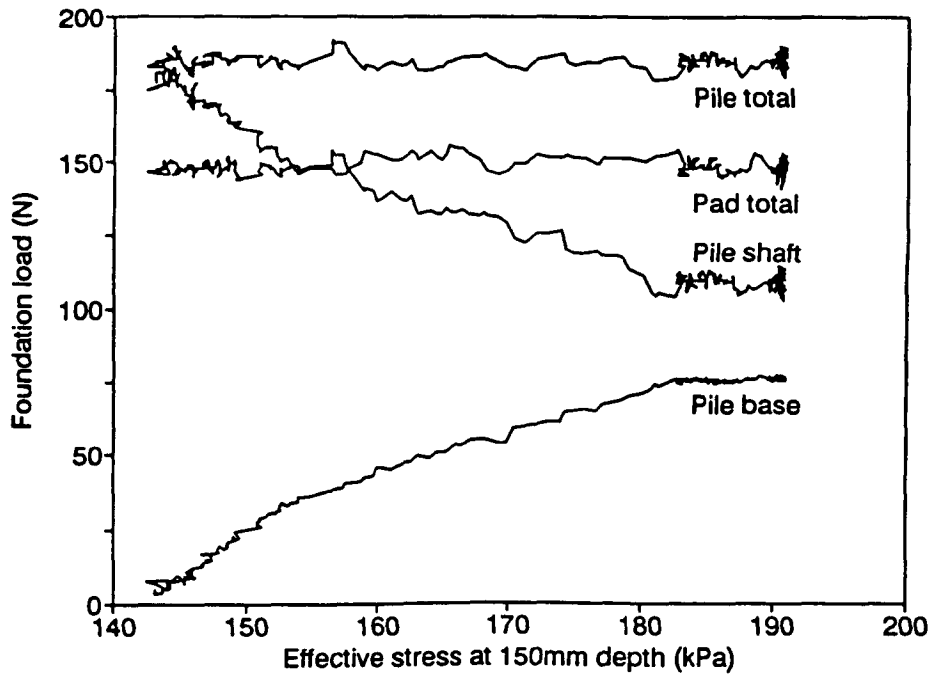


Figure A.RW3.3 Foundation loads against vertical effective stress at pile base level during rising groundwater event, test RW3

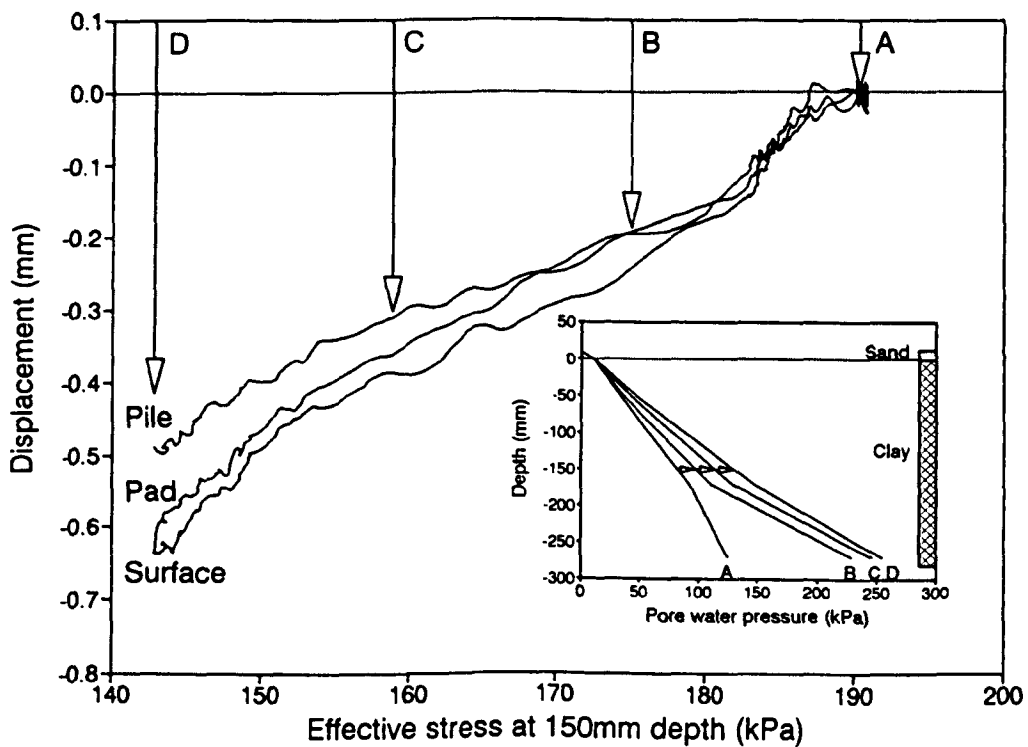


Figure A.RW3.4 Displacement against vertical effective stress at pile base level during rising groundwater event, test RW3

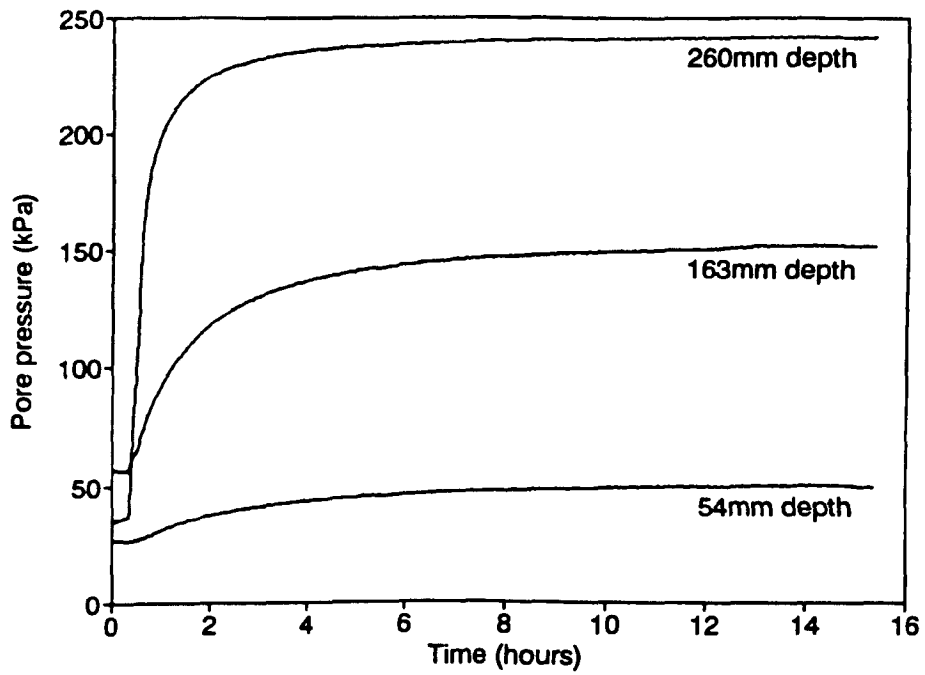


Figure A.RW4.1 Pore water pressure increase against time during rising groundwater event, test RW4

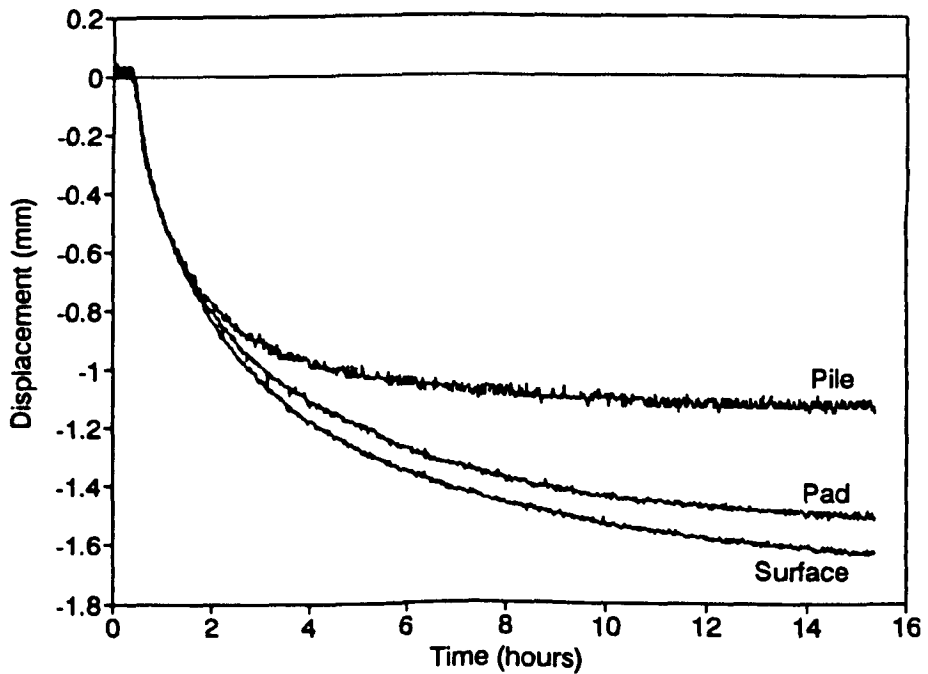


Figure A.RW4.2 Displacement against time during rising groundwater event, test RW4

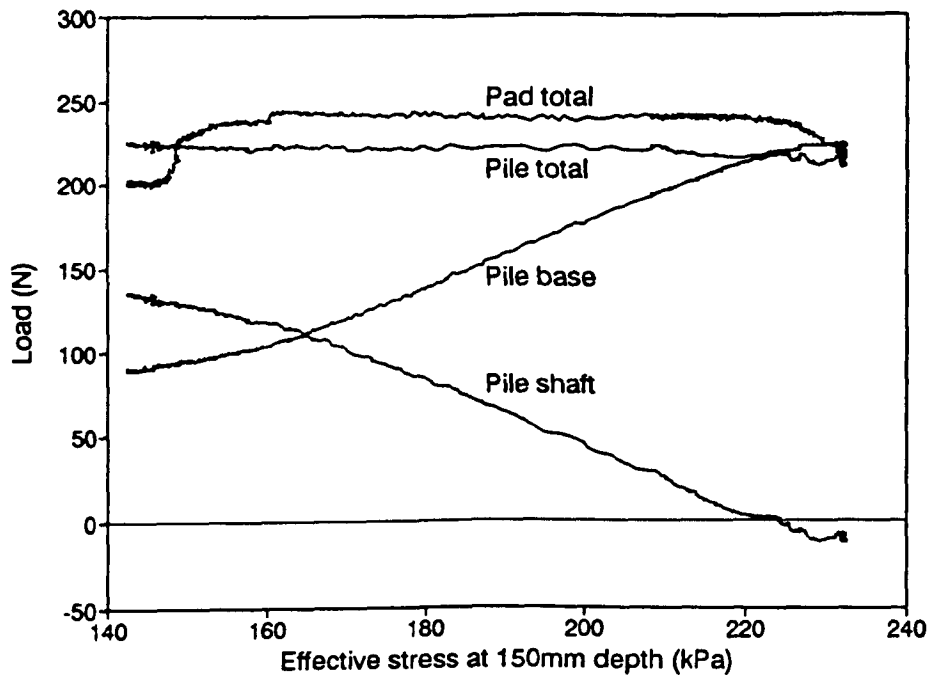


Figure A.RW4.3 Foundation loads against vertical effective stress at pile base level during rising groundwater event, test RW4

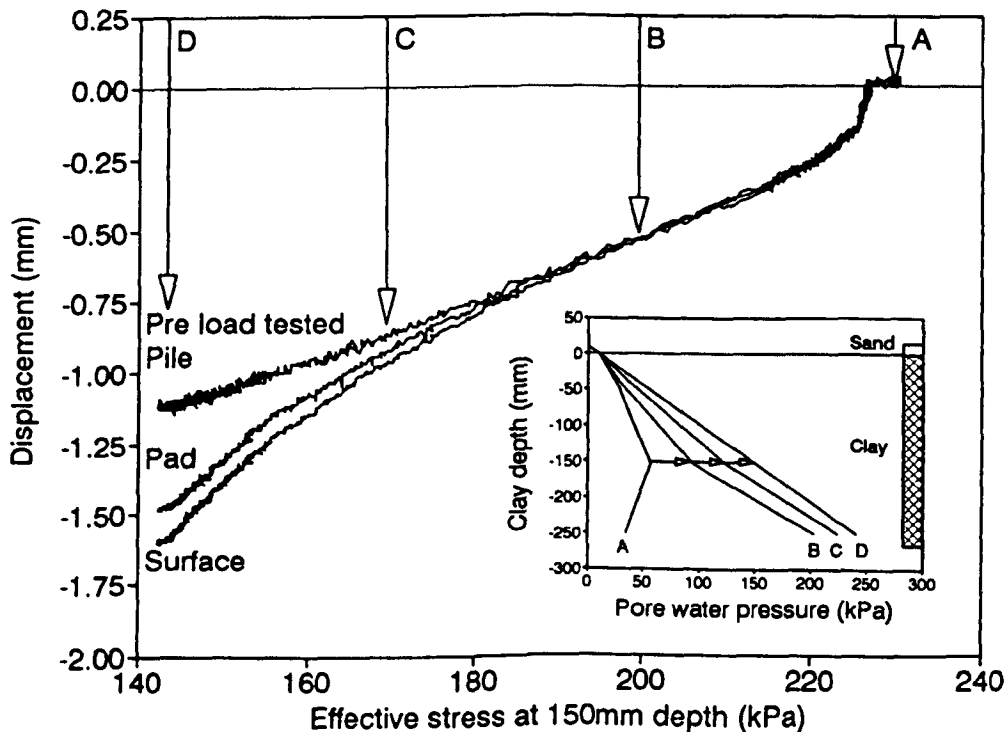


Figure A.RW4.4 Displacement against vertical effective stress at pile base level during rising groundwater event, test RW4

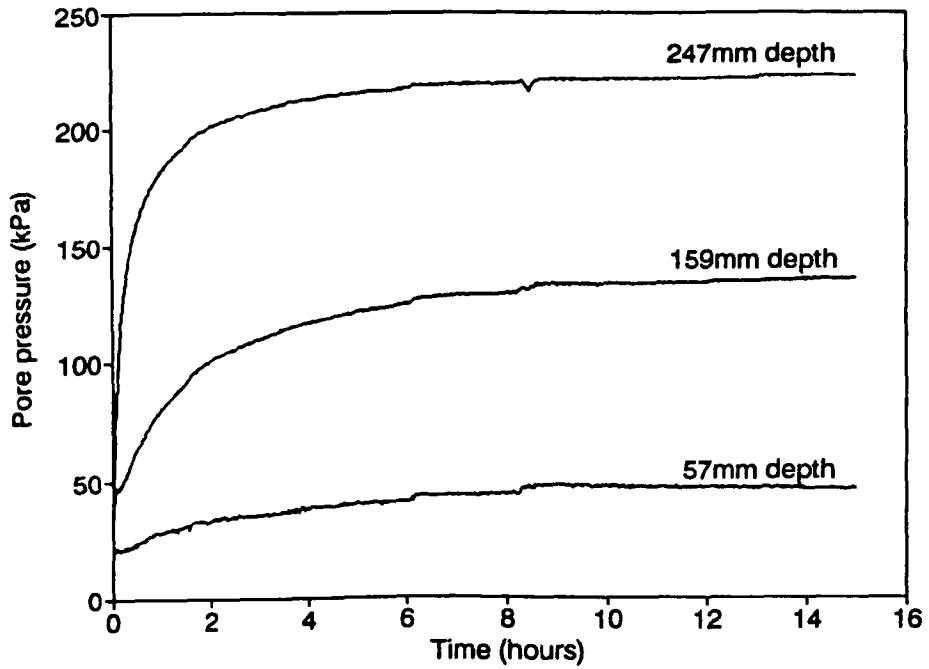


Figure A.RW6.1 Pore water pressure increase against time during rising groundwater event, test RW6

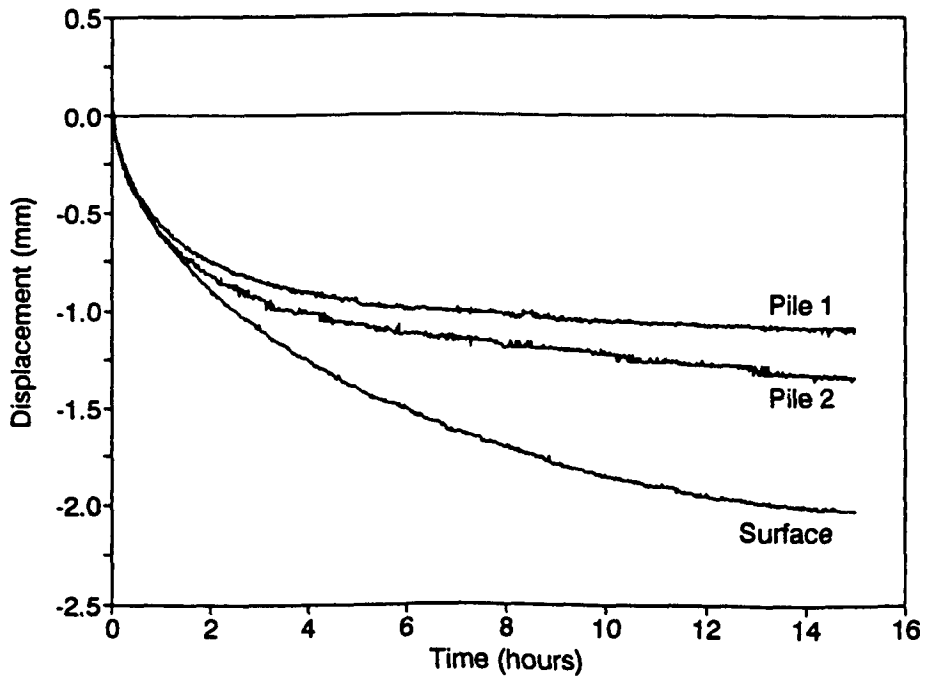


Figure A.RW6.2 Displacement against time during rising groundwater event, test RW6

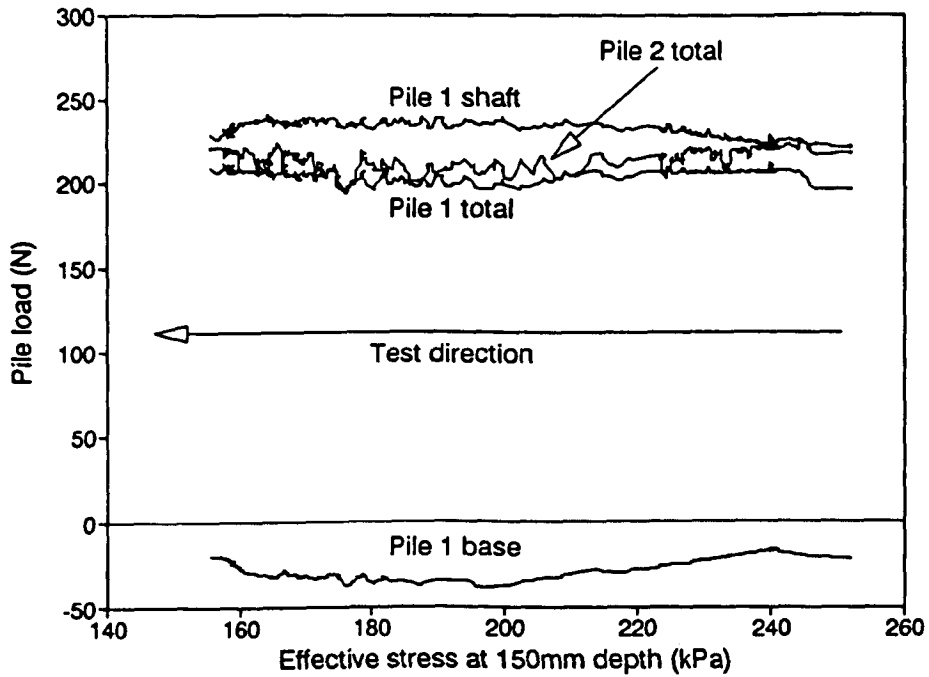


Figure A.RW6.3 Foundation loads against vertical effective stress at pile base level during rising groundwater event, test RW6

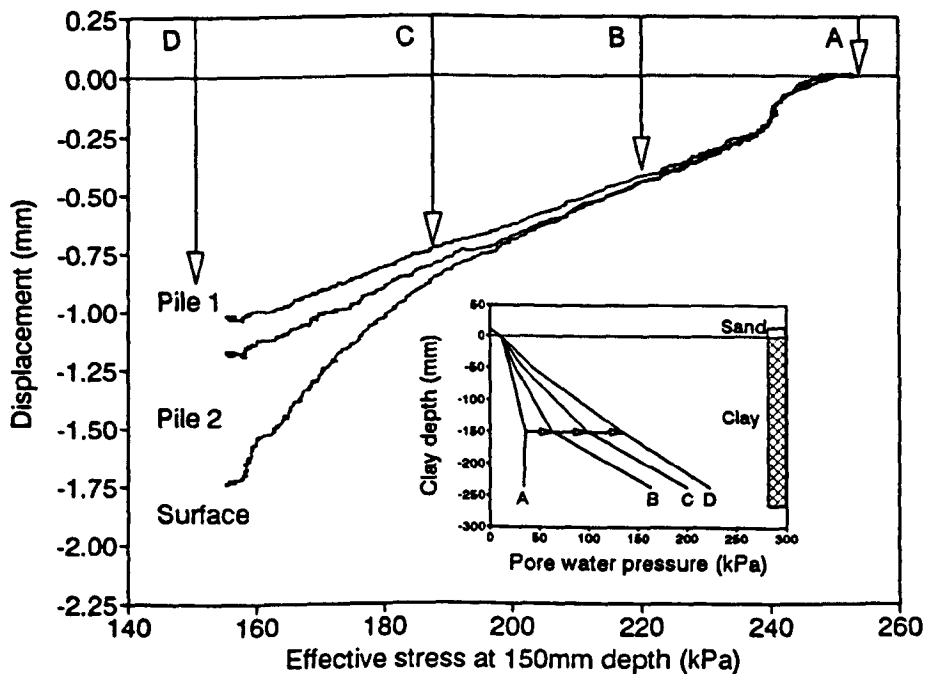


Figure A.RW6.4 Displacement against vertical effective stress at pile base level during rising groundwater event, test RW6

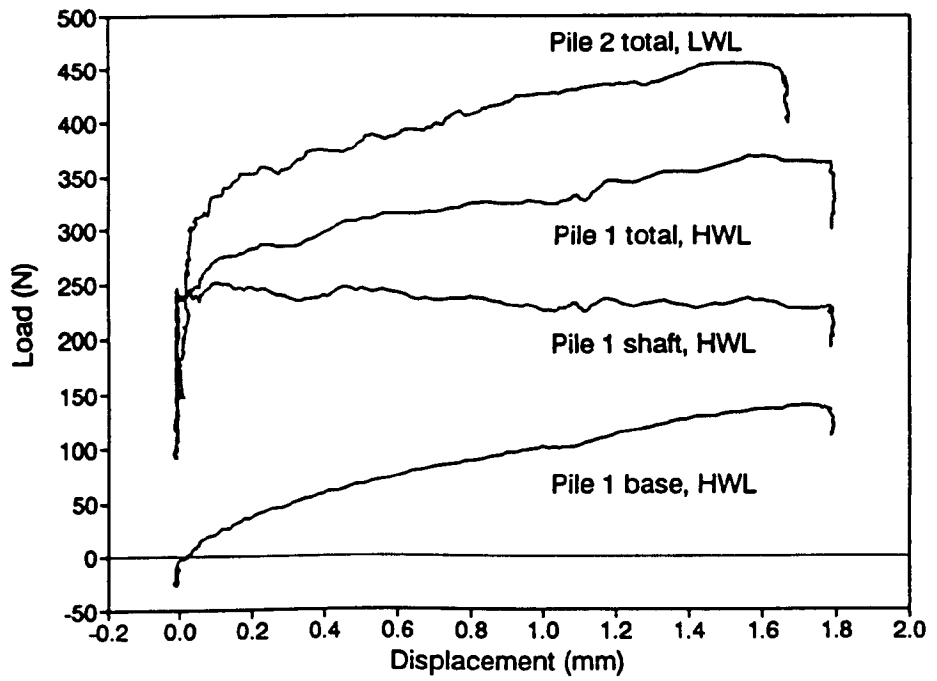


Figure A.RW6.5 Comparison of foundation load tests before (Pile 2) and after (Pile 1) rising groundwater event, test RW6

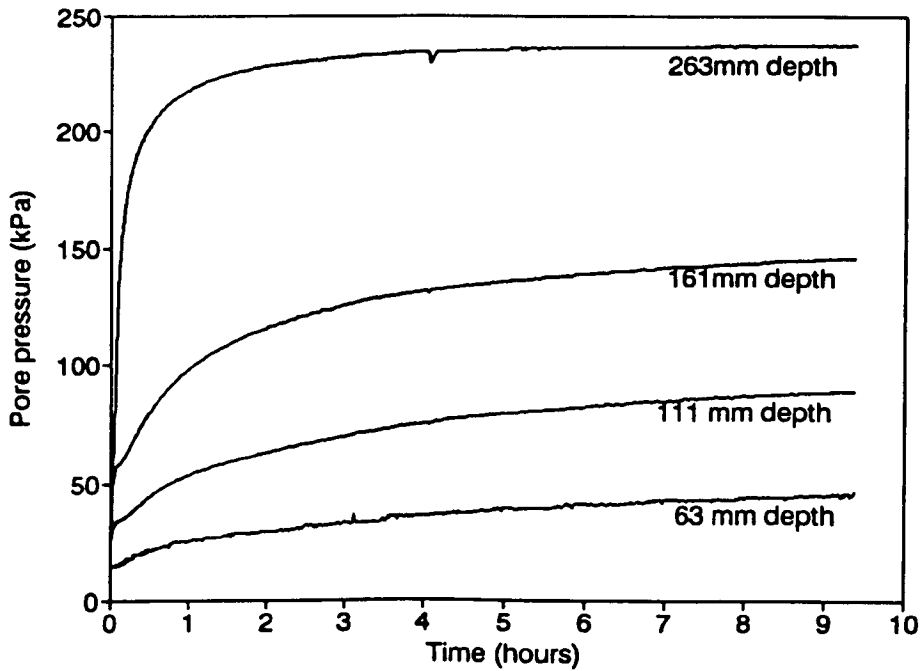


Figure A.RW7.1 Pore water pressure increase against time during rising groundwater event, test RW7

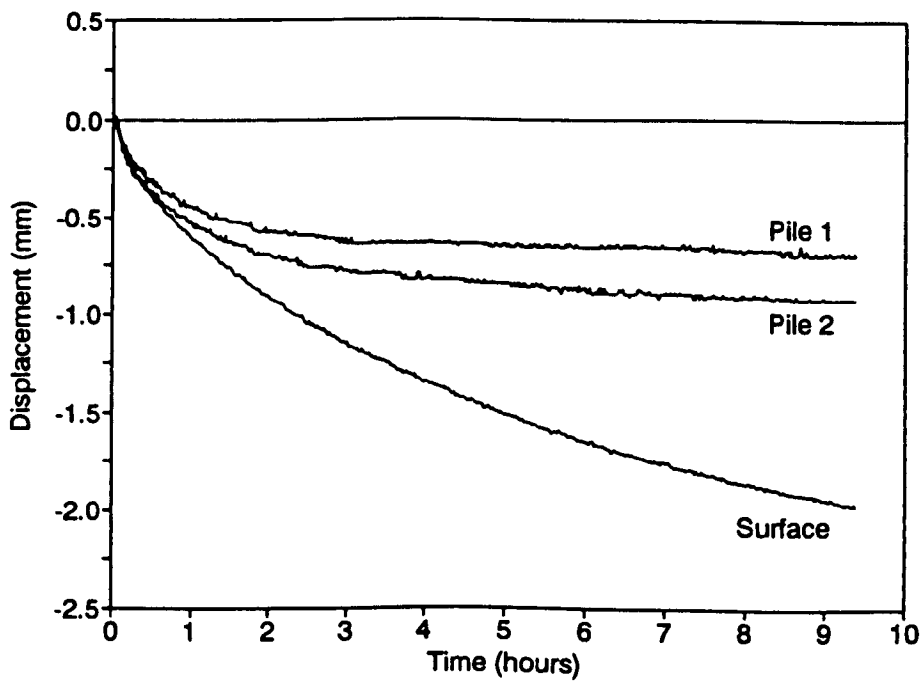


Figure A.RW7.2 Displacement against time during rising groundwater event, test RW7

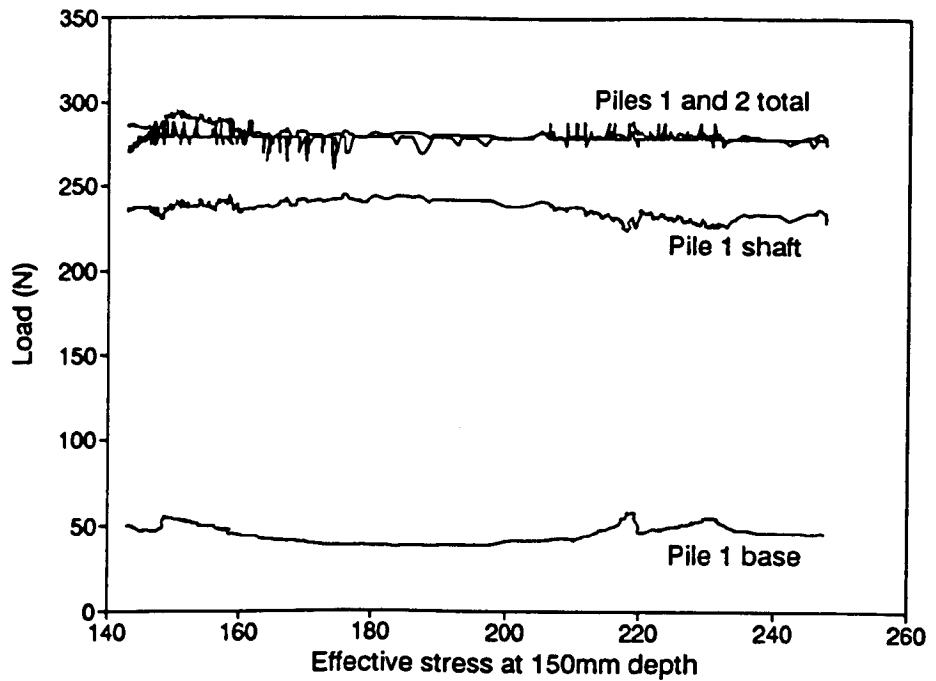


Figure A.RW7.3 Foundation loads against vertical effective stress at pile base level during rising groundwater event, test RW7

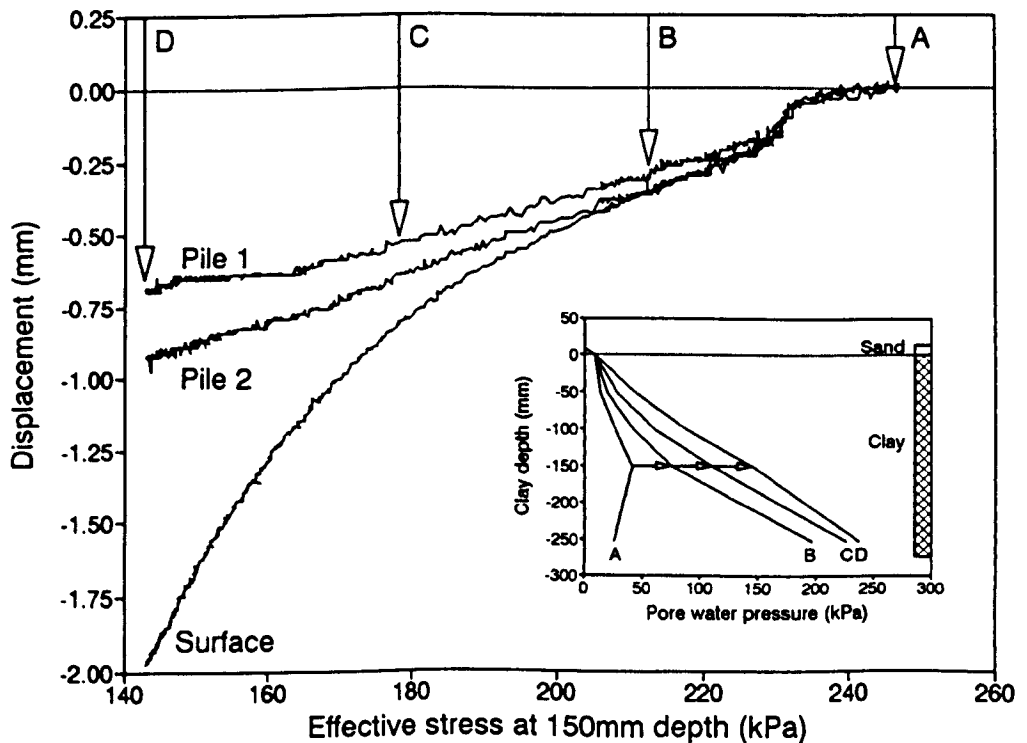


Figure A.RW7.4 Displacement against vertical effective stress at pile base level during rising groundwater event, test RW7

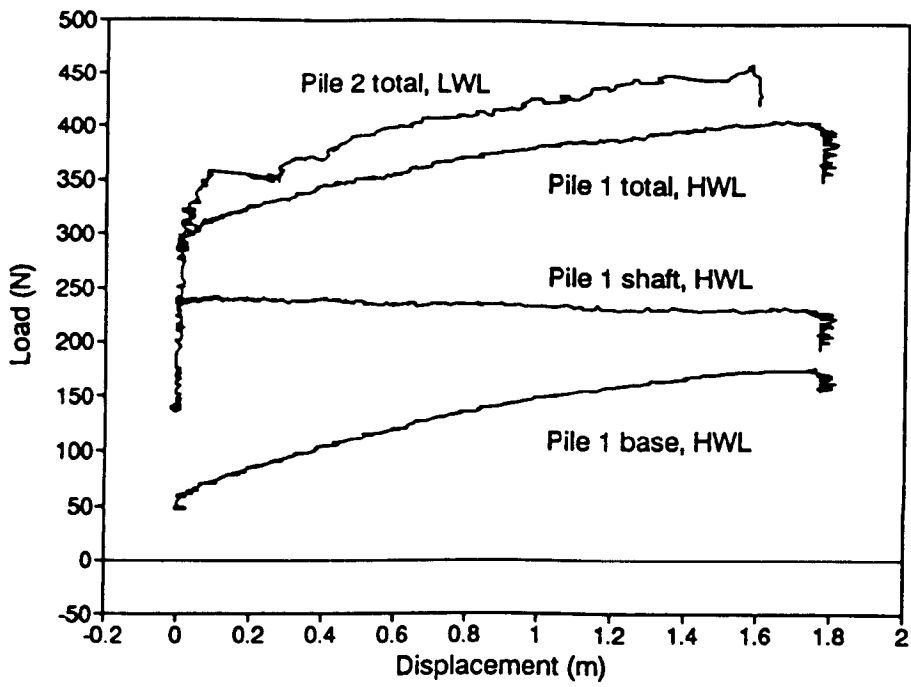


Figure A.RW7.5 Comparison of foundation load tests before (Pile 2) and after (Pile 1) rising groundwater event, test RW7

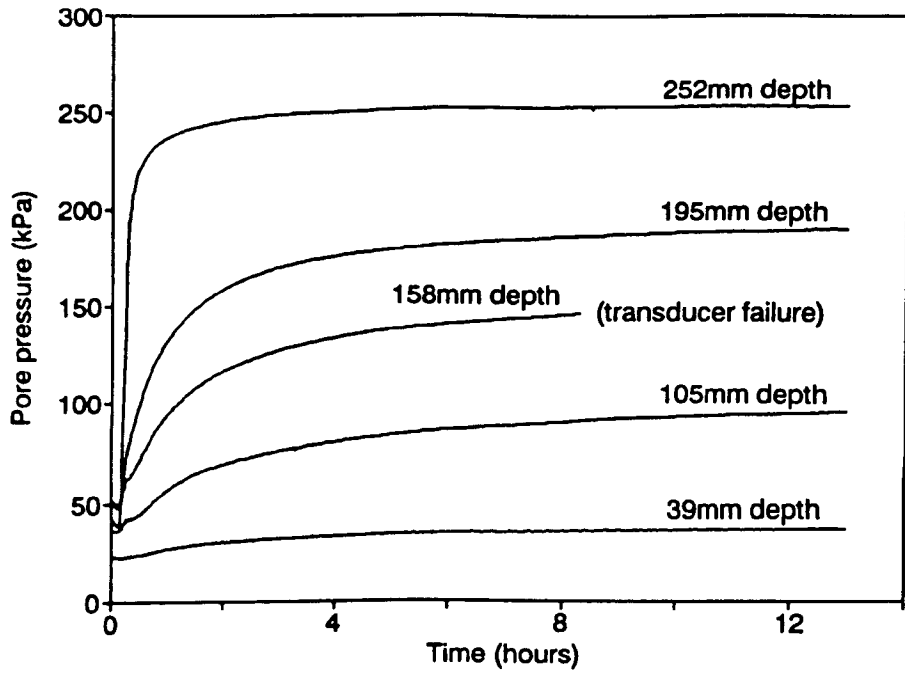


Figure A.RW10.1 Pore water pressure increase against time during rising groundwater event, test RW10

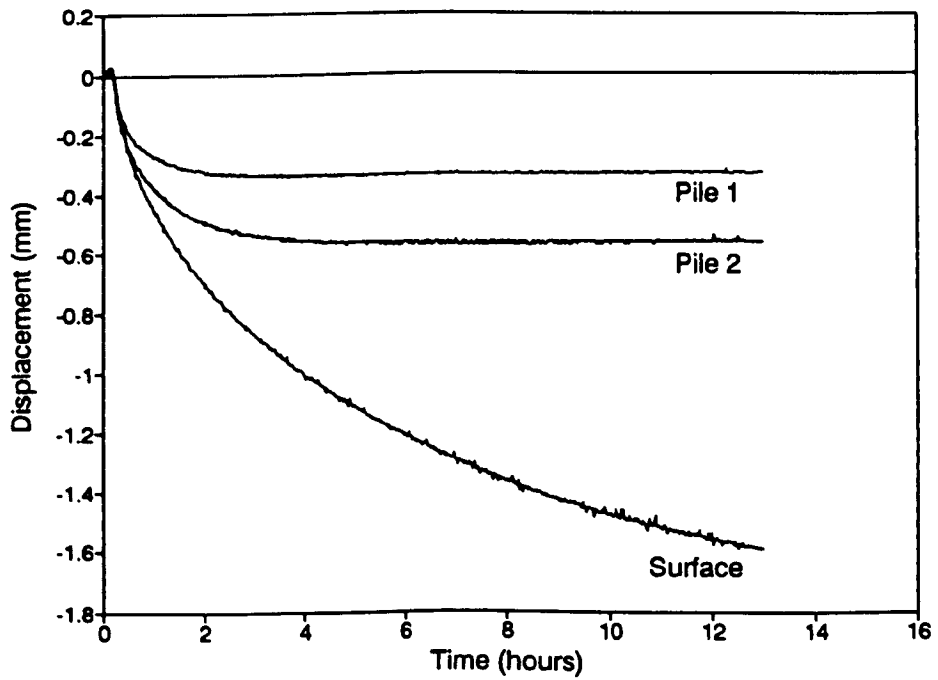


Figure A.RW10.2 Displacement against time during rising groundwater event, test RW10

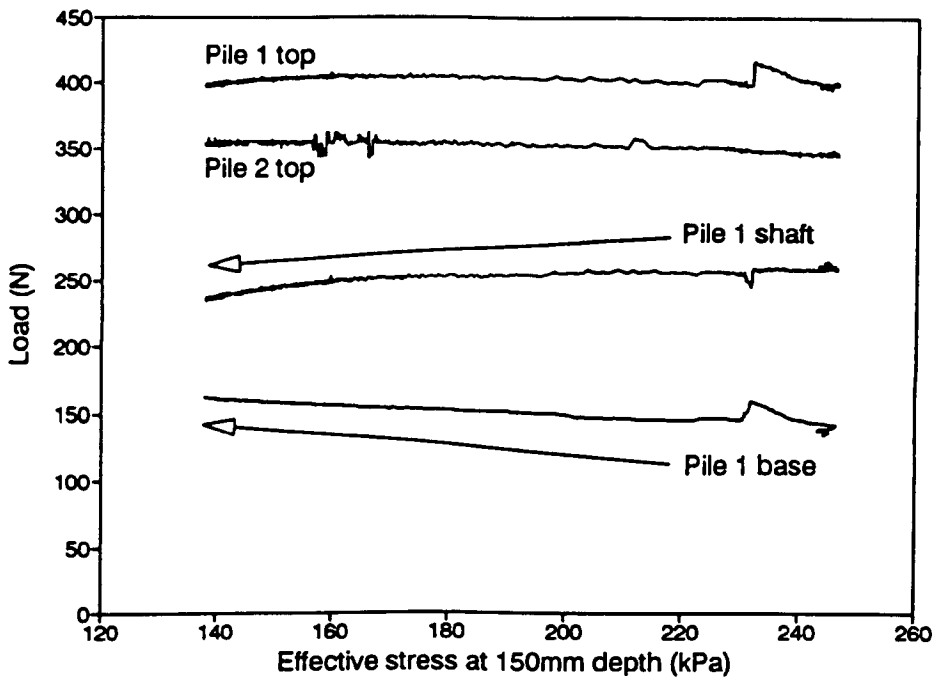


Figure A.RW10.3 Foundation loads against vertical effective stress at pile base level during rising groundwater event, test RW10

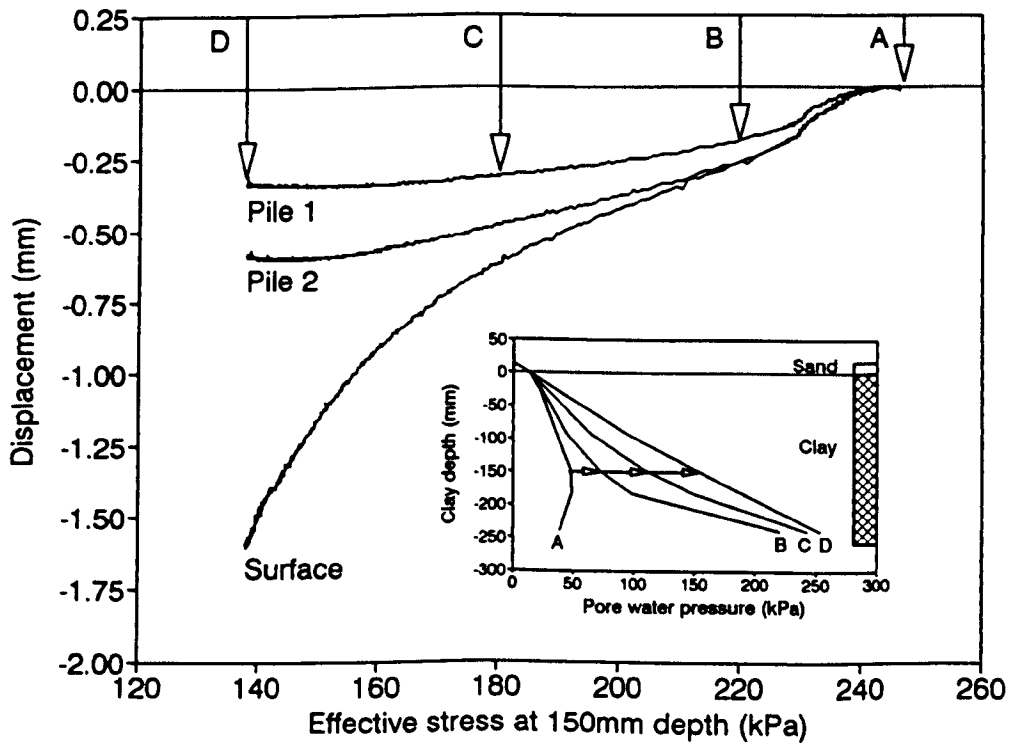


Figure A.RW10.4 Displacement against vertical effective stress at pile base level during rising groundwater event, test RW10

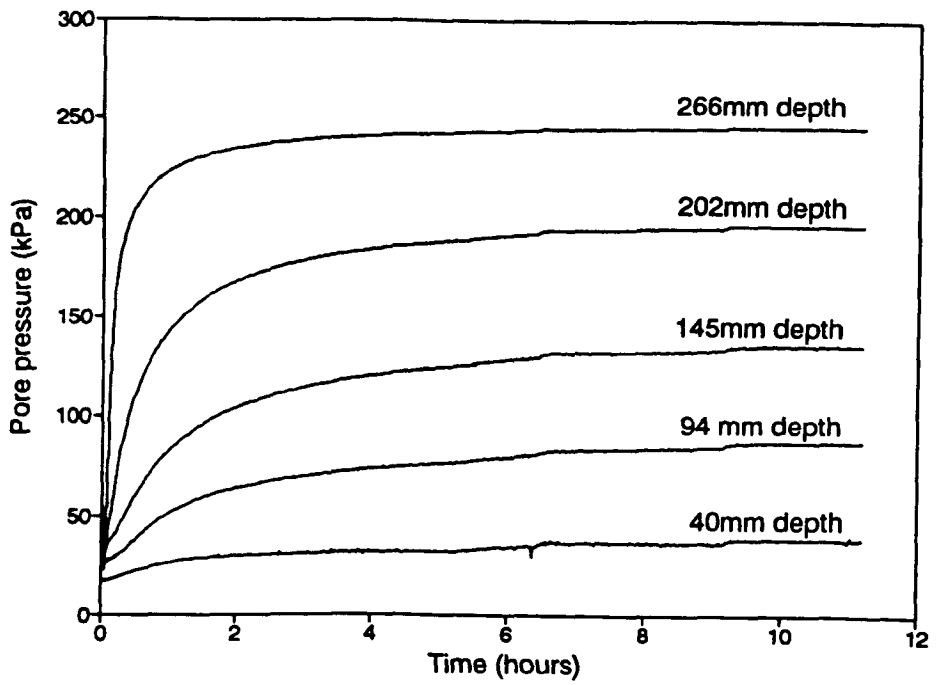


Figure A.RW11.1 Pore water pressure increase against time during rising groundwater event, test RW11

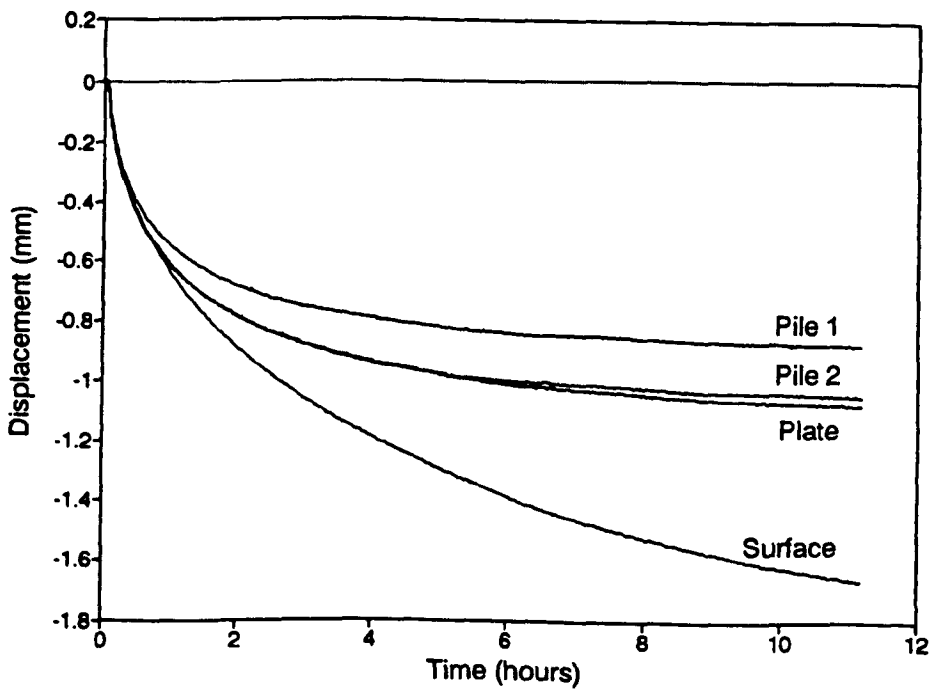


Figure A.RW11.2 Displacement against time during rising groundwater event, test RW11

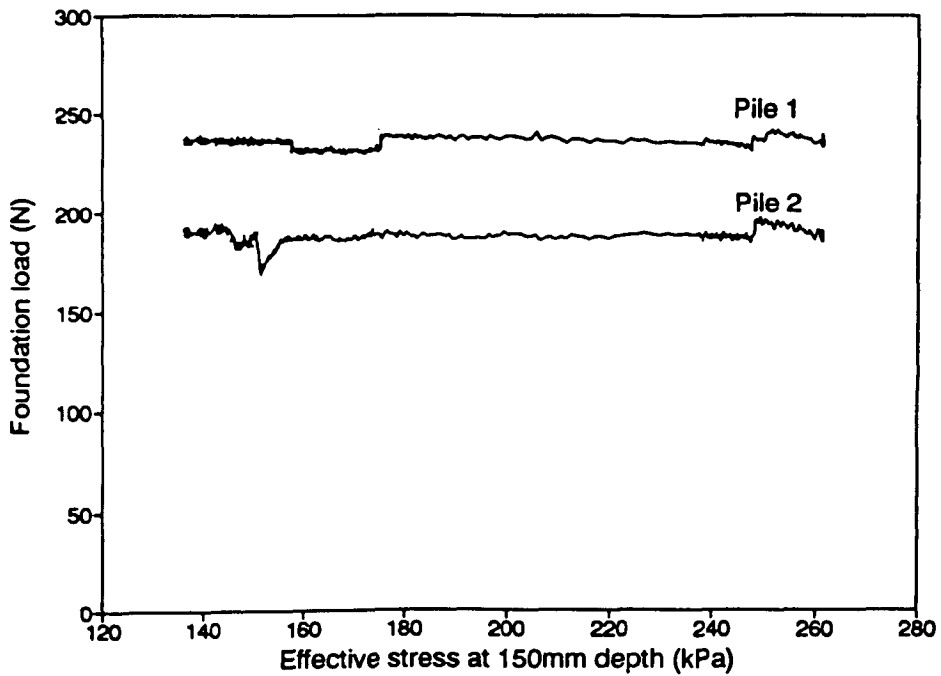


Figure A.RW11.3 Foundation loads against vertical effective stress at pile base level during rising groundwater event, test RW11

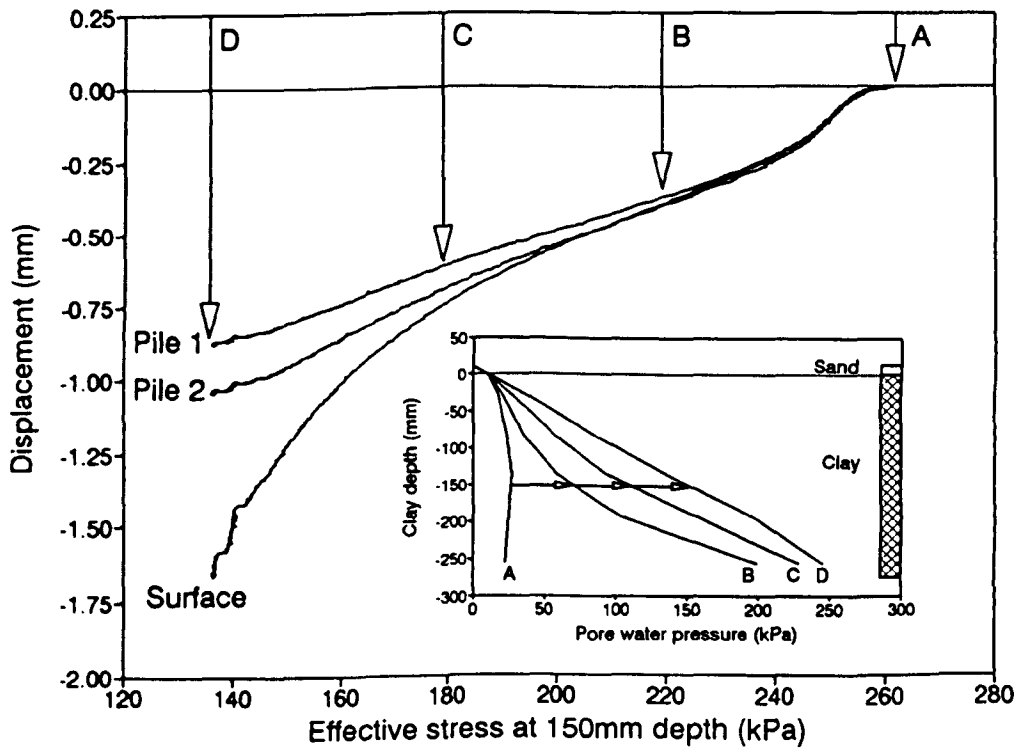


Figure A.RW11.4 Displacement against vertical effective stress at pile base level during rising groundwater event, test RW11

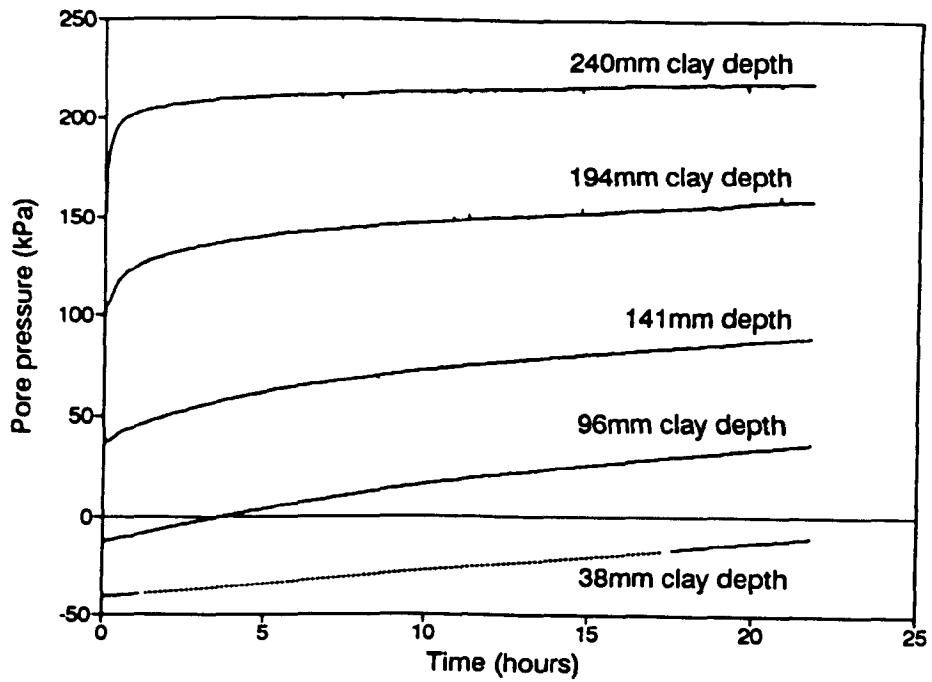


Figure A.RW12.1 Pore water pressure increase against time during rising groundwater event, test RW12

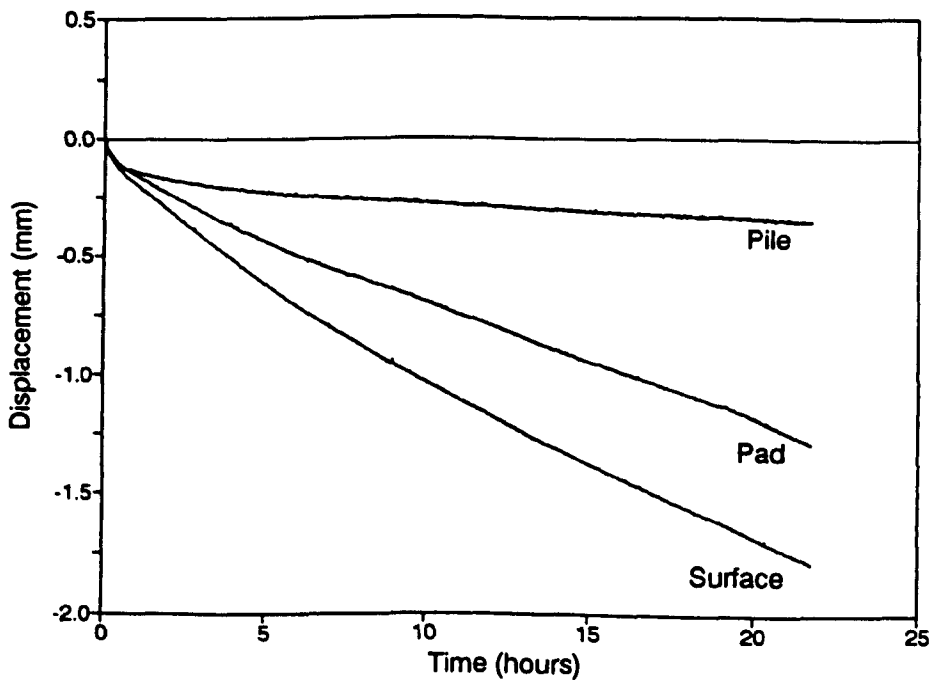


Figure A.RW12.2 Displacement against time during rising groundwater event, test RW12

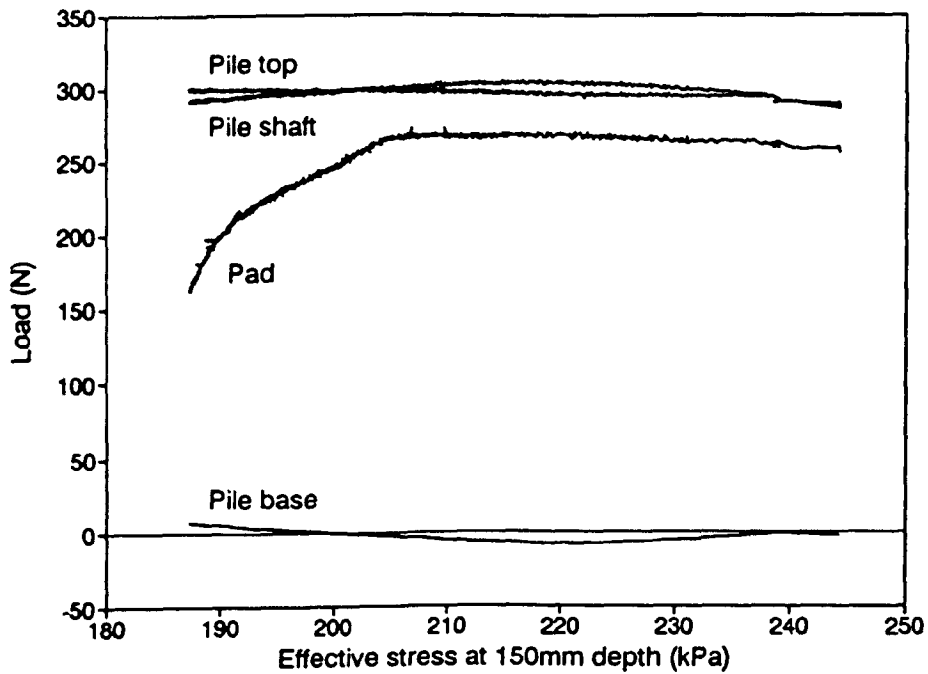


Figure A.RW12.3 Foundation loads against vertical effective stress at pile base level during rising groundwater event, test RW12

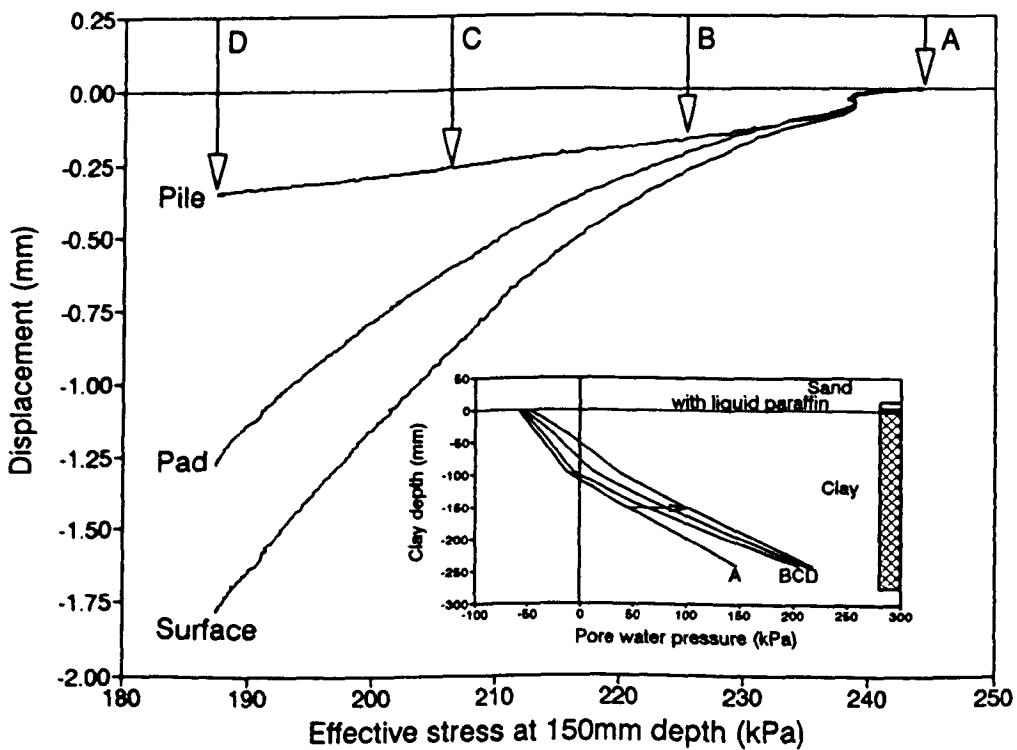


Figure A.RW12.4 Displacement against vertical effective stress at pile base level during rising groundwater event, test RW12

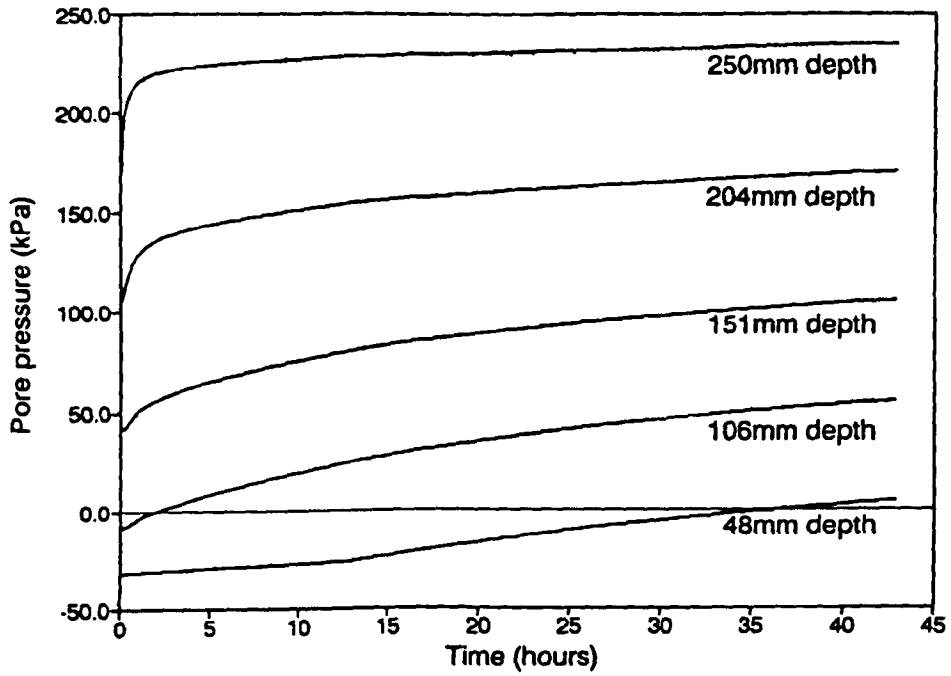


Figure A.RW13.1 Pore water pressure increase against time during rising groundwater event, test RW13

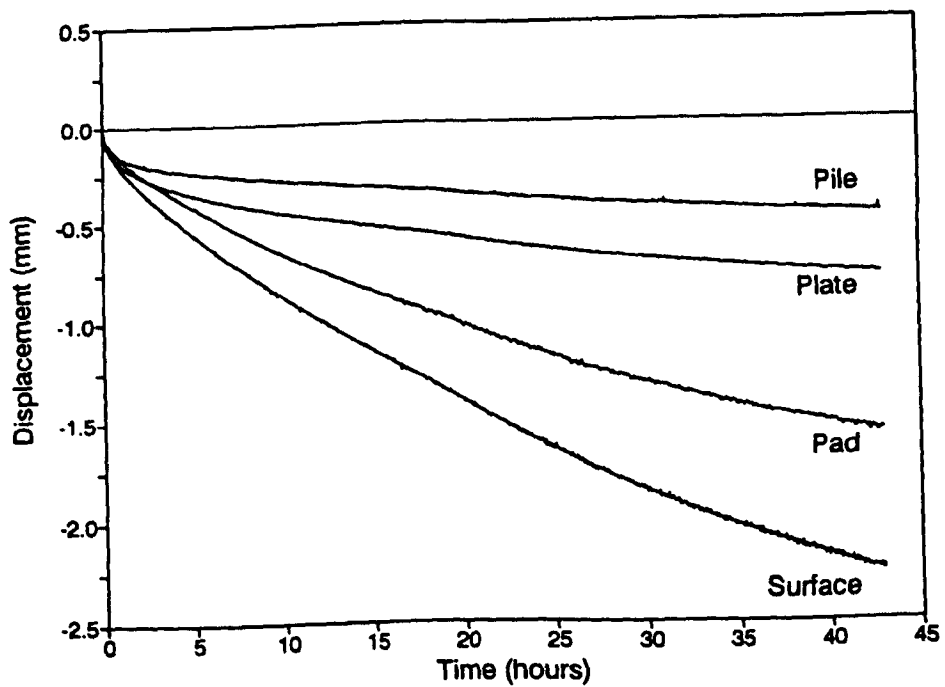


Figure A.RW13.2 Displacement against time during rising groundwater event, test RW13

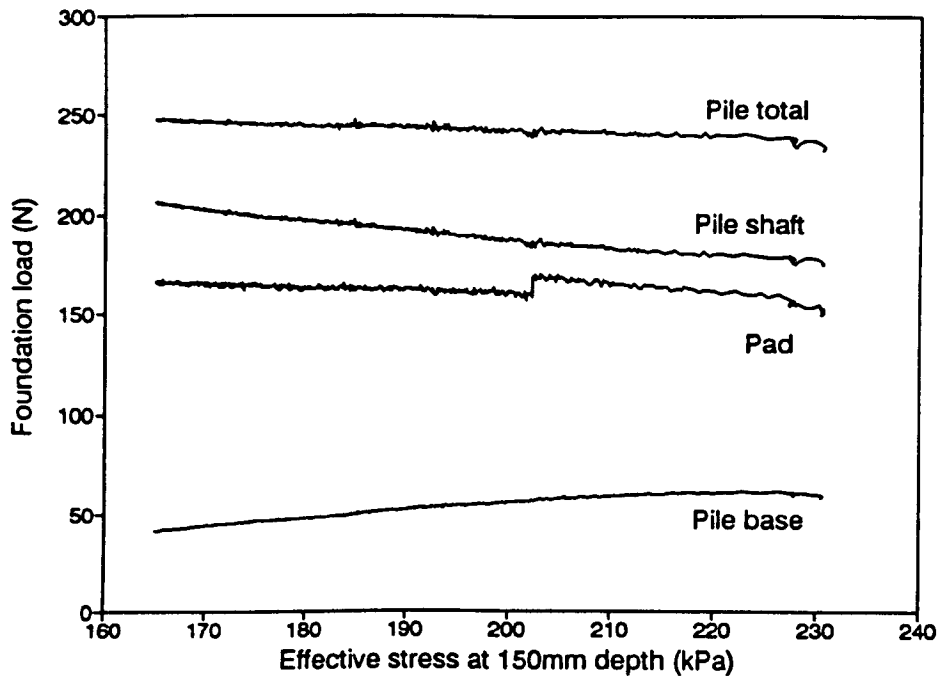


Figure A.RW13.3 Foundation loads against vertical effective stress at pile base level during rising groundwater event, test RW13

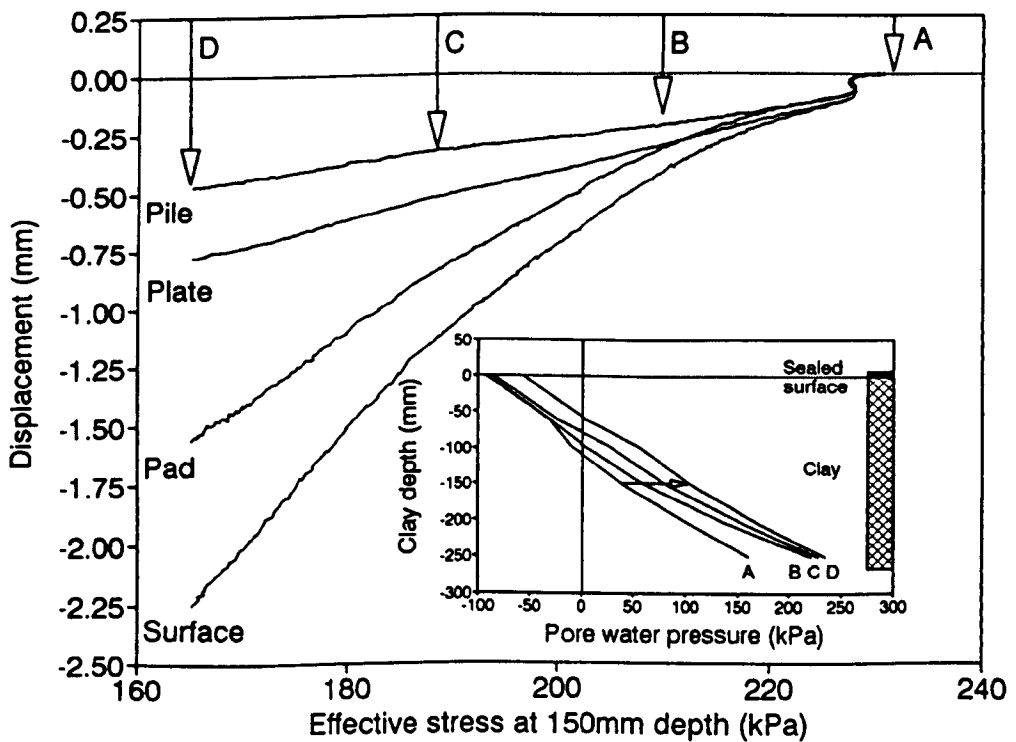


Figure A.RW13.4 Displacement against vertical effective stress at pile base level during rising groundwater event, test RW13

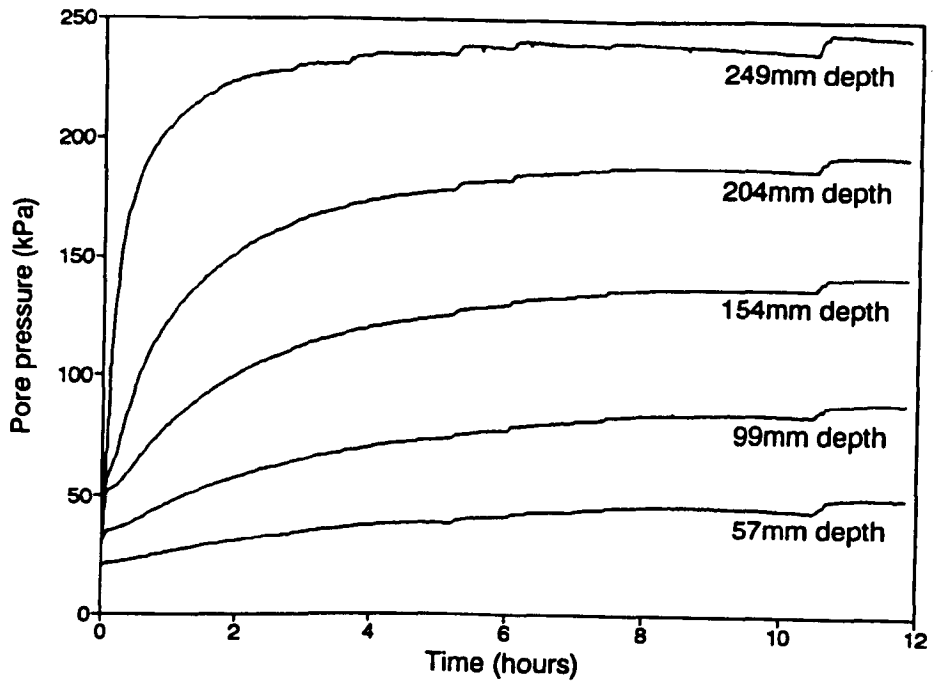


Figure A.RW14.1 Pore water pressure increase against time during rising groundwater event, test RW14

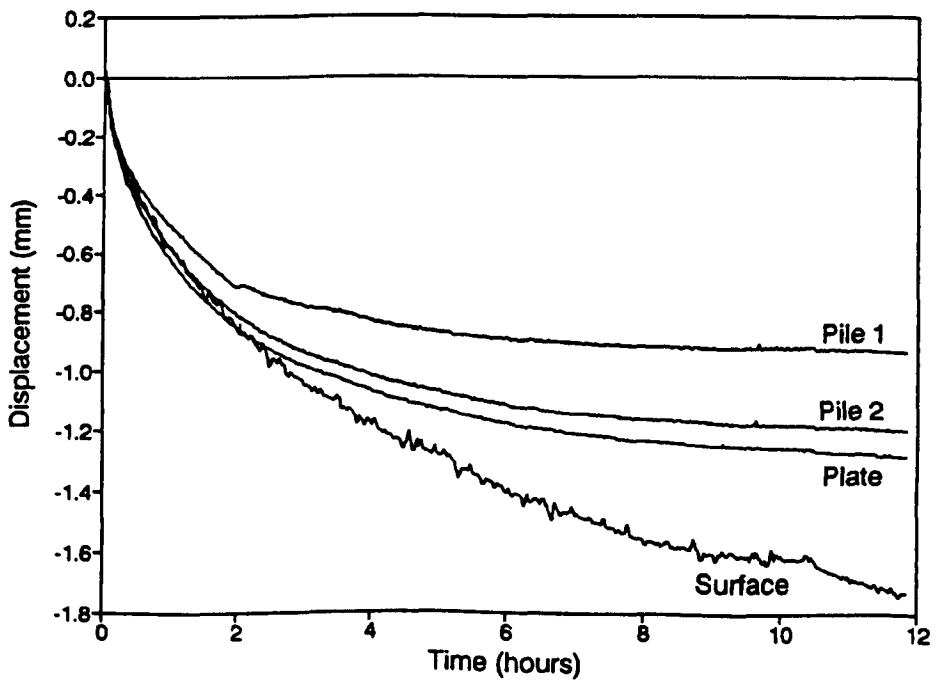


Figure A.RW14.2 Displacement against time during rising groundwater event, test RW14

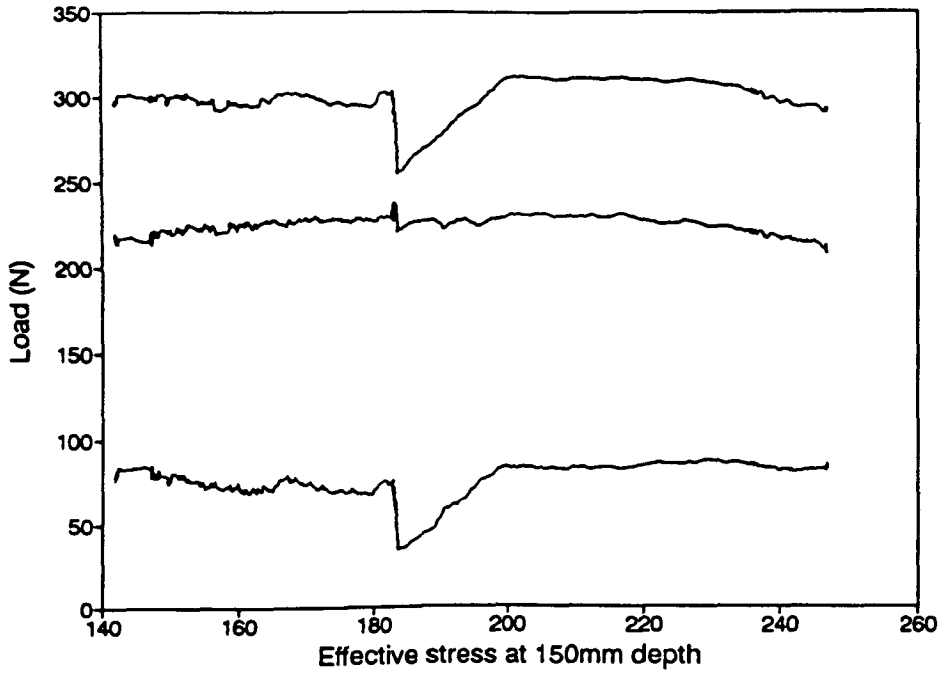


Figure A.RW14.3a Pile 1 load against vertical effective stress at pile base level during rising groundwater event, test RW14

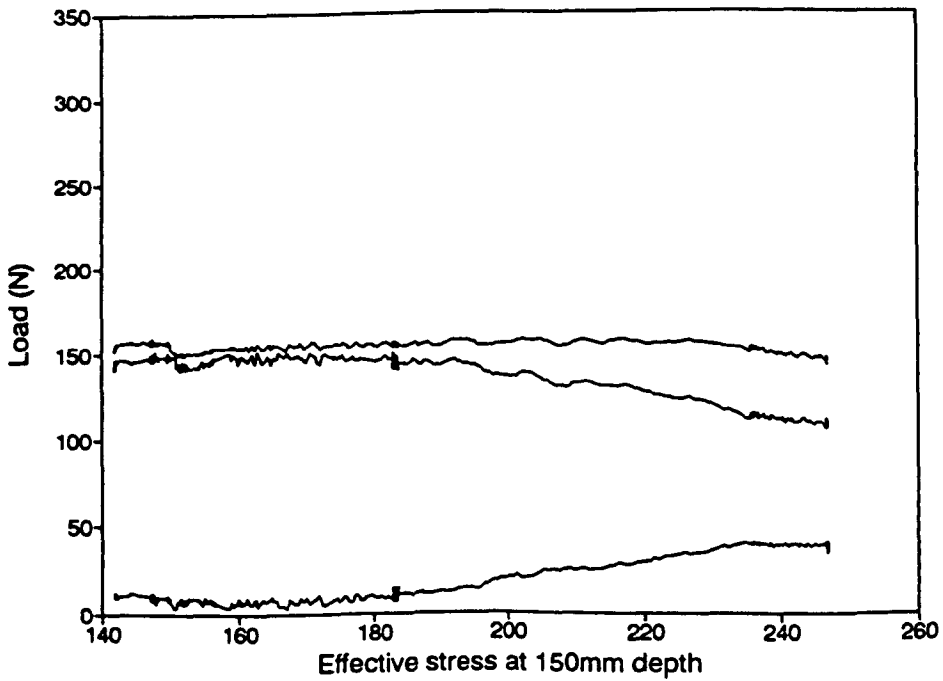


Figure A.RW14.3b Pile 2 load against vertical effective stress at pile base level during rising groundwater event, test RW14

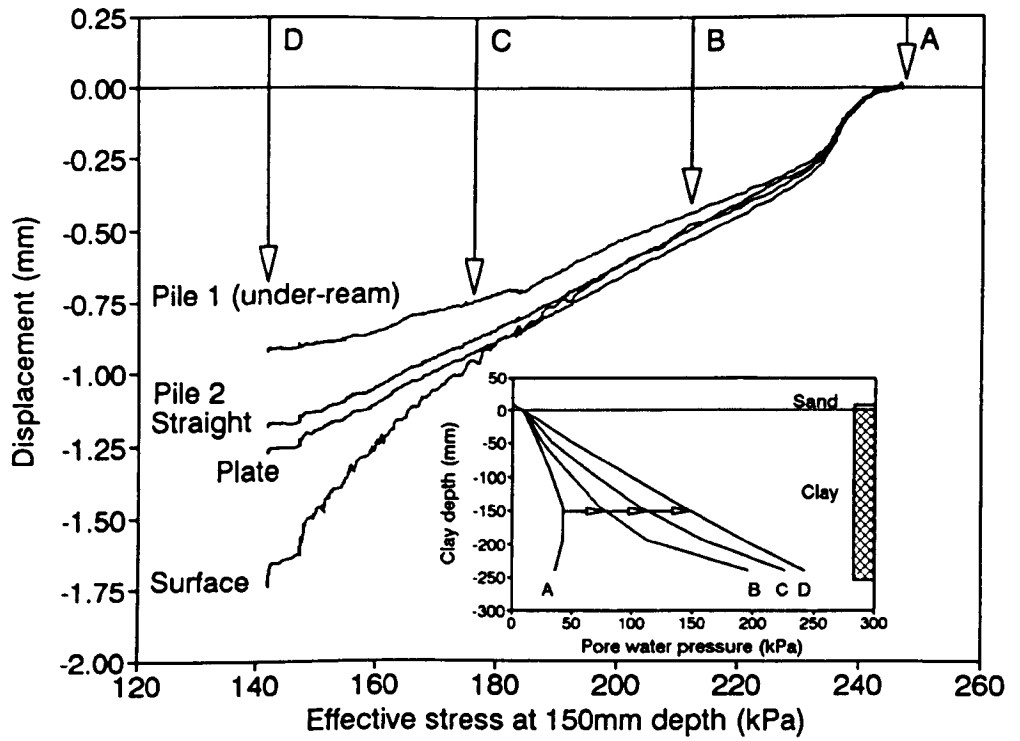


Figure A.RW14.4 Displacement against vertical effective stress at pile base level during rising groundwater event, test RW14

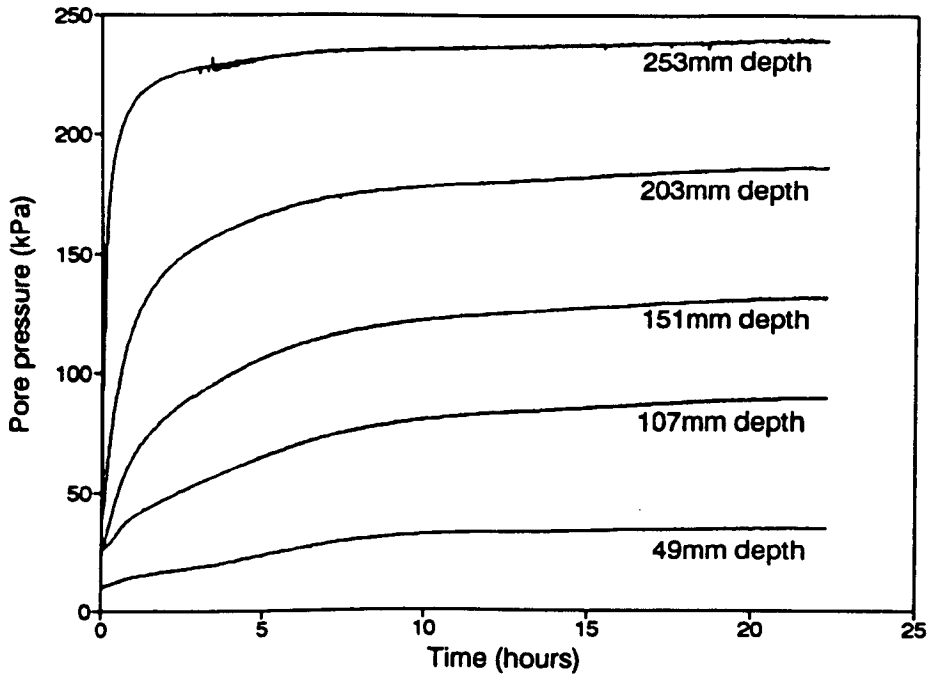


Figure A.RW15.1 Pore water pressure increase against time during rising groundwater event, test RW15

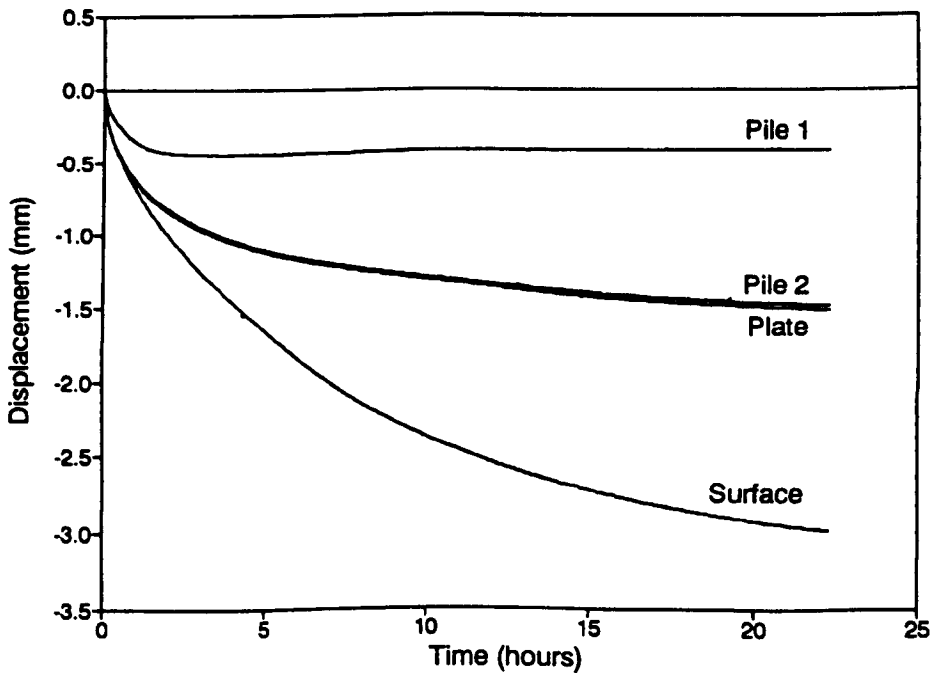


Figure A.RW15.2 Displacement against time during rising groundwater event, test RW15

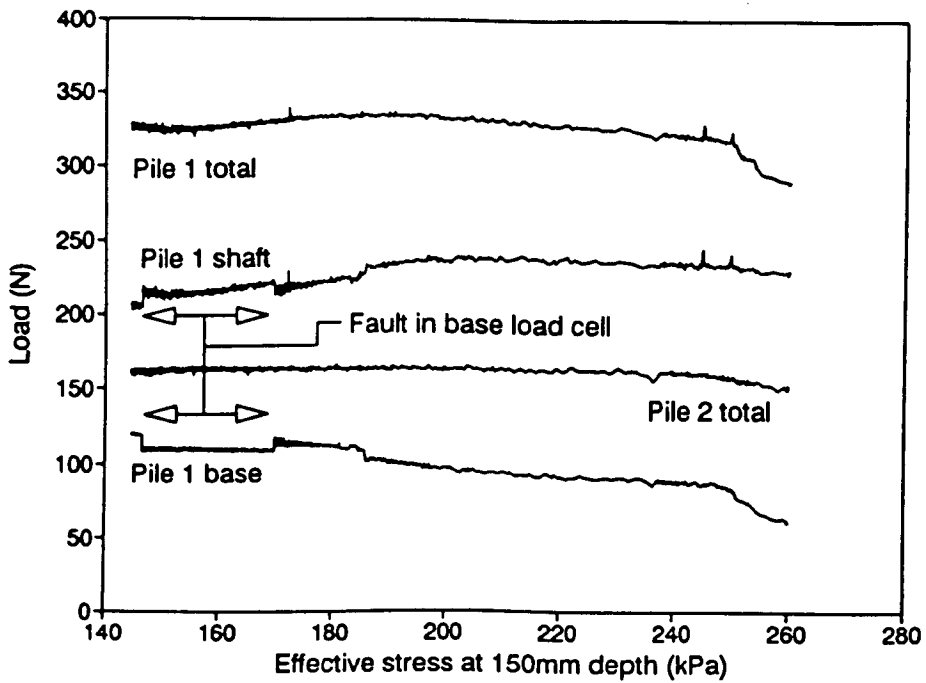


Figure A.RW15.3 Foundation loads against vertical effective stress at pile base level during rising groundwater event, test RW15

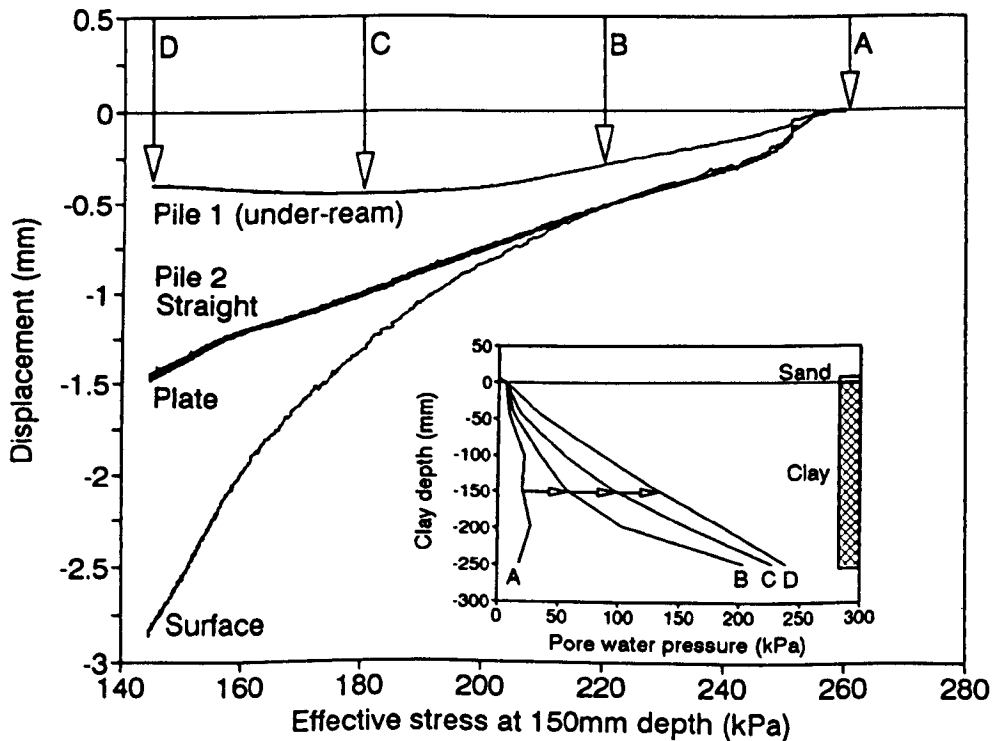


Figure A.RW15.4 Displacement against vertical effective stress at pile base level during rising groundwater event, test RW15

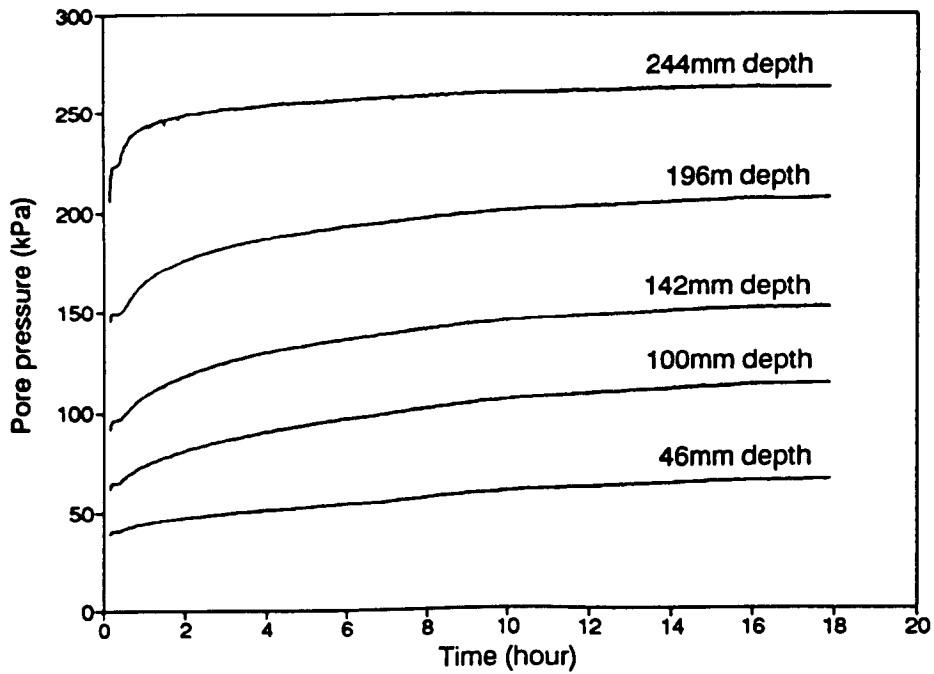


Figure A.RW16.1 Pore water pressure increase against time during rising groundwater event, test RW16

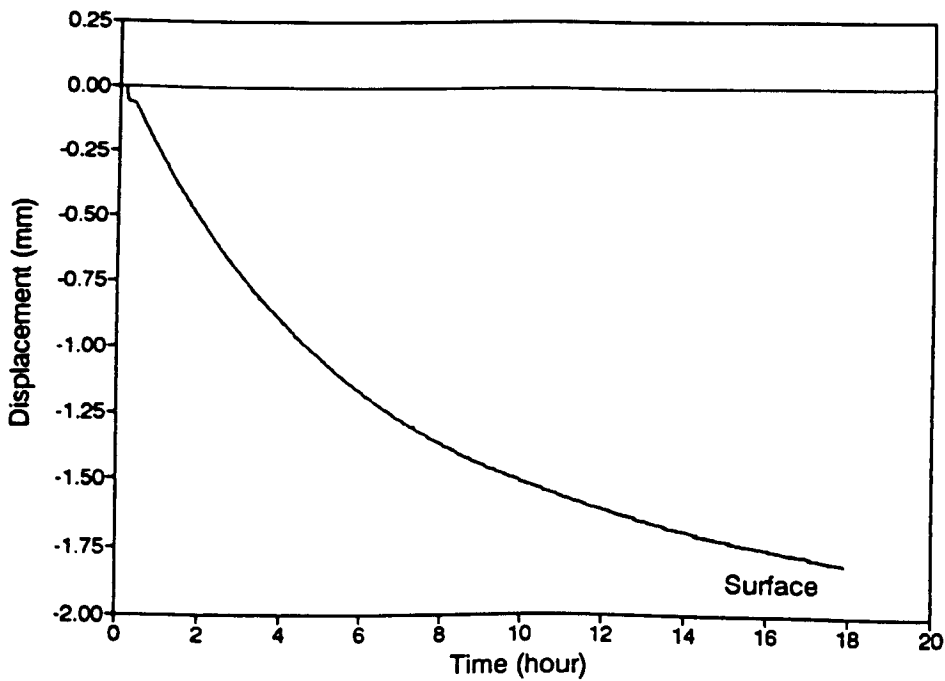


Figure A.RW16.2 Displacement against time during rising groundwater event, test RW16

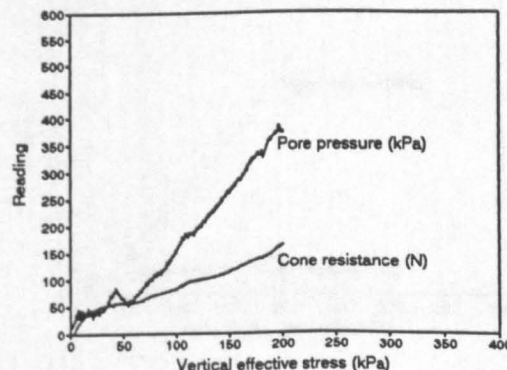
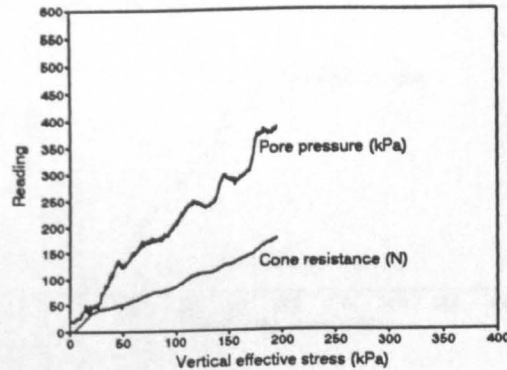
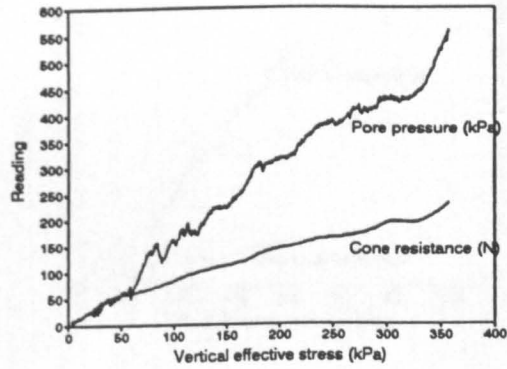
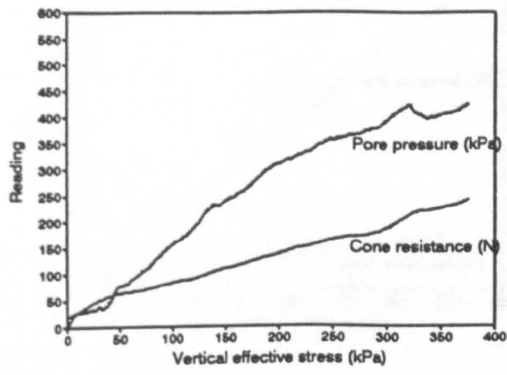


Figure A.RW16.3 Raw data from piezocone tests at 0.2mm/sec. From top to bottom: CPT1, CPT2, CPT4 and CPT5

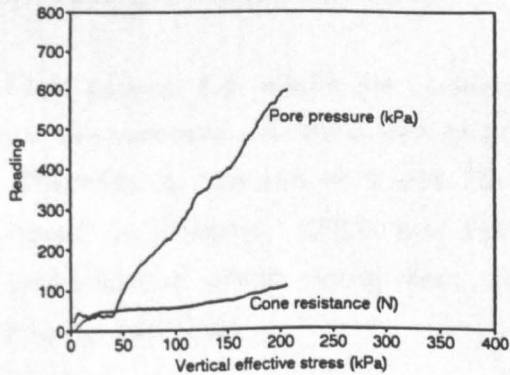
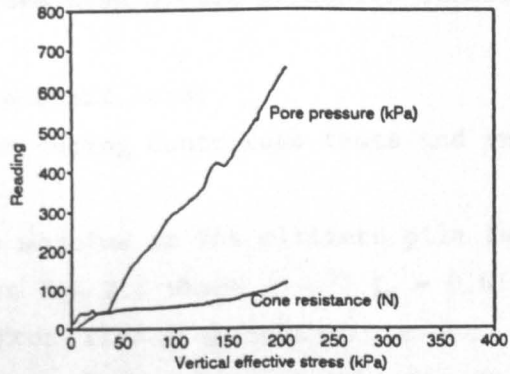
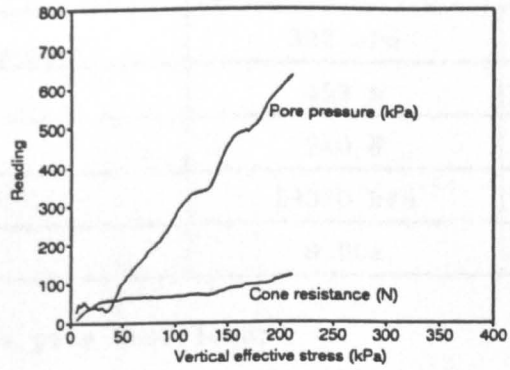
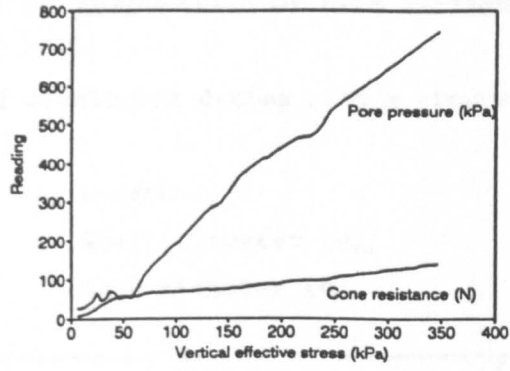


Figure A.RW16.4 Raw data from piezocone tests at 2.0mm/sec. From top to bottom: CPT3, CPT6, CPT7 and CPT8

APPENDIX B: CALCULATION OF PILE SETTLEMENT

Calculation of settlement during rising groundwater event for Pile 1 test RW14.

Data: Length : 150mm  
 Shaft diameter ( $d_s$ ) : 16mm  
 Base diameter ( $d_b$ ) : 23mm

	Before rising groundwater event	After rising groundwater event
$P'_{150\text{mm depth}}$	302 kPa	211 kPa
$P_b^{*1}$	459 N	321 N
$P_s^{*2}$	240 N	207 N
$E_{25}^{*3}$	19090 kPa	13340 kPa
$M_s^{*4}$	0.001	0.0013

- \*1 Ultimate pile base load:  
 Based on observation of pile load tests in section 5.7.2 and calculated mean normal effective stress.  $P_b = A_b 3.66 p'$ .
- \*2 Ultimate shaft load:  
 Measured during centrifuge tests and included in Table 5.3c.
- \*3 Young's modulus at 25% ultimate pile load:  
 Based on Eqn 2.8 where  $(1-\nu^2).I_p = 0.61$  and back analysis of pile test after rising groundwater event. Value quoted for before rising groundwater event is  $(p'_{LWL}/p'_{BWL})$  302/211 times that measured after the rising groundwater event.
- \*4 Flexibility factor for shaft settlement:  
 No direct measurement of this was possible during the centrifuge tests. Therefore  $M_s$  was set to 0.001 for initial conditions (in the range quoted by Fleming, 1992) and increased to 0.0013 after the rising groundwater event using data in Eqn 2.11 and appropriate values for  $r_s$  and  $G_{ave}$ .

Calculation of pile settlement in 'stationary soil' due to reduced effective stress and stiffness.

Component of pile base settlement:

$$\rho_b = \frac{0.6 P_b P_b}{E_{25} d_b \cdot (P_b - P_b)} \quad (\text{B.1})(2.10\text{bis})$$

Component of pile shaft settlement:

$$\rho_s = \frac{M_s d_s P_s}{P_s - P_s} \quad (\text{B.2})(2.11\text{bis})$$

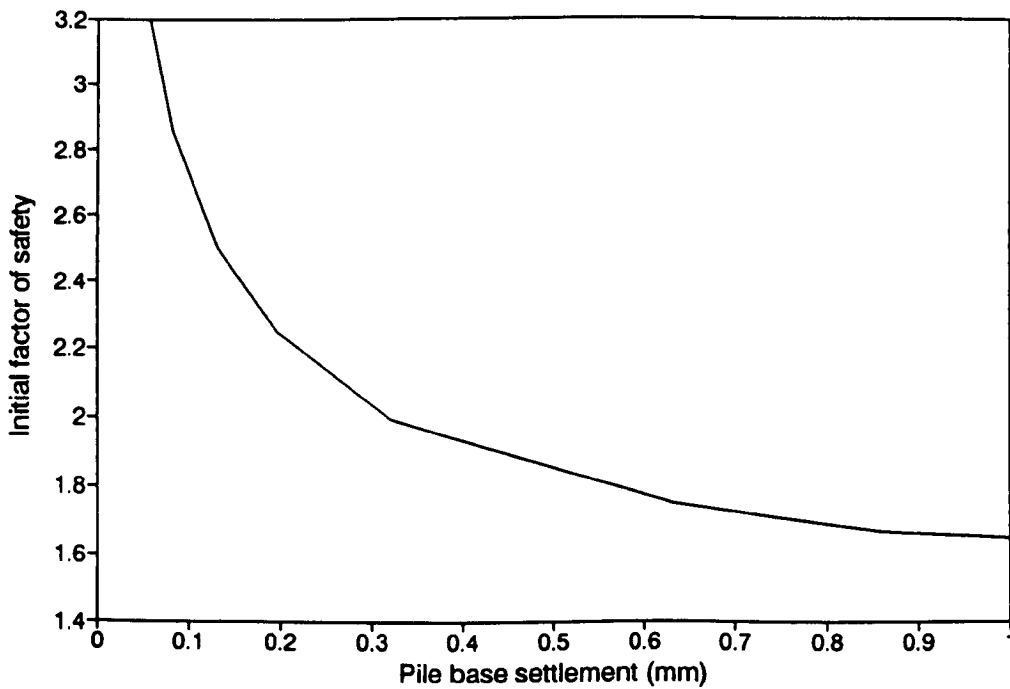


Figure B.1 Pile base settlement during rising groundwater event for varying initial factor of safety (After Fleming, 1992). Settlement due to rising groundwater event is the difference in pile settlements before and after rising groundwater event and assumes superposition.

Calculation of soil heave above pile base level may be carried out using appropriate soil parameters such as  $\kappa$ . For Speswhite Kaolin a value of  $\kappa = 0.05$  was assumed for the calculation of soil heave. Soil swelling in most centrifuge tests included both secondary primary unloading requiring a larger  $\kappa$  than would be needed if all swelling was on a secondary unload loop as used in the finite element analyses using the Schofield model in Chapter 6. Figure B2 shows soil heave above any given level so that settlement for piles of different depth or different neutral point can be obtained from one figure. At 0.15m depth the soil heave above this level is 0.7mm.

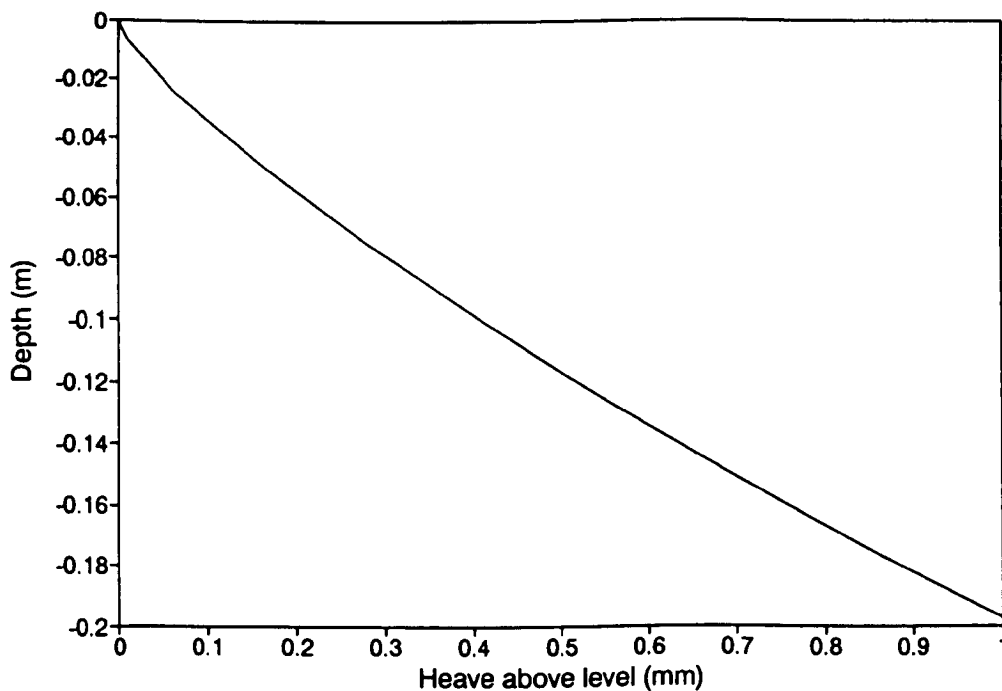


Figure B2 Soil heave due to rising groundwater event.

Overall pile settlement relative to ground surface for a pile with initial factor of safety of 2.1 is:

Pile base settlement		0.27 mm	
Soil heave	+	<u>0.70 mm</u>	
Total settlement		=	0.97 mm